

Dissertation zur Erlangung des Doktorgrades
der Fakultät für Chemie und Pharmazie der
Ludwig-Maximilians-Universität München

Theoretical Investigations of Radicals in Biology and Chemistry

von
Johnny Hioe
aus
Jakarta, Indonesien

2013

Erklärung

Diese Dissertation wurde im Sinne von §7 der Promotionsordnung vom 28. November 2011 von Herrn Prof. Dr. H. Zipse betreut.

Eidesstattliche Versicherung

Diese Dissertation wurde eigenständig und ohne unerlaubte Hilfe erarbeitet.

München, den

Johnny Hioe

Dissertation eingereicht am

1. Gutachter: Prof. Dr. H. Zipse
2. Gutachter: Prof. Dr. R. de Vivie-Riedle

Mündliche Prüfung am 22.10.2013

List of Publications

Full paper:

- J. Hioe, H. Zipse, “Radicals in enzymatic catalysis - a thermodynamic perspective”, *Faraday Disc.*, **2010**, *145*, 301 - 313.
- J. Hioe, G. Savasçı, H. Brandt, H. Zipse, “The stability of C_α-peptide radicals - why glycyl radical enzymes?”, *Chem. Eur. J.*, **2011**, *17*, 3781 - 3789.
- J. Hioe, H. Zipse, “Hydrogen transfer in SAM-mediated enzymatic radical reactions”, *Chem. Eur. J.*, **2012**, *18*, 16463 - 16472.
- J. Hioe, M. Mosch, D. M. Smith, H. Zipse, “Dissociation energies of C_α-H bonds in amino acids – a re-examination”, *RSC Advances*, **2013**, *3*, 12403 - 12408.

Review:

- J. Hioe, H. Zipse, “Radical stability and its role in synthesis and catalysis”, *Org. Biomol. Chem.*, **2010**, *8*, 3609 - 3617.

Book:

- J. Hioe, H. Zipse, “Radical stability - thermochemical aspects”, p. 449 - 476 in *Encyclopedia of Radical in Chemistry, Biology and Materials*, C. Chatgililoglu and A. Studer (eds.), John Wiley & Sons Ltd, Chichester, UK, 2012.

Danksagung

Diese Arbeit wurde in der Zeit von Dezember 2009 bis April 2013 unter der Anleitung von Prof. Dr. H. Zipse an der Fakultät für Chemie und Pharmazie der Ludwig-Maximilians-Universität München durchgeführt. Ich möchte vielen Personen herzlich für die Unterstützungen danken.

An der ersten Stelle möchte ich mich bei Prof. Dr. H. Zipse bedanken, für seine Anleitung, wissenschaftliche Diskussion und Lehre, die mir sehr viel bedeutet haben. Prof. Dr. H. Zipse hat mir nicht nur auf dem Gebiet der Wissenschaft viel beigebracht, sondern auch bei ausserplanmässigen Kletteraktivitäten, die mir besonders am Herzen liegen. Meinem Zweitgutachter, Prof. Dr. R. de Vivie-Riedle, danke ich herzlich für die freundliche Übernahme des Zweitgutachtens.

Des Weiteren möchte ich mich auch bei den Arbeitsgruppenmitgliedern von Prof. H. Zipse bedanken, die für mich mehr Freunde als wissenschaftliche Kollegen sind. Einen besonderen Dank möchte ich an Dr. B. Maryasin richten. Seine fruchtbaren (manchmal auch furchtbaren) Diskussionen und Ideen schätze ich sehr. Mein Dank gilt auch C. Zhang, die mit mir zusammen den Rechen-Cluster betreut hat, Dr. C. Lindner und Dr. R. Tandon, mit denen ich zusammen studiert und viele lustige Dinge erlebt habe und F. Achrainer, der mir einige Aspekte der Chemie näher gebracht hat, F. Barth, mit dem ich das Projekt "nicht-funktionierende Marcus-theorie" gemacht habe, P. Patschinski, der unsere treue Kaffeemaschine verwaltet hat, Dr. Y. Liu, mit dem ich Fussball gespielt habe und Dr. E. Larionov, mit dem ich auf den interessanten Rinnkendlsteig gegangen bin.

Wichtig sind auch Dr. D. M. Smith, Prof. Dr. V. Vrcek und dessen Mitarbeiter D. Sakic, mit denen ich zusammengearbeitet habe. Den Mitarbeitern von Prof. Dr. R. Gschwind, M. Hammer und M. Haindl, danke ich für das gemeinsame interessante Projekt. Meinen Studenten G. Savasçı, A. Hader, G. Bahadir, T. Tarade, M. Mosch und T. Driant, deren Ergebnisse für mich sehr wichtig sind, bin ich zu Dank verpflichtet. Bei Dr. K. Matsumoto, den ich auf dem Gebiet der theoretischen Chemie betreut habe, möchte ich mich für das Betreuungserlebnis und für den japanischen grünen Tee bedanken.

Ein herzlicher Dank richtet sich auch an S. Oesterling, mit dem ich viele Klettererlebnisse und Capoeirastunden verbracht habe. Meinen Eltern, Jeffrey Hioe und Tantri Megawati, und meinen Geschwister, Henny Megawati, Tony Kurniawan, Dr. Denny Hioe, die mich stets unterstützt haben, bin ich überaus dankbar. Zuletzt möchte ich diese Arbeit meiner Frau, Theresia Wijaya Kusuma, widmen. Ohne ihre liebevolle Unterstützung hätte ich mein Chemiestudium sicher nicht so gut geschafft.

“One could perhaps describe the situation by saying that God is a mathematician of a very high order, and He used very advanced mathematics in constructing the universe.”

P. A. M. Dirac

Für Theresia

Table of Contents

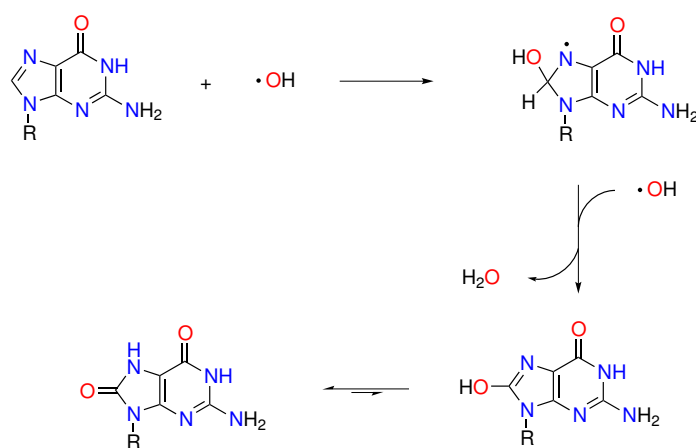
1	General Introduction	1
1.1	Theoretical calculation of the thermodynamic stability of radicals . . .	4
1.1.1	Choice of theoretical methods	4
1.1.2	Concept of radical stabilization energy (RSE)	6
2	Radicals in Enzymatic Catalysis - A Thermodynamic Perspective	15
2.1	Introduction	16
2.2	Computational Details	17
2.3	Results	17
2.4	Discussion	21
2.4.1	Enzymatic reaction mechanisms I: pyruvate formate lyase (PFL)	22
2.4.2	Enzymatic reaction mechanisms II: spore photoproduct lyase (SPL)	25
2.5	Conclusion	27
3	The Stability of C_α-Peptide Radicals - Why Glycyl Radical Enzymes?	33
3.1	Introduction	34
3.2	Results	35
3.3	Conclusion	49
4	Dissociation Energies of C_α-H Bonds in Amino Acids - a Reexamination	54
4.1	Introduction	55
4.2	Results	56
4.3	Conclusions	64
5	Hydrogen Transfer in SAM-Mediated Enzymatic Radical Reactions	67
5.1	Introduction	68
5.2	Results and Discussion	69
5.3	Conclusion	84

6	Radical Stability of Oxygen-centered Radicals - A Methodological Survey	90
6.1	Introduction	91
6.2	Results	91
6.3	Conclusion	114
7	Marcus-Analysis of Reaction Barriers for Hydrogen Transfer Reactions	119
7.1	Introduction	120
7.2	Results	120
7.3	Conclusion	128
8	Barrier in Spore Photoproduct Lyase	131
8.1	Introduction	132
8.2	Results	132
8.3	Conclusion	143
9	General Conclusion	147
A	Theoretical Methods	154
A.1	Composite methods	155
B	Supplementary Information	161

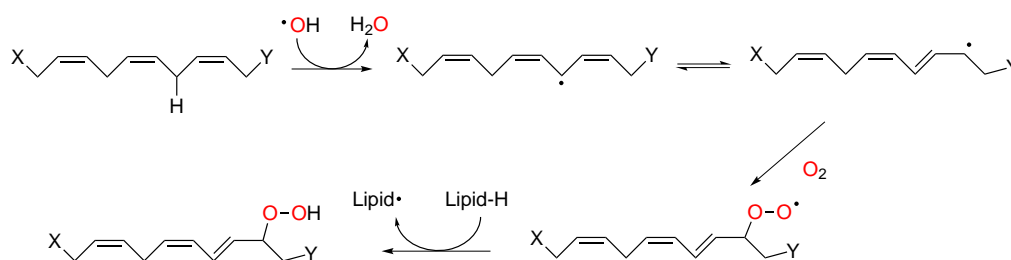
Chapter 1

General Introduction

Open-shell systems in the main group chemistry, which possess one or more unpaired electrons (*e.g.* radicals) are generally assumed to be chemically reactive towards other chemical compounds. This is partially supported by the observation of spontaneous dimerization or polymerization, which indicates that such open-shell intermediates are possibly thermodynamically or/and kinetically unstable. Consequently most radicals occur only in very low concentration. At cellular level several radicals are proven to react with macromolecules such as nucleic acids, lipids and proteins causing damages, which can further lead to single strand breaks and cross-linking. Just to name a prominent example, the oxidative stress of the DNA base guanine by reactive oxygen species (ROS), such as superoxide radical anion $\cdot\text{O}_2^-$, O_2^{2-} , nitric oxide $\text{NO}\cdot$, hydroxyl radical $\text{HO}\cdot$, which leads to oxo-guanine derivatives.^[1;2] Free radicals are suspected to be associated with the development of Parkinson's disease and Alzheimer.^[3]



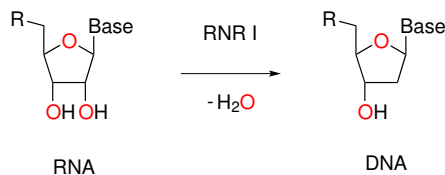
Scheme 1.1: Oxidative stress of guanine by two hydroxyl radicals leading to 8-oxo-guanine.^[4]



Scheme 1.2: Peroxidation of lipid by ROS.

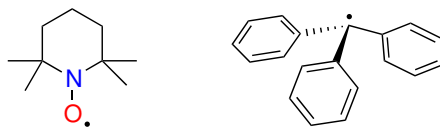
In contrast to the general assumption, scientific studies on enzymatic catalysis also evidenced that the apparently reactive open-shell intermediates are applied as tools, which opens the question of the stability of radicals and how the natural architectures manage to control the radicals. One of the most intensively studied enzymes of this class is ribonucleotide reductase (RNR class I) in anaerobic organisms, which

uses a variety of protein-bound radicals in its catalysis converting ribonucleic acid (RNA) into 2'-desoxyribonucleic acid (DNA) (Scheme 1.3).^[5-9]



Scheme 1.3: Reduction of ribonucleic acid to 2'-desoxyribonucleic acid catalyzed by the enzyme ribonucleotide reductase in anaerobes.

The important role of radicals is not only found in enzymology, but also in the field of synthetic and polymer chemistry. As an example, the "persistent" radical (2,2,6,6-tetramethylpiperidin-1-yl)oxyl (TEMPO) is used in organic synthesis as catalyst in the oxidation of primary alcohols to aldehydes, or as a radical trap in biochemistry (Scheme 1.4). The terms persistent and transient radical are in the literature connected to kinetic properties rather than thermodynamic stability. In fact, TEMPO, owing to the steric features near to the radical center, is even dull enough to be stored in a bottle. However, O-H bond strength of hydroxylamine is known to be one of the weakest, which indicates a high thermodynamic stability of the respective radicals.



Scheme 1.4: TEMPO and triphenylmethyl radical are examples of the persistent oxygen centered radicals.

1.1 Theoretical calculation of the thermodynamic stability of radicals

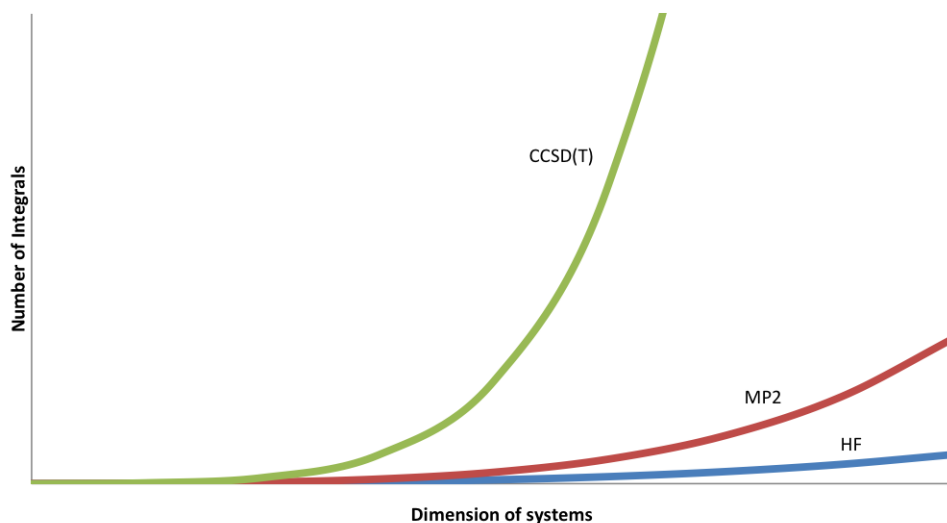
Particularly for biological systems, measuring thermodynamic stabilities and obtaining structural information for open-shell systems experimentally is extremely tedious and therefore often not feasible. Since the advent of quantum mechanics, the computational chemistry has developed in an exponential speed, and has been proven to be a powerful instrument for predicting, supporting, and comprehending the experimental outcomes. Furthermore the establishment of density functional theory (DFT) for small molecular systems by Kohn and Sham set the milestone in the computational chemistry being able to predict the chemical reaction in a quite accurate manner.^[10] Whenever experimental investigations on biological systems are very limited, quantum chemical studies may thus serve as a good alternative.

1.1.1 Choice of theoretical methods

However, it should be mentioned, that the theory has a major problem to calculate accurate energies of electronic structures. The Hartree-Fock theory (HF), being the most central method, covers about 99 % of the exact electronic energies. Unfortunately the 1 % (0.01 a.u. = 26.255 kJ mol⁻¹) is yet so necessary, since it may determine all of chemistry. Very highly correlated methods such as coupled clusters or configuration interactions (Table 1.1) using multi-determinant expansions of electronic wavefunction with huge basis sets do fill the missing correlation energy very well, yet they are restricted to small, or at best medium sized systems.

Table 1.1: Overview of cost scaling of common theoretical methods.

Methods	Scaling with number of basis functions	Determinant number	Variational of methods	Size-extensivity
Hartree-Fock	n^4	single determinant	variational	size-extensive
Hybrid DFT	n^4	single determinant	functional dependent	functional dependent
MP2	n^5	multi determinant	non-variational	size-extensive
MP4(SDQ)	n^6	multi determinant	non-variational	size-extensive
CISD	n^6	multi determinant	variational	non-size-extensive
CCSD	n^6	multi determinant	non-variational	size-extensive
MP4(SDTQ)	n^7	multi determinant	non-variational	size-extensive
CISD(T)	n^7	multi determinant	non-variational	non-size-extensive
CCSD(T)	n^7	multi determinant	non-variational	size-extensive
CISDT	n^8	multi determinant	variational	non-size-extensive
CCSDT	n^8	multi determinant	non-variational	size-extensive



Scheme 1.5: Conventional Hartree-Fock (HF) calculation scales to the power of 4 (n^4) with the basis set number. The first correction to HF, Møller-Plesset second order (MP2), scales to the power of 5 (n^5) due to the AO to MO integral transformation. With the power of 7 (n^7), coupled cluster single double with perturbative triples (CCSD(T)) is therefore very computational demanding. Full-CI is not affordable for systems with more than 3-4 atoms.

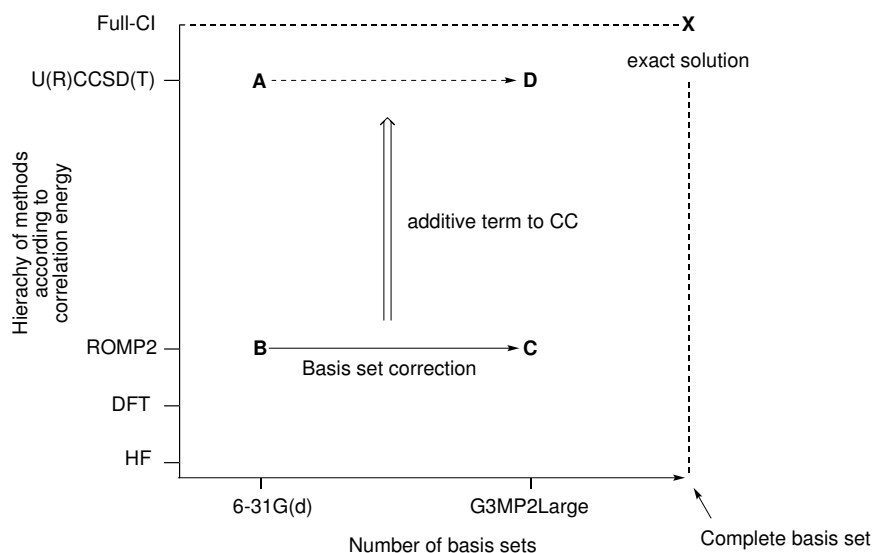
Fortunately computations of chemical reaction energies are indeed pretty accurate even for relatively low-level theories owing to the error compensation mechanism. Therefore, the construction of elegant schemes of reactions using appropriate electronic models, and the choice of methods are very crucial in the theory. Careless choice of reaction schemes and poorly chosen methods can yield numerical garbage and lead to misinterpretation. The biggest part in this dissertation will deal with the calculation of the thermodynamic stability of radicals and its application to assess the thermochemical effort, which is one of the important criterion in the enzymatic catalysis. The computation methods applied in the whole projects are tailor-made for predicting thermochemical properties. For radicals G3(MP2)-RAD from the Gaussian theories family is frequently used, whenever accurate reaction energies with 1 kcal mol⁻¹ statistical error from the experimental values are desired (Scheme 1.6).^[11;12] The G3(MP2)-RAD is a composite extrapolation procedure, which approximates coupled cluster energies at huge basis set by an addition of a basis set correction, which is performed at ROMP2-level of theory (Scheme 1.6).

The definition of total electronic energy in G3(MP2)-RAD is thus given by,

$$E_{\text{tot}}(\text{G3(MP2)-RAD}) = E_{\text{tot}}(\text{U(R)CCSD(T)/6-31G(d)}) + \text{B.C.} \quad (1.1)$$

With basis set correction term (B.C.) performed at ROMP2 level of theory,

$$\text{B.C.} = E_{\text{tot}}(\text{ROMP2(FC)/G3MP2Large}) - E_{\text{tot}}(\text{ROMP2(FC)/6-31G(d)}) \quad (1.2)$$



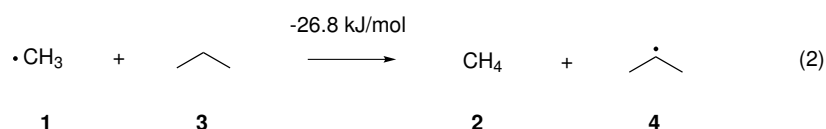
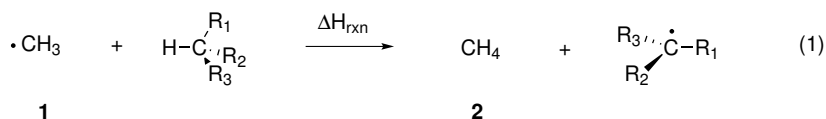
Scheme 1.6: Schematic figure of G3(MP2)-RAD.

Nevertheless, while G3(MP2)-RAD is able to give results sophisticatedly for most of the cases, the studies of oxygen centered radicals revealed that such systems are inadequately treated at G3(MP2)-RAD. Higher theoretical methods such as G4 is available and are shown to predict thermochemical properties of a large test set including oxygen-centered radicals better.^[13] The twist on these variants is that they are more costly than G3(MP2)-RAD, hence reducing the choice of the systems to a smaller window. Application of such methods for peptide based radicals is not affordable given the limited current computational power. A small chapter about minor revisions of G3(MP2)-RAD is hence dedicated to give better results for the sensitive case of oxygen centered radicals.

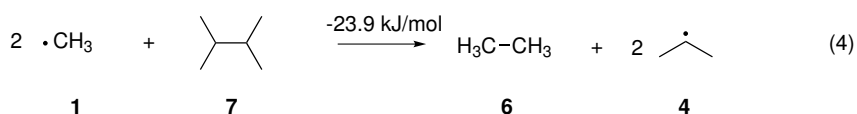
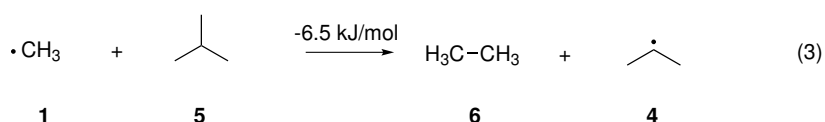
1.1.2 Concept of radical stabilization energy (RSE)

The stability of C-centered radicals can conveniently be expressed using the isodesmic H-transfer reaction shown in eqn. (1).^[14–18] The reaction enthalpy of this process is commonly referred to as the radical stabilization energy (RSE) of the newly formed radical $\bullet\text{CR}_1\text{R}_2\text{R}_3$ relative to the unsubstituted methyl radical $\bullet\text{CH}_3$ (**1**). For isopropyl radical **4**, for example, a RSE value of $-26.8 \text{ kJ mol}^{-1}$ is derived in this way and interpreted as the result of stabilizing (hyperconjugative) interactions between the two methyl groups and the radical center. It should be noted here that this reaction energy is, of course, exactly identical to the difference in the C-H bond dissociation energy in methane (**2**) of $\text{BDE}(\text{CH}_3\text{-H}) = +439.3 \pm 0.4 \text{ kJ mol}^{-1}$, and

that of the central C-H bond in propane (**3**) with BDE $(\text{CH}_3)_2\text{CH-H} = +412.5 \pm 1.7$ kJ mol^{-1} .^[19-21]

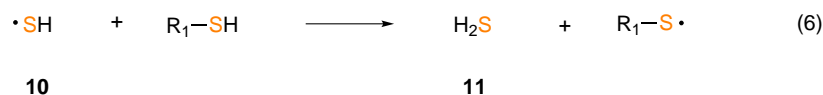
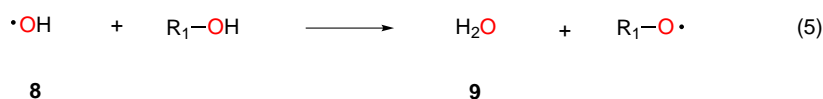


While it is convenient to interpret the RSE values derived from eqn. (1) as the result of stabilizing/destabilizing interactions between the unpaired spin and substituents $\text{R}_1\text{-R}_3$, this analysis ignores possible substituent effects in the closed-shell reference system $\text{H-C}(\text{R}_1\text{R}_2\text{R}_3)$.^[17;22-24] An alternative approach therefore defines radical stabilization energies with reference to a C-C bond cleavage (instead of C-H cleavage) process, as expressed by isodesmic eqn. (3). In this particular example methyl radical (**1**) formally abstracts a methyl group from isobutane (**5**), forming isopropyl radical (**4**) and ethane (**6**). Comparison of the defining eqns. (2) and (3) shows that only the closed shell reference compounds, not the open shell systems have been modified. The reaction energy for the example in eqn. (3) (and thus the RSE of radical **4**) now amounts to -6.5 kJ mol^{-1} , significantly less than that obtained from eqn. (2). Thus, while both approaches find the isopropyl radical (**4**) to be more stable than methyl radical (**1**), the actual degree of stabilization differs quite significantly.



A third way of quantifying the stability of isopropyl radical (**4**) is based on symmetric reference compound **7**. Cleavage of the fully apolar central C-C bond in **7** (due to symmetry) yields two isopropyl radicals (**4**). Comparison of this cleavage reaction with that of the central C-C bond in ethane (**6**) as expressed in eqn. (4) yields a reaction energy of $-23.9 \text{ kJ mol}^{-1}$. Due to the fact that eqn. (4) involves two methyl radicals (**1**) and two isopropyl radicals (**4**), the corresponding RSE value for radical **4** now equates to $-23.9/2 = -11.9 \text{ kJ mol}^{-1}$. This is quite similar to the result obtained from eqns. (3), but may also reflect some repulsive interactions between the two isopropyl fragments in the formal dimer **7**. While eqns. (3) and (4) are certainly more appropriate for the quantification of substituent effects on radical centers, the

approach described by eqns. (1) and (2) has the advantage of relating directly to an important elementary process in radical chemistry, the hydrogen transfer reaction between two radicals. These processes are of outstanding importance in synthetic as well as biological radical reactions and often involve hydrogen exchange between carbon- and heteroatom-centered radicals. The stabilities of these latter species can, of course, be defined in a completely analogous way as expressed for carbon-centered radicals in eqn. (1), and defining equations for oxygen- and sulfur-centered radicals are given in eqns. (5) and (6).



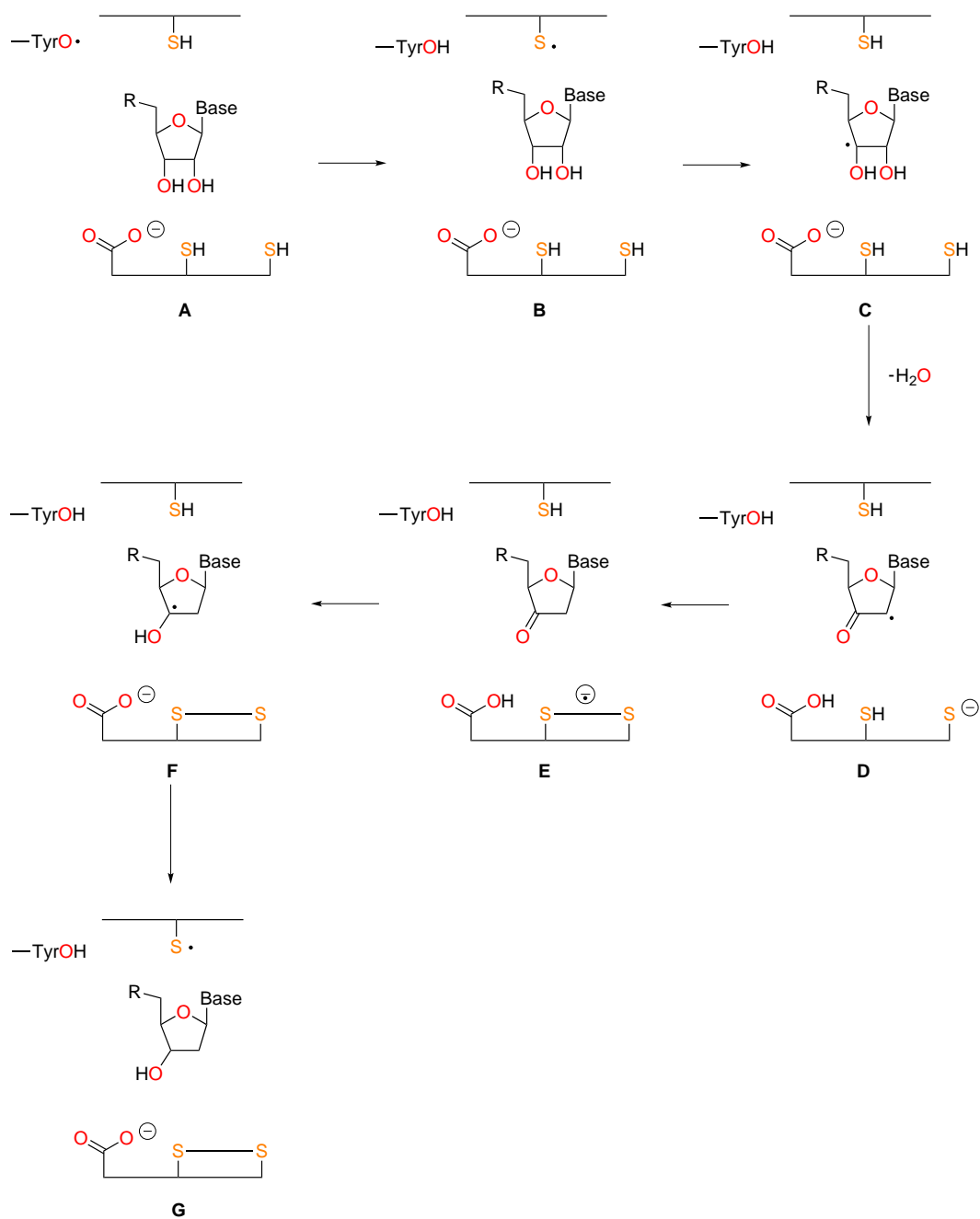
The radical stabilization energies of C-, O- and S-centered radicals are connected by the absolute X-H (X = C, O, S) bond dissociation energies. Using the experimental data for BDE(CH₃-H) = +439.3 ± 0.4 kJ mol⁻¹, BDE(HO-H) = +497.1 ± 0.3 kJ mol⁻¹, and BDE(HS-H) = +381.2 ± 0.1 kJ mol⁻¹, we thus are able to compare the stability of radicals with different centers in a pictorial manner for better understanding.

Application of radical stabilization energies in the example of RNR

In the case of RNR (Scheme 1.7), the reaction energies for the hydrogen transfer in the step **A** to **B**, **B** to **C**, **D** to **E** and **F** to **G** can be quantified easily using the data recollected from published work.^[5;17;18] The hydrogen transfer between tyrosyl radical and cysteine (**A/B**) can be modeled by *p*-me-phenoxy radical **12** and a dipeptide model for cysteinyl radical **13**. According to the RSE data (Figure 9.1)¹, the O-H and S-H bond strengths in **12** (+367.7 kJ mol⁻¹) and **13** (+366.8 kJ mol⁻¹) are very similar. Therefore the hydrogen transfer step between cysteinyl and tyrosyl radical is thermoneutral. Taking the fragment radical **14** and the cysteinyl radical **13** again for the step **B/C**, a relatively huge endothermicity (+31.7 kJ mol⁻¹) is observed, which is unusual for a reaction sequence that works under "normal" experimental condition.² The next hydrogen transfer step (**D/E**) occurs from cysteine to radical center at C2' of the ribose fragment. Taking 2-butanone-3-yl radical **15** as a model together with radical **13**, we obtain a reaction energy of -20.3 kJ mol⁻¹ for this step. Finally for the step **F/G**, the reaction energy can be assessed again with the same model as used for the step **B/C**. In contrast to the latter, the reaction energy is now inverted being exothermic by -31.7 kJ mol⁻¹.

¹RSE(**12**) = -129.4 kJ mol⁻¹, RSE(**13**) = -14.4 kJ mol⁻¹.

²For the discussion see ref. 17;25-28.



Scheme 1.7: Reduction of ribonucleic acid to 2'-deoxyribonucleic acid catalyzed by the enzyme ribonucleotide reductase in anaerobes. [6]

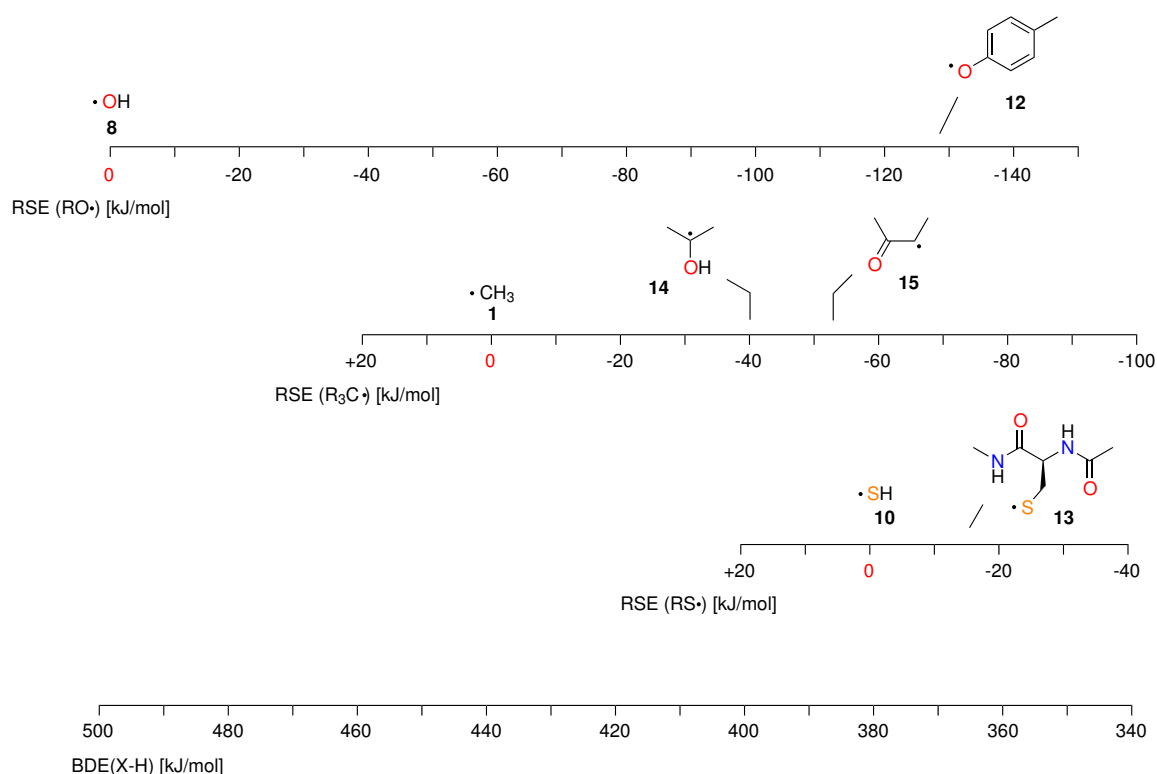
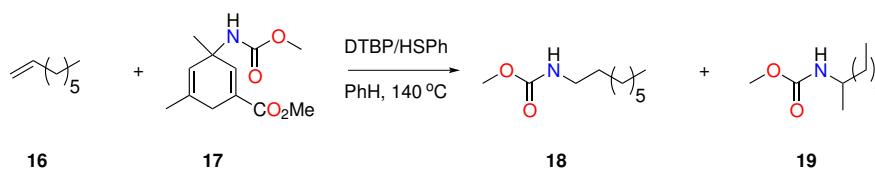


Figure 1.1: RSE data for radicals related to the RNR I substrate reaction in Scheme 1.1.

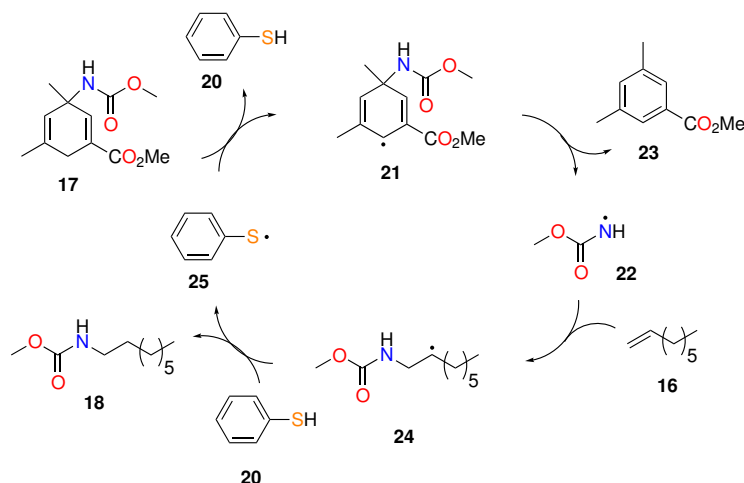
Application of radical stabilization energies in the example of polarity reversal catalysis (PRC)



Scheme 1.8: PRC as applied to the hydroamination of 1-octene (**16**).^[29]

Homolytic hydrogen transfer reactions can be accelerated considerably by tuning the polarity of the hydrogen atom donors and acceptors in an appropriate fashion. It is, for example, well known that electrophilic alkoxy radicals will abstract hydrogen from electron-rich C-H bonds faster than from electron-deficient substrates with comparable C-H bond energies. This insight has been developed into a general design concept for radical chain reactions commonly referred to as "polarity reversal catalysis (PRC)".^[30] While it is important to acknowledge that PRC builds on the concept of barrier reduction through lowering the intrinsic barriers for hydrogen transfer reactions, thermochemical criteria such as RSE data for the participating open shell species are nevertheless useful in defining the limits of this type of catalysis. A recent example for PRC catalysis involving combinations of different H-atom

donors is shown in Scheme 1.8.^[29;31] This involves the reaction of cyclohexadiene **17** acting not only as an organic H-atom donor, but also as a source of aminyl radicals. Both functions taken together allow for the hydroamination of unfunctionalized alkenes such as 1-octene (**16**), in this case yielding 50% of a 7 : 1 mixture of regioisomeric amides **18** and **19**. The reaction is initiated by 0.5 equiv. of di-*t*-butylperoxide (DTBP) in benzene solution, but proceeds significantly better in the presence of 0.2 equiv. thiophenol (HSPH, **20**). A reaction mechanism accounting for this finding is shown in Scheme 1.9.



Scheme 1.9: Radical chain reaction for the PRC example shown in Scheme 1.8.^[29]

Initial H-atom abstraction from cyclohexadiene **17** through peroxy radicals generated from DTBP yields radical **21** as one of the chain-carrying radicals in this system. Cyclohexadienyl radical **21** will eliminate aminyl radical **22** together with benzene derivative **23** through unimolecular C-N bond cleavage. Addition of aminyl radical **22** to 1-octene (**16**) can, in principle, proceed in anti-Markovnikov fashion to yield adduct radical **24** or in Markovnikov fashion yielding the regioisomeric adduct radical (not shown). Adduct radical **24** is converted to closed-shell product **18** through (fast) H-atom abstraction from thiophenol **20**, yielding thiyl radical **25** as the fourth chain-carrying radical in this system. Reaction of **25** with cyclohexadiene **17** then closes the catalytic cycle and regenerates the catalytic thiol **20**. The catalytic function of thiol **20** thus boils down to replacing one hydrogen transfer reaction between two carbon centers by two separate H-atom transfer steps between carbon and sulfur. The criteria for this type of catalysis can readily be visualized using radical stability scales for C- and S-centered radicals (Fig. 1.2). The H-S BDE in thiophenol (**20**) has recently been redetermined by Ashfold *et al.* through gas phase measurements at 0 K and a value of $\text{BDE}(\text{S-H}, \mathbf{20}, 0 \text{ K}) = +335.3 \pm 1.2 \text{ kJ mol}^{-1}$ has been derived.^[32] Combination of this value with that for the reference system H_2S (**11**) of $\text{BDE}(\text{S-H}, \mathbf{11}, 0 \text{ K}) = +376.2 \pm 0.1 \text{ kJ mol}^{-1}$ ^[33] yields $\text{RSE}(\mathbf{25}) = -40.9 \text{ kJ mol}^{-1}$ at 0 K.^[18] Using the (rather small) thermochemical corrections to 298.15 K used in the G3B3 scheme one can also predict a value of $\text{RSE}(\mathbf{25}) =$

$-40.8 \text{ kJ mol}^{-1}$ at 298.15 K. This implies that radical **25** is significantly more stable than aliphatic thiyl radicals such as methylthiyl radical (**26**) or cysteinyl radical **13**. Turning to the catalytic cycle shown in Scheme 1.9, the stability of radical **25** is relevant in two of the four steps. In the first of these, thiophenol (**20**) reacts with secondary radical **24**, whose stability may be assumed to be similar to that of isopropyl radical **4** or but-2-yl radical (**27**). Adopting the RSE data available for the latter of these systems at the G3 level of $\text{RSE}(\mathbf{27}) = -21.2 \text{ kJ mol}^{-1}$ implies a (highly favorable!) reaction energy of $-77.7 \text{ kJ mol}^{-1}$ for the hydrogen transfer between radical **24** and thiophenol **20**. The properties of cyclohexadiene **17** can be approximated with those of the parent cyclohexa-1,4-diene (**28**). The stability of the corresponding radical **29** of $\text{RSE}(\mathbf{29}) = -119.5 \text{ kJ mol}^{-1}$ at the G3 level is quite close to previous^[20] and more recent experimental and high-level theoretical studies.^[34] Assuming this value also to be valid for the more highly substituted cyclohexadiene radical **21** in Scheme 1.9 implies that the reaction of thiophenyl radical **25** with cyclohexadiene **17** is indeed exothermic by 20.6 kJ mol^{-1} . The art in designing and optimizing PRC reactions is thus connected to finding a thiol whose BDE(S-H) is located in-between that of the breaking C-H bond and that of the new C-H bond being made.

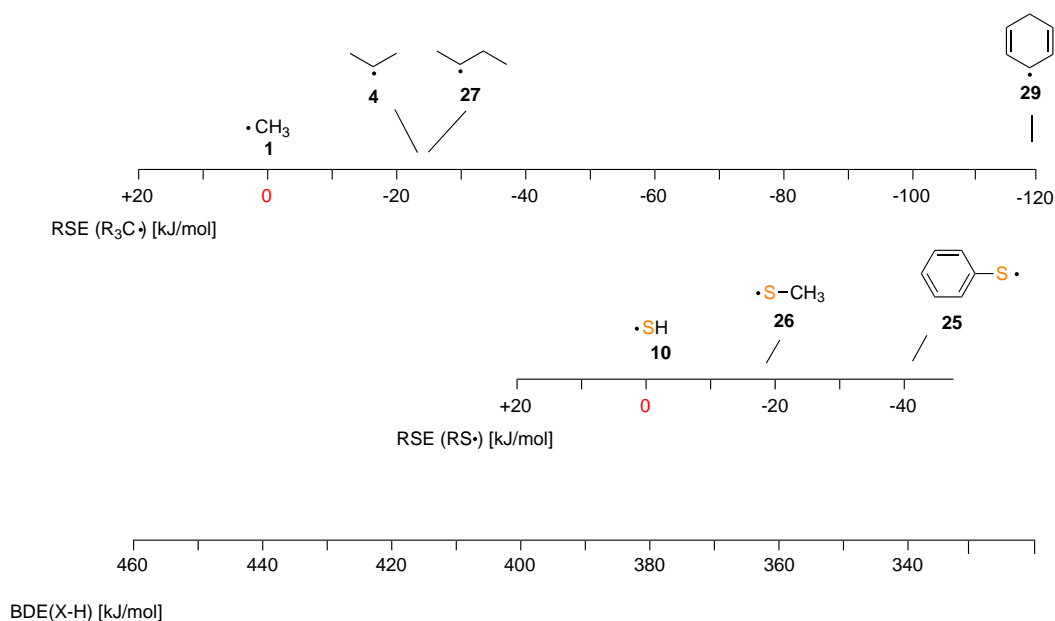


Figure 1.2: RSE data for radicals related to the reaction mechanism shown in Scheme 1.9.

Bibliography

- [1] S. Cuzzocrea, D. P. Riley, A. P. Caputi, and D. Salvemini. *Pharmacol. Rev.*, 53:135–159, 2001.

-
- [2] K. C. Cheng, D. S. Cahill, H. Kasai, S. Nishimura, and L. A. Loeb. *J. Biol. Chem.*, 267:166–172, 1992.
- [3] R. A. Floyd. *Free Radical Biology and Medicine*, 26(9-10):1346–1355, 1999.
- [4] N. R. Jena and P. C. Mishra. *J. Phys. Chem. B*, 109:14205–14218, 2005.
- [5] J. Hioe and H. Zipse. *Org. Biol. Chem.*, 8:3609–3617, 2010.
- [6] M. Bennati, F. Lendzian, M. Schmittl, and H. Zipse. *Biol. Chem.*, 386:1007–1022, 2005.
- [7] P. Nordlund and P. Reichard. *Annu. Rev. Biochem.*, 75:681–706, 2006.
- [8] J. Stubbe and W. A. van der Donk. *Chem. Rev.*, 98:705–762, 1998.
- [9] J. Stubbe, D. G. Nocera, C. S. Yee, and M. C. Y. Chang. *Chem. Rev.*, 103:2167–2201, 2003.
- [10] W. Kohn and L. J. Sham. *Phys. Rev.*, 140:A1133–A1138, 1965.
- [11] D. J. Henry, C. J. Parkinson, and L. Radom. *J. Phys. Chem. A*, 106:7927–7936, 2002.
- [12] D. J. Henry, M. B. Sullivan, and L. Radom. *J. Chem. Phys.*, 118:4849–4860, 2003.
- [13] L. A. Curtiss, P. C. Redfern, and K. Raghavachari. *J. Chem. Phys.*, 126:084108, 2007.
- [14] W. J. Hehre, R. Ditchfield, L. Radom, and J. A. Pople. *J. Am. Chem. Soc.*, 92:4796, 1970.
- [15] S. E. Wheeler, K. N. Houk, P. v. R. Schleyer, and W. D. Allen. *J. Am. Chem. Soc.*, 131:2547–2560, 2009.
- [16] H. Zipse. *Top. Curr. Chem.*, 263:163–189, 2006.
- [17] M. L. Coote, C. Y. Lin, and H. Zipse. *Carbon-Centered Free Radicals and Radicals Cations*, chapter "The Stability of Carbon-Centered Radicals", pages 83–104. M. D. E. Forbes (Ed.), John Wiley & Sons, 2010.
- [18] J. Hioe and H. Zipse. *Faraday Discuss.*, 145:301–313, 2010. and subsequent discussion, p. 381-409.
- [19] S. J. Blanksby and G. B. Ellison. *Acc. Chem. Res.*, 263:255–263, 2003.
- [20] Y.-R. Luo. *Comprehensive Handbook of Chemical Bond Energies*. CRC Press, 2007.
-

-
- [21] M. W. Jr. Chase. *NIST-JANAF Thermochemical Tables*. J. Phys. Chem. Ref. Data. Amer Inst of Physics, 4th edition, 1998.
- [22] A. A. Zavitsas. *J. Chem. Educ.*, 78:417–419, 2001.
- [23] N. Matsunaga, D. W. Rogers, and A. A. Zavitsas. *J. Org. Chem.*, 68:3158–3172, 2003.
- [24] A. A. Zavitsas. *J. Org. Chem.*, 73:9022–9026, 2008.
- [25] M. Mohr and H. Zipse. *Chem. Eur. J.*, 5:3046–3054, 1999.
- [26] H. Zipse. *Org. Biol. Chem.*, 1:692–699, 2003.
- [27] P. E. M. Siegbahn. *J. Am. Chem. Soc.*, 120:8417–8429, 1998.
- [28] V. Pelmenschikov, K.-B. Cho, and P. E. M. Siegbahn. *J. Comput. Chem.*, 25:311–321, 2004.
- [29] J. Guin, C. Mück-Lichtenfeld, S. Grimme, and A. Studer. *J. Am. Chem. Soc.*, 129:4498–4503, 2007.
- [30] B. P. Roberts. *Chem. Soc. Rev.*, 28:53–82, 1999.
- [31] A. F. Bella, L. V. Jackson, and J. C. Walton. *Org. Biomol. Chem.*, 2:421–428, 2004.
- [32] L. Devine, M. G. D. Nix, R. N. Dixon, and M. N. R. Ashfold. *J. Phys. Chem. A.*, 112:9563–9574, 2008.
- [33] R. C. Shiell, X. K. Hu, Q. J. Hu, and J. W. Hepburn. *J. Phys. Chem. A.*, 104:4339–4342, 2008.
- [34] Y. Gao, N. J. DeYonker, E. C. Garrett III, A. K. Wilson, T. R. Cundari, and P. Marshall. *J. Phys. Chem. A.*, 113:6955–6963, 2009.

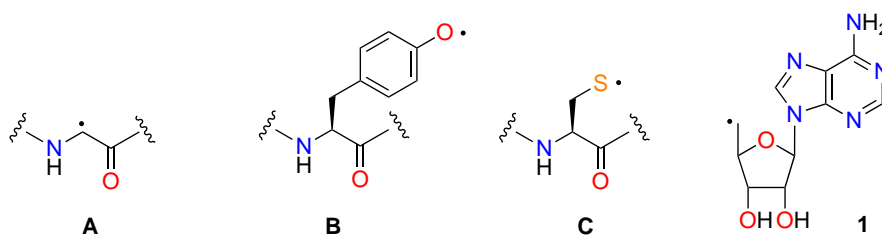
Chapter 2

Radicals in Enzymatic Catalysis - A Thermodynamic Perspective

Published in: J. Hioe, H. Zipse, *Faraday Disc.*, **2010**, *145*, 301-313.

2.1 Introduction

The use of open-shell intermediates represents one of the most daring and intriguing tools in enzymatic catalysis. A significant amount of structural data has been accumulated for these systems in the recent past, providing a detailed picture of the respective active sites and thus allowing for the reconstruction of the most likely reaction pathways under *in vivo* conditions. The most well known functional elements of radical enzymes are those in which open shell intermediates are generated directly at the protein backbone or at one of the side chain residues. In pyruvate formate lyase (PFL) and class I ribonucleotide reductase (RNR I), as two of the best-characterized radical enzymes,^[1-10] these include glycy radical **A**, tyrosyl radical **B** and cysteinyl radical **C** (Scheme 2.1). Radicals **A** also occur in other members of the "glycyl radical enzyme" (GRE) family such as benzylsuccinate synthase (Bss), 4-hydroxyphenylacetate decarboxylase (Hpd), or class III ribonucleotide reductase (RNR III).^[11] In addition to these protein-derived radicals, nature also employs a number of cofactor-derived radicals, C5'-desoxyadenosyl radical (**1**) being the most important representative of this class. Two completely independent pathways for the formation of **1** have evolved, the first one being the generation through thermally driven Co-C bond homolysis in vitamin B₁₂ (adenosylcobalamine, AdoCbl) and the second one being the redox-mediated generation from S-adenosylmethionine (SAM, AdoMet). Recent analyses of sequence databases have revealed that this latter class may be significantly larger than previously anticipated.^[1-7] Irrespective of its mode of generation, it is currently believed that the reaction of radical **1** with substrate molecules is an essentially homolytic hydrogen transfer process with favourable thermochemical driving force, yielding C5'-desoxyadenosine **1H** and a new substrate radical as the product. The substrates on which **1** acts vary widely and include proteins (as in the activating enzymes for pyruvate formate lyase (PFL) and class III ribonucleotide reductase),^[12;13] small molecules in biosynthetic pathways (as in biotin synthase (BioB)),^[14] intermediates of anaerobic fermentation pathways (as in the multitude of B₁₂-dependent carbon skeleton mutases),^[15] and damaged biopolymers (as in spore photoproduct lyase (SPL)).^[16-19] It is also noteworthy that the precursors to radical **1** act as catalytic cofactors with multiple turnovers in some of these transformations, while they are substrates (with single turnover) in others. Theoretical studies of the energy profiles of these processes have shown that the two steps of formation of **1** and of reaction with substrate molecules can be tightly coupled, thus avoiding unwanted side reactions of this highly reactive species.^[20-24] What led to the evolutionary selection of **A-C** and radical **1** as entries in the "radical toolbox" of enzymology is not immediately obvious on a structural basis alone, and we analyze here whether the thermodynamic stabilities of the protein- and the cofactor-derived radicals shown in Scheme 2.1 provide at least part of a rationalization.



Scheme 2.1: Structures of protein-derived glycylyl, tyrosyl, and cysteinyl radicals, and of cofactor derived C5'-adenosyl radical **1**.

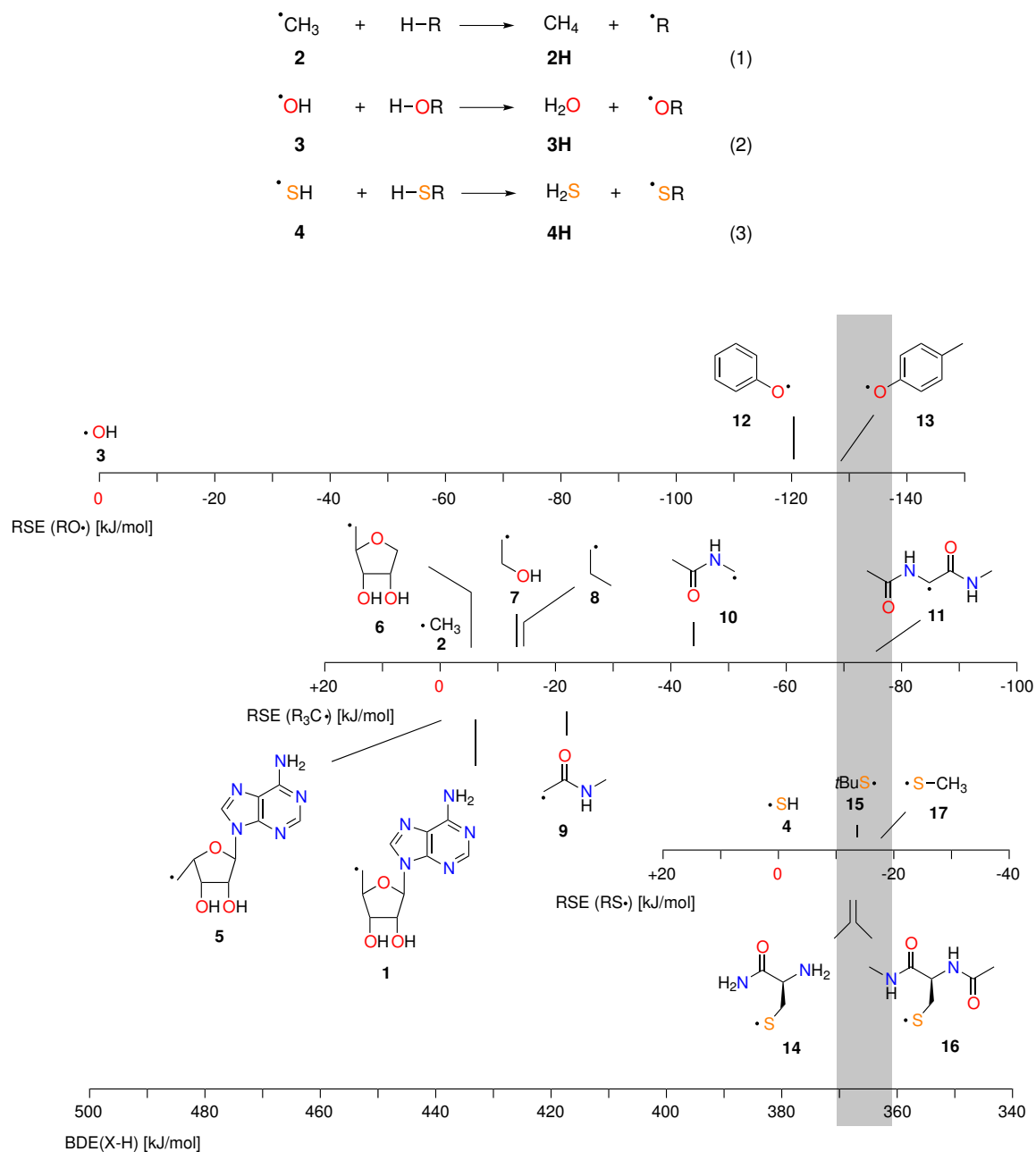
2.2 Computational Details

For the larger closed-shell systems the conformational space has been searched using the MM3 force field and the systematic search routine implemented in the TINKER program suite.^[25] The structures for radicals were then built from those of the respective closed-shell parents. All structures have then been reoptimized at the (U)B3LYP/6-31G(d) level of theory. Thermal corrections to enthalpies at 298.15 K have been calculated at this same level of theory using the rigid rotor / harmonic oscillator model and a scale factor of 0.9806. Refined energies have subsequently been obtained by single point calculations at the ROMP2/6-311+G(3df,2p) level of theory. Combination of these total energies with thermal corrections obtained at (U)B3LYP/6-31G(d) level yield the "ROMP2" enthalpies reported in Table 2.1. A second set of refined enthalpies was obtained using the G3(MP2)-RAD model developed by Radom *et al.*^[26;27] For selected systems enthalpies have also been calculated using the G3B3 compound method by Curtiss *et al.*^[28] A quantitative assessment of the predictive quality of these methods for thermochemical data by Radom *et al.* has documented a small advantage of G3B3 over the G3(MP2)-RAD procedure.^[26;27] The URCCSD(T) calculations required in the G3(MP2)-RAD method have been performed with the MOLPRO 2006.1 program package,^[29] and all other calculations have been performed using Gaussian 03, Revision D.01.^[30] All calculations have been performed in the gas phase.

2.3 Results

Radical stabilization energies (RSEs) have been calculated for C-, O-, and S-centred radicals as the reaction enthalpies at 298.15 K for isodesmic equations (1)-(3). These RSE values can be understood as the influence of the substitution pattern on the homolytic bond dissociation energies of the respective reference molecules CH₄, H₂O, and H₂S. When defined as given in eqns. (1)-(3), negative values imply a stabilizing effect of the substituents.^[31;32] Results for model systems for glycylyl, tyrosyl, and cysteinyl radicals have been collected in Table 2.1 together with those of closely related systems. In the following we restrict ourselves to the discussion of the best

data only (G3(MP2)-RAD or G3B3, if available). A graphical representation of these results is given in Scheme 2.2.



Scheme 2.2: Radical stabilization energies (RSE) of selected O-, C-, and S-centred radicals and bond dissociation energies (BDE) of the corresponding O-H, C-H, and S-H bonds.

The stability of C5'-adenosyl radical **1** (RSE= -6.8 kJ mol^{-1}) is closely similar to that of other primary alkyl radicals such as 2-hydroxyethyl radical (**7**) (RSE= $-13.3 \text{ kJ mol}^{-1}$) or *n*-propyl radical (**8**) (RSE= $-15.3 \text{ kJ mol}^{-1}$). Interaction of the adenine base located at the C1' position with the radical centre appears to play a limited role only in that the result obtained for the base-free model system **6** (RSE= -4.2

Table 2.1: Radical stabilization enthalpies (RSE, in kJ mol^{-1}) at 298.15 K of the systems shown in Scheme 2.2 and X-H bond dissociation energies of the respective closed shell compounds

System	ROMP2 ^a	G3(MP2)-RAD	G3B3	RSE exp. ^b	BDE(X-H) exp. ^b
•CH ₃ (2)	0.0	0.0	0.0	0.0	+439.3 ± 0.4
5	-0.7	-1.6	n.d. ^g		
6	-2.5	-3.9	-4.2		
1	-6.0	-6.8	n.d.		
•CH ₂ CH ₂ OH (7)	-9.6 ^c	-10.3 ^c	-13.3 ^c	-15.5	+423.8
•CH ₂ CH ₂ CH ₃ (8)	-11.5 ^c	-12.2 ^c	-15.3 ^c	-17.1	+422.2 ± 2.1
•CH ₂ C(O)NHCH ₃ (9)	n.d.	-23.0 ^c	n.d.		
•CH ₂ NHC(O)CH ₃ (10)	n.d.	-43.0 ^c	n.d.		
18	-42.8	-45.9	-47.3		
19	-56.1	-61.6	-60.2		
20	-78.8 ^c	-72.0 ^c	-70.5 ^c	-67.8	371.5 ± 1.7
11	-75.0	-74.1	-75.5		
•OH(3)	0.0	0.0	0.0	0.0	+497.1 ± 0.3
12	-149.2	-155.7	-121.6	-134.3 ^d (-125.6) ^e [-120] ^f	+362.8 ± 2.9 ^d (+371.5 ± 2.5) ^e [+377 ± 13] ^f
13	-154.7	-148.9	-129.4		
•SH(4)	0.0	0.0	0.0	0.0	+381.2 ± 0.1
14	-10.8	-11.9	-12.0		
•SC(CH ₃) ₃ (15)	-11.3	-12.1	-12.3	-18.9	+362.3 ± 9.2
16	-11.7	-13.7	-14.4		
•SCH ₃ (17)	-17.9	-18.1	-18.2	-15.5	+365.7 ± 2.1

^aData obtained at ROMP2/6-311+G(3df,2p)//UB3LYP/6-31G(d) level of theory.^bAll BDE data at 298.15 K taken from ref. 33, if no specified otherwise.^cTaken from ref. 32^dTaken from ref. 34^eTaken from ref. 35^fTaken from ref. 36^gn.d. = no data

kJ mol^{-1}) differs from that of **1** by only 2.6 kJ mol^{-1} . The magnitude of such an interaction can also be estimated by inversion of configuration at the C4' position as in **5**, positioning the adenine base and the radical centre on opposite sides of the connecting 5-membered ring system. The stability value for **5** is $\text{RSE} = -1.6 \text{ kJ mol}^{-1}$, a 5.2 kJ mol^{-1} difference to adenosyl radical **1**. Several cases are known in which radicals form tight complexes with π -systems and thus modify their reactivity in hydrogen abstraction reactions.^[37;38] However, the C5'-adenosyl radical **1** seems not to belong to this class of systems. Its rather moderate stability and its structure (Fig. 2.1) indicate that **1** can best be viewed as a primary alkyl radical with a large "handle" attached to it, facilitating the control of this species in an enzymatic catalysis context. The stability value calculated for **1** does, of course, not exclude that its generation from B₁₂ or SAM precursors bound to enzymes is aided by electrostatic interactions between the adenosine fragment and protein side chains.^[23;39] The gly-

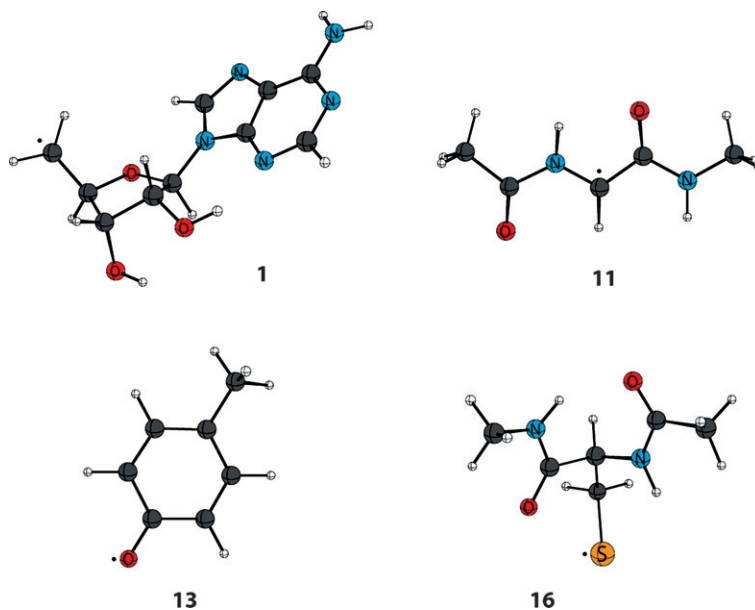


Figure 2.1: Structures of the preferred conformations of radicals **1**, **11**, **13**, and **16** as optimized at UB3LYP/6-31G(d) level of theory.

cyl radical **11** is significantly more stable than **1** with $RSE = -75.5 \text{ kJ mol}^{-1}$. This high stability arises due to the simultaneous presence of donor and acceptor substituents at the radical centre. The effect of the donor substituent alone as present in acetylaminoethyl radical **10** amounts to $RSE = -43.0 \text{ kJ mol}^{-1}$, while a single acceptor as in acetamide radical **9** leads to $RSE = -23.0 \text{ kJ mol}^{-1}$. If these two effects were additive, a combined $RSE = -66.0 \text{ kJ mol}^{-1}$ has to be expected. The actual value calculated for **11** is more negative by -9.5 kJ mol^{-1} , indicating a synergistic "push-pull" or "captodative" stabilization of this system.^[40–42] This value is somewhat smaller than calculated in previous studies of glycyl radical models, in which the C-terminal side of the glycyl systems were modelled by stronger acceptor substituents such as esters, acids or ketones.^[43–47] Previous studies of the stability of **11** at 0 K using a modified version of CBS-QB3 theory arrived at a value of $-13.3 \text{ kJ mol}^{-1}$ for the captodative stabilization of this system.^[48] Also, a recent theoretical study of glycine and glycine radical in aqueous solution indicates that solvent effects will have only a small effect on the captodative stabilization of this system.^[49] The effects of geometric distortion on radical stability may, in contrast, be quite substantial.^[50] The resonance interaction of donor and acceptor motifs described above is only fully effective in the extended conformation shown in Fig. 2.1, and any deviation from this planar structure will thus reduce the stability of the radical. The closed-shell parent system **11H**, in contrast, is characterized by two close-lying conformations, the (energetically most favourable) folded C_7 conformation and the extended C_5 conformation.^[51;52] This latter conformation of **11H** is located 4.2 kJ mol^{-1} higher in energy than the C_7 conformation at G3(MP2)-RAD level and is structurally quite similar to the extended conformation shown in Fig. 2.1 for radi-

cal **11**. A preference for this conformation in a fixed protein environment will thus change the stabilization energy of glycy radical **11** from -75.5 to -79.7 kJ mol $^{-1}$. The stability of phenoxy radical **12** and 4-methylphenoxy radical **13** (Scheme 2.2) has been referenced to that of $\bullet\text{OH}$ radical (**3**) as expressed in isodesmic equation (2). The results obtained for phenoxy radical **12** depend significantly more on the level of theory than those for C- or S-centred radicals. A comparison to experimental results is made difficult due to an ongoing debate on the correct gas-phase value for the O-H BDE in phenol (**12H**) itself. Earlier gas-phase measurements by DeTuri *et al.* predict $\text{BDE}(\text{O-H}) = 377 \pm 13$ kJ mol $^{-1}$, which, in combination with $\text{BDE}(\text{O-H}) = 497.1 \pm 0.3$ kJ mol $^{-1}$ for water, leads to $\text{RSE}(\mathbf{12}) = -120$ kJ mol $^{-1}$ with a significant error bar.^[36] Measurements by Kass *et al.* predict a somewhat lower O-H BDE value of 371.5 ± 2.5 kJ mol $^{-1}$ and thus $\text{RSE}(\mathbf{12}) = -125.6$ kJ mol $^{-1}$.^[35] A comparison of available gas- and solution-phase data, in combination with theoretical estimates, prompts Mulder *et al.* to propose an even lower O-H BDE of $+362.8 \pm 2.9$ kJ mol $^{-1}$, leading to $\text{RSE}(\mathbf{12}) = -134.3$ kJ mol $^{-1}$.^[34] The G3B3 value of $\text{RSE}(\mathbf{12}) = -121.6$ kJ mol $^{-1}$ obtained here is certainly more in support of the former two values than the latter. A slightly larger value of -124.7 ± 4.0 kJ mol $^{-1}$ has been derived from a combination of results obtained at G3, G3B3, and CBS-APNO level.^[53] Extrapolating CCSD energies to the basis set limit yields a value of -124.3 kJ mol $^{-1}$.^[54-56] Gas phase O-H BDE values for 4-methylphenol appear not to be available in the literature, but the stabilization of the phenoxy radical through introduction of the 4-CH $_3$ group as in **13** of 7.8 kJ mol $^{-1}$ (G3B3 value) is very close to that of 8.8 kJ mol $^{-1}$ derived from measurements in benzene solution for these two phenols.^[57] A slightly smaller value of 5.9 ± 4.5 kJ mol $^{-1}$ has been estimated by Richard *et al.* using a combination of experimental and theoretical data.^[58] The stability of the sulfur-centred radicals shown in Scheme 2.2 has been referenced to that of $\bullet\text{SH}$ radical (**4**) as expressed in isodesmic equation (3). The two models **14** and **16** used here for cysteinyl radicals have rather similar RSE values of -12.0 and -14.4 kJ mol $^{-1}$, respectively. These stabilities are rather similar to those of simple alkylthiyl radicals such as methylthiyl (**17**) or *t*-butylthiyl (**15**). It thus appears that the peptide functionality present in cysteinyl model systems **14** and **16** has only a limited effect on the properties of the radical centre itself.

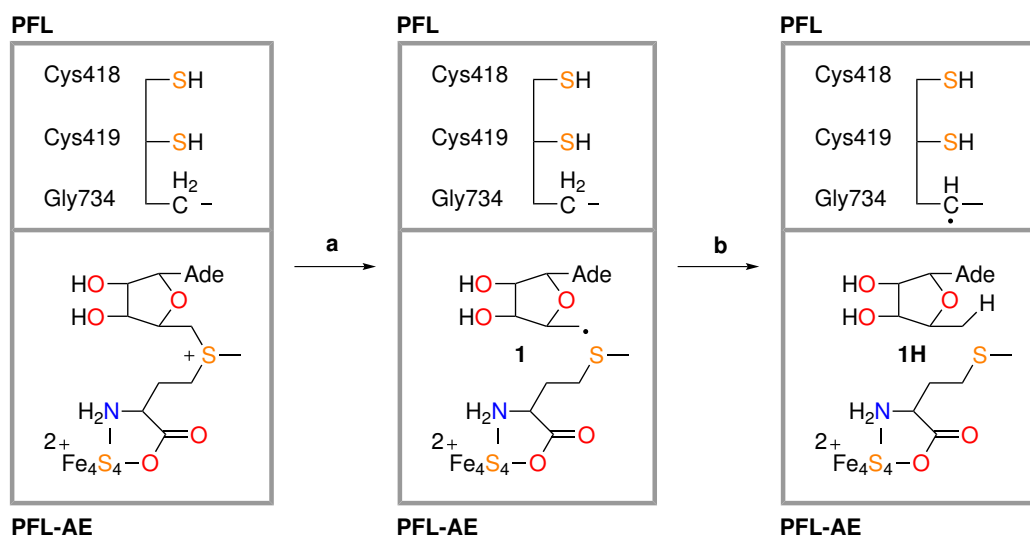
2.4 Discussion

The RSE values calculated for all C-, O- and S-centred radicals have been combined with the experimentally determined homolytic X-H bond dissociation energy (BDE) in the reference systems CH $_4$ (439.3 kJ mol $^{-1}$), H $_2$ O (497.1 kJ mol $^{-1}$) and H $_2$ S (381.2 kJ mol $^{-1}$) in order to allow for a comparison of the stabilities of all systems in Scheme 2.2. The zero point of the stability scale of O-centred radicals is located to the far left due to the high O-H BDE in water. The zero points of the scales for C-centred and S-centred radicals are shifted relative to the scale of O-centred radicals by 57.8 kJ mol $^{-1}$ and 115.9 kJ mol $^{-1}$, respectively, due to the much lower C-H and S-H BDE values in the reference compounds CH $_4$ and H $_2$ S. One major result of this comparison

is that the stabilities of radicals **13**, **11**, and **16** mimicking protein-derived tyrosyl, glycyl, and cysteinyl radicals are rather similar relative to each other. This implies that homolytic cleavage of the bonds leading to these radicals requires rather similar thermochemical effort with O-H BDE(**13H**) = +367.7 kJ mol⁻¹, C-H BDE(**11H**) = +363.8 kJ mol⁻¹, and S-H BDE(**16H**) = +366.8 kJ mol⁻¹ (indicated by the vertical grey bar in Scheme 2.2). The high stability of all three systems contrasts markedly with that of the cofactor-derived radical **1**, being 68.7 kJ mol⁻¹ less stable than glycyl radical **11**. This stability difference can also be expressed through the C-H BDE 432.5 kJ mol⁻¹ required to generate **1** from its closed shell parent **1H**. Despite the fact that the values derived here for small model systems will be modified in the full enzymatic system through interactions with adjacent functional groups, a general design criterion for radical enzymes thus emerges in that protein-bound radicals are of rather high stability from a thermochemical perspective, with only small differences between tyrosyl, glycyl, and cysteinyl radicals, while more reactive radicals are introduced through cofactors such as **1**. This large stability difference may also be the reason why protein-bound radicals, such as the glycyl radical in PFL, can be monitored for extended times (even hours) by EPR spectroscopy,^[59] while radical **1** is usually not detected under the conditions of enzymatic turnover. The thermodynamic data collected in Table 2.1 can be used in a straightforward manner for the validation of all enzyme-mediated reaction steps involving hydrogen atom transfer. This will in the following be illustrated for the proposed reaction mechanism of pyruvate formate lyase (PFL) and its activation through PFL activase (PFL-AE), and for the repair of thymidine dimers by spore photoproduct lyase (SPL).

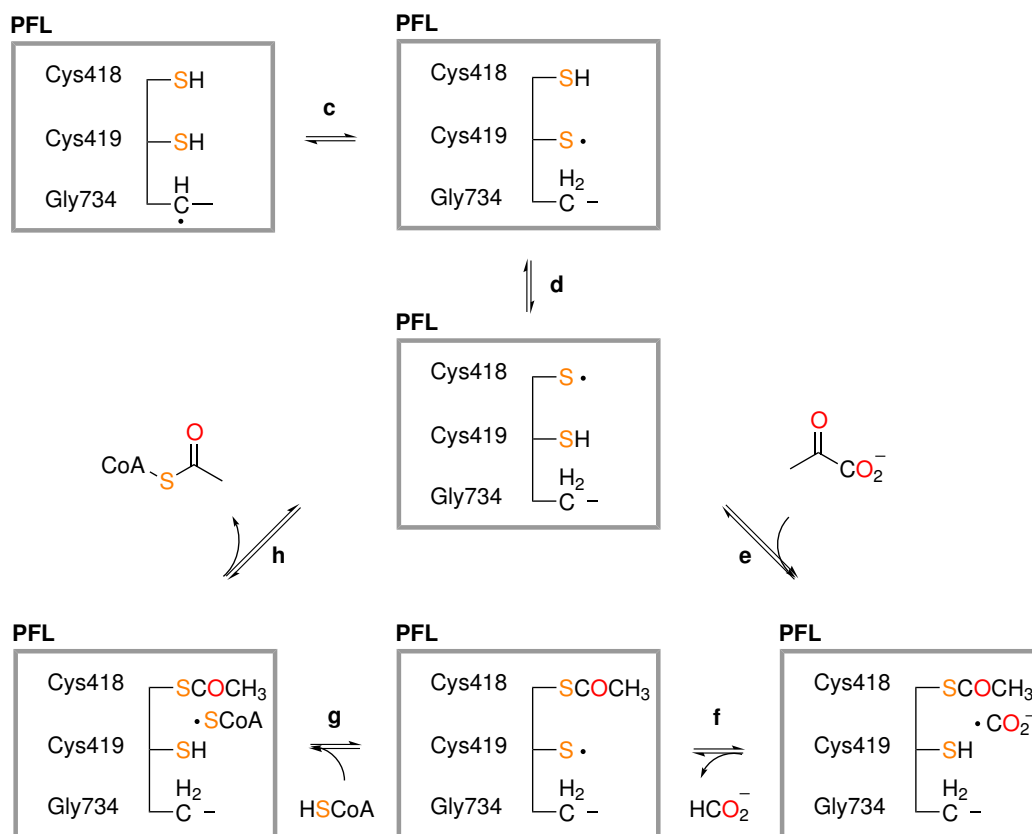
2.4.1 Enzymatic reaction mechanisms I: pyruvate formate lyase (PFL)

The essential steps for the PFL activation reaction are outlined in Scheme 2.3, starting from the complex of PFL and PFL-AE. Recent results from protein structure analyses suggest that the Gly734 residue in PFL is located close to the SAM cofactor in PFL-AE in this case.^[12] The first step of the activation process involves one-electron reduction of the Fe₄S₄²⁺ cluster in PFL-AE through flavodoxin and subsequent single electron transfer from the (reduced) Fe₄S₄¹⁺ cluster into the cationic C-S bond. This last step regenerates the oxidized Fe₄S₄²⁺ cluster and creates radical **1** in the enzyme binding pocket (Scheme 2.3). The lifetime of **1** generated under these conditions is expected to be quite limited due to its proximity to glycine residue Gly734. Hydrogen atom transfer between these two species is thus expected to be rapid, generating the glycyl radical in PFL and reduced radical **1H** as the final products of the activating step. The stability data for radicals **1** and **11** in Table 2.1 indicates that the last of these steps is exothermic by 68.7 kJ mol⁻¹. This rather favourable value will undoubtedly be modified by the differences in interactions between the radicals and their closed-shell parent systems with the protein environment, but it is hard to see how these changes can alter the intrinsically favourable



Scheme 2.3: Generation of the glycy radical in PFL at residue Gly734 through **a**: one-electron reduction of the $\text{Fe}_4\text{S}_4^{2+}$ cluster in PFL-AE and subsequent electron transfer into the C-S bond; and **b**: hydrogen atom transfer between C5'-adenosyl radical **1** and the glycine residue Gly734.

energetics of the hydrogen transfer step in a significant way. We may thus conclude that the energetics of the hydrogen transfer step leading to PFL activation will be quite favourable. The proposed substrate mechanism of PFL involves initial (and reversible) homolytic hydrogen atom transfer between glycine residue Gly734, and cysteine residues Cys418 and Cys419 (Scheme 2.4).^[59–65] Attack of the thiyl radical located at Cys418 on pyruvate bound in the active site then initiates cleavage of the substrate to yield formate radical anion and acetylated cysteine residue Cys418. The transient formate radical anion abstracts hydrogen from Cys419 in order to generate formate as the first product of the catalytic cycle. Binding of coenzyme A and hydrogen transfer to the cysteinyl radical at Cys419 then yields an open-shell CoA intermediate capable of abstracting the acetyl group from Cys418. This last step, together with removal of CoA-SAc from the binding pocket, completes the catalytic cycle of PFL. The thermochemical data in Table 2.1 can be used to assess the reaction enthalpy of the hydrogen transfer steps **c**, **d**, **f**, and **g** in this mechanism. Comparison of the stability of glycy radical **11** with that of cysteinyl radical **16** arrives, after consideration of the experimental X-H BDE differences in CH_4 and H_2S , at a reaction enthalpy for step **c** of the substrate mechanism of $+3.0 \text{ kJ mol}^{-1}$. Homolytic hydrogen transfer between two cysteinyl residues as in step **d** of the reaction mechanism will, of course, be thermoneutral. As long as the open and closed shell forms of the glycine and cysteine residues involved in these bond breaking/bond making processes interact with the surrounding protein in a comparable fashion, we may thus conclude that steps **c** and **d** in the PFL substrate mechanism are thermoneutral or, at most, weakly endothermic. Stability data for formate radical anion and thus the assessment of the thermochemistry of step **f** of the substrate mechanism are currently not available at G3 level. However, a recent compilation of radical stability data of



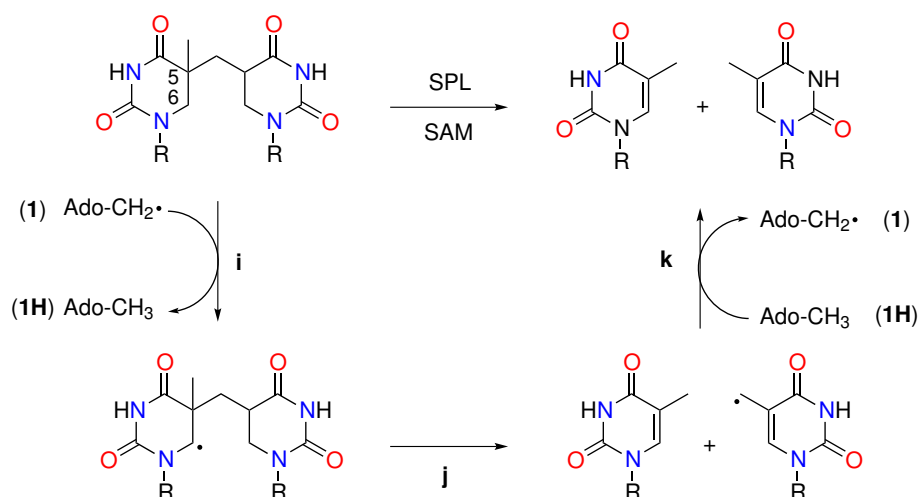
Scheme 2.4: The proposed substrate mechanism for PFL.

neutral radicals at G3(MP2)-RAD level lists the stability of the neutral formic acid radical $\bullet\text{CO}_2\text{H}$ as 14.2 kJ mol^{-1} relative to methyl radical **2**.^[32] Combination with the data for thiol radical (**16**) in Table 2.1 yields a reaction exothermicity of 58.3 kJ mol^{-1} for the hydrogen transfer between formic acid radical and cysteine model **16H**. Similarly, using the reaction of methylthiol (**17H**) with $\bullet\text{CO}_2\text{H}$ as a model for step **f**, Himo and Eriksson predict this hydrogen transfer step to be exothermic by 73.2 kJ mol^{-1} at the B3LYP/6-311+G(2d,2p)//B3LYP/6-311G(d,p) level.^[61;62] Using a much larger model for the enzyme binding site and formate radical anion coordinated to two guanidinium cations as the substrate model, Himo and Guo more recently estimate step **f** to be exothermic by 14.2 kJ mol^{-1} . These studies have been performed at the B3LYP/6-311+G(2d,2p)//B3LYP/6-31G(d,p) level including solvent effects through the COSMO continuum solvation model.^[64] Taken together all three theoretical approaches describe step **f** to be exothermic in nature, but also document how strongly the results for reactions of charge-separate substrates depend on details of the actual model systems. Finally, hydrogen transfer between the thiol terminus of coenzyme A and the cysteinyl radical at Cys419 as in step **g** can again be assumed to be intrinsically thermoneutral. For the substrate mechanism of PFL as well as the activation step involving PFL-AE we may thus conclude that all hydrogen transfer steps look good from a thermochemical perspective, being mostly

exothermic in nature or, at worst, mildly endothermic.

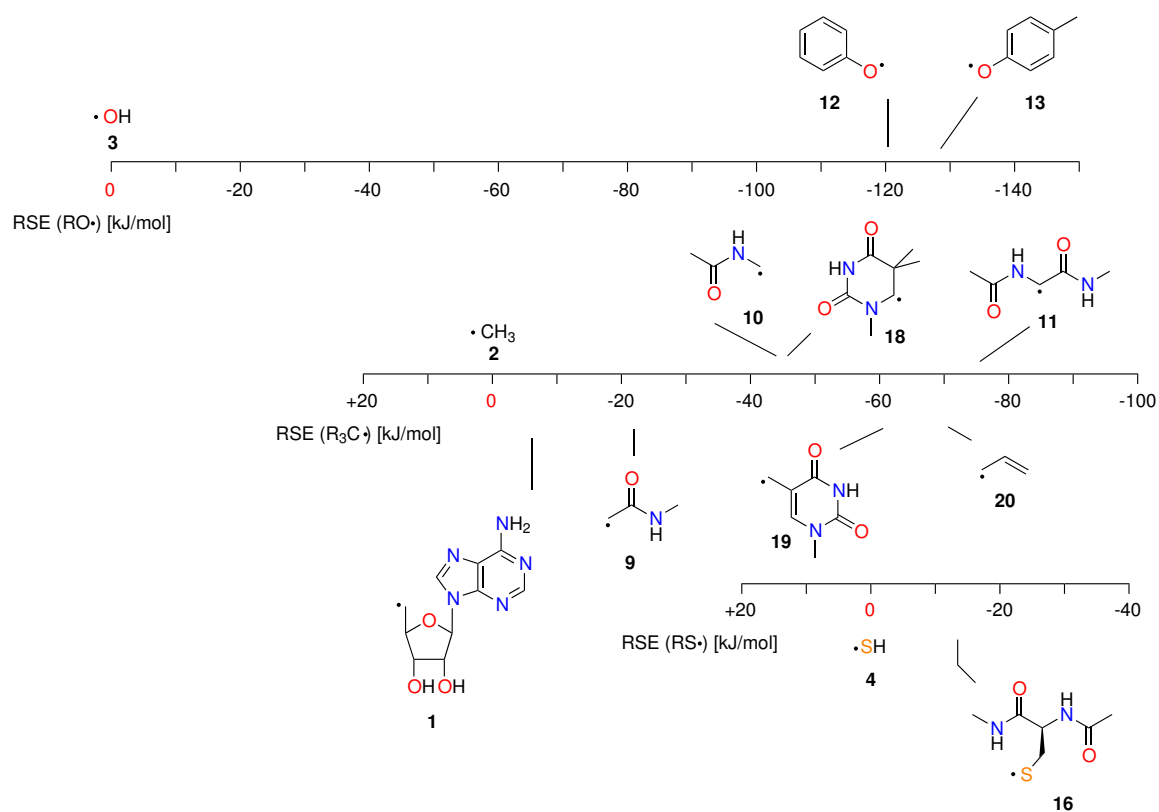
2.4.2 Enzymatic reaction mechanisms II: spore photoproduct lyase (SPL)

The essential steps for the SPL repair reaction of the thymidine photodimer as originally proposed by Mehl and Begley^[65] are shown in Scheme 2.5. These include redox-mediated generation of adenosyl radical **1** from the SAM cofactor and subsequent hydrogen abstraction from the C6 position of the spore photoproduct (step **i**). Cleavage of the C-C bond adjacent to the radical centre regenerates the first thymidine base together with a new allylic substrate radical (step **j**). Hydrogen transfer from the reduced cofactor **1H** to this product radical yields the second repaired thymidine base and regenerates adenosyl radical **1** (step **k**). Despite some recent



Scheme 2.5: The proposed substrate mechanism for SPL.

controversy over the stereochemistry of the photoproducts repaired by SPL at the C5 centre,^[16–19;66;67] this mechanism still stands as originally proposed. However, theoretical studies of this mechanism at the B3LYP/6-311+G(2d,2p)//B3LYP/6-31G(d) level by Himo *et al.* have shown that the last step **k** of this sequence is plagued by an unfavourable relative orientation of the reduced cofactor Ado-CH₃ and the product radical, and also by a rather unfavourable reaction energy.^[68] Using the thermochemical data in Table 2.1 we can assess the thermochemical viability of steps **i** and **k** of this mechanism with high accuracy. A graphical representation of the relevant data has also been compiled in Scheme 2.6. The stability of the first substrate radical shown in the mechanism in Scheme 2.5 can satisfactorily be modelled by that of radical **18** with $RSE(\mathbf{18}) = -47.3 \text{ kJ mol}^{-1}$. This value is only slightly larger than that obtained for radical **10** and thus quite typical for α -amide substituted radicals. Generation of **18** by hydrogen transfer from **18H** to adenosyl radical **1** is exothermic by 40.5 kJ mol^{-1} and thus perfectly feasible from a thermochemical point of view. The last step **k** in the repair mechanism in Scheme 2.5



Scheme 2.6: Radical stabilization energies (RSE) of O-, C-, and S-centred radicals relevant for the SPL-mediated repair of the thymidine photoproduct.

involves hydrogen transfer from reduced cofactor **1H** to the allylic product radical formed in the central repair step **j**. This allylic product radical can be represented satisfactorily by radical **19**, whose stability value amounts to $\text{RSE}(\mathbf{19}) = -60.2 \text{ kJ mol}^{-1}$. This value is somewhat lower than that of allyl radical **20** with $\text{RSE}(\mathbf{20}) = -70.5 \text{ kJ mol}^{-1}$, most likely due to the competition between allylic radical and vinylic amide resonance stabilization, but still significantly higher than that of the initial substrate radical **18**. This implies that step **k** of the catalytic cycle is significantly endothermic by 53.4 kJ mol^{-1} , a value closely similar to the 51.0 kJ mol^{-1} ($12.2 \text{ kcal mol}^{-1}$) obtained by Himo *et al.* on the basis of more economical DFT calculations.^[68] These results, if taken together with the data available for step **i** and **j**, make step **k** most certainly the slowest and thus the rate-limiting step of the catalytic cycle shown in Scheme 2.5. The endothermicity of this step may be reduced if formation of radical **1** is coupled to a second, thermochemically favourable process such as readdition of **1** to the methionine- $\text{Fe}_4\text{S}_4^{2+}$ cluster complex (the reverse of the initial generation process). However, the stability values for radicals **11**, **13**, and **16** in Scheme 2.6 show that the endothermic hydrogen abstraction from reduced cofactor **1H** competes with exothermic hydrogen abstraction from any close lying tyrosyl-OH-, cysteinyl-SH-, and backbone C(α)-H group. In case one of these thermochemically favourable processes wins over the endothermic regeneration of co-

factor radical **1**, the SAM cofactor will not act catalytically in substrate turnover as described in Scheme 2.5. The final product derived from SAM under these conditions is 5'-desoxyadenosine (**1H**), whose detection has been reported in some,^[19;66;69] but not all^[16;17] of the experimental studies on the SPL reaction mechanism. That allylic product radicals may be too stable to abstract hydrogen from 5'-desoxyadenosine in an efficient manner is actually not unique to the SPL mechanism in Scheme 2.5, but has been proposed earlier as an explanation for the suicide inhibition of lysine 2,3-aminomutase (2,3-LAM) by trans-4,5-dehydrolysine.^[70] Taken together, all arguments described above are not sufficient to unequivocally decide, whether SPL belongs into the class of radical enzymes using SAM as a cofactor (with multiple substrate turnovers per SAM and regeneration of radical **1** in the catalytic cycle) or whether SPL should be grouped with those enzymes using SAM as a cosubstrate (with single substrate turnover per SAM and no regeneration of radical **1** in the catalytic cycle). The radical stability data in Scheme 2.6 illustrate that a third alternative with multiple substrate turnovers per SAM, but no regeneration of radical **1** in the catalytic cycle, exists under the condition that glycy-, tyrosyl-, or thiy-radicals are also involved in substrate turnover. This could, for example, be realized by combining initial substrate activation by radical **1**, trapping of product radical by an active site residue, and subsequent multiple substrate turnovers by an active site radical. This is closely related to what is achieved in the PFL-AE/PFL combination, with the only difference that SAM-derived radical **1** directly activates the glycine-cysteine-cysteine triad and not the actual pyruvate substrate. The data presented in Scheme 2.6 are sufficient to make such a sequence plausible on thermochemical grounds. Whether such a sequence applies to SPL will, of course, ultimately be decided by the functional groups available in the active site.

2.5 Conclusion

On a generally applicable stability scale for open-shell intermediates, the protein-bound radicals derived from tyrosyl, cysteinyl, and glycy residues are of comparable (and high) stability. The cofactor-derived 5'-desoxyadenosyl radical **1** is significantly less stable (by ca. 70 kJ mol⁻¹) and thus closely similar to other primary alkyl radicals. The stability data can be used to assess the thermochemical effort connected to hydrogen transfer steps in enzymatic reaction mechanisms. Application of this concept to the currently proposed reaction mechanisms of PFL-AE/PFL and SPL have identified the regeneration of C5'-adenosyl radicals in the latter case as thermochemically stressful.

Acknowledgements

We thank the Deutsche Forschungsgemeinschaft for financial support through project DFG Zi 436/13-1 and the SFB 739.

Bibliography

- [1] H. J. Sofia, G. Chen, B. G. Hetzler, J. F. Reyes-Spindola, and N. E. Miller. *Nucleic Acids Res.*, 29:1097–1106, 2001.
- [2] P. A. Frey and S. J. Booker. *Adv. Protein Chem.*, 58:1–45, 2001.
- [3] J. Cheek and J. B. Broderick. *J. Biol. Inorg. Chem.*, 6:209–226, 2001.
- [4] P. A. Frey and O. T. Magnusson. *Chem. Rev.*, 103:2129–2148, 2003.
- [5] Y. Nicoleta and C. L. Drennan. *Nucleic Acids Res.*, 32:4015–4025, 2004.
- [6] E. N. G. Marsh, A. Patwardhan, and M. S. Huhta. *Bioorg. Chem.*, 32:326–340, 2004.
- [7] P. A. Frey, A. D. Hegeman, and F. J. Ruzicka. *Crit. Rev. Biochem. Mol. Biol.*, 43:63–68, 2008.
- [8] M. Bennati, F. Lenzian, M. Schmittel, and H. Zipse. *Biol. Chem.*, 386:1007–1022, 2005.
- [9] P. Nordlund and P. Reichard. *Annu. Rev. Biochem.*, 75:681–706, 2006.
- [10] J. Stubbe. *Curr. Opin. Chem. Biol.*, 7:183–188, 2003.
- [11] T. Selmer, A. J. Pierik, and J. Heider. *Biol. Chem.*, 386:981–988, 2005.
- [12] J. L. Vey, J. Yang, M. Li, W. E. Broderick, J. B. Broderick, and C. L. Drennan. *Proc. Natl. Acad. Sci. U. S. A.*, 105:16137–16141, 2008.
- [13] J. Tamarit, E. Mulliez, C. Meier, A. Trautwein, and M. Fontecave. *J. Biol. Chem.*, 274:31291–31296, 1999.
- [14] F. Berkovitch, Y. Nicolet, J. T. Wan, J. T. Jarrett, and C. L. Drennan. *Science*, 303:76–79, 2004.
- [15] R. Banerjee. *Chem. Rev.*, 103:2083–2094, 2003.
- [16] J. Cheek and J. B. Broderick. *J. Am. Chem. Soc.*, 124:2860–2861, 2002.
- [17] J. M. Buis, J. Cheek, E. Kalliri, and J. B. Broderick. *J. Biol. Chem.*, 281:25994–26003, 2006.
- [18] T. Chandra, S. C. Silver, E. Zilinskas, E. M. Shepard, W. E. Broderick, and J. B. Broderick. *J. Am. Chem. Soc.*, 131:2420–2421, 2009.
- [19] M. G. Friedel, O. Berteau, J. C. Pieck, M. Atta, S. Ollagnier de Choudens, M. Fontecave, and T. Carell. *Chem. Commun.*, pages 445–447, 2006.
- [20] T. Kamachi, T. Toraya, and K. Yoshizawa. *Chem. Eur. J.*, 13:7864–7873, 2007.

- [21] P. M. Kozlowski, T. Kamachi, T. Toraya, and K. Yoshizawa. *Angew. Chem. Int. Ed.*, 46:980–983, 2007.
- [22] J. Kuta, S. Patchkovskii, M. Z. Zgierski, and P. M. Kozlowski. *J. Comput. Chem.*, 27:1429–1437, 2006.
- [23] R. A. Kwiecień, I. V. Khavrutskii, D. G. Musaev, K. Morokuma, R. Banerjee, and P. Paneth. *J. Am. Chem. Soc.*, 128:1287–1292, 2006.
- [24] K. P. Jensen and U. Ryde. *J. Am. Chem. Soc.*, 127:9117–9128, 2005.
- [25] J. W. Ponder. Tinker 4.2, 2004. Washington University, St. Louis.
- [26] D. J. Henry, C. J. Parkinson, and L. Radom. *J. Phys. Chem. A*, 106:7927–7936, 2002.
- [27] D. J. Henry, M. B. Sullivan, and L. Radom. *J. Chem. Phys.*, 118:4849–4860, 2003.
- [28] A. G. Baboul, L. A. Curtiss, P. C. Redfern, and K. Raghavachari. *J. Chem. Phys.*, 110:7650–7657, 1999.
- [29] H.-J. Werner, P. J. Knowles, R. Lindh, F. R. Manby, M. Schütz, P. Celani, T. Korona, A. Mitrushenkov, G. Rauhut, T. B. Adler, R. D. Amos, A. Bernhardsson, A. Berning, D. L. Cooper, M. J. O. Deegan, A. J. Dobbyn, F. Eckert, E. Goll, C. Hampel, G. Hetzer, G. Knizia, T. Hrenar, C. Köppl, A. W. Lloyd, Y. Liu, R. A. Mata, A. J. May, S. J. McNicholas, W. Meyer, M. E. Mura, A. Nicklaß, P. Palmieri, K. Pflüger, R. Pitzer, M. Reiher, U. Schumann, H. Stoll, A. J. Stone, R. Tarroni, T. Thorsteinsson, M. Wang, and A. Wolf. MOLPRO, version 2006.1, *a package of ab initio programs*.
- [30] M. J. Frisch, G. W. Trucks, H. B. Schlegel, G. E. Scuseria, M. A. Robb, J. R. Cheeseman, J. A. Montgomery, Jr., T. Vreven, K. N. Kudin, J. C. Burant, J. M. Millam, S. S. Iyengar, J. Tomasi, V. Barone, B. Mennucci, M. Cossi, G. Scalmani, N. Rega, G. A. Petersson, H. Nakatsuji, M. Hada, M. Ehara, K. Toyota, R. Fukuda, J. Hasegawa, M. Ishida, T. Nakajima, Y. Honda, O. Kitao, H. Nakai, M. Klene, X. Li, J. E. Knox, H. P. Hratchian, J. B. Cross, V. Bakken, C. Adamo, J. Jaramillo, R. Gomperts, R. E. Stratmann, O. Yazyev, A. J. Austin, R. Cammi, C. Pomelli, J. Ochterski, P. Y. Ayala, K. Morokuma, G. A. Voth, P. Salvador, J. J. Dannenberg, V. G. Zakrzewski, S. Dapprich, A. D. Daniels, M. C. Strain, O. Farkas, D. K. Malick, A. D. Rabuck, K. Raghavachari, J. B. Foresman, J. V. Ortiz, Q. Cui, A. G. Baboul, S. Clifford, J. Cioslowski, B. B. Stefanov, G. Liu, A. Liashenko, P. Piskorz, I. Komaromi, R. L. Martin, D. J. Fox, T. Keith, M. A. Al-Laham, C. Y. Peng, A. Nanayakkara, M. Challacombe, P. M. W. Gill, B. G. Johnson, W. Chen, M. W. Wong, C. Gonzalez, and J. A. Pople, 2004. GAUSSIAN 03 (Revision D.01), Gaussian, Inc., Wallingford, CT.

- [31] H. Zipse. *Top. Curr. Chem.*, 263:163–189, 2006.
- [32] M. L. Coote, C. Y. Lin, and H. Zipse. *Carbon-Centered Free Radicals and Radicals Cations*, chapter "The Stability of Carbon-Centered Radicals", pages 83–104. M. D. E. Forbes (Ed.), John Wiley & Sons, 2010.
- [33] Y.-R. Luo. *Comprehensive Handbook of Chemical Bond Energies*. CRC Press, 2007.
- [34] P. Mulder, H.-G. Korth, D. A. Pratt, G. A. DiLabio, L. Valgimigli, G. F. Pedulli, and K. U. Ingold. *J. Phys. Chem. A*, 109:2647–2655, 2005.
- [35] D. R. Reed, M. C. Hare, A. Fattahi, G. Chung, M. S. Gordon, and S. R. Kass. *J. Am. Chem. Soc.*, 125:4643–4651, 2003.
- [36] V. F. DeTuri and K. M. Ervin. *Int. J. Mass Spectrom. Ion Processes*, 175:123–132, 1998.
- [37] K. U. Ingold, J. Lusztyk, and K. D. Raner. *Acc. Chem. Res.*, 23:219–225, 1990.
- [38] A. K. Croft and H. M. Howard-Jones. *Phys. Chem. Chem. Phys.*, 9:5649–5655, 2007.
- [39] N. Dölker, F. Maseras, and P. E. M. Siegbahn. *Chem. Phys. Lett.*, 386:174–178, 2004.
- [40] H. G. Viehe, R. Merenyi, L. Stella, and Z. Janousek. *Angew. Chem. Int. Ed. Engl.*, 18:917, 1979.
- [41] H. G. Viehe, Z. Janousek, R. Merenyi, and L. Stella. *Acc. Chem. Res.*, 18:148–154, 1985.
- [42] C. J. Easton. *Chem. Rev.*, 97:53–82, 1997.
- [43] A. K. Croft, C. J. Easton, and L. Radom. *J. Am. Chem. Soc.*, 125:4119–4124, 2003.
- [44] D. Yu, A. Rauk, and D. A. Armstrong. *J. Am. Chem. Soc.*, 117:1789–1796, 1995.
- [45] D. A. Armstrong, D. Yu, and A. Rauk. *Can. J. Chem.*, 74:1192–1199, 1996.
- [46] A. Rauk, D. Yu, and D. A. Armstrong. *J. Am. Chem. Soc.*, 119:208–217, 1997.
- [47] F. M. Welle, H.-D. Beckhaus, and C. Rüchardt. *J. Org. Chem.*, 62:552–558, 1997.
- [48] G. P. F. Wood, D. Moran, R. Jacob, and L. Radom. *J. Phys. Chem. A*, 109:6318–6325, 2005.

- [49] G. P. F. Wood, M. S. Gordon, L. Radom, and D. M. Smith. *J. Chem. Theory Comput.*, 4:1788–1794, 2008.
- [50] A. Rauk, D. Yu, J. Taylor, G. V. Shustov, D. A. Block, and D. A. Armstrong. *Biochemistry*, 38:9089–9096, 1999.
- [51] T. M. Watson and J. D. Hirst. *J. Phys. Chem. A*, 106:7858–7867, 2002.
- [52] G. V. Papamokos and I. N. Demetropoulos. *J. Phys. Chem. A*, 108:7291–7300, 2004.
- [53] G. da Silva, C. Chen, and J. W. Bozzelli. *Chem. Phys. Lett.*, 424:42–45, 2006.
- [54] B. J. C. Cabral and S. Canuto. *Chem. Phys. Lett.*, 406:300–305, 2005.
- [55] G. A. DiLabio and P. Mulder. *Chem. Phys. Lett.*, 417:566–569, 2006.
- [56] B. J. C. Cabral and S. Canuto. *Chem. Phys. Lett.*, 417:570–572, 2006.
- [57] M. Lucarini, P. Pedrielli, G. F. Pedulli, S. Cabiddu, and C. Fattuoni. *J. Org. Chem.*, 61:9259–9263, 1996.
- [58] L. S. Richard, C. E. S. Bernardes, H. P. Diogo, J. P. Leal, and M. E. Minas da Piedade. *J. Phys. Chem. A*, 111:8741–8748, 2007.
- [59] A. F. V. Wagner, M. Frey, F. A. Neugebauer, W. Schäfer, and J. Knappe. *Proc. Natl. Acad. Sci. U. S. A.*, 89:996–1000, 1992.
- [60] A. Becker and W. Kabsch. *J. Biol. Chem.*, 277:40036–40042, 2002.
- [61] F. Himo and L. A. Eriksson. *J. Am. Chem. Soc.*, 120:11449–11455, 1998. for a discussion of technical aspects of calculations on PFL model systems see ref [62].
- [62] K. Condic-Jurkic, V. T. Perchyonok, H. Zipse, and D. M. Smith. *J. Comput. Chem.*, 29:2425–2433, 2008.
- [63] C. V. Parast, K. K. Wong, S. A. Lewisch, and J. W. Kozarich. *Biochemistry*, 34:2393–2399, 1995.
- [64] J.-D. Guo and F. Himo. *J. Phys. Chem. B*, 108:15347–15354, 2004.
- [65] R. A. Mehl and T. P. Begley. *Org. Lett.*, 1:1065–1066, 1999.
- [66] J. C. Pieck, U. Hennecke, A. J. Pierik, M. G. Friedel, and T. Carell. *J. Biol. Chem.*, 281:36317–36326, 2006.
- [67] E. Bürckstümmer and T. Carell. *Chem. Commun*, pages 4037–4039, 2008.
- [68] J.-D. Guo, Y. Luo, and F. Himo. *J. Phys. Chem. B*, 107:11188–11192, 2003.

- [69] R. Rebeil and W. L. Nicholson. *Proc. Natl. Acad. Sci. U. S. A.*, 98:9038–9043, 2001.
- [70] W. Wu, S. Booker, K. W. Lieder, V. Bandarian, G. H. Reed, and P. A. Frey. *Biochemistry*, 39:9561–9570, 2000.

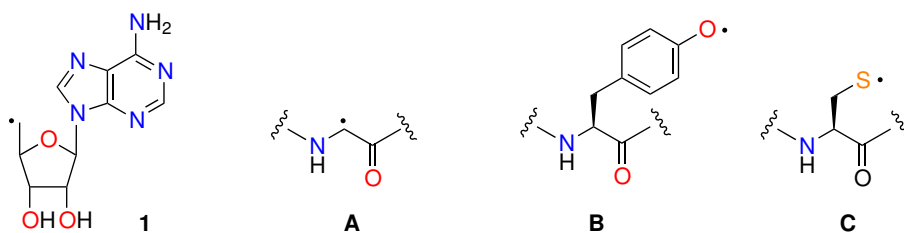
Chapter 3

The Stability of C_α-Peptide Radicals - Why Glycyl Radical Enzymes?

Published in: J. Hioe, G. Savasçı, H. Brandt, H. Zipse, *Chem. Eur. J.*, **2011**, *17*, 3781-3789.

3.1 Introduction

It is firmly established today that a large number of enzymes employ radicals and radical ions at some stage in their respective substrate reactions. The open-shell intermediates generated in this context may be grouped into three categories:^[1] 1) Substrate radicals such as the radical-ion intermediates in photolyases,^[2] 2) cofactor radicals such as the 5'-deoxy-5'-adenosyl radical **1** generated from coenzyme B₁₂ or S-adenosylmethionine (SAM),^[2-7] and 3) protein radicals generated either at the backbone or one of the side chain residues.^[3;4] Despite the multitude of possibilities for generating radicals at backbone and side-chain positions, there appear to be only three protein-derived radicals that are used in enzymatic catalysis. The most prominent of these is the glycy radical (**A**), the key residue in the "glycyl radical enzyme" (GRE) family (Scheme 3.1).^[3;4] Known reaction mechanisms in this class of enzymes also involve a second open-shell residue, the cysteinyl radical (**B**). Finally, the tyrosyl radical (**C**) is also known to play a role in a number of systems. A recent comparison of the respective C-H, S-H, and O-H bond dissociation energies (BDE) leading to radicals **A-C** found these to be remarkably similar at around +365±5 kJ mol⁻¹, whereas the C-H BDE leading to radical **1** is significantly higher at +433 kJ mol⁻¹.^[8] This finding implies that radicals **A-C** are all of similar (high) stability and that hydrogen transfer reactions between these residues will have practically no thermochemical driving force. This latter aspect touches on the fundamental

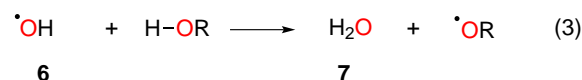
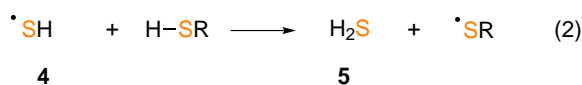
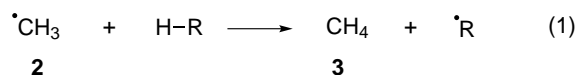


Scheme 3.1: Structures of 5'-deoxy-5'-adenosyl (**1**), glycy (**A**), cysteinyl (**B**), and tyrosyl (**C**) radicals.

question of how to design active sites for enzymes handling thermochemically (and kinetically) "hot" species such as radicals. A thermochemical design criterion may be formulated such that, on the protein side, only those species that are (due to their stability) not able to abstract hydrogen atoms from other residues in the active site in an exergonic fashion will be involved. That this criterion is fulfilled by glycy radical (**A**) is not immediately obvious as this system is the least substituted of all C $_{\alpha}$ -peptide radicals. In view of the known stabilizing influence of alkyl substituents on radical centers^[9-11] we may, for example, ask why there are no "alanyl radical enzymes" or why the C $_{\alpha}$ variants of radicals **B** and **C** are not more stable than **A**? To address this question we have studied the thermodynamic stability of dipeptide radicals derived from glycine, alanine, phenylalanine, tyrosine, cysteine, and proline. The term "dipeptide" refers in this context to systems composed of single amino acids with N- and C-terminal amide groups.

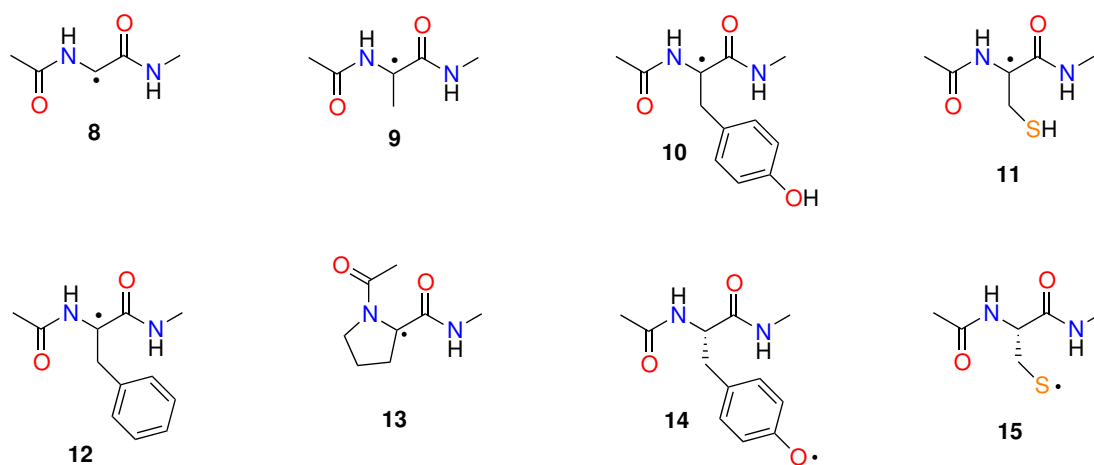
3.2 Results

The thermodynamic stabilities of C-, S-, and O-centered radicals have in recent studies been quantified by isodesmic reactions (1)-(3).^[8] By using these reactions the thermodynamic stabilities of C-, S-, and O-centered radicals can be expressed relative to that of the unsubstituted parent systems $\cdot\text{CH}_3$ (**2**), $\cdot\text{SH}$ (**4**), and $\cdot\text{OH}$ (**6**). These relative stabilities are often referred to as "radical stabilization energies" (RSE) and interpreted as the effects of substituents on the radical center. In combination with the experimentally determined^[12] bond dissociation energies (BDEs) of CH_4 (BDE(C-H)= +439.3 kJ mol⁻¹), H_2S (BDE(S-H)= +381.2 kJ mol⁻¹), and H_2O (BDE(O-H)= +497.1 kJ mol⁻¹), RSE values can be directly converted into the corresponding BDE values. The reaction energies for reactions (1)-(3) were calculated by using the G3B3^[13] method for smaller systems and the IMOMO(G3B3, G3(MP2)-RAD)^[10;14-16] method for larger systems. The accuracy of the G3B3 and G3(MP2)-RAD^[17;18] methods feeding into the IMOMO scheme in predicting radical stability has recently been compared for a larger set of radicals by Radom and co-workers and the accuracy was found to be slightly better for the G3B3 scheme (mean absolute deviation (MAD)= 3.2 kJ mol⁻¹) than for the G3(MP2)-RAD scheme (MAD = 5.1 kJ mol⁻¹).^[17;18] As illustrated for the thiyl radical **15** in Table 3.1, predictions made with the IMOMO(G3B3, G3(MP2)-RAD) approach are similar to those made at the G3B3 level. The following discussion is therefore based on G3B3 values for all small systems and IMOMO(G3B3, G3(MP2)-RAD) values for all larger systems. The glycy radical **A** is described here by using the N-acetyl-glycine-methylamide dipeptide model **8** (Scheme 3.2), the stability of which relative to the methyl radical (**2**) is RSE(**8**)= -75.5 kJ mol⁻¹ at the G3B3 level.^[8] This is a highly stabilized species due to push-pull (captodative)^[19-21] interactions between the donor and acceptor substituents connected to the formal radical center.^[9;22-24] In view of the highly stabilized nature of the glycy radical **8** the effects of additional



alkyl substituents, as in the alanyl dipeptide radical **9**, may be quite small, as is also found in other stabilized systems. The difference between a typical secondary radical such as the isopropyl radical (**16**) with RSE(**16**)= -23.7 kJ mol⁻¹ and a tertiary radical such as the *tert*-butyl radical (**17**) with RSE(**17**) = -29.8 kJ mol⁻¹, for example, amounts to only -6.1 kJ mol⁻¹ at the G3B3 level.^[10] By using experimentally measured thermochemical data the stability difference between **16** and **17** is slightly larger at (-10.1 \pm 2.9) kJ mol⁻¹ (Table 3.1). In more highly stabilized

systems the effects are significantly smaller. The stability of the α -methylbenzyl radical **18** with $\text{RSE}(\mathbf{18}) = -66.6 \text{ kJ mol}^{-1}$, for example, hardly differs from that of the α,α -dimethylbenzyl radical (**19**) with $\text{RSE}(\mathbf{19}) = -64.2 \text{ kJ mol}^{-1}$ at the G3B3 level. Determination of the stability of the alanyl radical **9** yields $\text{RSE}(\mathbf{9}) = -67.0 \text{ kJ mol}^{-1}$, 8.5 kJ mol^{-1} less than found for the glycyl radical **8**. This finding is in line with earlier results by Radom and co-workers for slightly smaller glycyl and alanyl peptide ester systems.^[22;23;25] Through comparison of model systems of different size, this earlier study concluded that the lower stability of the alanyl system is due to repulsive interactions between the added methyl group at the C $_{\alpha}$ position and the adjacent peptide bond.



Scheme 3.2: Structures of radicals **8-15** derived from glycine, alanine, tyrosine, cysteine, phenylalanine, and proline dipeptides.

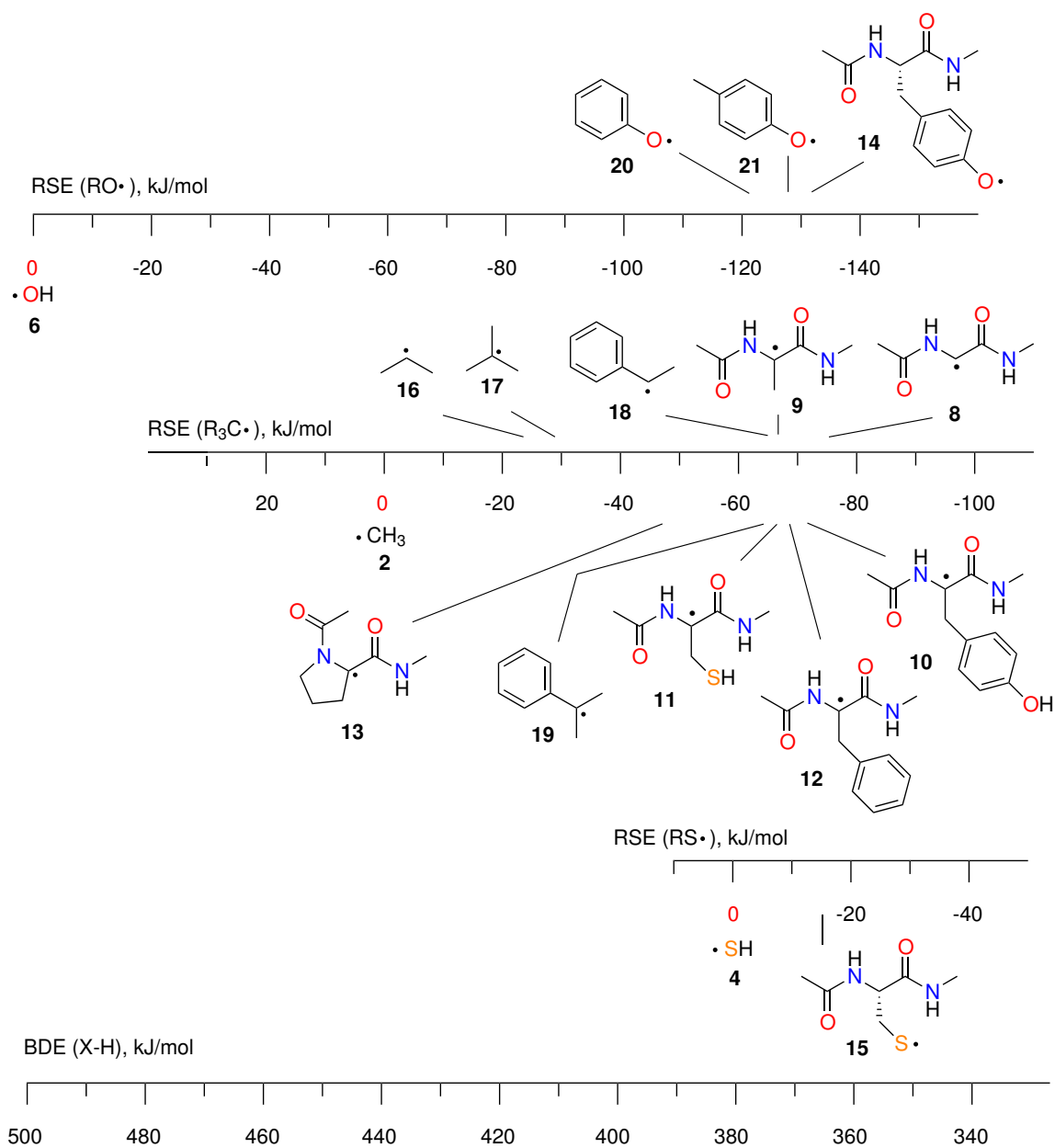


Figure 3.1: RSE and BDE data (in kJ mol⁻¹, from Table 3.1) for selected O-, C-, and S-centered radicals as obtained at the G3B3 (small systems) and IMOMO(G3B3,G3(MP2)-RAD) (large systems) levels of theory.

Table 3.1: Radical stabilization energies (RSEs) and, in part, bond dissociation energies (BDEs) derived from theoretically calculated and experimentally measured thermochemical data (in kJ mol⁻¹).

System	ROMP2 ^a	G3(MP2)-RAD	G3B3 or IMOMO ^b	RSE exp. ^c	BDE(X-H) exp. ^c
•CH ₃ (2)	0.0	0.0	0.0	0.0	+439.3 ± 0.4
•CH(CH ₃) ₂ (16)	-23.3 ^d	-23.0 ^e	-23.7(G3B3)	-28.8	+410.5 ± 2.9
•C(CH ₃) ₃ (17)	-28.3 ^d	-28.5 ^e	-29.8(G3B3)	-38.9	+400.4 ± 2.9
13	-42.6 ^f	-46.3	-47.8 (IMOMO)	n.a.	n.a.
•CH ₂ C ₆ H ₅ (23)		-61.0	-55.1(G3B3)	-69.0	+370.3 ± 6.3
11	-64.1 ^f	-64.7, ^f -64.8	-66.3(IMOMO)	n.a.	n.a.
9	-64.6 ^f	-64.8, ^f -65.5	-67.0(IMOMO)	n.a.	n.a.
18	-59.7[d]	-68.3 ^e	-66.6 (G3B3), -62.4(IMOMO)	-82.0	+357.3 ± 6.3
12	-66.4 ^f	-68.3, ^f -69.1	-68.6(IMOMO)	n.a.	n.a.
10	-66.6 ^f	-68.1, ^f -69.4	-70.6(IMOMO)	n.a.	n.a.
19	-62.1 ^d	-69.7 ^e	-64.2(G3B3), -63.8(IMOMO)	n.a.	n.a.
8	-75.0 ^f	-74.0, ^f -74.1	-75.5(G3B3) ^g	n.a.	n.a.
•OH (6)	0.0	0.0	0.0	0.0	+497.1 ± 0.3
14	-147.6 ^f	-151.0 ^f	-131.5(IMOMO)	n.a.	n.a.
20	-149.2	-155.7	-121.6(G3B3) ^g	-134.3	+362.8 ± 2.9
21	-154.7	-148.9	-129.4(G3B3) ^g	-136.9	+360.2 ± 2.1
•SH(4)	0.0	0.0	0.0	0.0	+381.2 ± 0.1
15	-11.7	-13.7	-14.4(G3B3) ^g , -13.8(IMOMO)	n.a.	n.a.
•SCH ₃ (22)	-17.9	-18.1	-18.2(G3B3)	-15.5	+365.7 ± 2.1

^aData obtained at ROMP2/6-311+G(3df,2p)//UB3LYP/6-31G(d) level of theory.

^bData obtained at the IMOMO(G3B3,G3(MP2)-RAD) level of theory.

^cAll BDE data at 298.15 K taken from ref. 12 unless specified otherwise.

^dTaken from ref. 9.

^eTaken from ref. 10.

^fBest conformer only.

^gTaken from ref. 8.

The stabilities of the other C $_{\alpha}$ dipeptide radicals **10**, **11**, and **12** shown in Scheme are quite similar to that of the alanyl system **9** (Table 3.1, Figure 3.1). It is only the C $_{\alpha}$ dipeptide radical **13** derived from proline that is significantly less stable than the acyclic peptide radicals with $\text{RSE}(\mathbf{13}) = -47.8 \text{ kJ mol}^{-1}$. This implies that of all the C $_{\alpha}$ dipeptide radicals studied here, it is indeed the least-substituted glycyl radical **8** that is most stable! Together with stability data for tyrosyl and cysteinyl radicals **14** and **15**, respectively, this confirms the previously formulated design criterion for the active sites of radical enzymes: Open-shell intermediates located at the protein cannot abstract hydrogen from other residues in an exergonic fashion.

Conformational space of C $_{\alpha}$ -peptide radicals:

The radical stability data collected in Table 3.1 are based on Boltzmann-averaged enthalpies for dipeptide radicals and their corresponding closed shell parent systems. The full conformational freedom implicated in this type of averaging procedure may not be available in the context of enzymatic catalysis when the open-shell peptide residues are part of a protein chain. The effects induced by conformational restrictions through the protein secondary and tertiary structures on the radical stabilization energy can be analyzed by the calculation of RSE values for radicals and closed-shell parent systems belonging to the same conformational subpopulation.^[26] Taking glycine as a first example, we note that glycine dipeptide radical **8** has distinctly different conformational preferences compared with its closed-shell parent system **8H** (Figure 3.2). The conformations of open- and closed-shell systems will be described in the following by using the Φ (C-N-C-C) and Ψ (N-C-C-N) backbone angles together with the established terminology for closed-shell peptide systems and the N- and C-terminal peptide bonds being either trans (t) or cis (c).^[27;28] All conformations within an energy window of 50 kJ mol^{-1} were characterized at the G3(MP2)-RAD level of theory (see appendix B), but only those located within 30 kJ mol^{-1} of the best conformer are discussed here.

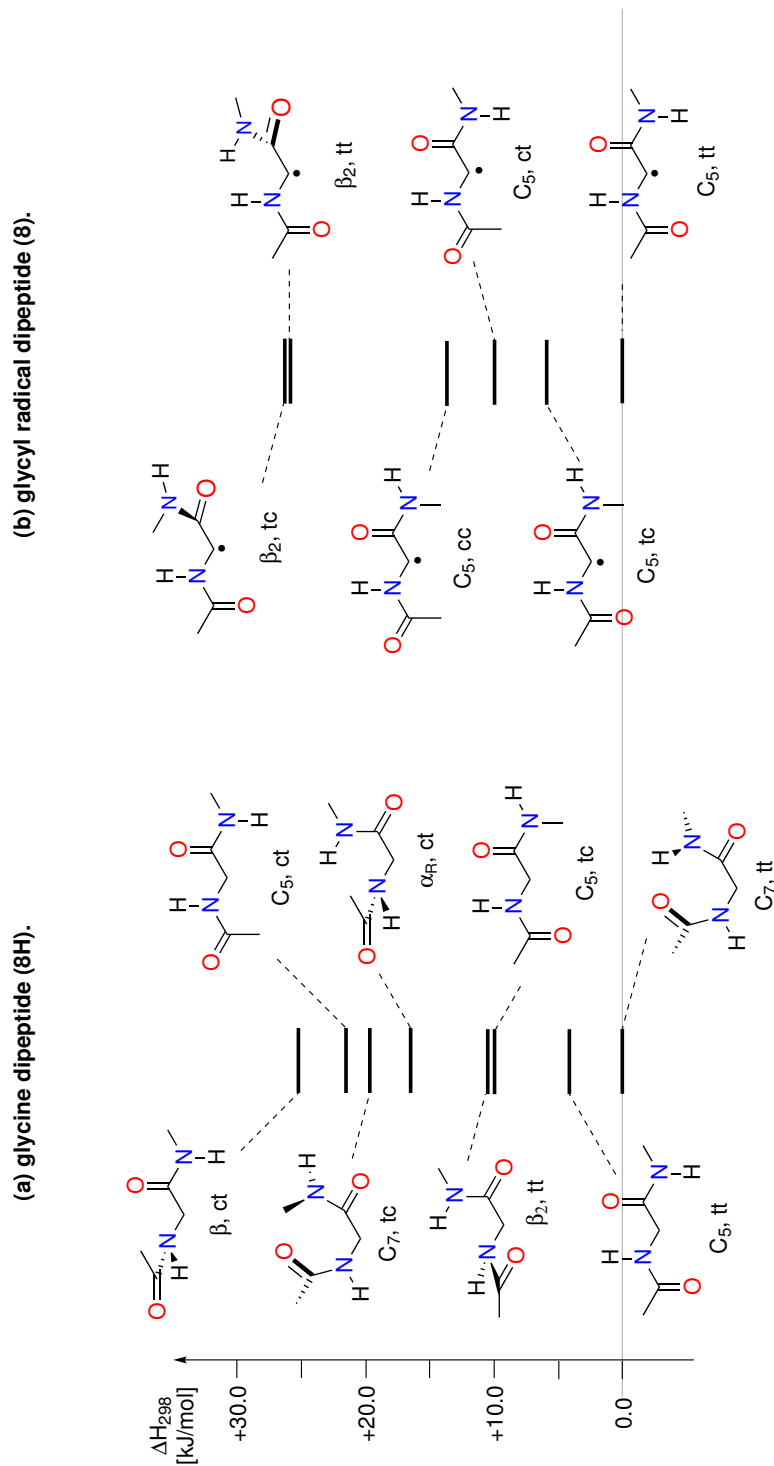


Figure 3.2: Relative enthalpies at 298 K for conformers of glycine dipeptide **8H** and the corresponding radical **8** as obtained at the G3(MP2)-RAD level of theory. All conformations within an energy window of 30 kJ mol $^{-1}$ are shown.

The glycine dipeptide system **8H** has been studied repeatedly before and is known to adopt the C $_7$ conformation preferentially (Figure 3.2a).^[29-34] In practically quantitative agreement with other recent high-level studies,^[32;33] the C $_5$ conformation is located 4.2 kJ mol $^{-1}$ higher, as determined at the G3(MP2)-RAD level, followed by the β_2 conformation at +11.5 kJ mol $^{-1}$. The cis peptide conformers are generally not considered to be competitive and thus are often excluded in conformational studies of peptides. We find here, however, that the most favorable of these conformations (C $_5$, tc) is energetically more stable than the β_2 conformation at +10.7 kJ mol $^{-1}$ and that the best conformation with two cis peptide bonds (β_2 , cc, not shown) is located +30.3 kJ mol $^{-1}$ above the global minimum C $_7$ structure. Other cis peptide conformations are significantly less stable, but still fall within the 50 kJ mol $^{-1}$ window considered in this study. For the radical **8** the most stable structure corresponds to the C $_5$ conformation with all the peptide bonds in the trans orientation. The C $_7$ and β_2 conformations of radical **8** are much less favorable at +31.4 (not shown) and +26.7 kJ mol $^{-1}$, respectively, due to less efficient orbital overlap between the radical center and the attached donor and acceptor units. Conformations with peptide bonds in the cis orientation are surprisingly stable at the radical stage and the most favorable of these structures (C $_5$, tc) is thus located only +6.0 kJ mol $^{-1}$ above the global minimum (Figure 3.2b). The conformational preferences noted for glycine dipeptide **8H** (the C $_7$ conformation being the most stable) and its radical **8** (the C $_5$ conformation being the most stable) also recur in a similar way in the other dipeptide systems studied here. The additional substituents present at the C $_{\alpha}$ position do, however, lead to steric effects in the C $_5$ conformation at the radical stage. This is exemplified by the alanine dipeptide **9H**, the smallest of the substituted systems, the conformational energies of which are displayed in Figure 3.3.

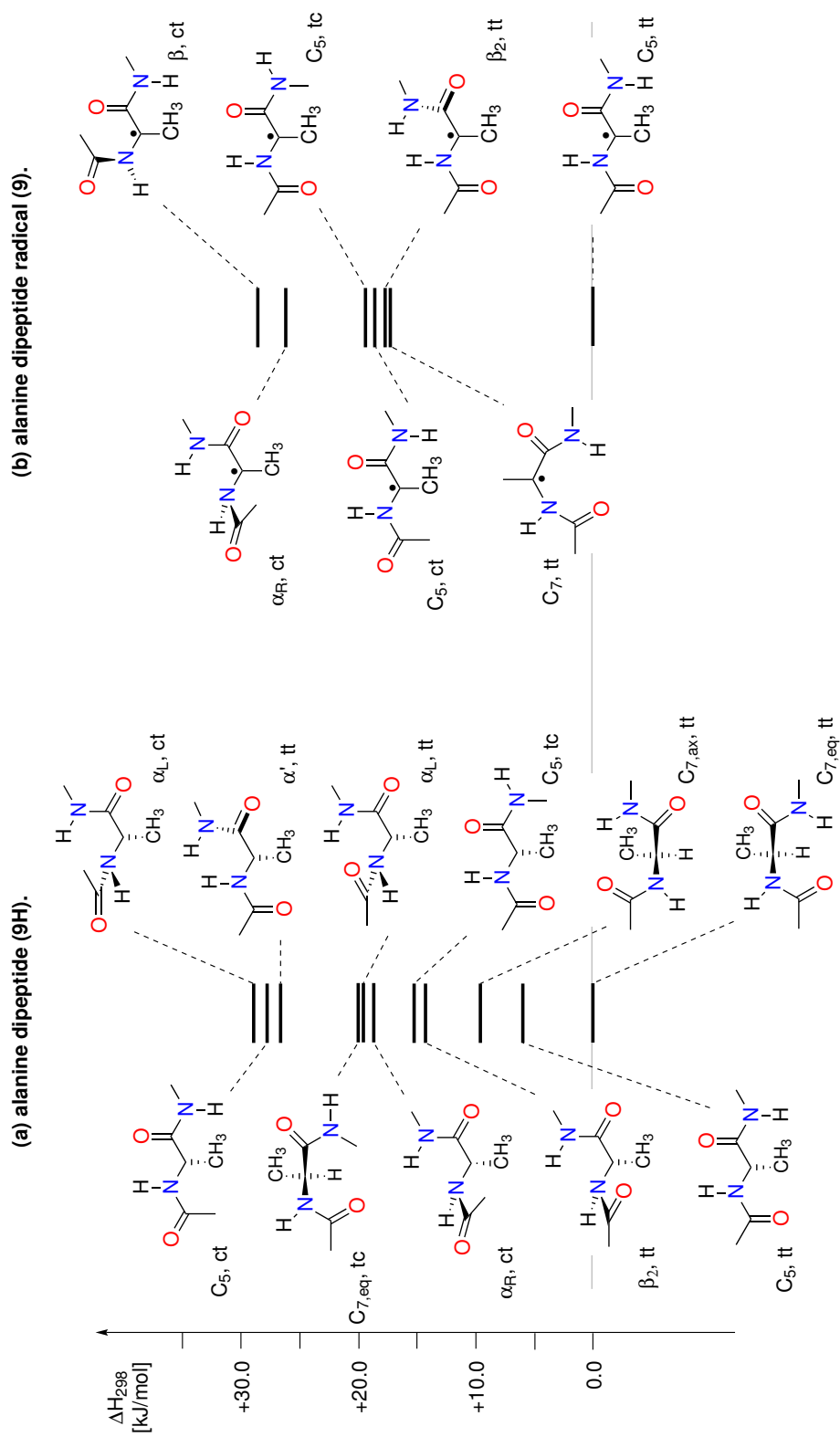
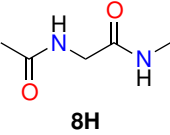
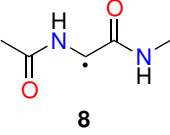
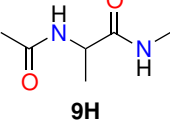
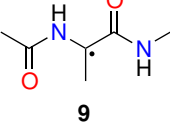
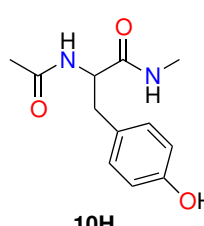
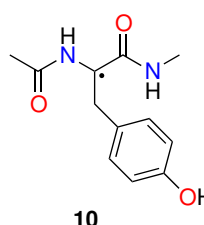
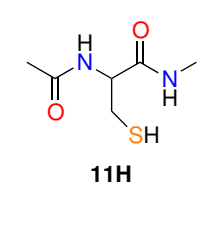
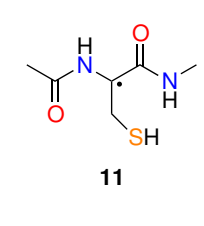
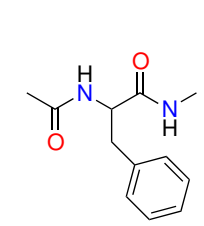
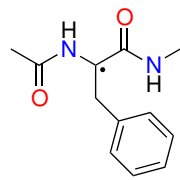
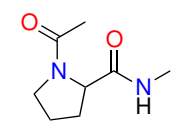
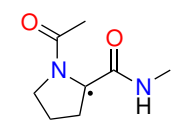


Figure 3.3: Relative enthalpies at 298 K for conformers of alanine dipeptide **9H** and the corresponding radical **9** as obtained at the G3(MP2)-RAD level of theory. All conformations within an energy window of 30 kJ mol⁻¹ are shown.

Table 3.2: Conformational enthalpies ($\Delta H_{298,\text{rel}}$) of dipeptide radicals and their corresponding closed-shell parent systems (G3(MP2)-RAD).

Systems	Backbone geometry	Φ [°]	Ψ [°]	Peptide bond conformations	$\Delta H_{298,\text{rel}}$ [kJ mol $^{-1}$]
 8H	C $_7$	-82.2	68.6	trans-trans	+0.0
	C $_5$	180.0	180.0	trans-trans	+4.2
	C $_5$	-179.9	-179.8	trans-cis	+10.7
	β_2	-122.7	21.8	trans-trans	+11.5
	α_R	-94.5	-1.7	cis-trans	+16.5
	C $_7$	-93.9	117.4	trans-cis	+19.6
	C $_5$	180.0	180.0	cis-trans	+23.7
	β	-74.9	-151.7	cis-trans	+27.0
 8	C $_5$	180.0	180.0	trans-trans	+0.0
	C $_5$	179.9	179.5	trans-cis	+6.0
	C $_5$	180.0	180.0	cis-trans	+10.3
	C $_5$	180.0	180.0	cis-cis	+13.6
	β_2	-176.4	14.9	trans-trans	+26.7
	β_2	-173.9	13.6	trans-cis	+27.4
 9H	C $_{7\text{eq.}}$	-82.9	72.9	trans-trans	+0.0
	C $_5$	-158.1	164.1	trans-trans	+6.1
	C $_{7\text{ax.}}$	72.8	-56.3	trans-trans	+9.8
	β_2	-126.7	20.9	trans-trans	+14.3
	C $_5$	-157.1	158.7	trans-cis	+15.8
	α_R	-94.1	-4.0	cis-trans	+18.8
	α_L	68.2	26.8	trans-trans	+19.5
	C $_{7\text{eq.}}$	-96.5	111.6	trans-cis	+20.4
	α'	-169.1	-39.3	trans-trans	+26.8
	C $_5$	-151.1	150.6	cis-trans	+27.8
	α_L	74.5	26.1	cis-trans	+29.0
 9	C $_5$	180.0	180.0	trans-trans	+0.0
	C $_7$	-31.9	6.5	trans-trans	+17.4
	β_2	-167.7	15.2	trans-trans	+17.7
	C $_5$	-170.6	177.1	cis-trans	+18.6
	C $_5$	-175.1	172.8	trans-cis	+19.3
	α_R	-62.5	-10.9	cis-trans	+26.2
	β	-37.2	168.4	cis-trans	+28.7

 <p>10H</p>	C ₅	-158.7	170.8	trans-trans	+0.0
	C _{7eq.}	-82.8	78.2	trans-trans	+2.8
	β_2	-122.4	19.5	trans-trans	+5.7
	C _{7ax.}	72.3	-54.9	trans-trans	+6.3
	C _{7eq.}	-108.0	7.4	cis-trans	+14.7
	C ₅	-155.5	162.0	trans-cis	+16.3
	α'	-174.6	-32.1	trans-trans	+18.0
	β_2	-133.2	15.1	cis-trans	+17.5
	C ₅	-133.5	142.7	cis-trans	+22.1
	β_2	-125.2	58.5	trans-cis	+22.8
	C _{7eq.}	-99.2	109.9	trans-cis	+24.2
	α_L	49.4	43.4	trans-trans	+25.6
	α_L	69.9	35.6	cis-trans	+28.3
 <p>10</p>	C ₅	-170.3	177.2	trans-trans	+0.0
	C ₇	40.6	-19.3	trans-trans	+14.6
	β_2	-165.0	17.7	trans-trans	+18.1
	C ₅	171.1	-178.4	cis-trans	+21.0
	C ₅	-171.6	172.4	trans-cis	+25.6
	α_R	-61.8	-14.6	cis-trans	+26.9
 <p>11H</p>	C _{7eq.}	-82.5	66.0	trans-trans	+0.0
	C ₅	-160.4	173.0	trans-trans	+8.7
	C _{7ax.}	75.6	-54.9	trans-trans	+18.6
	β_2	-131.9	25.8	trans-trans	+19.2
	β_2	-125.5	62.4	trans-cis	+23.4
	α_L	68.0	26.3	trans-trans	+23.7
	β_2	-126.3	19.4	cis-trans	+24.0
	C ₅	-155.5	133.4	trans-cis	+27.0
 <p>11</p>	C ₅	-168.3	172.2	trans-trans	+0.0
	C ₇	-38.7	16.6	trans-trans	+16.4
	C ₅	-178.0	173.2	trans-cis	+21.0
	β_2	-172.1	16.6	trans-trans	+23.4
	C ₅	-177.0	171.6	cis-trans	+26.8
 <p>12H</p>	C ₅	-159.0	170.8	trans-trans	+0.0
	C _{7eq.}	-82.8	78.8	trans-trans	+3.0
	β_2	-120.6	17.6	trans-trans	+5.7
	C _{7ax.}	76.2	-54.9	trans-trans	+5.8
	C ₅	-158.7	140.4	trans-cis	+11.0
	C _{7eq.}	-102.4	6.9	cis-trans	+14.5
	β_2	-132.3	15.2	cis-trans	+17.8
	C _{7eq.}	-99.7	110.1	trans-cis	+23.3
β_2	-125.2	57.2	trans-cis	+23.7	

	α'	-172.6	-33.5	trans-trans	+17.7
	α_L	49.0	44.1	trans-trans	+24.5
	α_L	69.5	35.4	cis-trans	+28.2
	α_R	-81.4	-27.6	cis-trans	+29.9
	C ₅	-171.7	177.3	trans-trans	+0.0
	C ₇	40.0	-18.2	trans-trans	+15.0
	β_2	-164.5	17.6	trans-trans	+18.3
	C ₅	170.8	-178.2	cis-trans	+21.0
	α_R	-62.5	-14.3	cis-trans	+26.9
	C ₅	175.0	177.4	trans-cis	+28.4
	C _{7eq.}	-84.0	71.0	trans-trans	+0.0
	α_R	-93.0	-1.8	cis-trans	+11.9
	β	-74.0	144.5	cis-trans	+23.9
	β	-76.9	123.9	trans-cis	+24.6
	C ₇	-26.4	2.2	trans-trans	+0.0
	β	-40.9	171.9	cis-trans	+4.3
	α_R	-54.8	-9.8	cis-trans	+8.4
	β	-41.5	167.3	cis-cis	+16.3

As already found for glycine dipeptide **8H**, the C₇ conformation is the most favorable for the alanine dipeptide **9H**. This is in line with the results obtained in a number of previous studies.^[28;31;33;35;36] The relative conformational energies calculated here at the G3(MP2)-RAD level are quite similar to those found previously at the MP2 level.^[28] We note again, however, that cis peptide conformations are energetically competitive with some of the α and β conformations. The energetically best cis peptide conformation (C₅, tc) is located 15.8 kJ mol⁻¹ above the global minimum. For radical **9** the C₅ conformation is again by far the most stable structure (Table 3.2). The cis peptide conformations derived from the C₅ conformer are now much less favorable than in the case of the glycine dipeptide radical **8** due to steric hindrance between the peptide substituents and the methyl substituent at C $_{\alpha}$. This leaves us with the C₇ conformation as the second best conformer in radical **9** at +17.4 kJ mol⁻¹ closely followed by the β_2 conformer at +17.7 kJ mol⁻¹. The only dipeptide radical with systematically different conformational preferences is the proline dipeptide radical **13** for which the C₅ conformation cannot be formed due to the presence of the pyrrolidine ring system. In this case the C₇ conformation is the most favorable for the proline dipeptide radical **13** as well as the parent dipeptide

13. The distinctly different conformational preferences of the dipeptide radicals and their corresponding closed-shell parent systems have dramatic consequences for the stability of peptide radicals of restricted conformational flexibility. The isodesmic reactions (1)-(3) used before for the calculation of RSE values can also be employed for systems of reduced conformational mobility under the condition that comparable conformations are selected on the radical and the non-radical side. The stability of radical **8** in its most stable conformation (C $_5$, tt), for example, can be calculated according to reaction (4). The RSE value obtained for the C $_5$, tt conformation (RSE(**8**, C $_5$, tt) = -78.2 kJ mol $^{-1}$) is quite similar to the Boltzmann-averaged value of RSE(**8**) = -74.1 kJ mol $^{-1}$ (G3(MP2)-RAD level) because the C $_5$, tt conformer is similarly favorable for radical **8** and its closed-shell parent **8H**. However, RSE calculations on other conformations of radical **8** yield rather different stability values (Table 3.3). On the low side this includes the C $_7$ conformation with RSE(**8**, C $_7$, tt) = -42.6 kJ mol $^{-1}$ whereas the largest RSE value is calculated for the C $_5$ conformation with both peptide bonds in the cis conformation with RSE(**8**, C $_5$, cc) = -90.7 kJ mol $^{-1}$ (Table 3.3).^[26]

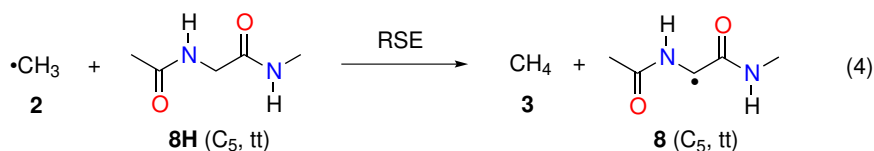
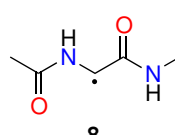
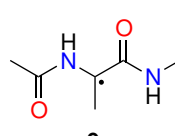
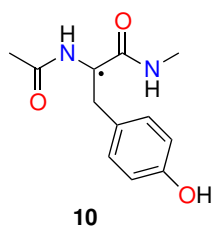
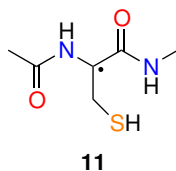


Table 3.3: RSE values of conformationally restricted dipeptide radicals (G3(MP2)-RAD).

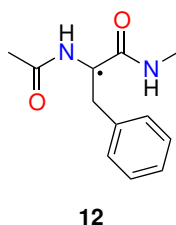
Systems	Backbone geometry	Peptide bond conformations	RSE [kJ mol $^{-1}$]
	C $_7$	trans-trans	-42.6
	α_R	cis-trans	-46.0
	β_2	trans-trans	-58.8
	β	cis-trans	-62.1
	β_2	cis-cis	-72.2
	C $_5$	trans-trans	-78.2
	C $_5$	trans-cis	-79.6
	C $_5$	cis-trans	-87.4
	C $_5$	cis-cis	-90.7
		C $_7$	trans-trans
α_R		cis-trans	-57.4
α_L		trans-cis	-59.4
α_R		trans-cis	-59.7
C $_5$		trans-cis	-61.3
β_2		trans-trans	-61.4
β_2		cis-cis	-63.7
C $_5$		cis-cis	-64.9
α_R		cis-cis	-65.1
α_L		cis-trans	-67.5
α_L		cis-cis	-68.7
C $_5$		trans-trans	-70.9



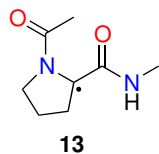
α'	trans-trans	-73.9
C ₅	cis-trans	-73.9
α'	trans-cis	-77.8
β_2	trans-trans	-55.7
C ₇	trans-trans	-56.3
β_2	trans-cis	-57.9
C ₅	trans-cis	-59.3
α_L	trans-cis	-59.4
β_2	cis-cis	-63.5
C ₅	cis-cis	-66.1
α'	trans-trans	-68.0
C ₅	trans-trans	-68.1
α_L	cis-cis	-69.4
α_L	cis-trans	-69.5
C ₅	cis-trans	-70.4
α_R	cis-cis	-70.6
α_R	cis-trans	-71.4
α_R	trans-cis	-72.5
α'	trans-cis	-84.2



C ₇	trans-trans	-48.3
β_2	cis-trans	-56.4
C ₅	cis-cis	-57.0
β_2	trans-trans	-60.5
β_2	cis-cis	-62.5
α_L	trans-cis	-66.0
α_L	cis-trans	-69.2
C ₅	trans-cis	-70.7
α'	trans-trans	-71.4
C ₅	cis-trans	-72.9
C ₅	trans-trans	-73.4
α_L	cis-cis	-73.6
α_R	trans-cis	-75.2
α_R	cis-trans	-77.0
α_R	cis-cis	-77.2
β_2	trans-cis	-81.4
α'	trans-cis	-83.5
α'	cis-trans	-86.2



C ₅	trans-cis	-50.9
β_2	trans-trans	-55.8
C ₇	trans-trans	-56.3
α_L	trans-cis	-57.3
C ₅	cis-cis	-58.5
β_2	trans-cis	-58.5
β_2	cis-cis	-64.3
α'	trans-trans	-67.7
C ₅	trans-trans	-68.3
α_L	cis-trans	-69.6
α_L	cis-cis	-70.2
α_R	cis-cis	-71.0
α_R	cis-trans	-71.3



α_R	trans-cis	-71.4
C_5	cis-trans	-77.5
α'	trans-cis	-82.9
β	trans-cis	-39.1
C_7	trans-trans	-46.3
α_R	cis-trans	-49.8
β	cis-cis	-63.8
β	cis-trans	-65.9

RSE values for conformationally restricted dipeptide radicals can be calculated in an analogous fashion for all other systems shown in Scheme 3.2. In all cases it is found that the RSE values vary significantly with the selected peptide conformation (Table 3.3). The C_7 conformations are typically of low stability (strong C $_{\alpha}$ -H bonds) whereas higher stabilities (weak C $_{\alpha}$ -H bonds) are found for the C_5 conformation. In practice this means that the stability values of peptide radicals cover a certain range and are a function of the accessible conformational space, as graphically displayed in Figure 3.4. The large dependence of radical stability on the selected conformations may be seen as a technical complication in RSE calculations because accurate values can only be obtained after covering the complete conformational space of radicals and non-radicals. However, the more important implication of the conformational dependence of RSE values is that radical enzymes can tune the stability of radicals located at the protein backbone (and thus the strength of the corresponding C-H bonds) through conformational control at the spin-carrying site. Of all the dipeptide radicals shown in Figure 3.4 it is the glycine dipeptide radical **8** that shows the largest dispersion of RSE values (ranging from -42.6 to -90.7 kJ mol $^{-1}$). This is similar to the range of 44.7 kJ mol $^{-1}$ for C-H BDE values estimated for selected glycine dipeptides in a recent study on the potential for oxidative damage to peptides.^[37] Use of the glycine residue as one of the spin-carrying sites in radical enzymes may thus be motivated by both the high absolute stability of the corresponding dipeptide radical as well as the ability to tune this stability over a wide range of energies.^[8] Structural effects of C $_{\alpha}$ substituents: The influence of C $_{\alpha}$ substituents on radical stability was in the previous paragraph attributed to steric effects. These steric effects are also responsible for characteristic changes in the three-dimensional structures of the dipeptide radicals. This will be exemplified again by using the glycine dipeptide **8H** and its radical **8** as unstrained reference systems. The energetically most favorable conformations of these two systems are shown in Figure 3.5 together with those for alanine dipeptide **9H** and the alanyl radical **9**. The two closed-shell dipeptide systems **8H** and **9H** both prefer a C_7 conformation with both peptide bonds in a trans orientation. As can be inferred from the length of the internal hydrogen bond (204 pm) as well as the largely similar OCN and CNC angles on the N-terminal side it is clear that introduction of the methyl group into **9H** does not lead to significant distortions in the dipeptide structure. This is quite different to the corresponding

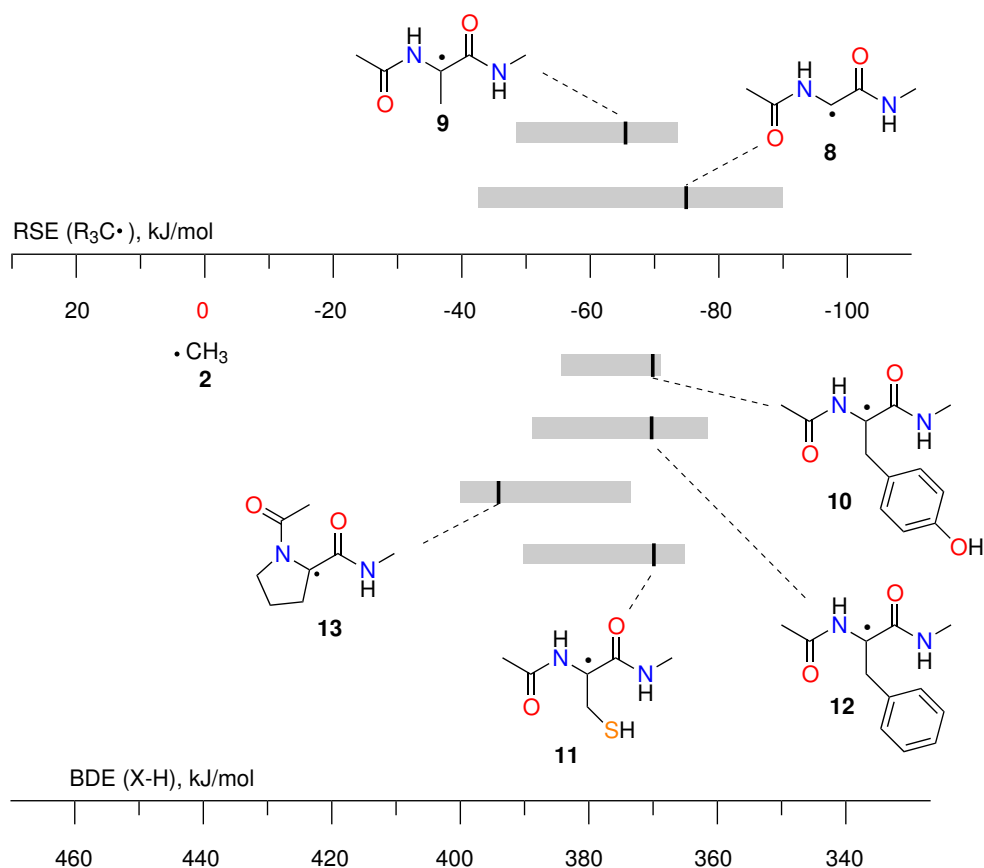


Figure 3.4: Radical stabilization energies (RSE) of selected O-, C-, and S-centred radicals and bond dissociation energies (BDE) of the corresponding O-H, C-H, and S-H bonds.

radicals **8** and **9** in which the extended C₅ conformation is preferred in both systems. Introduction of the methyl substituent in **9** now leads to an increase in the OCN and CNC bond angles as a consequence of repulsive interactions between the methyl substituent at the C $_{\alpha}$ position and the N-terminal peptide group. Structural changes on the C-terminal side are, in comparison, rather minor. These results are in full agreement with previous observations made by Radom and co-workers on smaller peptide ester models.^[22;23]

3.3 Conclusion

Calculations performed at the G3B3, G3(MP2)-RAD, and IMOMO(G3B3,G3(MP2)-RAD) levels of theory have firmly established that substituents at the C $_{\alpha}$ position of dipeptide radicals have a destabilizing effect. Electronic stabilization effects of the attached substituent are overridden by repulsive interactions between the substituents and the amide groups of the protein backbone making C $_{\alpha}$ radicals derived from alanyl, cysteinyl, tyrosyl, phenylalanyl, or prolyl residues less stable than the nonsubstituted glycyl radical. Conformational analysis of the dipeptide radicals and

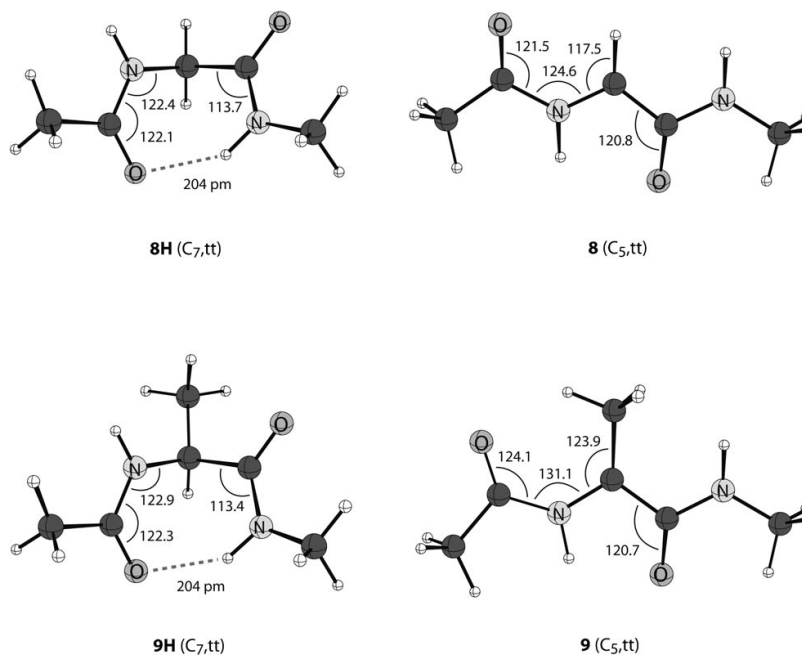


Figure 3.5: Structures of the energetically most favorable conformations of glycine dipeptide **8H**, glycyI dipeptide radical **8**, alanine dipeptide **9H**, and alanyl dipeptide radical **9**.

their respective closed-shell parents also indicates that radical stability varies quite significantly as a function of the selected conformation. The glycine residue is found to provide the largest variation of radical stability with changes in peptide conformation. Aside from the large intrinsic stability of the glycyI radical, this offers a second argument for the existence of the large glycyI radical enzyme (GRE) family of enzymes. These arguments are based on thermodynamic quantities exclusively and do not exclude the involvement of kinetic factors in hydrogen transfer processes.^[37–40]

Bibliography

- [1] W. Buckel and B. T. Golding. *Annu. Rev. Microbiol.*, 60:27–49, 2006.
- [2] A. Sancar. *Chem. Rev.*, 103:2203–2237, 2003.
- [3] H. Eklund and M. Fontecave. *Structure*, 7:R257–R262, 1999.
- [4] T. Selmer, A. J. Pierik, and J. Heider. *Biol. Chem.*, 386:981–988, 2005.
- [5] O. T. Magnusson P. A. Frey. *Chem. Rev.*, 32:2129–2148, 2003.
- [6] R. Banerjee. *Chem. Rev.*, 103:2083–2094, 2003.
- [7] P. A. Frey, A. D. Hegeman, and F. J. Ruzicka. *Crit. Rev. Biochem. Mol. Biol.*, 43:63–68, 2008.

- [8] H. Zipse J. Hioe. *Faraday Discuss.*, 145:301–313, 2010. and subsequent discussion, p. 381-409.
- [9] H. Zipse. *Top. Curr. Chem.*, 263:163–189, 2006.
- [10] M. L. Coote, C. Y. Lin, and H. Zipse. *Carbon-Centered Free Radicals and Radicals Cations*, chapter "The Stability of Carbon-Centered Radicals", pages 83–104. M. D. E. Forbes (Ed.), John Wiley & Sons, 2010.
- [11] Y. Feng, L. Liu, J.-T. Wang, H. Huang, and Q.-X. Guo. *J. chem. Inf. Comput. Sci.*, 43:2005 – 2013, 2003.
- [12] Y.-R. Luo. *Comprehensive Handbook of Chemical Bond Energies*. CRC Press, 2007.
- [13] A. G. Baboul, L. A. Curtiss, P. C. Redfern, and K. Raghavachari. *J. Chem. Phys.*, 110:7650–7657, 1999.
- [14] T. Vreven and K. Morokuma. *J. Chem. Phys.*, 111:8799–8803, 1999.
- [15] T. Vreven and K. Morokuma. *J. Comput. Chem.*, 21:1419–1432, 2000.
- [16] E. I. Izgorodina, D. R. B. Brittain, J. L. Hodgson, E. H. Krenske, C. Y. Lin, M. Namazian, and M. L. Coote. *J. Phys. Chem. A*, 111:10754–10768, 2007.
- [17] D. J. Henry, C. J. Parkinson, and L. Radom. *J. Phys. Chem. A*, 106:7927–7936, 2002.
- [18] D. J. Henry, M. B. Sullivan, and L. Radom. *J. Chem. Phys.*, 118:4849–4860, 2003.
- [19] H. G. Viehe, Z. Janousek, R. Merenyi, and L. Stella. *Acc. Chem. Res.*, 18:148–154, 1985.
- [20] R. Sustmann and H.-G. Korth. *Adv. Phys. Org. Chem.*, 26:131–178, 1991.
- [21] C. J. Easton. *Chem. Rev.*, 97:53–82, 1997.
- [22] A. K. Croft, C. J. Easton, K. Kociuba, and L. Radom. *Tetrahedron: Asymmetry*, 14:2919–2926, 2003.
- [23] A. K. Croft, C. J. Easton, and L. Radom. *J. Am. Chem. Soc.*, 125:4119–4124, 2003.
- [24] G. P. F. Wood, D. Moran, R. Jacob, and L. Radom. *J. Phys. Chem. A*, 109:6318–6325, 2005.
- [25] B. J. W. Barratt, C. J. Easton, D. J. Henry, I. H.W. Li, L. Radom, and J. S. Simpson. *J. Am. Chem. Soc.*, 126:13306–13311, 2004.

- [26] G. Yang, Y. Zu, and L. Zhou. *J. Phys. Org. Chem.*, 21:34, 2008.
- [27] I. Hudky, R. Kiss, and A. Perczel. *J. Mol. Struct.: THEOCHEM*, 675:177–183, 2004.
- [28] R. Vargas, J. Garza, B. P. Hay, and D. A. Dixon. *J. Phys. Chem. A*, 106:3213–3218, 2002.
- [29] W. D. Cornell, I. R. Gould, and P. A. Kollman. *J. Mol. Struct.: THEOCHEM*, 392:101–109, 1997.
- [30] K. Bisetty, J. Gomez Catalan, H. G. Kruger, and J. J. Perez. *J. Mol. Struct.: THEOCHEM*, 731:127–137, 2005.
- [31] G. Pohl, A. Perczel, E. Vass, G. Magyarfalvi, and G. Tarczay. *Phys. Chem. Chem. Phys.*, 9:4698–4708, 2007.
- [32] J. Kaminsky and F. Jensen. *J. Chem. Theory Comput.*, 3:1774–1788, 2007.
- [33] H. Fujitani, A. Matsuura, S. Sakai, H. Sato, and Y. Tanida. *J. Chem. Theory Comput.*, 5:1155–1165, 2009.
- [34] L. Schäfer, C. VanAlsenoy, and J. N. Scarsdale. *J. Chem. Theory Comput.*, 76:1439–1444, 1982.
- [35] K. Möhle and H.-J. Hofmann. *J. Chem. Theory Comput.*, 4:53–60, 1998.
- [36] J. N. Scarsdale, C. VanAlsenoy, V. J. Klimkowski, and K. Schäfer. *J. Am. Chem. Soc.*, 105:3438–3445, 1983.
- [37] H. F. Lu and S. H. Lin. *J. Comput. Chem.*, 28:783–794, 2007.
- [38] D. Moran, R. Jacob, G. P. F. Wood, M. L. Coote, M. J. Davies, R. A. J. O’Hair, C. J. Easton, and L. Radom. *Helv. Chim. Acta*, 89:2254–2272, 2006.
- [39] Z. I. Watts and C. J. Easton. *J. Am. Chem. Soc.*, 131:11323–11325, 2009.
- [40] L. Zeng, T. Kaoudi, and C. H. Schiesser. *Tetrahedron Lett.*, 47:7911–7914, 2006.
- [41] J. W. Ponder. Tinker 4.2, 2004. Washington University, St. Louis.
- [42] H.-J. Werner, P. J. Knowles, R. Lindh, F. R. Manby, M. Schütz, P. Celani, T. Korona, A. Mitrushenkov, G. Rauhut, T. B. Adler, R. D. Amos, A. Bernhardsson, A. Berning, D. L. Cooper, M. J. O. Deegan, A. J. Dobbyn, F. Eckert, E. Goll, C. Hampel, G. Hetzer, T. Hrenar, G. Knizia, C. Köppl, Y. Liu, A. W. Lloyd, R. A. Mata, A. J. May, S. J. McNicholas, W. Meyer, M. E. Mura, A. Nicklaß, P. Palmieri, K. Pflüger, R. Pitzer, M. Reiher, U. Schumann, H. Stoll, A. J. Stone, R. Tarroni, T. Thorsteinsson, M. Wang, and A. Wolf. MOLPRO, version 2006.1, a package of *ab initio* programs.

- [43] M. J. Frisch, G. W. Trucks, H. B. Schlegel, G. E. Scuseria, M. A. Robb, J. R. Cheeseman, J. A. Montgomery, Jr., T. Vreven, K. N. Kudin, J. C. Burant, J. M. Millam, S. S. Iyengar, J. Tomasi, V. Barone, B. Mennucci, M. Cossi, G. Scalmani, N. Rega, G. A. Petersson, H. Nakatsuji, M. Hada, M. Ehara, K. Toyota, R. Fukuda, J. Hasegawa, M. Ishida, T. Nakajima, Y. Honda, O. Kitao, H. Nakai, M. Klene, X. Li, J. E. Knox, H. P. Hratchian, J. B. Cross, V. Bakken, C. Adamo, J. Jaramillo, R. Gomperts, R. E. Stratmann, O. Yazyev, A. J. Austin, R. Cammi, C. Pomelli, J. Ochterski, P. Y. Ayala, K. Morokuma, G. A. Voth, P. Salvador, J. J. Dannenberg, V. G. Zakrzewski, S. Dapprich, A. D. Daniels, M. C. Strain, O. Farkas, D. K. Malick, A. D. Rabuck, K. Raghavachari, J. B. Foresman, J. V. Ortiz, Q. Cui, A. G. Baboul, S. Clifford, J. Cioslowski, B. B. Stefanov, G. Liu, A. Liashenko, P. Piskorz, I. Komaromi, R. L. Martin, D. J. Fox, T. Keith, M. A. Al-Laham, C. Y. Peng, A. Nanayakkara, M. Challacombe, P. M. W. Gill, B. G. Johnson, W. Chen, M. W. Wong, C. Gonzalez, and J. A. Pople, 2004. GAUSSIAN 03 (Revision D.01), Gaussian, Inc., Wallingford, CT.

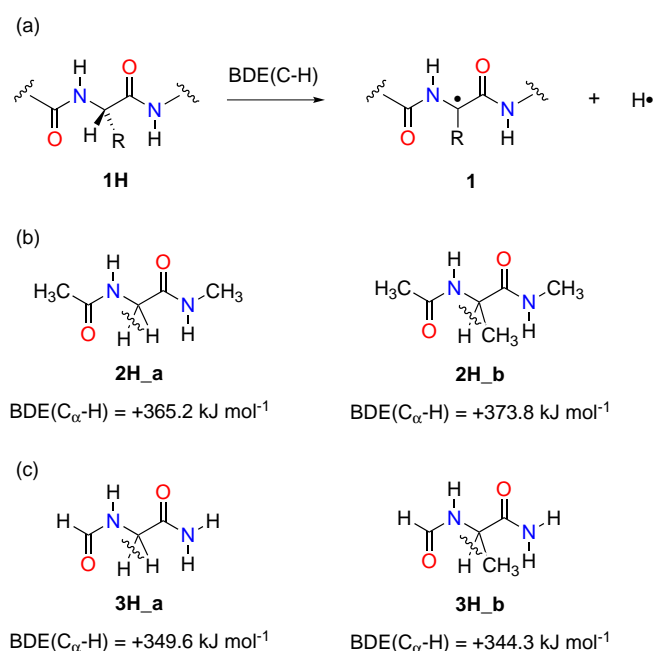
Chapter 4

Dissociation Energies of C_α-H Bonds in Amino Acids - a Reexamination

Published in: J. Hioe, M. Mosch, D. M. Smith, H. Zipse, *RSC Advances*, **2013**,
3, 12403 - 12408.

4.1 Introduction

The abstraction of hydrogen atoms from amino acids, peptides and proteins is of outstanding relevance for processes as diverse as the oxidative damage to proteins and the catalysis of unusual substrate rearrangements through radical enzymes. The bond dissociation energies of the C-H bonds (BDE(C-H)) involved in these hydrogen transfer reactions thus represent important parameters in assessing the likelihood of these processes. Experimental data for individual C $_{\alpha}$ -H bonds in amino acids and peptides is still rather limited and the bulk of BDE data has thus been obtained from quantum chemical studies. As is described in Scheme 4.1 for the question of C $_{\alpha}$ -H bond energies, theoretical studies are typically not performed on complete proteins or peptides **1H**, but on smaller dipeptide or amino acid models instead. Using theoretical methods designed for the description of open shell systems such as G3(MP2)-RAD, we have recently found the BDE(C $_{\alpha}$ -H, **2H_a**) = +365.2 kJ mol $^{-1}$) to be significantly smaller than those in alanine dipeptide (BDE(C $_{\alpha}$ -H, **2H_b**) = +373.8 kJ mol $^{-1}$).^[1-4]



Scheme 4.1: (a) Definition of C $_{\alpha}$ -H bond dissociation energies (BDE(C $_{\alpha}$ -H)) in peptides; (b) BDE(C $_{\alpha}$ -H) values obtained for glycine and alanine dipeptide models **2H_a** and **2H_b** (ref. 1-4); (c) BDE(C $_{\alpha}$ -H) values obtained for glycine and alanine dipeptide models **3H_a** and **3H_b** (ref. 5;6).

Together with BDE data for other dipeptide radicals this was taken to reflect steric interactions between the C $_{\alpha}$ substituents and the amide groups present on the N- and C-terminal side of the central amino acid radicals. Combining results obtained from B3LYP/6-31G(d) calculations for peptide model **3H** and earlier work by Rauk *et al.*,^[7;8] Julian *et al.* predict BDE(C $_{\alpha}$ -H, **3H_a**) = +349.6 kJ mol $^{-1}$ for glycine

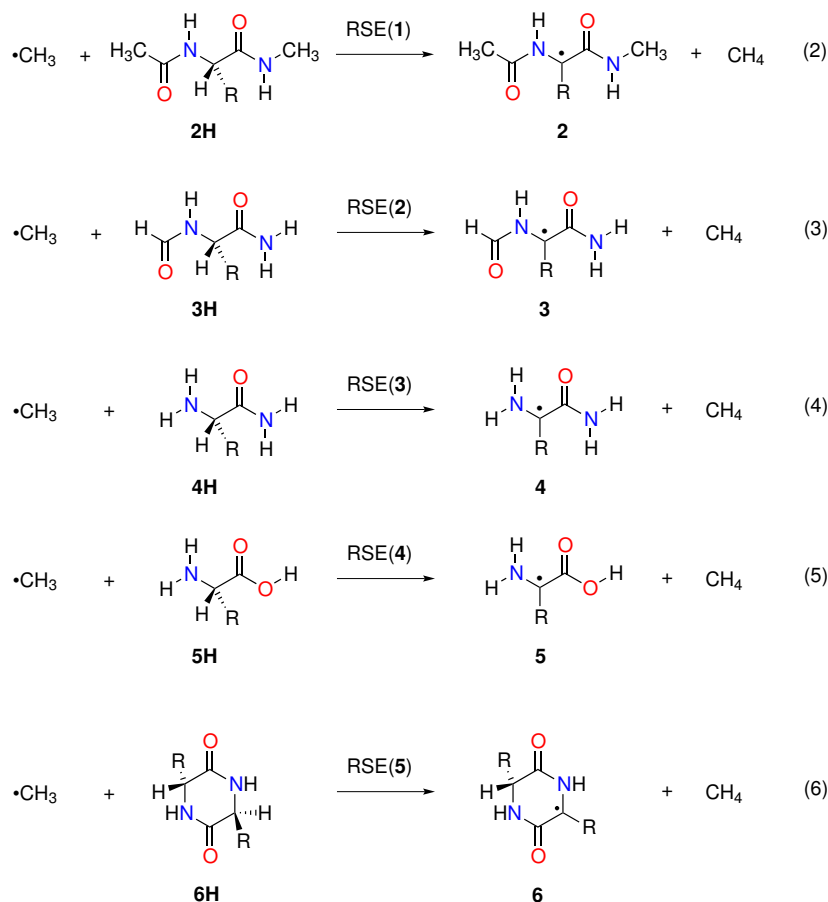
peptide **3H_a** and $\text{BDE}(\text{C}_\alpha\text{-H}, \mathbf{3H_b}) = +344.3 \text{ kJ mol}^{-1}$ for alanine peptide **3H_b**.^[5] These values are practically identical to those reported earlier by Rauk *et al.*^[6] These BDE values are not only significantly smaller than those obtained for dipeptide model **2H** at G3(MP2)-RAD level, but also imply lower BDE values for alanine residues as compared to glycine. This apparent contradiction may be due to various factors such as the choice of model system, the choice of theoretical method, and the strategy for calculating reaction energies. Using the examples of glycine and alanine we show in the following how these factors impact $\text{BDE}(\text{C-H})$ values for the C_α position in peptide models. Furthermore, we show that a carefully chosen combination of the said factors is sufficient to allay any apparent inconsistency related to the relative stabilities of glycine and alanine peptide radicals.

4.2 Results

The calculation of C-H bond dissociation energies is most easily approached using hydrogen transfer reactions between the system of interest and a (thermochemically) well characterized reference system. For carbon-centered radicals the most often used reference system is methane (CH₄), whose C-H bond energy is accurately known as $\text{BDE}(\text{C-H}) = +439.4 \pm 0.4 \text{ kJ mol}^{-1}$.^[9] The reaction energy for isodesmic hydrogen transfer reaction with this reference system as shown, for example, for peptide radical **2_a** in Scheme 4.2, is often referred to as the radical stabilization energy (RSE) of radical **2_a** relative to methyl radical $\bullet\text{CH}_3$. Summation of the RSE value for a particular radical with the (experimental) $\text{BDE}(\text{C-H})$ value of the reference system then yields the $\text{BDE}(\text{C-H})$ value for the system under investigation. The $\text{BDE}(\text{C-H})$ value in model peptide **2H_a**, for example, can thus be calculated using equation 4.1. The reaction energy calculated for hydrogen transfer between methyl radical ($\bullet\text{CH}_3$) and peptide model **2H_a** amounts to $\text{RSE}(\mathbf{2_a}) = -74.1 \text{ kJ mol}^{-1}$ at the G3(MP3)-RAD level of theory, and combination of this value with the $\text{BDE}(\text{C-H})$ value in methane according to eq. 4.1 then yields a C_α-H bond dissociation energy of $\text{BDE}(\text{C}_\alpha\text{-H}, \mathbf{2H_a}) = +365.2 \text{ kJ mol}^{-1}$ for peptide model **2H_a**. Following this procedure $\text{BDE}(\text{C}_\alpha\text{-H})$ values have been computed for all amino acid and peptide models in Scheme 4.2 and compiled in Table 4.1.

$$\text{BDE}(\text{C-H}, \mathbf{2H_a}) = \text{BDE}(\text{C-H}, \text{CH}_4) + \text{RSE}(\mathbf{2_a}) \quad (4.1)$$

Choice of electronic structure method: The $\text{BDE}(\text{C}_\alpha\text{-H})$ value obtained for glycine dipetide **2H_a** at G3(MP2)-RAD level is in good agreement with that obtained with the even more elaborate G3B3 scheme,^[10] $\text{BDE}(\text{C}_\alpha\text{-H}, \mathbf{2H_a}) = +363.8 \text{ kJ mol}^{-1}$. Both values are significantly larger than the value of $\text{BDE}(\text{C}_\alpha\text{-H}, \mathbf{2H_a}) = +337.7 \text{ kJ mol}^{-1}$ obtained with the more economical B3LYP/6-31G(d) approach.



a: R = H; **b:** R = CH₃

Scheme 4.2: Isodesmic reactions (2) - (6) for the calculation of radical stabilization energies of amino acid, peptide radicals **2** - **5** derived from glycine (**5H**_a, R = H) and alanine (**5H**_b, R = CH₃) and peptide anhydrides **6H**.

This is also found for all other amino acids, peptide models and peptide anhydrides **2H-6H** studied here. Previous studies^[9] indicate that G3B3 and G3(MP2)-RAD methods predict BDE values with an accuracy of 3 - 5 kJ mol⁻¹. This implies that the BDE(C $_{\alpha}$ -H) data obtained at B3LYP/6-31G(d) level are too low by 20 - 30 kJ mol⁻¹. BDE(C $_{\alpha}$ -H) data for glycine **5H**_a have also been evaluated with the G3X(MP2)-RAD and the more elaborate G4-5H and W1RO schemes (Table 4.1).^[11-13] G3X(MP2)-RAD theory^[13] differs from G3(MP2)-RAD in that geometry optimizations are performed at B3LYP/6-31G(2df,p) (instead of B3LYP/6-31G(d)) level, and in adding a basis set correction term at the (restricted open shell) Hartree-Fock level. Results obtained for **5H**_a with both methods are practically identical, which implies that the basis set used in geometry optimizations is not critical for obtaining accurate BDE data. G4-5H theory is a variant of G4 theory^[14] whose performance in the description of hydrogen transfer reactions is particularly good, while the even more expensive W1RO theory^[15;16] is expected to deliver sub-kcal/mol accuracy in predicting the thermochemistry of a wide variety of systems. Both ap-

proaches yield effectively the same BDE data as obtained at the G3B3 level, thus confirming the quality of these predictions. The subsequent discussion will thus focus on the G3B3 results exclusively.

Table 4.1: RSE and BDE(C α -H) values of amino acid/peptide models at various levels of theory using the isodesmic reactions (2) - (5) in Scheme 2

System	RSE B3LYP ^a	BDE B3LYP ^a	RSE G3(MP2)-RAD	BDE G3(MP2)-RAD	RSE Other	BDE Other
2a	-101.6	+337.7	-74.1	+365.2	-75.5 ^b	+363.8 ^b
2b	-98.9	+340.5	-65.5	+373.8	-67.0 ^c	+372.3 ^c
3a	-100.4	+338.9	-75.9	+363.4	-77.6 ^b -78.4 ^d	+361.7 ^b +360.9 ^d
3b	-101.0	+338.3	-69.6	+369.7	-71.2 ^b	+368.1 ^b
4a	-108.1	+331.2	-85.6	+353.7	-87.7 ^b -88.9 ^d	+351.6 ^b +350.4 ^d
4b	-113.8	+325.5	-87.1	+352.1	-89.9 ^b	+349.4 ^b
5a	-118.8	+320.5	-95.8	+343.5	-96.0 ^e -97.8 ^f -99.0 ^b -99.1 ^d -101.4 ^g	+343.3 ^e +341.5 ^f +340.3 ^b +340.2 ^d +337.9 ^g
5b	-130.8	+308.5	-102.5	+336.8	-106.4 ^b	+332.9 ^b
6a	-98.3	+341.0	-77.9	+361.4	-80.1 ^b -82.8 ^h	+359.2 ^b +359.1 ^h +340 ± 15 ⁱ
6b	-114.6	+324.7	-87.7	+351.6	-90.1 ^b -93.7 ^h	+349.2 ^b +348.1 ^h +323 ± 15 ⁱ

^aUB3LYP/6-31G(d)

^bG3B3

^cIMOMO(G3B3,G3(MP2)-RAD)

^dG4-H

^eG3X(MP2)-RAD

^fG2MP2

^gW1RO

^hPCM/G3B3

ⁱExperimental values in aqueous solution (ref. 17)

Choice of model system: The value of BDE(C α -H, **2H_a**) = +363.8 kJ mol⁻¹ for glycine dipeptide model **2H_a** is significantly smaller as compared to that calculated for the alanine-based dipeptide model **2H_b** with BDE(C α -H, **2H_b**) =

+372.3 kJ mol⁻¹. This implies that glycy radical **2_a** is more stable than alanine radical **2_b** by +8.5 kJ mol⁻¹. On moving from dipeptide **2H** to the smaller peptide models, this difference is found to diminish to +6.4 kJ mol⁻¹ in dipeptide model **3H** and reverse to -2.2 kJ mol⁻¹ in peptide model **4H**. Finally, in the bare amino acids the BDE(C $_{\alpha}$ -H) in alanine (**5H_b**) amounts to BDE(C $_{\alpha}$ -H, **5H_b**) = +332.9 kJ mol⁻¹, which is 7.4 kJ mol⁻¹ less than in glycine with BDE(C $_{\alpha}$ -H, **5H_a**) = +340.3 kJ mol⁻¹. We note in passing that the BDE(C $_{\alpha}$ -H) value obtained here for glycine **5H_a** at G3B3 level is slightly higher than the value of BDE(C $_{\alpha}$ -H, **5H_a**) = +331 kJ mol⁻¹ based on G2(MP2) theory reported by Rauk.^[7:8] As is shown in a pictorial manner in Figure 4.1, the move to smaller and smaller peptide models and, eventually, to amino acids is accompanied by a cross-over in the relative stabilities of glycy and alanyl radicals, the larger model systems predicting lower BDE(C $_{\alpha}$ -H) values for glycine as compared to alanine. This trend is due to two opposing effects of the C $_{\alpha}$ substituents at the radical stage: (a) an inductively stabilizing effect onto the C $_{\alpha}$ radical center; and (b) steric repulsion with the amide substituents at the N- and C-terminal side. The alanyl radical **5_b** is more stable than glycy radical **5_a** due to the electron-donating effect of the methyl group attached to the radical center. Extension of the peptide models on the N- and C-terminal side as in **3H** and **2H** now adds steric effects large enough to overcompensate the beneficial electronic effect and thus leads to higher stability of the glycy peptide radicals. This is also fully in line with earlier conclusions by Radom *et al.* on the stability of peptide ester radicals.^[18] The conformational consequences of these interactions will be discussed below.

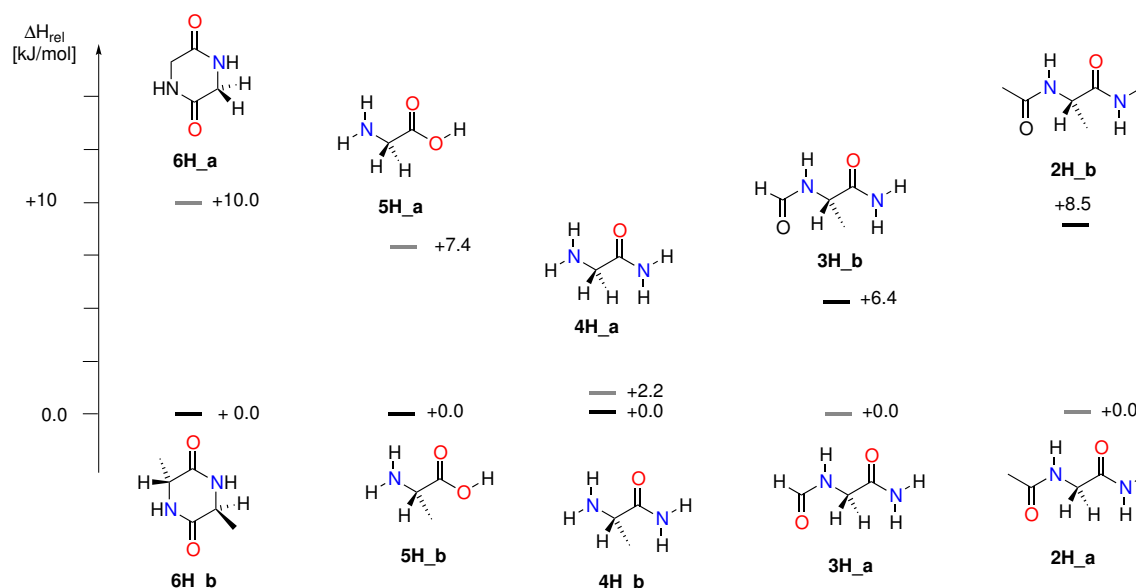


Figure 4.1: Relative C $_{\alpha}$ -H BDE between glycine and alanine at G3B3 level of theory.

Choice of reference system: The stabilization energies reported in Table 4.1 and Figure 4.1 are based on Boltzmann-averaged enthalpies for all species and the reference system CH₄/•CH₃. In order to test whether different reference systems lead

to substantially different results, BDE(C $_{\alpha}$ -H) values in glycine and alanine dipeptide models and anhydrides **2H-6H** were recalculated using the CH $_3$ NH $_2$ /•CH $_2$ NH $_2$ and the propene/allyl radical reference systems. Experimental BDE(C-H) values are known for both of these systems and these bond energies are closely similar to those in the peptide models studied here. We note in passing that the experimental bond energy in CH $_3$ NH $_2$ /•CH $_2$ NH $_2$ of BDE(C $_{\alpha}$ -H, exp.) = +392.9 ± 9.4 kJ mol $^{-1}$ can be closely matched at G3B3 level with BDE(C-H, G3B3) = +392.4 kJ mol $^{-1}$ using the isodesmic equation approach with the CH $_4$ /•CH $_3$ reference system. This is also found for the bond strength of the allylic C-H bond in propene with BDE(C-H, exp.) = +368.6 ± 2.9 kJ mol $^{-1}$ and BDE(C-H, G3B3) = +368.8 kJ mol $^{-1}$. As shown schematically in Figure 4.2 the BDE(C $_{\alpha}$ -H) values obtained at G3B3 level for dipeptide models **3H_a** and **3H_b** are closely similar for all three reference systems, the BDE(C $_{\alpha}$ -H) in **3H_b** being larger by *ca.* 6 kJ mol $^{-1}$ than that in **3H_a**. This is distinctly different for the B3LYP level, where the BDE(C $_{\alpha}$ -H) values are found to vary by more than 10 kJ mol $^{-1}$ in absolute terms as a function of the reference system and where glycine and alanine dipeptides **3H_a** and **3H_b** are predicted to have essentially the same BDE(C $_{\alpha}$ -H) values. Similar observations can also be made for all other dipeptide models and amino acids in Table 4.1/Figure 4.1 (see SI for full details).

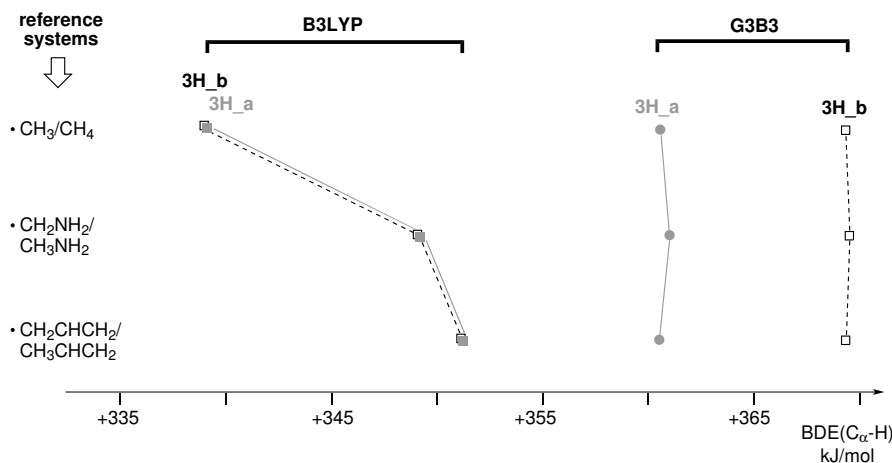


Figure 4.2: Influence of reference system and theoretical method on the BDE(C $_{\alpha}$ -H) values for glycine and alanine dipeptide models **3H_a** and **3H_b**.

Conformational selection: The reaction enthalpies obtained for isodesmic reactions (2) - (6) (and thus the BDE(C $_{\alpha}$ -H) values) depend significantly on the conformers chosen for reactants and products. The BDE values listed in Table 4.1 have been obtained using Boltzmann-averaged enthalpies over all relevant conformers. It is important to note at this point that conformational preferences are rather different for closed-shell dipeptides and their respective C $_{\alpha}$ radicals. For peptide models **3H_a/b** and radicals **3_a/b** the required information on conformational energies has been compiled in Table 4.2. For both radicals **3_a** and **3_b** the extended C $_5$ conformation is found to be most stable, while the closed shell parent dipeptides

3H_a and **3H_b** prefer the folded C $_7$ conformation. For these latter systems, the C $_5$ conformation represents the second best conformer, located +1.9 kJ mol $^{-1}$ (in **3H_a**) and +4.2 kJ mol $^{-1}$ (in **3H_b**) higher in energy. That the C $_5$ /C $_7$ energy difference is not identical in these dipeptide models is due to the steric effects induced by the C $_{\alpha}$ methyl substituent present in **3H_b**. These results are consistent with previous studies of C $_{\alpha}$ -peptide radicals.^[3] Table 4.3 compiles BDE(C $_{\alpha}$ -H) values of peptide models **3H_a/b** using a restricted conformational space with CH $_4$ /•CH $_3$ as the reference system. For glycine model **3H_a** the BDE(C $_{\alpha}$ -H) value of +360.0 kJ mol $^{-1}$ obtained through locking the system in a C $_5$ conformation is almost identical to that obtained with full Boltzmann averaging (+361.7 kJ mol $^{-1}$, G3B3 data from Table 4.1). Differences are somewhat larger for the alanine system **3H_b**, where the system in its C $_5$ conformation has a clearly lower BDE(C $_{\alpha}$ -H) value of +364.1 kJ mol $^{-1}$ as compared to that obtained with Boltzmann averaging of +368.1 kJ mol $^{-1}$. Significantly larger variations in BDE(C $_{\alpha}$ -H) values are observed when locking the dipeptide systems in the C $_7$ conformation, which is particularly unfavorable for dipeptide radicals. Similar trends can also be observed at the B3LYP level of theory (Table 4.3). This implies that relative glycine/alanine dipeptide BDE(C $_{\alpha}$ -H) values also depend on the conformational selection made for radicals as well as for closed shell parents.

Table 4.2: Relative energies of dominant conformers for peptide **3H_a/b** and peptide radical **3_a/b**.

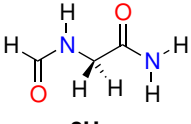
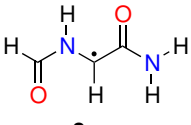
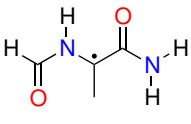
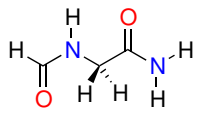
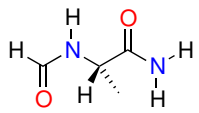
Systems	Backbone geometry	Peptide bond conformations	$\Delta H_{298,\text{rel.}}$ B3LYP [kJ mol $^{-1}$]	$\Delta H_{298,\text{rel.}}$ G3B3 [kJ mol $^{-1}$]
 3H_a	C $_7$	trans	+0.0	+0.0
	C $_5$	trans	+0.1	+1.9
	C $_7$	cis	+12.4	+14.4
	C $_5$	cis	+15.4	+20.0
 3_a	C $_5$	trans	+0.0	+0.0
	C $_5$	cis	+7.6	+9.2
	β_2	trans	+27.3	+26.2
	α_L	trans	+29.0	+30.8
	α_R	cis	+40.9	+40.5
 3H_b	C $_{7\text{ax.}}$	trans	+0.0	+0.0
	C $_5$	trans	+4.3	+4.2
	C $_{7\text{eq.}}$	trans	+10.2	+9.4
	α'	cis	+15.2	+17.3
	C $_5$	cis	+18.9	+21.5
	α_R	cis	+24.3	+24.3
	β_2	trans	+26.4	+25.3
	C $_{7\text{eq.}}$	cis	+27.3	+26.8
 3_b	C $_5$	trans	+0.0	+0.0
	C $_5$	cis	+6.9	+5.2
	β_2	cis	+17.8	+15.7
	C $_{7\text{eq.}}$	trans	+20.0	+19.4
	β_2	trans	+20.5	+17.8
	α_L	cis	+28.5	+25.5

Table 4.3: C $_{\alpha}$ -H BDE of conformational restricted peptide model **3H_a/b**

Systems	Backbone geometry	Peptide bond conformations	BDE B3LYP [kJ mol $^{-1}$]	BDE G3B3 [kJ mol $^{-1}$]
 3H_a	C $_5$	trans	+338.5	+360.0
	C $_5$	cis	+330.8	+351.2
 3H_b	C $_5$	trans	+334.4	+364.1
	C $_5$	cis	+326.6	+352.1
	C $_7$	trans	+358.7	+387.8
	β_2	trans	+332.7	+360.9

Comparison to experimental studies: The BDE(C $_{\alpha}$ -H) values obtained for glycine- and alanine anhydride (**6H_a** and **6H_b**) at G3(MP2)-RAD and G3B3 level in the gas phase are significantly larger than the experimental values obtained with photoacoustic calorimetry in aqueous solution (BDE $_{\text{exp.}}$ (C $_{\alpha}$ -H, **6H_a**) = 340 \pm 15 kJ mol $^{-1}$; BDE $_{\text{exp.}}$ (C $_{\alpha}$ -H, **6H_b**) = 325 \pm 15 kJ mol $^{-1}$).^[17] This might only partially be due to aqueous solvation effects. The application of a continuum solvation model (PCM) for water, at the B3LYP/6-31G(d) level, lowers the BDE(C $_{\alpha}$ -H) value of **6H_a** by only 0.13 kJ mol $^{-1}$ and that of **6H_b** by 1.10 kJ mol $^{-1}$, respectively. The deviations between experiment and theory may, in part, also be due to the large uncertainties of the measurements in water.^[17] Kinetic studies by Schöneich *et al.* measuring C $_{\alpha}$ -H-abstraction rate constants from peptides N-Ac-Gly/Ala-NH $_2$ by thiyl radicals have established that the abstraction from glycine N-Ac-Gly-NH $_2$ is approximately three times faster than from alanine N-Ac-Ala-NH $_2$, which may be rationalized by lower BDE(C $_{\alpha}$ -H) values in glycine as compared to alanine.^[19]

Table 4.4: Rate constants for hydrogen abstraction by thiyl radicals^[19] and BDE(C $_{\alpha}$ -H) values for selected peptide models.

System	Rate [M $^{-1}$ s $^{-1}$]	C-H BDE a [kJ mol $^{-1}$]
6H_a	8.0 x 10 4	+359.2 a
N-Ac-Gly-NH $_2$	3.2 x 10 4	+363.8 b (2H_a)
N-Ac-Ala-NH $_2$	1.0 x 10 4	+372.3 c (2H_b)
N-Ac-Pro-NH $_2$	0.18 x 10 4	+391.5 c (Proline) b

^aG3B3^bTaken from ref. 3.^cIMOMO(G3B3,G3(MP2)-RAD)

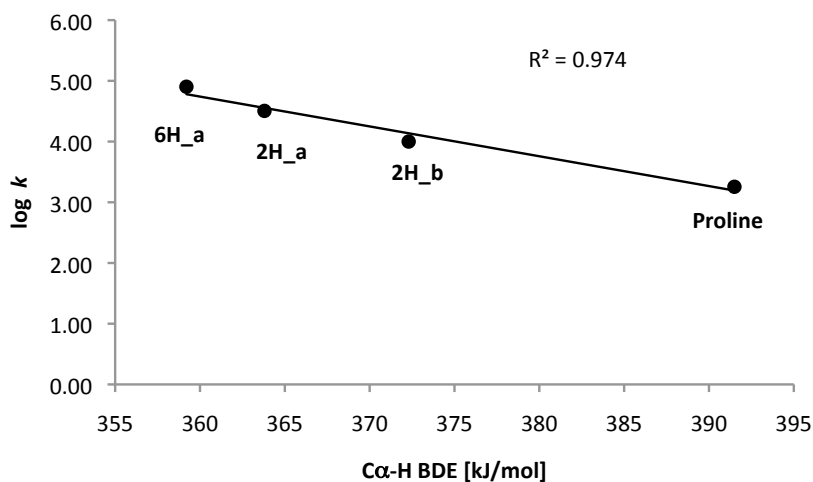


Figure 4.3: Correlation of BDE(C $_{\alpha}$ -H) values obtained at the G3B3 level with rate data for H-abstraction.^[19]

In contrast to the B3LYP values for peptide models **3H_a**/**3H_b** published earlier,^[6] the G3B3 results obtained here for peptide models **2H_a**/**2H_b** containing the full acetyl group on the N-terminal position predict lower BDE(C $_{\alpha}$ -H) values for glycine as compared to alanine by about 7 - 8 kJ mol $^{-1}$ (regardless of the choice of reference system). Glycine anhydride **6H_a** is shown in the same experimental study to react with the thiyl radical faster than either the glycine or alanine dipeptide models. This observation can also be rationalized by the G3B3 data in Table 4.1, which shows lower bond energies for **6H_a** as compared to **2H_a**. Additional consideration of BDE(C $_{\alpha}$ -H) values for the dipeptide proline model reported earlier at the G3B3 level,^[3] the kinetic data reported by Schöneich *et al.* can be correlated rather well with the respective bond energies (Table 4.4, Figure 4.3). This is in remarkable contrast to the poor correlation obtained earlier with B3LYP BDE(C $_{\alpha}$ -H) values for the smaller dipeptide models **3H_a**/**3H_b** by Rauk.

4.3 Conclusions

BDE(C $_{\alpha}$ -H) values in amino acids and peptide models can be computed quite reliably using an appropriate combination of electronic structure methods, sufficient conformational sampling and an experimentally well-characterized reference system. Results obtained using the G3(MP2)-RAD and G3B3 schemes are in good agreement with those obtained with benchmark quality methods such as W1RO, while this is not so for calculations obtained from hybrid density functional methods such as B3LYP. The choice of reference system is much less critical when one of the G3-level methods is used. Some care is required in selecting conformations for high-level calculations, as the conformational preferences of radicals and non-radicals differ substantially. Importantly, our results confirm that glycyI peptide radicals are more stable than analogous radicals derived from alanine (or other α -amino acids) and

thus resolve an apparent inconsistency, which had emerged from previous work in the literature.

Bibliography

- [1] J. Hioe and H. Zipse. *Faraday Discuss.*, 145:301–313, 2010. and subsequent discussion, p. 381-409.
- [2] J. Hioe and H. Zipse. *Org. Biol. Chem.*, 8:3609–3617, 2010.
- [3] J. Hioe, G. Savasci, H. Brand, and H. Zipse. *Chem. Eur. J.*, 17:3781–3789, 2011.
- [4] J. Hioe and H. Zipse. *Chem. Eur. J.*, 18:16463–16472, 2012.
- [5] B. N. Moore and R. R. Julian. *Phys. Chem. Chem. Phys.*, 14:3148–3154, 2012.
- [6] A. Rauk, D. Yu., J. Taylor, G. V. Shustov, D. A. Block, and D. A. Armstrong. *Biochemistry*, 38:9089–9096, 1999.
- [7] D. Yu, A. Rauk, and D. A. Armstrong. *J. Am. Chem. Soc.*, 117:1789–1796, 1995.
- [8] D. A. Armstrong, D. Yu, and A. Rauk. *J. Am. Chem. Soc.*, 119:208–217, 1997.
- [9] Y.-R. Luo. *Comprehensive Handbook of Chemical Bond Energies*. CRC Press, 2007.
- [10] A. G. Baboul, L. A. Curtiss, P. C. Redfern, and K. Raghavachari. *J. Chem. Phys.*, 110:7650–7657, 1999.
- [11] B. Chan, M. L. Coote, and L. Radom. *J. Chem. Theory Comput.*, 6:2647, 2010.
- [12] R. J. O’Reilly, A. Karton, and L. Radom. *Int. J. Quant. Chem.*, 112:1862–1878, 2012.
- [13] D. J. Henry, M. B. Sullivan, and L. Radom. *J. Chem. Phys.*, 118:4849–4860, 2003.
- [14] L. A. Curtiss, P. C. Redfern, and K. Raghavachari. *J. Chem. Phys.*, 126:7650–7657, 2007.
- [15] J. M. L. Martin and G. de Oliveira. *J. Chem. Phys.*, 111:1843–1856, 1999.
- [16] S. Parthiban and J. M. L. Martin. *J. Chem. Phys.*, 114:6014–6029, 2001.
- [17] M. Jonsson, D. D. M. Wayner, D. A. Armstrong, D. Yu, and A. Rauk. *J. Chem. Soc. Perkin Trans.*, 2:1967, 1998.

- [18] A. K. Croft, C. J. Easton, and L. Radom. *J. Am. Chem. Soc.*, 124:4119–4124, 2003.
- [19] T. Nauser and C. Schöneich. *J. Am. Chem. Soc.*, 125:2003–2004, 2003.
- [20] H.-J. Werner, P. J. Knowles, R. Lindh, F. R. Manby, M. Schütz, P. Celani, T. Korona, A. Mitrushenkov, G. Rauhut, T. B. Adler, R. D. Amos, A. Bernhardsson, A. Berning, D. L. Cooper, M. J. O. Deegan, A. J. Dobbyn, F. Eckert, E. Goll, C. Hampel, G. Hetzer, T. Hrenar, G. Knizia, C. Köppl, Y. Liu, A. W. Lloyd, R. A. Mata, A. J. May, S. J. McNicholas, W. Meyer, M. E. Mura, A. Nicklaß, P. Palmieri, K. Pflüger, R. Pitzer, M. Reiher, U. Schumann, H. Stoll, A. J. Stone, R. Tarroni, T. Thorsteinsson, M. Wang, and A. Wolf. MOLPRO, version 2012.1, *a package of ab initio programs*.
- [21] M. J. Frisch, G. W. Trucks, H. B. Schlegel, G. E. Scuseria, M. A. Robb, J. R. Cheeseman, J. A. Montgomery, Jr., T. Vreven, K. N. Kudin, J. C. Burant, J. M. Millam, S. S. Iyengar, J. Tomasi, V. Barone, B. Mennucci, M. Cossi, G. Scalmani, N. Rega, G. A. Petersson, H. Nakatsuji, M. Hada, M. Ehara, K. Toyota, R. Fukuda, J. Hasegawa, M. Ishida, T. Nakajima, Y. Honda, O. Kitao, H. Nakai, M. Klene, X. Li, J. E. Knox, H. P. Hratchian, J. B. Cross, V. Bakken, C. Adamo, J. Jaramillo, R. Gomperts, R. E. Stratmann, O. Yazyev, A. J. Austin, R. Cammi, C. Pomelli, J. Ochterski, P. Y. Ayala, K. Morokuma, G. A. Voth, P. Salvador, J. J. Dannenberg, V. G. Zakrzewski, S. Dapprich, A. D. Daniels, M. C. Strain, O. Farkas, D. K. Malick, A. D. Rabuck, K. Raghavachari, J. B. Foresman, J. V. Ortiz, Q. Cui, A. G. Baboul, S. Clifford, J. Cioslowski, B. B. Stefanov, G. Liu, A. Liashenko, P. Piskorz, I. Komaromi, R. L. Martin, D. J. Fox, T. Keith, M. A. Al-Laham, C. Y. Peng, A. Nanayakkara, M. Challacombe, P. M. W. Gill, B. G. Johnson, W. Chen, M. W. Wong, C. Gonzalez, and J. A. Pople, 2009. GAUSSIAN 09 (Revision C.01), Gaussian, Inc., Wallingford, CT.

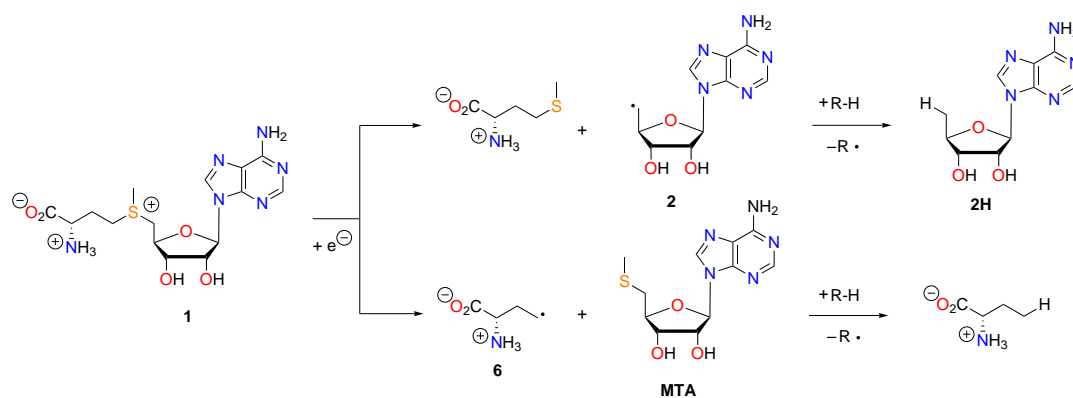
Chapter 5

Hydrogen Transfer in SAM-Mediated Enzymatic Radical Reactions

Published in: J. Hioe, H. Zipse, *Chem. Eur. J.*, **2012**, *18*, 16463 - 16472.

5.1 Introduction

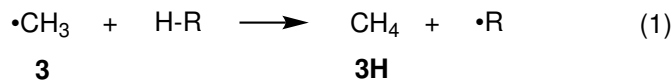
S-Adenosylmethionine (SAM, **1**) is an important cofactor in enzyme-mediated radical reactions.^[1–4] The mechanism of action of this sulfonium species is believed to involve initial coordination to a protein-bound $[\text{Fe}_4\text{S}_4]$ cluster, whose one electron reduction triggers the cleavage of one of the C-S bonds in SAM through a dissociative electron-transfer process (Scheme 5.1). This SET step is commonly believed to generate a transient C5'-adenosyl radical **2**, whose subsequent reaction with a hydrogen atom donor generates the (experimentally observed) C5'-desoxyadenosine **2H** byproduct. The observation of 5'-deoxy-5'-(methylthio)adenosine (MTA) in recent studies of the SAM-dependent activation of glycerol dehydratase^[5] and diphthamide biosynthesis^[6] hints at the formation of radical **6** as a possible alternative intermediate in reductive SAM cleavage. This latter radical may subsequently engage in the same radical reactions as adenosyl radical **2**. Based on the analysis of sequence databases it is currently believed that more than 3000 radical SAM enzymes exist,^[1;2;7] a small number of which has been biochemically characterized. It is generally assumed that the use of SAM in radical enzymes can either be stoichiometric or catalytic. Using a combination of experimentally measured and theoretically calculated thermochemical data it has recently been shown for pyruvate formate lyase activating enzyme (PFL-AE) as a representative of the first subgroup that hydrogen abstraction by adenosyl radical **2** is highly exothermic.^[8;9] Applying the same type of analysis to the mechanism proposed for spore photoproduct lyase (SPL) as a representative of the second (catalytic) subgroup it was found that at least one of the hydrogen-transfer steps in the catalytic cycle is significantly endothermic.^[8;9] To establish thermochemical profiles for a larger number of SAM-dependent enzymes of both subgroups we now report new results for the hydrogen transfer energetics in glycerol dehydratase (GD), biotin synthase (BioB), coproporphyrinogen III oxidase (HemN), fosfomycin synthase (Fom3), and RNA methylating enzyme RlmN. The hydrogen-transfer energetics for all of these systems will subsequently be used to identify mechanistic limits for the enzyme subgroups using SAM in a stoichiometric or catalytic fashion.



Scheme 5.1: Generation of C5'-desoxyadenosine by single electron transfer from a protein-bound iron-sulfur cluster.

5.2 Results and Discussion

The stability of carbon-centered radicals $R\cdot$ can be quantified using a formal hydrogen-transfer reaction between a closed-shell precursor $R-H$ and an unbiased reference radical such as $CH_3\cdot$ (**3**) as given in Equation (1). The reaction enthalpy at 298.15



K for this process as defined by equation (2) is often termed radical stabilization energy (RSE) of radical $R\cdot$, which implies that the reference system is given a stability value of 0.0 kJ mol⁻¹.^[8-14] Using this definition, negative RSE values imply a higher stability of radicals $R\cdot$ as compared to the reference radical $CH_3\cdot$ (**3**). Combination

$$RSE(R\cdot) = H_{298}(R\cdot) + H_{298}(CH_4) - H_{298}(R-H) - H_{298}(\cdot CH_3) \quad (2)$$

of the (theoretically calculated) RSE values with the experimentally measured bond dissociation energy (BDE) for $H-CH_3$ (**3H**, +439.3 ± 0.4 kJ mol⁻¹)^[15] offers a convenient way for the calculation of BDE values in hydrocarbons $R-H$ according to Equation (3). In a completely analogous manner, the stability of N-centered radi-

$$BDE(R-H) = BDE(CH_3-H) + RSE(R\cdot) \quad (3)$$

cals can also be defined with ammonia (**4H**) and the aminyl radical $NH_2\cdot$ (**4**) as the reference system (see appendix B). RSE values can, in principle, be calculated using experimentally measured or theoretically calculated enthalpies. Due to the lack of experimental data for the systems studied here, we use a hierarchy of different theoretical methods with generally increasing predictive value in the order B3LYP < ROMP2 < G3(MP2)-RAD < G3(+2d,MP2)-RAD ≈ G3B3 (Table 5.1). Where available, estimates of the respective BDE values from experimental data have also been added. From all these methods the G3(MP2)-RAD level is the most broadly tested for the prediction of thermochemical stabilities of radicals.^[16-18] All energies given below correspond to reaction enthalpies at 298.15 K (ΔH_{298}), but we note that owing to the nature of the defining stability equation (1), rather similar results are obtained when using energies at 0 K (ΔE_0) or free energies at 298.15 K (ΔG_{298}). Figure 5.1 summarizes the calculated RSE and BDE values at G3(MP2)-RAD level in a pictorial manner.

Table 5.1: Radical stabilization energies (RSE, in kJ mol⁻¹) of radicals, which are involved in adenosyl chemistry.

System	B3LYP ^a	ROMP2 ^b	G3(MP2)-RAD	G3(+2d,MP2)-RAD	G3B3	RSE exp.	BDE(X-H) exp.
36	+42.8	+64.6	+57.3	+56.0	+53.6	n.a.	n.a.
35	+39.2	+61.7	+54.9	+53.5	+51.5	n.a.	n.a.
38	+30.3	+50.5	+44.0	+43.1	+50.7	+29.3	+468.6 ± 8.4 ^c
37	+25.5	+47.4	+42.8	+41.6	+40.5	n.a.	n.a.
33	+24.2	+41.7	+36.9	+35.9	+42.0	+32.9	+472.2 ± 2.2 ^d
31	+8.4	+27.8	+24.0	+22.8	+20.7	n.a.	n.a.
32	+9.1	+27.0	+23.3	+22.2	+25.5	-29.3	+410.0 ± 8.4 ^c
34	+2.3	+22.3	+17.0	+15.4	+20.6	0.0	+439.3 ± 0.8 ^c
42	-5.5	+5.3	+3.3	+2.4	+2.1	n.a.	n.a.
41	-9.3	+3.3	+0.9	+0.1	n.a.	n.a.	n.a.
3	0.0	0.0	0.0	0.0	0.0	0.0	+439.3 ± 0.4 ^e
2	n.a.	n.a.	-6.9	n.a.	n.a.	n.a.	n.a.
11a	-20.6	-9.0	-10.3	-10.5	n.a.	n.a.	n.a.
7	-19.1(-18.9 ^f)	-10.6(-10.5 ^f)	-11.7(-11.6 ^f)	n.a.	n.a.	n.a.	n.a.
20	-32.3(-31.8 ^f)	-13.8(-12.8 ^f)	-16.2(-15.0 ^f)	n.a.	n.a.	n.a.	n.a.
11b	-38.3	-18.8	-21.1	-21.5	n.a.	n.a.	n.a.
21	-56.2(-55.6 ^f)	-31.1(-30.4 ^f)	-32.9(-32.4 ^f)	n.a.	n.a.	n.a.	n.a.
17	-56.9	-40.1	-39.9	-40.5	-41.4	n.a.	n.a.
43	-44.4	-39.3	-41.0	-42.7	-42.9	-47.3	+392.0 ± 5.9 ^e
44	-45.1	-39.4	-41.3	n.a.	n.a.	n.a.	n.a.
24	n.a.	n.a.	-45.9	n.a.	-47.3	n.a.	n.a.
25	n.a.	n.a.	-61.6	n.a.	-60.2	n.a.	n.a.
14	-82.8(-82.8 ^f)	-57.8(-56.8 ^f)	-61.4(-60.9 ^f)	n.a.	n.a.	n.a.	n.a.
5	n.a.	n.a.	-74.1	n.a.	-75.5	n.a.	n.a.
4	0.0	0.0	0.0	0.0	0.0	0.0	+450.1 ± 0.2 ^e
39	-21.3	+2.7	-15.5	-13.9	-8.7	n.a.	n.a.
40	-120.5	-95.5	-108.0	-109.0	n.a.	n.a.	n.a.

^aΔH₂₉₈ B3LYP/6-31G(d).^bΔH₂₉₈ ROMP2/G3MP2Large.^cSee ref. 19^dSee ref. 20^eSee ref. 21^fBest conformer only.

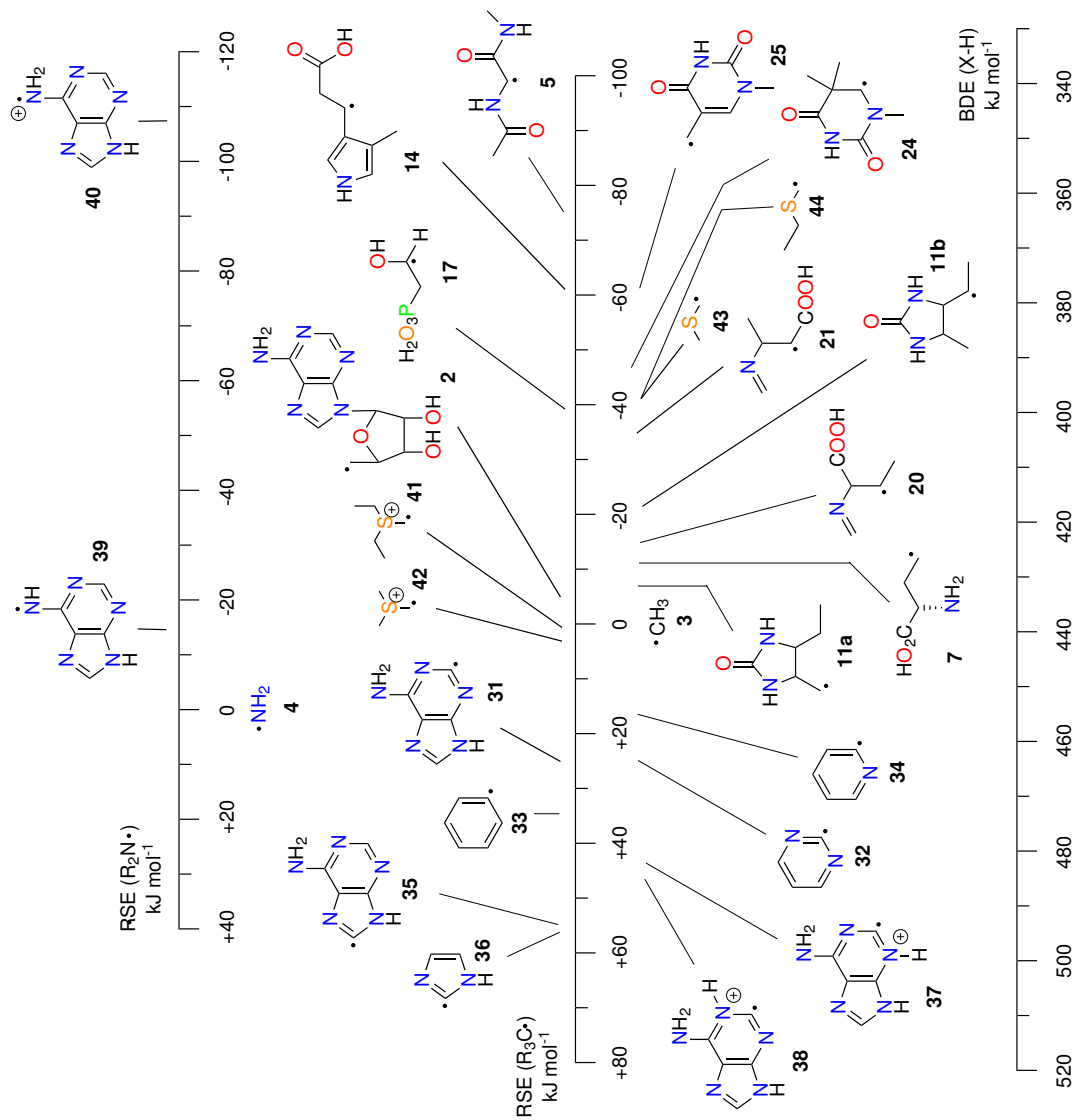
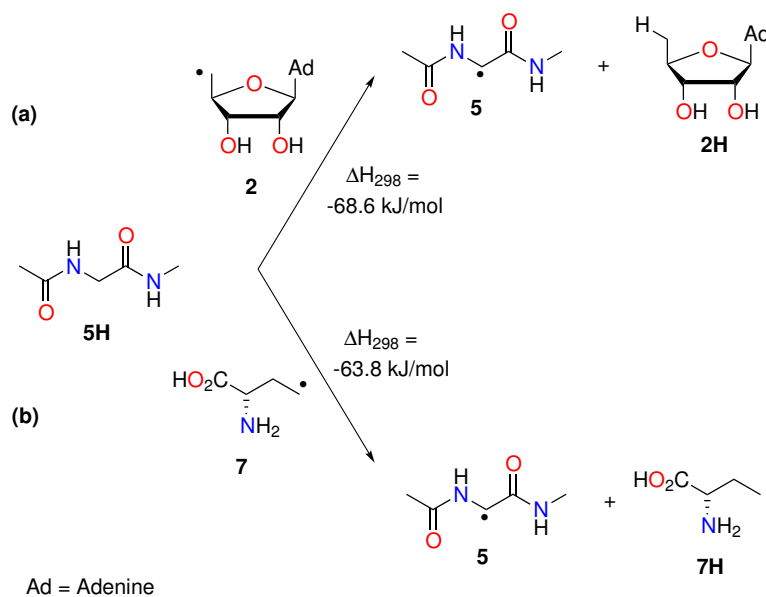


Figure 5.1: RSE and BDE scales for C- and N-centered radicals (ΔH_{298} , G3(MP2)-RAD [kJ mol^{-1}]).

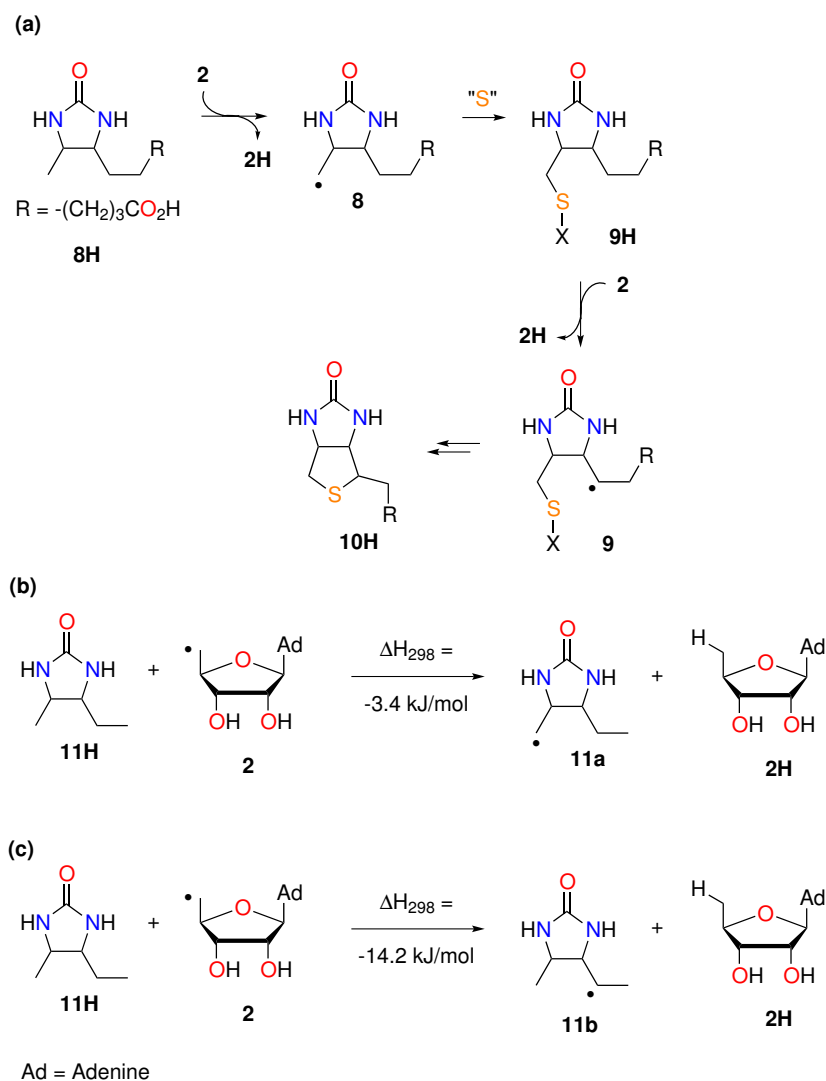
Radical enzymes using SAM as co-substrate:

The most prominent class of enzymes using SAM as a co-substrate is that of glycy radical enzymes (GRE), whose activation involves the combined action of SAM (1), an activating enzyme, and a one-electron reducing agent. Reductive electron transfer to SAM is in these systems followed by generation of adenosyl radical **2** and hydrogen abstraction from the C(α)-position of glycine residues (Scheme 5.2). Well-studied enzymes of this class include pyruvate formate lyase (PFL, PFL-AE), anaerobic ribonucleotide reductase (ARR, ARR-AE), B₁₂-independent glycerol dehydratase (GD, GDAE), and benzylsuccinate synthase (Bss, Bss-AE).^[1;5;22] The thermodynamics of the hydrogen abstraction step involving adenosyl radical **2** and glycine residues can be assessed by comparing the stability data of glycy radical **5** with $RSE(\mathbf{5}) = -75.5 \text{ kJ mol}^{-1}$ and adenosyl radical **2** (Scheme 5.2a).^[23] This yields a strongly exothermic reaction with $\Delta H_{298} = -68.6 \text{ kJ mol}^{-1}$.^[8;9] It has been mentioned above that 5'-deoxy-5'-(methylthio)adenosine (MTA) has been observed in recent studies of the SAM-dependent activation of glycerol dehydratase, hinting at radical **6** as a possible alternative intermediate in reductive SAM cleavage.^[5] The stability of 3-amino-3-carboxypropyl radical **7**, used here as a neutral model for zwitterionic radical **6**, is predicted to be $RSE(\mathbf{7}) = -11.7 \text{ kJ mol}^{-1}$. This is closely similar to other primary carbon-centered radicals and also to adenosyl radical **2**. The reaction of glycine dipeptide **5** with radical **7** is therefore similarly exothermic as before with $\Delta H_{298} = -63.8 \text{ kJ mol}^{-1}$ (Scheme 5.2b). MTA has recently also been observed in the context of diphthamide biosynthesis and the formation of radicals **6/7** in SAM-dependent enzymes may thus be more widespread than previously believed.^[6]



Scheme 5.2: H-abstraction from glycine dipeptide model **5H** using a) adenosyl radical **2** or b) 3-amino-3-carboxypropyl radical **7**.

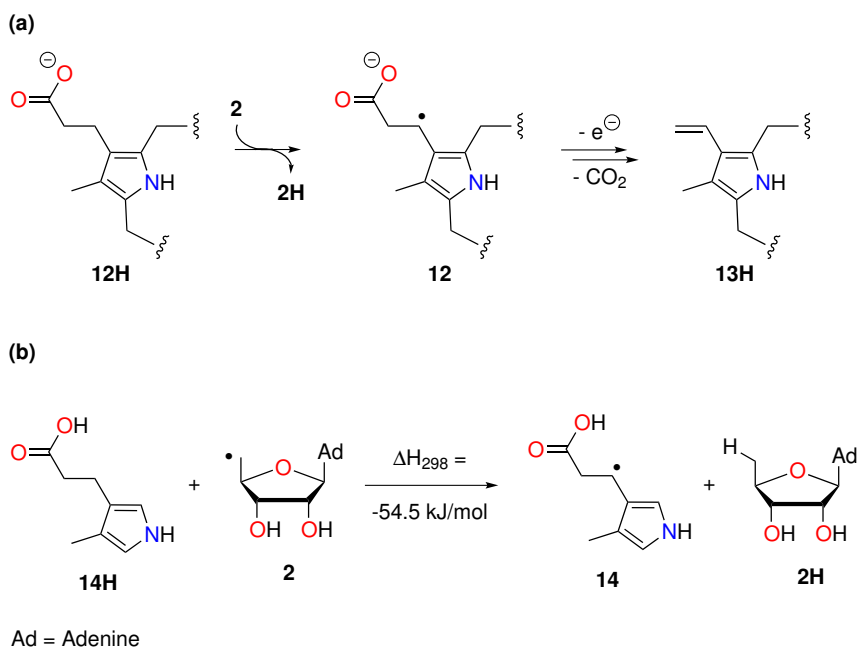
A second prominent system involving SAM-mediated radical chemistry is biotin synthase (BioB).^[1;24;25] As in the glycy radical enzymes, SAM functions as a co-substrate in this case and the SAM-derived adenosyl radical **2** is involved in C-H abstraction reactions in an irreversible fashion. The primary substrate in this transformation is dethiobiotin (**8H**), whose reaction with a first equivalent of SAM-derived radicals **2** yields substrate radical **8** and desoxyadenosine **2H**. Trapping of radical **8** with a sulfur-donor yields closed-shell intermediate **9H**, whose reaction with a second SAM-derived adenosyl radical **2** yields the second substrate radical **9** and generates the final product biotin **10H** through a concluding cyclization step (Scheme 5.3a). The two substrate radicals **8** and **9** in this mechanism can be classified as primary and secondary alkyl radicals, whose characteristics can readily be assessed using the radicals **11a** and **11b**. The stability of primary radical **11a** formed in the first step of the substrate mechanism is rather similar to that of other primary alkyl radicals with $\text{RSE}(\mathbf{11a}) = -10.3 \text{ kJ mol}^{-1}$, and its formation through reaction of **11H** with adenosyl radical **2** is therefore almost thermoneutral with $\Delta H_{298} = -3.4 \text{ kJ mol}^{-1}$ (Scheme 5.3b). Secondary radical **11b** formed in the second step of the substrate mechanism is slightly more stable with $\text{RSE}(\mathbf{11b}) = -21.1 \text{ kJ mol}^{-1}$. Generation of this species through reaction of adenosyl radical **2** with **11H** is correspondingly more exothermic, but the reaction enthalpy remains small at $\Delta H_{298} = -14.2 \text{ kJ mol}^{-1}$ (Scheme 5.3c). Taken together we can conclude that both H-abstraction steps in the biotin synthase substrate reaction are mildly exothermic. The situation is largely similar in lipoyl synthase (LipA), in which SAM-derived adenosyl radicals **2** are believed to activate the C8 and C6 positions of the octanoate substrate, again giving rise to primary and secondary alkyl radicals of prototypical stability.^[1]



Scheme 5.3: a) Substrate mechanism of biotin synthase and H-abstraction from desoxybiotin model **11H** with adenosyl radical **2** generating b) substrate radical **11a** or c) substrate radical **11b**.

A third example involving SAM-derived adenosyl radicals as co-substrates is coproporphyrinogen III oxidase (HemN).^[1;2;26] This enzyme catalyzes the oxidative decarboxylation of two of the four propionate side chains in coproporphyrinogen III and thus a key step of porphyrin biosynthesis under anaerobic conditions. Each decarboxylation step is considered to be an independent event involving initial hydrogen abstraction through adenosyl radical **2** from a position on the propionate side chain next to one of the pyrrole rings and subsequent one-electron oxidation and decarboxylation of intermediate radical **12** to yield product **13H** with a vinyl side chain (Scheme 5.4a). The unpaired spin in substrate radical **12** is formally located next to an aromatic π -system and the stability of this radical may thus be similar to that of other (hetero)benzylic radicals. Using substrate model **14H** this is indeed found to be the case with $RSE(\mathbf{14}) = -61.4 \text{ kJ mol}^{-1}$, a value closely similar

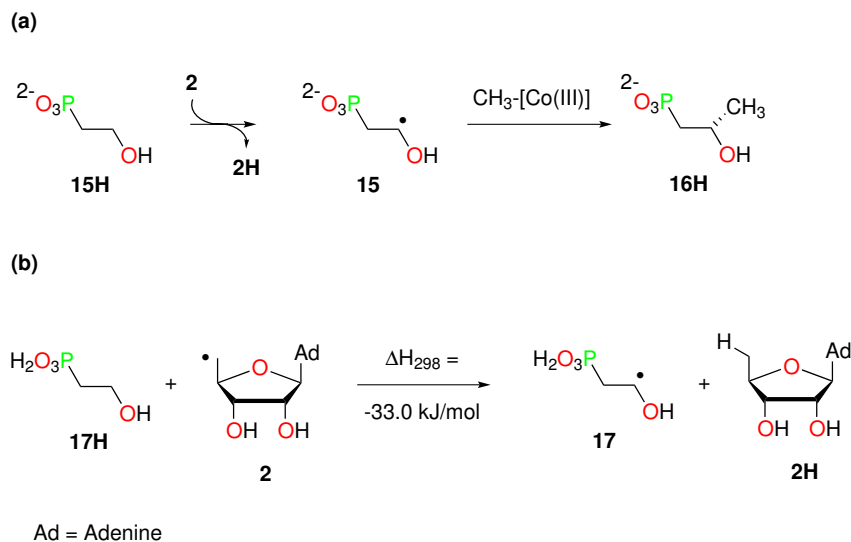
to that of the prototypical benzyl radical $\text{RSE}(\text{PhCH}_2\cdot) = -61.0 \text{ kJ mol}^{-1}$.^[13] Generation of substrate radical **14** through reaction of **14H** with adenosyl radical **2** is thus predicted to be significantly exothermic with $\Delta H_{298} = -54.5 \text{ kJ mol}^{-1}$ (Scheme 5.4b).



Scheme 5.4: a) Substrate mechanism of coproporphyrinogen III oxidase and b) reaction of adenosyl radical **2** with substrate model **14H**.

A somewhat less well explored area of SAM derived radical chemistry concerns the methylation of antibiotics as is, for example, the case in the penultimate step of fosfomycin biosynthesis.^[1;2] This reaction is catalyzed by enzyme Fom3 and uses SAM and methylcobalamine (MeCbl) as cofactors in the methylation of hydroxyethyl phosphonate **15H** (Scheme 5.5a). The current working mechanism involves initial reaction of SAM-derived adenosyl radical **2** with hydroxyethyl phosphonate to yield substrate radical **15**. This latter species reacts with methylcobalamine in an otherwise unknown methyl radical transfer step to yield the methylated phosphonate **16H**. The stability of substrate radical **15** is mainly determined by the hydroxy substituent attached to the radical center, whose stabilizing effect is due to lone pair electron donation.^[11-13] A prototypical example for this type of system is the ethanol-1-yl radical with $\text{RSE}(\cdot\text{CH}(\text{OH})\text{CH}_3) = -38.3 \text{ kJ mol}^{-1}$. The model substrate radical **17** chosen here is only marginally more stable with $\text{RSE}(\mathbf{17}) = -39.9 \text{ kJ mol}^{-1}$, indicating only a small influence of the phosphonate side chain. This implies that reaction of substrate model **17H** with adenosyl radical **2** is exothermic by $\Delta H_{298} = -33.0 \text{ kJ mol}^{-1}$ (Scheme 5.5b). We note in passing that the stability of radicals with α -hydroxy substituents depends markedly on the hydrogen bonding environment of the hydroxy group, coordination with anionic H-bond acceptors leading to more stable radicals. This point has been explored in large detail in

the context of the substrate mechanism of class I ribonucleotide reductase (RNR I).^[27–30]

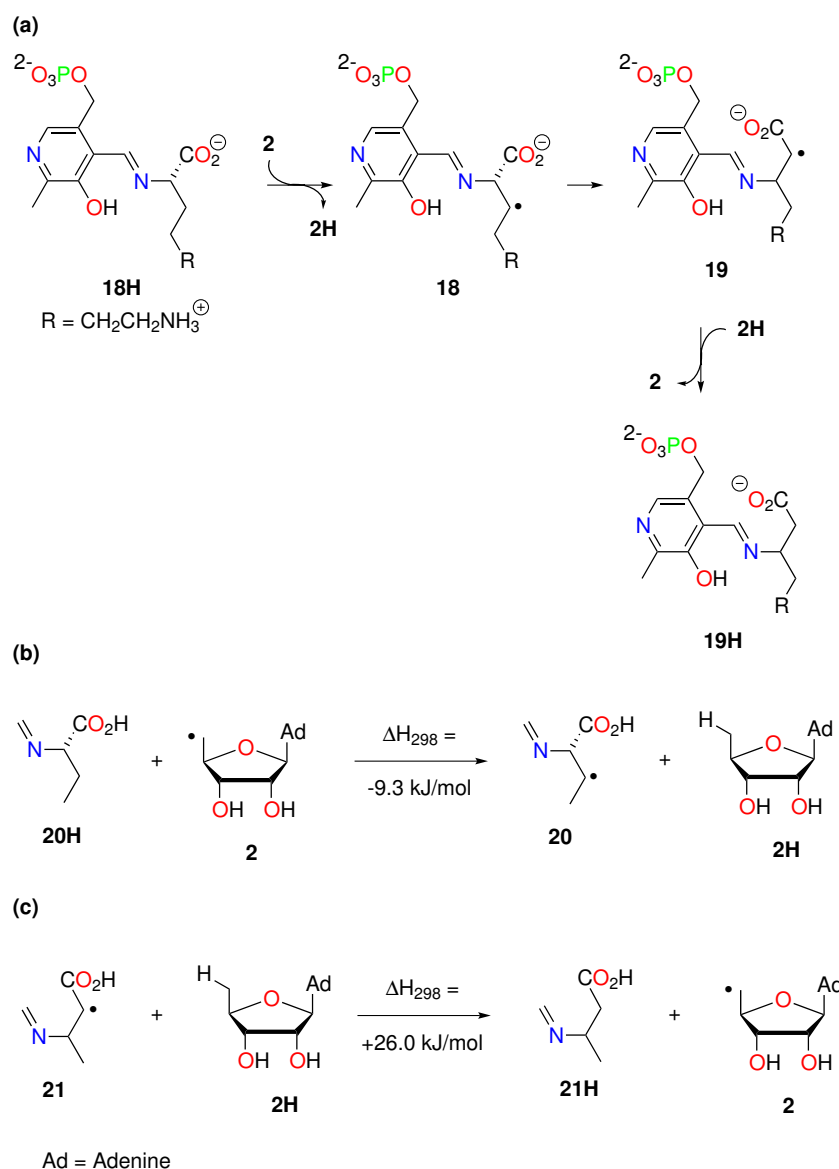


Scheme 5.5: a) Substrate mechanism of Fom3 and b) reaction of adenosyl radical **2** with substrate model **17H**.

Radical enzymes using SAM as co-catalyst:

Lysine-2,3-aminomutase (LAM) catalyzes the relocation of the amino group from the C(α) to the adjacent C(β) position in lysine and is one of the best studied radical enzymes using SAM in a catalytic fashion.^[1;2] An additional cofactor required by LAM for substrate turnover is pyridoxal-5'-phosphate (PLP), whose reaction with the substrate amino group provides the actual aldimine substrate **18H** for the radical reaction (Scheme 5.6a). Generation of adenosyl radical **2** in the active site and subsequent hydrogen transfer generates a first substrate radical **18**. Migration of the imine group then proceeds through an addition/elimination mechanism to furnish a second substrate radical **19**.^[31] This latter species then reabstracts one of the C5' hydrogen atoms in C5'-dehydroadenosine **2H** and thus regenerates adenosyl radical **2**. The two substrate radicals **18** and **19** proposed in this mechanism differ significantly in their stability. Radical **18** is a secondary aliphatic radical, whose stability can be estimated with the model radical **20**. In view of its structure it is not surprising that the stability of this latter species of $\text{RSE}(\mathbf{20}) = -16.2 \text{ kJ mol}^{-1}$ is rather similar to that of other secondary aliphatic radicals. The stability of the prototypical isopropyl radical, for example, amounts to $\text{RSE}(\cdot\text{CH}(\text{CH}_3)_2) = -23.0 \text{ kJ mol}^{-1}$.^[13] The second substrate radical **19** is significantly more stable due to resonance delocalization of the unpaired spin into the carboxylate group p-system. The stability of model radical **21** amounts to $\text{RSE}(\mathbf{21}) = -32.9 \text{ kJ mol}^{-1}$, in close proximity to radicals of similar structure such as the propanoic acid-2-yl radical with $\text{RSE}(\cdot\text{CH}(\text{CH}_3)\text{COOH}) = -41.9 \text{ kJ mol}^{-1}$.^[13] Using the stability values for radicals **20** and **21**, the reaction enthalpy for reaction of adenosyl radical **2** with precursor

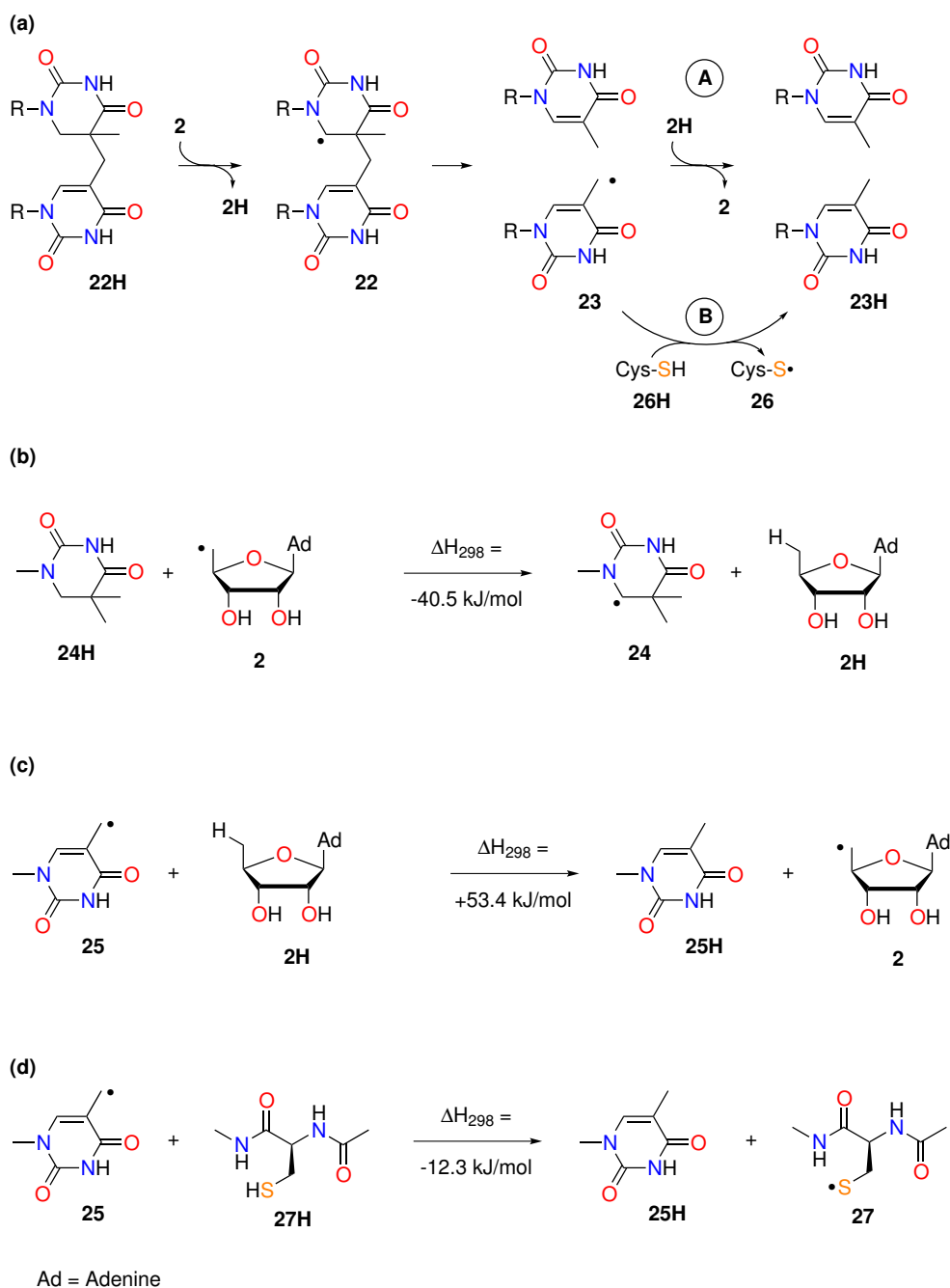
20H equates to $\Delta H_{298} = -9.3 \text{ kJ mol}^{-1}$ (Scheme 5.6b) and that for reaction of substrate radical **21** with desoxyadenosine **2H** to $\Delta H_{298} = +26.0 \text{ kJ mol}^{-1}$ (Scheme 5.6c). In contrast to the results obtained for enzymes using SAM-derived adenosyl radicals in a stoichiometric fashion, we now see here that the catalytic use of SAM involves a final endothermic step linked to regeneration of the (intrinsically unstable) adenosyl radical **2**. The endothermicity of the final step is due to the resonance delocalization of the unpaired spin into the attached carboxylate group, which is held in place in the enzyme active site through an arginine salt bridge.^[32] Through orientational control of the carboxylate group relative to the radical center, the endothermicity of the last step can thus be tuned towards smaller endothermicities. The energetics of fully decoupling carboxylate group and radical center can be assessed through calculation of the respective rotational barrier, which amounts to $+36.9 \text{ kJ mol}^{-1}$ in radical **21** at the G3(MP2)-RAD level. This large value implies that even a moderate degree of rotation around the bond linking radical center and carboxylate group may be sufficient to modulate the endothermicity of the final step significantly.



Scheme 5.6: a) Part of the substrate mechanism of LAM, b) reaction of adenosyl radical **2** with substrate model **20H**. c) Reaction of product radical **21** with desoxyadenosine **2H**.

A second system, in which a catalytic role of SAM has been proposed, is that of spore photoproduct lyase (SPL).^[1;2;33] This enzyme repairs damaged thymine bases in the genome of bacterial endospores and is one of the few SAM-dependent radical enzymes acting on a polymeric substrate. As shown in Scheme 5.7a the thymine dimer generated through UV irradiation contains a C-C cross link between two adjacent thymine bases. Cleavage of this cross link is initiated through hydrogen abstraction of SAM-derived adenosyl radicals **2** from a position directly adjacent to the C-C cross link. Subsequent rupture of the C-C bond in substrate radical **22** restores the two thymine bases, one in its fully intact closed-shell form and one as an allyl radical (**23**). One of the most often proposed mechanisms (here termed path

A) then calls for hydrogen transfer between radical **23** and desoxyadenosine **2H**, which leads to a fully repaired second thymine base and adenosyl radical **2**.^[1;2;34-44] A second mechanism (**B**) based on the analysis of deuterium labeling experiments invokes hydrogen transfer between a cystein residue present in the active site and substrate radical **23**, which also leads to a fully repaired thymine base, but relocates the regeneration of adenosyl radical **2** (and/or the SAM cofactor) to a later stage of the catalytic cycle.^[2;33;45-48] This mechanism is strongly supported by the recently solved SPL crystal structure from *G. thermodenitrificans*.^[49] The thermodynamic requirements of the initial hydrogen-transfer step can be assessed using substrate model **24H**, whose reaction with adenosyl radical **2** is exothermic by $\Delta H_{298} = -40.4$ kJ mol⁻¹. This large exothermicity is due to the stabilizing nature of the amide nitrogen neighbor in radical **24** and its stability of $\text{RSE}(\mathbf{24}) = -47.3$ kJ mol⁻¹ is therefore quite comparable to that of other α -amino- or α -amidoalkyl radicals.^[8;9] The second substrate radical **23** obtained after C-C bond cleavage can formally be classified as an allylic radical, but the additional substituents present in the system may also influence its stability. For model radical **25** a stability value of $\text{RSE}(\mathbf{25}) = -60.2$ kJ mol⁻¹ is obtained, slightly less than for the prototypical allyl radical with $\text{RSE}(\bullet\text{CH}_2\text{CHCH}_2) = -71.5$ kJ mol⁻¹.^[13] These values imply a large positive reaction enthalpy for the reaction of radical **25** with desoxyadenosine **2H** of $\Delta H_{298} = +53.4$ kJ mol⁻¹.



Scheme 5.7: a) Substrate mechanism of the SPL-catalyzed repair process. b) Reaction of adenosyl radical **2** with substrate model **24H**. c) Reaction of product radical **25** with desoxyadenosine **2H**. d) Reaction of product radical **25** with cysteine dipeptide **27H**.

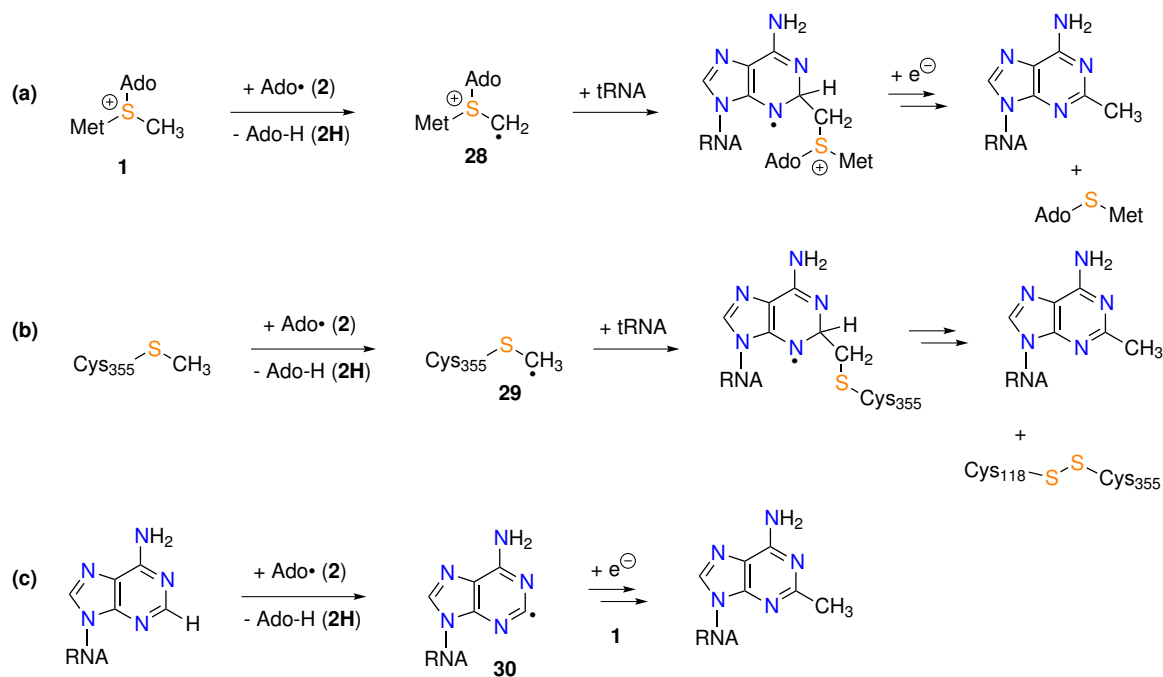
The thermochemically demanding character of path **A** contrasts with that of path **B**, in which hydrogen transfer occurs between substrate radical **23** and a cysteine thiol group. Using the S-H bond dissociation energy in cysteine dipeptide **27H** of $\text{BDE}(\text{S-H}) = +366.8 \text{ kJ mol}^{-1}$ obtained in a recent theoretical study^[8;9] and the allylic C-H bond strength in **25H** of $\text{BDE}(\text{C-H}) = +379.1 \text{ kJ mol}^{-1}$, a reaction enthalpy of ΔH_{298}

= $-12.3 \text{ kJ mol}^{-1}$ is calculated for path **B**. From a thermochemical point of view path **B** is thus significantly more attractive than path **A**. The fate of the cysteinyl radical generated in path **B** is, unfortunately, not known at the moment and the question, how the catalytic cycle can be closed to arrive at adenosyl radical **2** or, at the very least, the initial substrate radical **22** thus remains open at the moment. The simple most catalytic mechanism involves the direct reaction of the finally generated cysteinyl radical **26** with the next substrate molecule **22H**. The data given in Scheme 5.7 can be used to evaluate the thermodynamic requirements of such a process, as the stability value for substrate radical **24** of $\text{RSE}(\mathbf{24}) = -47.3 \text{ kJ mol}^{-1}$ equates to $\text{BDE}(\text{C-H}) = +392.0 \text{ kJ mol}^{-1}$ in substrate model **24H**. Comparison to the $\text{BDE}(\text{S-H})$ value for cystein dipeptide **27H** yields a reaction enthalpy of $\Delta H_{298} = +25.2 \text{ kJ mol}^{-1}$ for the hydrogen-transfer reaction between substrate **24H** and cysteinyl radical **27**. Compared to the current literature mechanism involving adenosyl radical **2** in the initial and terminal reaction steps and with a "steep" thermochemical profile of $-40.5 \text{ kJ mol}^{-1}$ for the first and $+53.4 \text{ kJ mol}^{-1}$ for the last step, the alternative catalytic cycle involving cysteinyl radical **26** shows a comparatively "flat" thermochemical profile of $+25.2 \text{ kJ mol}^{-1}$ for the first and $-12.3 \text{ kJ mol}^{-1}$ for the last reaction step. In this latter case the SAM-induced generation of adenosyl radical **2** would merely be required to initiate the process, but not to propagate it. It should be added at this point that, due to the almost identical thermochemical stability of cysteinyl and tyrosyl radicals,^[10;23] the role of cysteine discussed here can also be filled by tyrosine. Together with the finding that the recently solved SPL protein structure contains a tyrosine residue in the active site, this may imply an even more direct involvement of protein based radicals in the SPL substrate mechanism.

Radical enzymes using SAM in RNA methylation:

It has recently been proposed in studies on mechanistic aspects of RNA methylation reactions that the radical chemistry of SAM may be significantly more complex than portrayed in Scheme 5.1. In a mechanism proposed by Fujimori *et al.* for the methylation of ribosomal RNA catalyzed by enzymes RlmN and Cfr, a first equivalent of SAM is utilized for the generation of C5'-adenosyl radical **2** as outlined in Scheme 5.8, whose reaction with a second equivalent of SAM leads to formation of a previously unknown sulfonylmethyl radical species **28** (Scheme 5.8a).^[50] Subsequent addition of this radical to the C2 position of the adenosine ring system, followed by further reduction and hydrogen-transfer steps, leads to C2-methylated adenosine. The same reaction was also studied by Booker *et al.*, who suggest that a first equivalent of SAM is used (without a redox step) for the methylation of cysteine residue Cys355. A second equivalent of SAM is then employed to generate adenosyl radical **2**, followed by hydrogen abstraction from the cysteine-bound methyl group (Scheme 5.8b).^[51-53] The previously unknown thiylmethyl radical **29** generated in this step then adds to the C2 position of the adenosine ring system, followed by a sequence of redox and proton transfer steps needed to ultimately generate C2-methylated adenosine.^[51;52;54] In both of these studies the equally possible direct activation of the adenosine C2 position through hydrogen abstraction

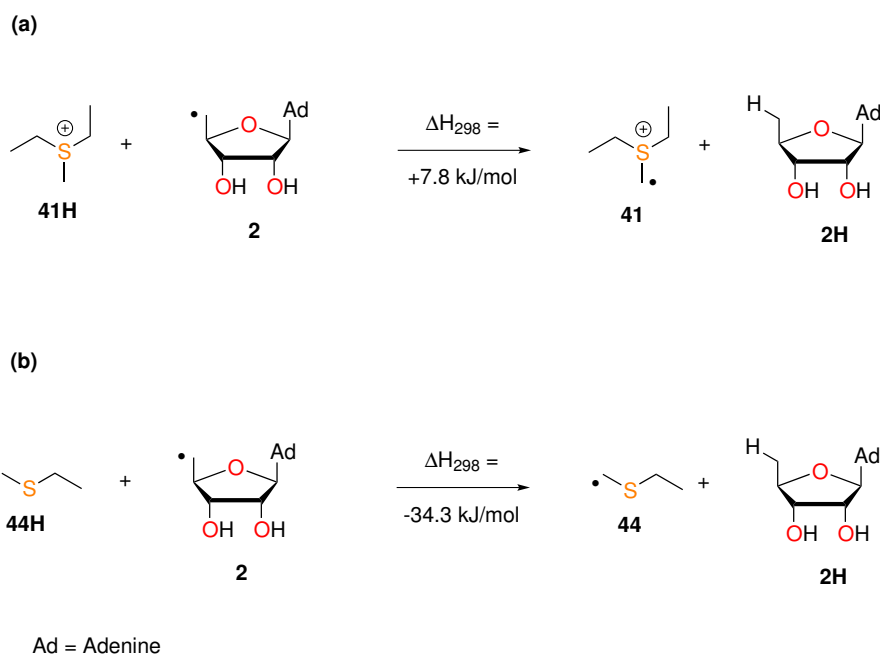
by adenosyl radical **2** (Scheme 5.8c) proposed in other studies of SAM-dependent enzymatic transformations was considered to be energetically too costly (and thus unlikely).^[55–57] From the stability data collected in Figure 5.1 and Table 5.1, we note that the C2-adenine radical **31** is similarly stable as the structurally related pyrimidine radical **32**, both of which are more stable than phenyl radical **33**, but less stable than C2-pyridine radical **34**. The stability values for pyridine radical **34** and pyrimidine radical **32** are at variance with experimental data obtained from fitting activation barriers for C-H bond rupture processes at higher temperature. These studies had predicted significantly more stable radicals and thus lower C-H BDE values for these systems.^[19] The same discrepancy had already been noted in earlier theoretical studies using a broad variety of methods.^[20;58] In addition to using validated compound methods such as G3(MP2)-RAD, the stability of pyrimidine radical **32** has also been determined using the more accurate U(R)CCSD(T)/CBS approach (see the Supporting Information for details). The U(R)CCSD(T)/CBS value for RSE(**32**) = +19.5 kJ mol⁻¹ is very close to that obtained at G3(MP2)-RAD level (+23.3 kJ mol⁻¹) and all following arguments will therefore be made using RSE values obtained at G3(MP2)-RAD level for all systems involved. The RSE value for C5'-adenosyl radical **2** amounts to -6.9 kJ mol⁻¹,^[8;9] a value lower than any of the aromatic σ -type radicals selected here.



Scheme 5.8: Possible methylation mechanisms of the C2 position of the adenosine ring.

Hydrogen abstraction by radical **2** from the C2 position of adenine yielding radical **31** is therefore endothermic by +30.9 kJ mol⁻¹, while hydrogen abstraction from the C8 position yielding radical **35** is endothermic by +61.8 kJ mol⁻¹. The stability of adenine-C8 radical **35** is quite similar to that of imidazol-2-yl radical **36** with

RSE(**36**) = +57.3 kJ mol⁻¹. The annulated pyrimidine ring in radical **35** thus seems to have only a limited influence on its stability. Additional consideration of adenine radicals bearing a proton at either N1 (radical **37**) or N3 (radical **38**) also shows that protonation of adenine will further increase the C-H bond energy at the C2 position. The (thermochemically) most attractive H-abstraction from adenine actually involves attack at the amino group hydrogens, yielding a spin-delocalized radical **39**. Protonation of this neutral species is highly favorable and the resulting radical cation **40** therefore one of the most stable radicals studied here. Under the conditions of enzymatic catalysis this will, of course, remain without any practical consequence. In conclusion it thus appears that hydrogen abstraction from the C2 and C8 positions in adenine involving adenosyl radical **2** will not be favorable from a thermochemical point of view. The RNA methylation mechanism proposed by Fujimori *et al.* involves hydrogen transfer between C5'-adenosyl radical **2** and SAM, generating sulfonylmethyl radical **28** as the first radical intermediate.^[50;55] This latter structure is modeled here using sulfonylmethyl radical **41**, whose stability value amounts to RSE(**41**) = +0.9 kJ mol⁻¹ at G3(MP2)-RAD level. Combination with the data for C5'-adenosyl radical **2** yields a reaction enthalpy for the hydrogen-transfer reaction shown in Scheme 5.9a of +7.8 kJ mol⁻¹. It should be added that the low stability of radical **41** seems to be typical for radicals carrying dialkylsulfonyl substituents, as a very similar stability value is also found for the sulfonylmethyl radical **42** (Figure 5.1). The alternative mechanism suggested by Booker *et al.* involves hydrogen transfer between adenosyl radical **2** and the methylated Cys355, and subsequent addition of the newly formed cysteinylmethyl radical to the C2 position of adenine. The energetics of this initial hydrogen-transfer step can be estimated with good accuracy using the RSE values for C5'-adenosyl radical **2** of RSE(**2**) = -6.9 kJ mol⁻¹ and for methylthioethyl radical **44** of RSE(**44**) = -41.3 kJ mol⁻¹.^[12] Combination of these values yields a reaction enthalpy of -34.4 kJ mol⁻¹. Comparing all hydrogen-transfer steps proposed in recent experimental studies of SAM-mediated adenosine methylation, we can thus conclude that the formation of a cysteine-derived thiomethyl radical **29** as proposed by Booker *et al.* is the only thermochemically favorable process, while formation of the SAM-derived radical cation **28** proposed by Fujimori *et al.* is mildly endothermic. The formation of adenine C2- and C8-radicals through hydrogen abstraction by adenosyl radical **2** is, in contrast, significantly more endothermic.



Scheme 5.9: Reaction of adenosyl radical **2** with a) substrate model **41H** and b) substrate model **44H**.

5.3 Conclusion

The thermodynamics of hydrogen-transfer reactions involving adenosyl radical **2** have been quantified for selected SAM-dependent enzymes. These include reactions using SAM in a stoichiometric fashion (as in glycyl radical enzyme activases) and those using SAM in a catalytic fashion (as is the case of LAM). An overview over all derived reaction enthalpies for hydrogen-transfer reactions is given in Figure 5.2. It is readily seen in this presentation that all reactions known to use SAM as a co-substrate involve exothermic hydrogen-transfer reactions between SAM-derived radicals and the respective substrates. The exothermicity is largest for the glycyl radical enzyme activases irrespective of whether adenosyl radical **2** or 3-amino-3-carboxypropyl radical **7** is used as the reaction partner. The least exothermic reactions are those in biotin synthase, in which relatively unstable primary and secondary hydrocarbon radicals are generated in the primary substrate activation steps. In contrast, all reactions using SAM in a catalytic fashion combine one exothermic with one endothermic hydrogen-transfer step in the catalytic cycle. The thermochemical profile of the LAM-catalyzed hydrogen-transfer reactions is found to be quite similar to that of the (hypothetical) SPL mechanism involving a chain-carrying cysteinyl radical. The alternative SPL mechanism involving a catalytic adenosyl radical **2** features hydrogen-transfer steps with significantly larger exo- and endothermicities. All reactions proposed in the context of RNA base methylation implicate a non-catalytic role of SAM. Should these reactions indeed proceed through direct attack of adenosyl radical **2** on the adenine C2 and C8 hydrogens, then these would rep-

resent the first radical reactions stoichiometric in SAM with large endothermicities. Reactions involving the initial formation of dialkylsulfonium methyl radicals such as **41** or thioalkylmethyl radical such as **44** are much more in line with all other stoichiometric SAM-mediated reactions. The latter of these two options is the most appealing on thermochemical grounds.

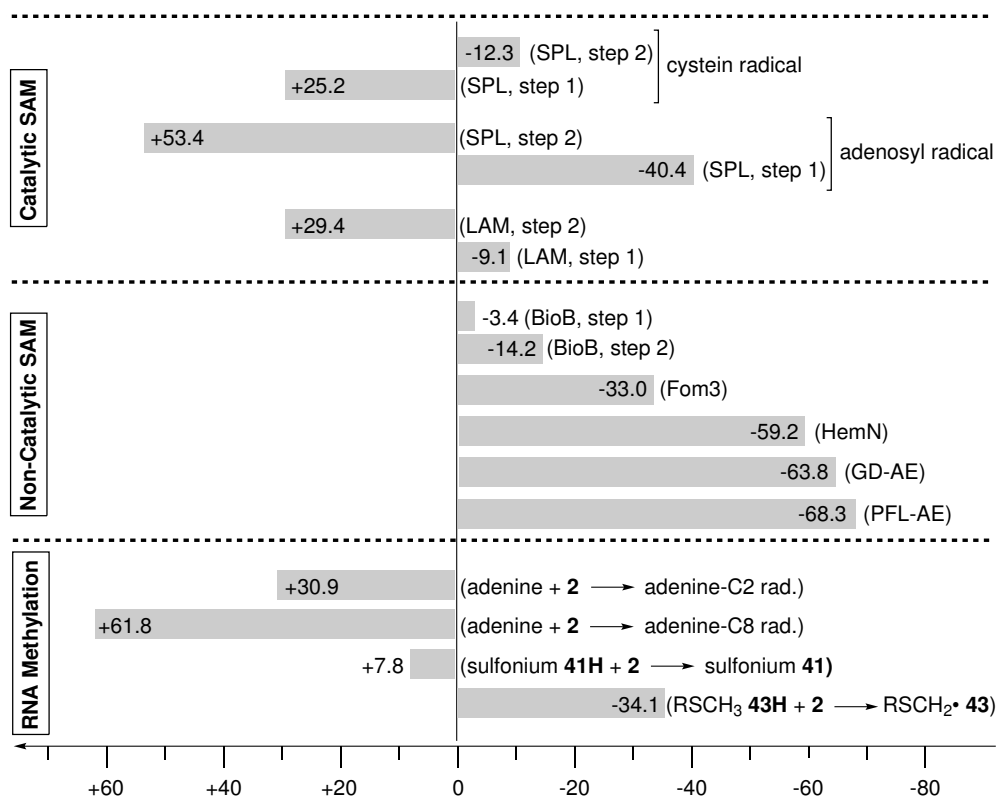


Figure 5.2: Thermochemical profiles for all discussed hydrogen-transfer reactions in SAM-mediated enzymatic radical reactions.

Acknowledgements

Financial support for this project by the Deutsche Forschungsgemeinschaft (grant Nos. Zi 436/13-1 and SFB 749) is gratefully acknowledged. We thank David M. Smith and Thomas Carell for valuable comments and suggestions.

Bibliography

- [1] P. A. Frey, A. D. Hegeman, and F. J. Ruzicka. *Crit. Rev. Biochem. Mol. Biol.*, 43:63–68, 2008.
- [2] E. N. Marsh, D. P. Patterson, and L. Li. *ChemBioChem.*, 11:604–621, 2010.
- [3] J. L. Vey and C. L. Drennan. *Chem. Rev.*, 111:2487–2506, 2011.

-
- [4] Q. Zhang, W. A. van der Donk, and W. Liu. *Acc. Chem. Res.*, 45:555–564, 2012.
- [5] W. N. Lanzilotta J. M. Demick. *Biochemistry*, 50:440–442, 2011.
- [6] Y. Zhang, X. Zhu, A. T. Rorelli, M. Lee, B. Dzikovski, R. M. Koralewski, E. Wang, J. Freed, C. Krebs, S. E. Ealick, and H. Lin. *Nature*, 465:891–896, 2010.
- [7] H. J. Sofia, G. Chen, B. G. Hetzler, J. F. Reyes-Spindola, and N. E. Miller. *Nucleic Acids Res.*, 29:1097–1106, 2001.
- [8] J. Hioe and H. Zipse. *Faraday Discuss.*, 145:301–313, 2010. and subsequent discussion, p. 381-409.
- [9] J. Hioe and H. Zipse. *Org. Biol. Chem.*, 8:3609–3617, 2010.
- [10] D. Griller and K. Ingold. *Acc. Chem. Res.*, 9:13–19, 1976.
- [11] H. Zipse. *Top. Curr. Chem.*, 263:163–189, 2006.
- [12] M. L. Coote, C. Y. Lin, and H. Zipse. *Carbon-Centered Free Radicals and Radicals Cations*, chapter "The Stability of Carbon-Centered Radicals", pages 83–104. M. D. E. Forbes (Ed.), John Wiley & Sons, 2010.
- [13] J. Hioe and H. Zipse. *Encyclopedia of Radicals in Chemistry, Biology and Materials*, chapter "Radical Stability-Thermochemical Aspects", pages 449–476. John Wiley & sons, 2012.
- [14] M. L. Coote, C. Y. Lin, A. L. J. Beckwith, and A. A. Zavitsas. *Phys. Chem. Chem. Phys.*, 12:9597–9610, 2010.
- [15] Y.-R. Luo. *Comprehensive Handbook of Chemical Bond Energies*. CRC Press, 2007.
- [16] D. J. Henry, C. J. Parkinson, P. M. Mayer, and L. Radom. *J. Phys. Chem. A*, 105:6750–6756, 2001.
- [17] D. J. Henry, C. J. Parkinson, and L. Radom. *J. Phys. Chem. A*, 106:7927–7936, 2002.
- [18] D. J. Henry, M. B. Sullivan, and L. Radom. *J. Chem. Phys.*, 118:4849–4860, 2003.
- [19] J. H. Kiefer, Q. Zhang, R. D. Kern, J. Yao, and B. Jursic. *J. Phys. Chem. A*, 101:7061–7073, 1997.
- [20] Y. Feng, J.-T. Wang, L. Liu, and Q.-X. Guo. *J. Phys. Org. Chem.*, 16:883–890, 2003.
-

- [21] K. M. Ervin and V. F. DeTuri. *J. Phys. Chem. A*, 106:9947–9956, 2002.
- [22] J. L. Vey, J. Yang, M. Li, W. E. Broderick, J. B. Broderick, and C. L. Drennan. *Proc. Natl. Acad. Sci. U. S. A.*, 105:16137–16141, 2008.
- [23] J. Hioe, G. Savasci, H. Brand, and H. Zipse. *Chem. Eur. J.*, 17:3781–3789, 2011.
- [24] M. Fontecave, S. Ollagnier de Choudens, and E. Mulliez. *Chem. Rev.*, 103:2149–2166, 2003.
- [25] C. J. Fugate and J. T. Jarrett. *BBA - Proteins and Proteomics*, 1824:1213–1222, 2012.
- [26] G. Layer, J. Reichlet, D. Jahn, and D. W. Heinz. *Protein Sci.*, 19:1213–1222, 2010.
- [27] R. Lenz and B. Giese. *J. Am. Chem. Soc.*, 119:2789–2794, 1997.
- [28] M. Mohr and H. Zipse. *Chem. Eur. J.*, 5:3046–3054, 1999.
- [29] M. Bennati, F. Lenzian, M. Schmittel, and H. Zipse. *Biol. Chem.*, 386:1007–1022, 2005.
- [30] P. Nordlund and P. Reichard. *Annu. Rev. Biochem.*, 75:681–706, 2006.
- [31] G. M. Sandala, D. M. Smith, and L. Radom. *J. Am. Chem. Soc.*, 128:16004–16005, 2006.
- [32] B. W. Lepore, F. J. Ruzicka, P. A. Frey, and D. Ringe. *Proc. Natl. Acad. Sci. U. S. A.*, 102:13819–13824, 2005.
- [33] L. Li. *BBA - Proteins and Proteomics*, 1824:1264–1277, 2012.
- [34] R. A. Mehl and T. P. Begley. *Org. Lett.*, 1:1065–1066, 1999.
- [35] R. Rebeil and W. L. Nicholson. *Proc. Natl. Acad. Sci. U. S. A.*, 98:9038–9043, 2001.
- [36] M. G. Friedel, O. Berteau, J. C. Pieck, M. Atta, S. Ollagnier de Choudens, M. Fontecave, and T. Carell. *Chem. Commun.*, pages 445–447, 2006.
- [37] J. C. Pieck, D. Kuch, F. Grolle, U. Linne, C. Haas, and T. Carell. *J. Am. Chem. Soc.*, 128:1404–1405, 2006.
- [38] J. C. Pieck, U. Hennecke, A. J. Pierik, M. G. Friedel, and T. Carell. *J. Biol. Chem.*, 281:36317–36326, 2006.
- [39] E. Bürckstümmer and T. Carell. *Chem. Commun*, pages 4037–4039, 2008.

- [40] K. Heil, A. C. Kneuttinger, S. Schneider, U. Lischke, and T. Carell. *Chem. Eur. J.*, 17:9651–9657, 2011.
- [41] J. Cheek and J. B. Broderick. *J. Am. Chem. Soc.*, 124:2860–2861, 2002.
- [42] J. M. Buis, J. Cheek, E. Kalliri, and J. B. Broderick. *J. Biol. Chem.*, 281:25994–26003, 2006.
- [43] T. Chandra, S. C. Silver, E. Zilinskas, E. M. Shepard, W. E. Broderick, and J. B. Broderick. *J. Am. Chem. Soc.*, 131:2420–2421, 2009.
- [44] S. C. Silver, T. Chandra, E. Zilinskas, S. Ghose, W. E. Broderick, and J. B. Broderick. *J. Biol. Inorg. Chem.*, 15:943–955, 2010.
- [45] L. Yang, G. Lin, D. Liu, K. J. Dria, J. Telsler, and L. Li. *J. Am. Chem. Soc.*, 133:10434–10447, 2011.
- [46] G. Lin, C.-H. Chen, M. Pink, J. Pu, and L. Li. *Chem. Eur. J.*, 17:9658–9668, 2011.
- [47] A. Chandor-Proust, O. Berteau, T. Douki, D. Gasparutto, S. Ollagnier-De-Choudens, M. Fontecave, and M. Atta. *J. Biol. Chem.*, 283:36361–36368, 2008.
- [48] A. Chandor, O. Berteau, T. Douki, D. Gasparutto, Y. Sanakis, S. Ollagnier-De-Choudens, M. Atta, and M. Fontecave. *J. Biol. Chem.*, 281:26922–26931, 2006.
- [49] A. Benjdia, K. Heil, T. R. M. Barends, T. Carell, and I. Schlichting. *Nucleic Acids Res.*, 40:9308–9318, 2012.
- [50] F. Yan and D. G. Fujimori. *Proc. Natl. Acad. Sci. U. S. A.*, 108:3930–3934, 2011.
- [51] T. L. Grove, J. S. Brenner, M. I. Radle, J. H. Ahlum, B. J. Landgraf, C. Krebs, and S. J. Booker. *Science*, 332:604–607, 2011.
- [52] J. Stubbe. *Science*, 332:544, 2011.
- [53] T. L. Grove, M. I. Radle, C. Krebs, and S. J. Booker. *J. Am. Chem. Soc.*, 133:19586–19589, 2011.
- [54] A. K. Boal, T. L. Grove, M. I. McLaughlin, N. H. Yennawar, S. J. Booker, and A. C. Rosenzweig. *Science*, 332:1089–1092, 2011.
- [55] F. Yan, J. M. LaMarre, R. Röhlich, J. Wiesner, H. Jomaa, A. S. Mankin, and D. G. Fujimori. *J. Am. Chem. Soc.*, 132:3953–3964, 2010.
- [56] F. Pierrel, T. Douki, M. Fontecave, and M. Atta. *J. Biol. Chem.*, 279:47555–47563, 2004.

- [57] H. L. Hernandez, F. Pierrel, E. Elleingand, R. Garcia-Serres, B. H. Huynh, M. K. Johnson, M. Fontecave, and M. Atta. *Biochemistry*, 46:5140–5147, 2007.
- [58] C. Barckholtz, T. A. Barckholtz, and C. M. Hadad. *J. Am. Chem. Soc.*, 121:491–500, 1999.
- [59] H.-J. Werner, P. J. Knowles, R. Lindh, F. R. Manby, M. Schütz, P. Celani, T. Korona, A. Mitrushenkov, G. Rauhut, T. B. Adler, R. D. Amos, A. Bernhardsson, A. Berning, D. L. Cooper, M. J. O. Deegan, A. J. Dobbyn, F. Eckert, E. Goll, C. Hampel, G. Hetzer, T. Hrenar, G. Knizia, C. Köppl, Y. Liu, A. W. Lloyd, R. A. Mata, A. J. May, S. J. McNicholas, W. Meyer, M. E. Mura, A. Nicklaß, P. Palmieri, K. Pflüger, R. Pitzer, M. Reiher, U. Schumann, H. Stoll, A. J. Stone, R. Tarroni, T. Thorsteinsson, M. Wang, and A. Wolf. MOLPRO, version 2012.1, *a package of ab initio programs*.
- [60] M. J. Frisch, G. W. Trucks, H. B. Schlegel, G. E. Scuseria, M. A. Robb, J. R. Cheeseman, J. A. Montgomery, Jr., T. Vreven, K. N. Kudin, J. C. Burant, J. M. Millam, S. S. Iyengar, J. Tomasi, V. Barone, B. Mennucci, M. Cossi, G. Scalmani, N. Rega, G. A. Petersson, H. Nakatsuji, M. Hada, M. Ehara, K. Toyota, R. Fukuda, J. Hasegawa, M. Ishida, T. Nakajima, Y. Honda, O. Kitao, H. Nakai, M. Klene, X. Li, J. E. Knox, H. P. Hratchian, J. B. Cross, V. Bakken, C. Adamo, J. Jaramillo, R. Gomperts, R. E. Stratmann, O. Yazyev, A. J. Austin, R. Cammi, C. Pomelli, J. Ochterski, P. Y. Ayala, K. Morokuma, G. A. Voth, P. Salvador, J. J. Dannenberg, V. G. Zakrzewski, S. Dapprich, A. D. Daniels, M. C. Strain, O. Farkas, D. K. Malick, A. D. Rabuck, K. Raghavachari, J. B. Foresman, J. V. Ortiz, Q. Cui, A. G. Baboul, S. Clifford, J. Cioslowski, B. B. Stefanov, G. Liu, A. Liashenko, P. Piskorz, I. Komaromi, R. L. Martin, D. J. Fox, T. Keith, M. A. Al-Laham, C. Y. Peng, A. Nanayakkara, M. Challacombe, P. M. W. Gill, B. G. Johnson, W. Chen, M. W. Wong, C. Gonzalez, and J. A. Pople, 2009. GAUSSIAN 09 (Revision C.01), Gaussian, Inc., Wallingford, CT.

Chapter 6

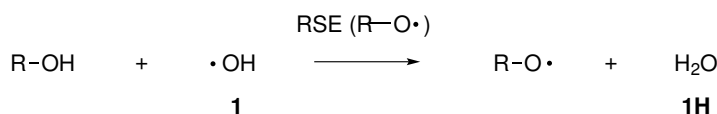
Radical Stability of Oxygen-centered Radicals - A Methodological Survey

6.1 Introduction

Oxygen-centered radicals play a central role in a large number of oxidation processes such as combustion or aging. The theoretical description of the stability of these species complements experimental studies in an ideal way as thermochemical data for open shell systems are difficult to determine experimentally. One recent example for the combination of theoretical and experimental data in oxidation processes concerns the development of more powerful anti-oxidants.^[1-3] The theoretical methods used in these types of studies range from DFT-based methods (for big systems) to highly elaborate wavefunction-based compound schemes such as G4 or the Weizman-family of methods.^[4;5] The G3(MP2)-RAD method^[6;7] is based on the G3(MP2) compound scheme^[8] and has been developed by Radom *et al.* as an option for medium-sized systems. Due to its rather favourable price/performance ratio this method has recently developed into a quasi standard for theoretical studies involving radicals of different character.^[9-15] Several variants of the G3(MP2)-RAD scheme have been proposed, either for particular situations or for technical reasons. A minor modification of G3(MP2)-RAD has been proposed by Coote *et al.* in which the Pople-style double and triple zeta basis sets are replaced by the respective cc-pVDZ and cc-pVTZ Dunning basis sets.^[16] The addition of diffuse basis functions on non-hydrogen atoms in geometry optimizations and CCSD(T) single point calculations has been proposed for the treatment of charged open-shell systems. This extended method is commonly referred to as G3(MP2)(+)-RAD(p) model.^[17-19] Open shell systems composed of more than approx. 20 non-hydrogen atoms are difficult to treat with one of the variants of G3 theory. Theoretical studies on these systems therefore resort to either one of the many DFT methods^[16;20-22] or to a combination of geometry optimization at DFT level with subsequent single point calculations at ROMP2(FC)/6-311+G(3df,2p) level.^[16;23] Given the rather good predictive power of the G3(MP2)-RAD scheme it is surprising to see its comparatively poor performance in the description of oxygen-centered radicals such as the phenoxy radical (**2**).^[9] We therefore analyze here whether simple modifications of the G3(MP2)-RAD scheme exist whose performance is substantially improved without raising the cost of computation to that of the G3^[24] or G4 methods.

6.2 Results

The stability of O-centered radicals will be assessed by an isodesmic reaction describing a hydrogen atom transfer with H₂O (**1H**) and HO• (**1**) as the reference systems (Scheme 6.1). Table 6.1 comprises stability data for 14 O-centered radicals calculated at the two higher level calculation methods G3(MP2)-RAD and G3B3. Where available experimental data will be also included.



Scheme 6.1: Isodesmic reaction used to define the stability of oxygen-centered radical.

The relative stability scale of O-centered radicals is rather broad when compared to that of C-centered radicals.^[9] Simple alkyl substituents (systems **4**, **5**, and **6**) stabilize the oxy-radicals by about 40 - 60 kJ mol⁻¹. The presence of strong electron withdrawing groups such as fluorine (system **3**) diminishes the stability of methoxy radical (**6**) by 51.8 kJ mol⁻¹, showing the electrophilic nature of oxy-radicals. Aromatic substitution (systems **2**, **7**, **8**, **12**) has a strong stabilization effect to the radicals owing to the delocalization of the unpaired electron into the attached π -system.^[9;25]

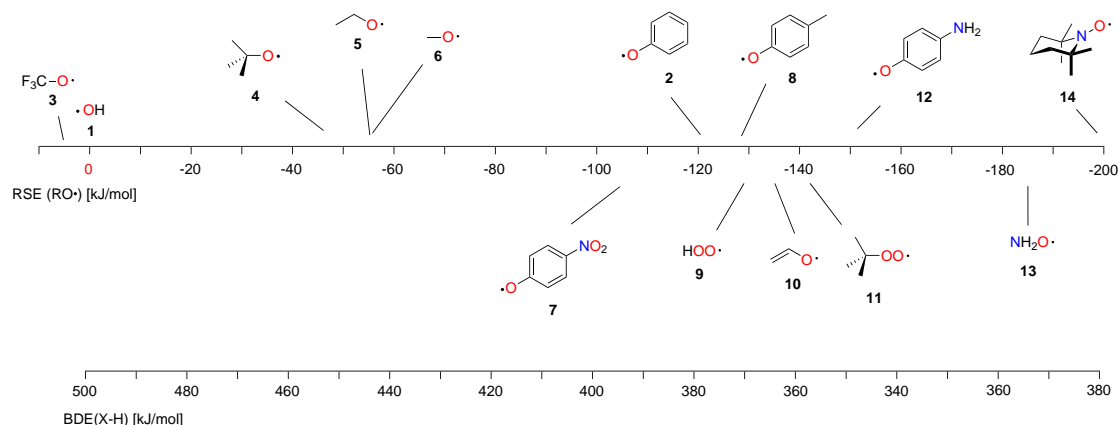


Figure 6.1: RSE scale of O-centered radicals at ΔH_{298} G3B3.

When comparing the results of the theoretical methods with the experimental data (Table 6.1), we observe that both G3B3 and G3(MP2)-RAD are mostly able to predict the radical stability well. Figure 6.2 depicts the comparison and linear correlation between G3(MP2)-RAD and G3B3 data. Obviously larger scattering occurs for highly stabilized radicals, which is very likely generated by three data points represented by systems **2**, **7** and **8** (Figure 6.2 and Table 6.1). These systems are lying above the correlation line and thus indicate that those RSEs calculated at G3(MP2)-RAD are clearly too negative when compared to RSEs at G3B3. The deviations of G3(MP2)-RAD to G3B3 are in the range of 1-4 kJ mol⁻¹, with the exception of systems **2** (-33.8 kJ mol⁻¹), **7** (-48.1 kJ mol⁻¹) and **8** (-19.2 kJ mol⁻¹).

Table 6.1: Radical stabilization enthalpies (RSE, in kJ mol^{-1}) at 298.15 K of 14 O-centered radicals at G3(MP2)-RAD and G3B3 level.

System	RSE G3(MP2)-RAD ^a	RSE G3B3 ^b	Deviation		RSE exp. ^c
	A	B	A-B		
CF ₃ O• (3)	+4.3	+4.5	+0.2		+0.0
HO• (1)	+0.0	+0.0	+0.0		+0.0
<i>t</i> -BuO• (4)	-46.7	-47.3	+0.6		-52.2 ± 2.8
CH ₃ CH ₂ O• (5)	-54.9	-55.4	+0.5		-56.1 ± 5.9
CH ₃ O• (6)	-55.2	-55.6	-0.4		-56.8 ± 3.0
<i>p</i> -NO ₂ -PhO• (7)	-153.9	-105.8	-48.1		-103.0 ± 5.9 ^d
PhO• (2)	-154.9	-121.1	-33.8		-128.1 ± 1.3 ^d ; -132.9 ± 0.5 ^f
<i>p</i> -me-PhO• (8)	-148.0	-128.8	-19.2		-136.9 ± 2.1 ^d ; -141.3 ± 0.6 ^f
HOO• (9)	-127.8	-129.3	+1.5		-131.4 ± 0.3
CH ₂ CHO• (10)	-134.3	-137.5	+3.2		-145.1 ± 5.0
<i>t</i> -BuOO• (11)	-139.1	-141.0	+1.9		-144.8 ± 8.8
<i>p</i> -NH ₂ -PhO• (12)	-153.5	-152.9	-0.6		-165.8 ± 13.0 ^e
NH ₂ O• (13)	-164.6	-164.2	-0.4		n.a.
TEMPO• (14)	-198.6	-198.5	-0.1		-205.5

^aScaling factor 0.9806; With full cartesian basis functions.

^bScaling factor 0.960; With full cartesian basis functions.

^cAs recommended by Luo (ref 26) if not mentioned otherwise.

^dMeasurement in solution phase at 298 K; see ref. 27

^eMeasurement in solution phase at 298 K; see ref. 28

^fMeasurement in gas phase at 0 K; see ref. 29;30

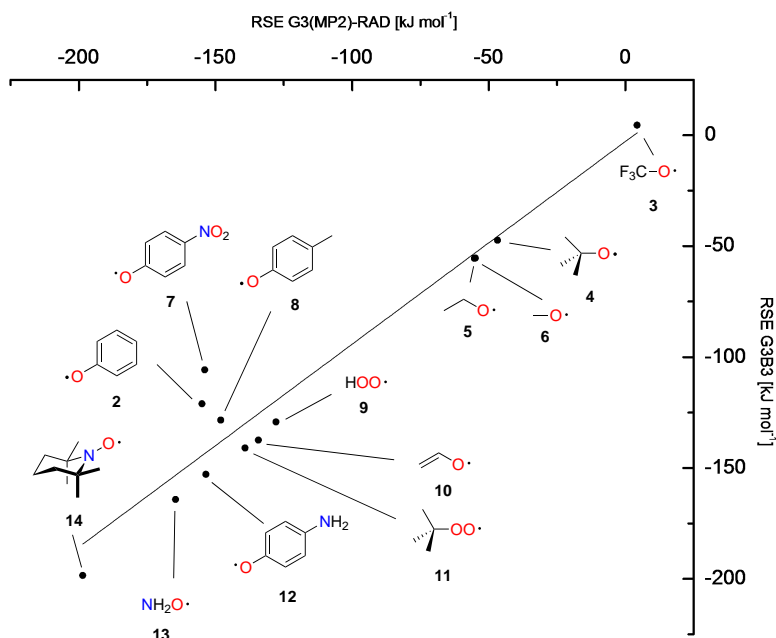


Figure 6.2: Correlation of RSE (G3B3) vs. RSE (G3(MP2)-RAD). Linear fit equation $\Delta H_{298}(\text{G3B3}) = 0.91414\Delta H_{298}(\text{G3(MP2)-RAD}) - 2.80234$ with correlation coefficient 0.91835. Reference system **1** is excluded.

Table 6.2: Radical stabilization enthalpies (RSE, in kJ mol⁻¹) at 298.15 K of phenoxy radical (**2**) and *p*-me-phenoxy radical (**8**) at different level of theories.

System	Methods	Basis sets	RSE
PhO• (2)	Exp.		-125.1
	B3LYP	6-31G(d) ^a	-126.6
	B2PLYP	6-31G(d)	-107.8
	ROMP2(FC)	6-31G(d) ^a	-106.4
		6-311+G(3df,2p) ^a	-148.4
		G3MP2Large ^a	-146.2
	SCS-ROMP2(FC)	6-31G(d) ^a	-107.4
	SCS-ROMP2(FC)	G3MP2Large ^a	-149.8
	U(R)CCSD(T)	6-31G(d) ^a	-115.1
	G3(MP2)-RAD ^a		-154.9
	G3(MP2)-RAD ^{a:c}		-157.5
	G3(MP2)-RAD ^d		-152.3
	G3-RAD ^a		-151.2
	G3B3 ^b		-121.1
	G4 ^e		-126.9
	G4-5H ^e		-120.2
	G4(MP2) ^e		-125.0
	G4(MP2) (w/o HLC) ^e		-114.0
	U(R)CCSD(T)	CBS ^{a:f}	-127.7
	W1RO		-128.1
<i>p</i> -me-PhO• (8)	Exp.		-133.8
	B3LYP	6-31G(d) ^a	-133.7
	B2PLYP	6-31G(d)	-113.7
	ROMP2(FC)	6-31G(d) ^a	-125.2
		6-311+G(3df,2p) ^a	-153.8
		G3MP2Large ^a	-152.0
	SCS-ROMP2(FC)	6-31G(d) ^a	-125.9
	SCS-ROMP2(FC)	G3MP2Large ^a	-154.3
	U(R)CCSD(T)	6-31G(d) ^a	-121.2
	G3(MP2)-RAD ^a		-148.0
	G3(MP2)-RAD ^{a:c}		-149.6
	G3(MP2)-RAD ^d		-146.7
	G3-RAD ^a		-144.0
	G3B3 ^b		-128.8
	G4 ^e		-135.6
	G4-5H ^e		-127.5
	G4(MP2) ^e		-136.8
	G4(MP2) (w/o HLC) ^e		-121.7
	U(R)CCSD(T)	CBS ^{a:f}	-135.3
	W1RO		-135.6

^aB3LYP/6-31G(d) geometry; Scaling factor 0.9806; With full cartesian basis functions.^bB3LYP/6-31G(d) geometry; Scaling factor 0.960; With full cartesian basis functions.^cUsing spin scaled MP2 in the basis correction term.^dModified G3(MP2)-RAD using Dunning basis sets (see ref. 16); No scaling factor.^eB3LYP/6-31G(2df,p) geometry; Scaling factor 0.9854; With full cartesian basis functions.^fCBS extrapolation (see appendix B); With full cartesian basis functions.

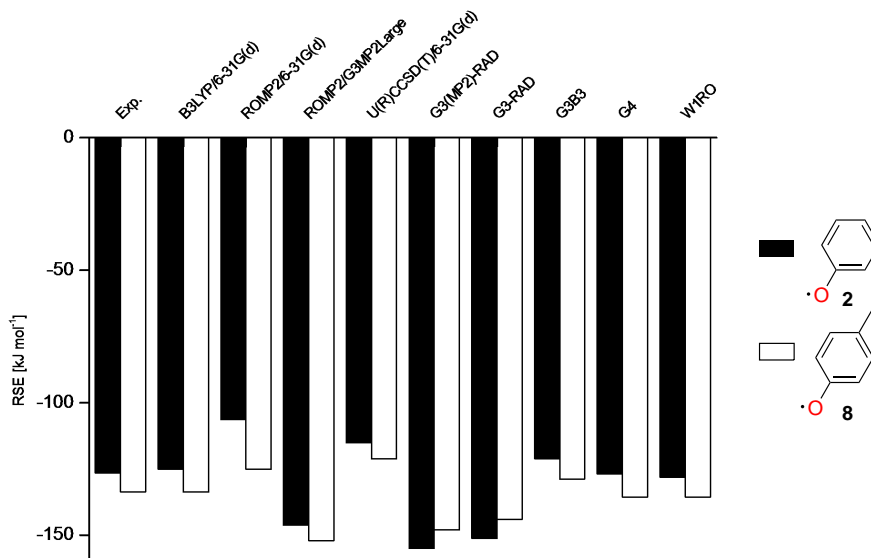
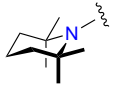


Figure 6.3: Graphical comparison between RSE of phenoxy radical (**2**) and *p*-me-phenoxy radical (**8**) at different levels of theory.

In addition to the large deviation Table 6.1 shows that G3(MP2)-RAD is qualitatively wrong in predicting the inductive effect of substituents at *para*-positions (RSE (**2**) = -154.9 kJ mol⁻¹; RSE (**7**) = -154.9 kJ mol⁻¹, RSE (**8**) = -148.0 kJ mol⁻¹, RSE (**12**) = -153.5 kJ mol⁻¹). Remarkably B3LYP, ROMP2(FC) and U(R)CCSD(T) (Figure 6.3) are able to predict the qualitative trend of methyl substituent of phenoxy radical correctly, while some of the G3 methods (G3(MP2)-RAD, and G3-RAD), which apply restricted openshell wavefunction in the basis set correction term, (Table 6.1) have failed to give the desired trend. However it is very obvious from Table 6.2 that all ROMP2 with either G3MP2Large or 6-311G+(3df,p), both non spin-scaled and spin-scaled, are yielding rather low RSEs (RSE (**2**) = -146.2 kJ mol⁻¹, RSE (**8**) = -152.0 kJ mol⁻¹ at ROMP2/G3MP2Large), which deviate largely from the experimental values. This is in contrast to the results at ROMP2/6-31G(d) level, where the RSEs are predicted too high for both phenoxy radical (**2**) (RSE (**2**) = -106.4 kJ/mol⁻¹) and *p*-me-phenoxy radical (**8**) (RSE (**8**) = -125.2 kJ/mol⁻¹). Further analysis of the correlation energy in ROMP2 calculation shows that a significant increase in $E_0^{(2)}$ of the product side in the isodesmic reaction (Scheme 6.1) occurs when the basis function is switched from 6-31G(d) to G3(MP2)Large. This particularity emerges in phenoxy radical and substituted phenoxy radicals (Table 6.3). Moreover, Table 6.3 also shows that the correlation energy is very important in the calculation of electron donor stabilized radical, such as TEMPO• (**14**), and resonance stabilized radicals, such as phenoxy radical (**2**). The ratio of the effect of correlation energy to the RSE ($\Delta E_0^{(2)}/\text{RSE}$) for the isodesmic reaction 6.1 is 78.5% in the case of phenoxy radical(**2**) at ROMP2/6-31G(d), and 39.7% in the case of TEMPO• (**14**). In contrast to the latter, RSE of alkyl-substituted oxy radical *t*-BuO• (**4**) obtained at ROHF/6-31G(d) level of theory is rather similar to that of

ROMP2/6-31G(d), since the sum of $\Delta E_0^{(2)}$ is very small (-3.0 kJ mol $^{-1}$).

Table 6.3: Components of $\Delta E_0^{(2)}$ (product – reactant) [kJ mol $^{-1}$] of isodesmic reaction (Scheme 6.1) for R = C $_4$ H $_9$, Ph and C $_9$ H $_{17}$ N.

	ROMP2			
Δ Singles	6-31G(d)	-1.0	-12.6	-6.5
	G3MP2Large ^a	-1.2	-10.6	-6.7
$\Delta\alpha/\alpha$	6-31G(d)	+0.9	-5.7	+0.0
	G3MP2Large ^a	+0.8	-11.4	+0.2
$\Delta\beta/\beta$	6-31G(d)	-2.5	-19.1	-34.9
	G3MP2Large ^a	-3.4	-21.7	-36.5
$\Delta\alpha/\beta$	6-31G(d)	-0.4	-46.1	-39.9
	G3MP2Large ^a	-1.9	-75.0	-45.0
$\Delta E_0^{(2)}$	6-31G(d)	-3.0	-83.5	-81.3
	G3MP2Large	-5.9	-118.7	-88.0

^aWith full cartesian basis functions.

Moving to more expensive methods such as G4, G3B3, U(R)CCSD(T)/CBS with Schwartz extrapolation scheme^[31;32] and W1RO the stability trend can be recovered (Figure 6.3). Interestingly G4(MP2) (Table 6.2), whose computational effort is marginally above G3(MP2)-RAD, is able to predict the stability similar to the values computed at G4 and even U(R)CCSD(T)/CBS. We note here that these methods use different higher level correction (HLC) parameters for open-shell and closed-shell system, which may have a significant contribution to the RSE depending on the applied reaction scheme. In all G3-theories, Δ HLC term is vanishing when isodesmic reaction (Scheme 6.1) is applied due to cancelation at the educt- and product-side. In contrast, Δ HLC in G4 and G4(MP2) is not zero when applying isodesmic reactions because of the different dimension of the unpaired electron's carrier at the left- and right-side. Hence the effect of the non-vanishing HLC for our reaction scheme is particularly huge for the RSE calculation of phenoxy-radical (**2**) and its derivatives. Recent work has solved the dilemma over the increasing HLC by introducing a damping parameter, which determines the maximum correction for spin polarization effect in radicals.^[33] The most expensive method applied in this study, W1RO, has given an RSE value for phenoxy radical (**2**) of -128.1 kJ mol $^{-1}$, which is close to U(R)CCSD(T)/CBS (-127.8 kJ mol $^{-1}$).

Geometrical dependency: To track the origin of the error in G3(MP2)-RAD, we performs calculations at G3(MP2)-RAD level of theory of phenoxy radical (**2**) and *p*-me-phenoxy radical (**8**) with different DFT-geometries.

Table 6.4: ΔE_{tot} (Methods//B3LYP/6-31G(d) – E_{tot} Methods//B3LYP/6-31G(2df,p)) of single point calculations using B3LYP geometries with different basis sets.

System	Methods	ΔE_{tot} [kJ mol ⁻¹]
H ₂ O (1H)	ROHF/6-31G(d)	+1.28
	ROMP2/6-31G(d)	-0.22
	ROHF/G3MP2Large	+1.81
	ROMP2/G3MP2Large	+0.39
	U(R)CCSD(T)/6-31G(d)	-0.36
HO• (1)	ROHF/6-31G(d)	+0.77
	ROMP2/6-31G(d)	+0.01
	ROHF/G3MP2Large	+1.04
	ROMP2/G3MP2Large	+0.38
	U(R)CCSD(T)/6-31G(d)	-0.18
PhOH (2H)	ROHF/6-31G(d)	+2.92
	ROMP2/6-31G(d)	-0.83
	ROHF/G3MP2Large	+3.94
	ROMP2/G3MP2Large	+0.70
	U(R)CCSD(T)/6-31G(d)	-1.80
PhO• (2)	ROHF/6-31G(d)	+1.10
	ROMP2/6-31G(d)	+17.60
	ROHF/G3MP2Large	+4.82
	ROMP2/G3MP2Large	-1.32
	U(R)CCSD(T)/6-31G(d)	-1.58
<i>p</i> -me-PhO (8H)	ROHF/6-31G(d)	+3.16
	ROMP2/6-31G(d)	-0.71
	ROHF/G3MP2Large	+4.26
	ROMP2/G3MP2Large	+0.97
	U(R)CCSD(T)/6-31G(d)	-1.80
<i>p</i> -me-PhO• (8)	ROHF/6-31G(d)	+3.62
	ROMP2/6-31G(d)	+14.39
	ROHF/G3MP2Large	+5.32
	ROMP2/G3MP2Large	-1.00
	U(R)CCSD(T)/6-31G(d)	-2.04

Table 6.4 shows that at ROMP2/6-31G(d) is very sensitive to the geometry of phenoxy radical (**2**) and *p*-me-phenoxy radical (**8**). In both cases the global minima of the radicals are shifted by +17.60 kJ mol⁻¹ for phenoxy radical (**2**), and respectively +14.39 kJ mol⁻¹ *p*-me-phenoxy radical (**8**). Other methods seem to be marginally affected by the geometry variation. As a consequence, for phenoxy radical (**2**),

less stabilization ($\text{RSE}(\mathbf{2}) = -135.1 \text{ kJ mol}^{-1}$) is obtained by applying B3LYP/6-31G(2df,p) geometry. Furthermore, we observe minor shortening of C-O bond with B3LYP/6-31G(2df,p)-geometry in phenoxy-radical ($\mathbf{2}$)¹. This indicates that RSEs of the phenoxy radical ($\mathbf{2}$) is very sensitive to the C-O bond length. Further detailed examination reveals that the influence of C-O bond length is particularly huge in the ROMP2/6-31G(d) single point calculation used in G3(MP2)-RAD (Table 6.4). Additional diffuse functions (6-31+G(d)) tend to pull again the RSE of phenoxy radical ($\mathbf{2}$) into more negative region ($\text{RSE}(\mathbf{2}) = -149.6 \text{ kJ mol}^{-1}$). Using the correlation consistent basis set (cc-pVDZ), which is fitted to high correlated methods, gives marginal effects to increase the RSE of phenoxy radical ($\mathbf{2}$) ($-149.5 \text{ kJ mol}^{-1}$). Double hybrid DFT^[34] (B2PLYP/6-31G(d)) and Truhlar’s MPW1K functional^[35] with 6-31+G(d) have similar magnitude in reducing the stability of phenoxy radical ($\mathbf{2}$)² as B3LYP/cc-pVDZ. From Table 6.5, it is obvious that RSE-fluctuation is also presence in *p*-me-phenoxy radical ($\mathbf{8}$). However this seems to converge to RSE values of about -130 kJ mol^{-1} to -133 kJ mol^{-1} . Finally, Figure 6.4 concludes that none of the geometrical variations for G3(MP2)-RAD can yield the expected stability trend.

Table 6.5: Radical stabilization enthalpies (RSE, in kJ mol^{-1}) at 298.15 K of phenoxy radical ($\mathbf{2}$) and *p*-me-phenoxy radical ($\mathbf{8}$) at G3(MP2)-RAD with different geometries.

System	Methods	Geometry	RSE
PhO• ($\mathbf{2}$)	G3(MP2)-RAD	B3LYP/6-31G(d)	-154.9
		B3LYP/6-31G(2df,p)	-135.1
		B3LYP/6-31+G(2df,p)	-143.1
		B3LYP/cc-pVDZ	-149.5
		MPW1K/6-31+G(d)	-146.9
		B2PLYP/6-31G(d)	-147.7
<i>p</i> -me-PhO• ($\mathbf{8}$)	G3(MP2)-RAD	B3LYP/6-31G(d)	-148.0
		B3LYP/6-31G(2df,p)	-131.1
		B3LYP/6-31+G(2df,p)	-131.0
		B3LYP/cc-pVDZ	-131.6
		MPW1K/6-31+G(d)	-132.9
		B2PLYP/6-31G(d)	-130.2

¹d(C-O) B3LYP/6-31G(d) = 1.258 Å; d(C-O) B3LYP/6-31G(2df,p) = 1.249 Å

²RSE($\mathbf{2}$) B2PYLP/6-31G(d) = $-147.7 \text{ kJ mol}^{-1}$; RSE($\mathbf{2}$) MPW1K/6-31+G(d) = $-146.9 \text{ kJ mol}^{-1}$

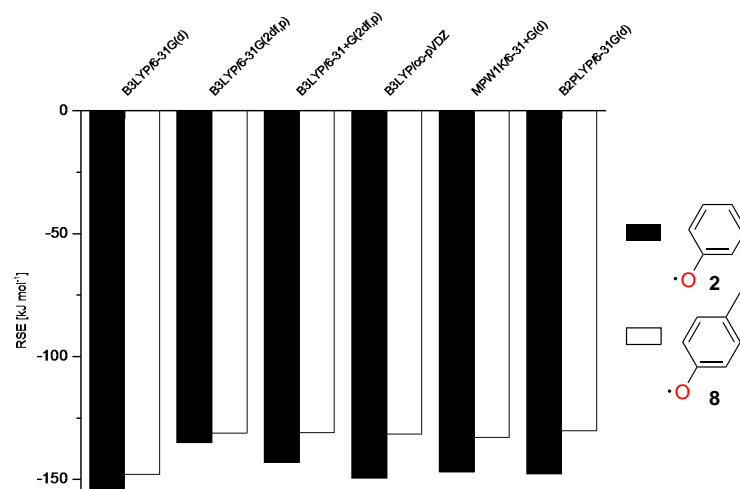


Figure 6.4: Graphical comparison between RSE of phenoxy radical (**2**) and *p*-me-phenoxy radical (**8**) at G3(MP2)-RAD using different optimized geometry.

Basis set variations in the basis set correction term: The accuracy of all composite methods relies heavily on the basis set correction term, which is added to single point configuration interaction or coupled cluster calculation. In G3(MP2)-RAD (Figure 6.5), the magnitude of the basis set correction at ROMP2(FC) (point **C** - point **B**) and at U(R)CCSD(T) are assumed to be identical (point **D** - point **A**).

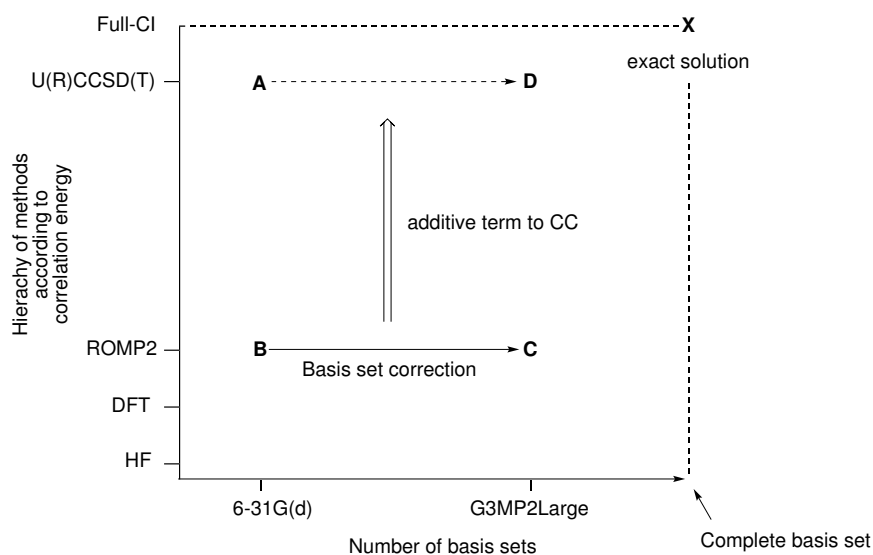


Figure 6.5: Schematic picture of G3(MP2)-RAD.

The total electronic energy in G3(MP2)-RAD is given by,

$$E_{\text{tot}}(\text{G3(MP2)-RAD}) = E_{\text{tot}}(\text{U(R)CCSD(T)/6-31G(d)}) + \text{B.C.} + \text{HLC} \quad (6.1)$$

with B.C. (basis set correction),

$$\text{B.C.} = E_{\text{tot}}(\text{ROMP2(FC)/G3MP2Large}) - E_{\text{tot}}(\text{ROMP2(FC)/6-31G(d)}) \quad (6.2)$$

and HLC (higher level correction) for molecules,

$$\text{HLC} = -0.009413 \, n\beta - 0.003969(n\alpha - n\beta) \quad (6.3)$$

$n\alpha$ = number of α -valence electrons

$n\beta$ = number of β -valence electrons

The thermal correction is performed at the geometry optimization method and using scaling factor 0.9806.

$$H_{298}(\text{G3(MP2)-RAD}) = E_{\text{tot}}(\text{G3(MP2)-RAD}) + H_{298}(\text{B3LYP/6-31G(d)}) - E_{\text{tot}}(\text{B3LYP/6-31G(d)}) \quad (6.4)$$

Principally, it is possible to construct any arbitrary basis set correction scheme by shifting the starting basis (point **A** and **B**) to another basis (point **A'** and point **B'**). Our main objective is therefore to find a reasonable starting basis point **x** and simultaneously to avoid a substantial increase in the computational cost (Figure 6.6 and eq. 6.5 - eq. 6.6).

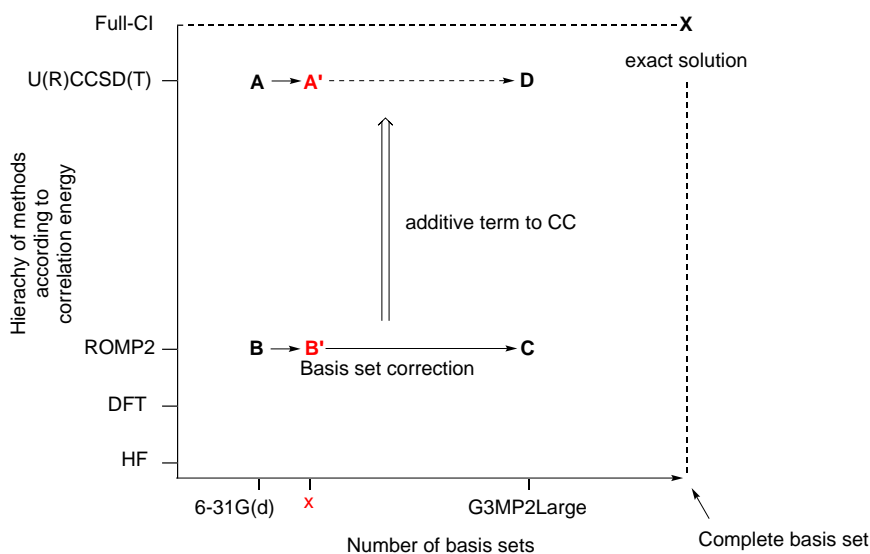


Figure 6.6: Schematic picture of G3(MP2)-RAD-modification by shifting the starting basis point **x**.

The modified G3(x,MP2)-RAD will then be defined as,

$$E_{\text{tot}}(\text{G3}(\mathbf{x},\text{MP2})\text{-RAD}) = E_{\text{tot}}(\text{U(R)CCSD(T)}/\mathbf{x}) + \text{B.C.} \quad (6.5)$$

$$\text{B.C.} = E_{\text{tot}}(\text{ROMP2(FC)}/\text{G3MP2Large}) - E_{\text{tot}}(\text{ROMP2(FC)}/\mathbf{x}) \quad (6.6)$$

During the search for the starting basis point, RSE calculations of phenoxy radical (**2**) at ROMP2(FC)- and U(R)CCSD(T)-level with many possible combination of basis sets are performed. Figure 6.7 and 6.8 demonstrate how large the RSE varies with the number of basis functions used. Our results show that in contrast to ROMP2(FC), U(R)CCSD(T) is by far more robust to basis function alterations. The calculated RSEs of phenoxy radical (**2**) at U(R)CCSD(T) range from $-113.1 \text{ kJ mol}^{-1}$ to $-128.0 \text{ kJ mol}^{-1}$, while at ROMP2(FC) these range from $-102.3 \text{ kJ mol}^{-1}$ to $-150.9 \text{ kJ mol}^{-1}$. Figure 6.7 also shows two groups of data points: The red dots \bullet are located at high RSEs ($-102.3 \text{ kJ mol}^{-1}$ to $-131.8 \text{ kJ mol}^{-1}$) and the black dots \bullet are located at a lower RSE region ($-139.1 \text{ kJ mol}^{-1}$ to $-150.9 \text{ kJ mol}^{-1}$). According to our results, a systematic jump in radical stability at ROMP2(FC)-level is observed whenever a combination of two d-polarization functions and a diffuse function, or three d-polarization functions is applied in the MP2 calculations. Additional f-polarization functions to non-hydrogen atom, p-polarization functions to hydrogen atoms, and triple ζ -splitting seem not to have a big influence in lowering the RSE (-113 kJ mol^{-1} to -126 kJ mol^{-1}).

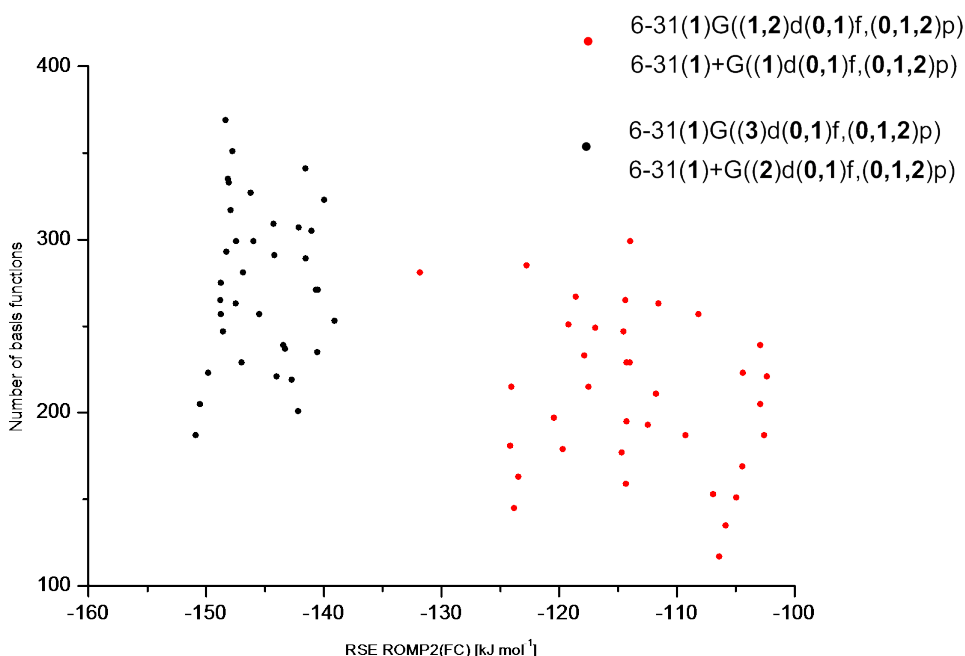


Figure 6.7: Variation of the RSE of phenoxy radical (**2**) with the number of basis functions at ROMP2(FC) level of theory.

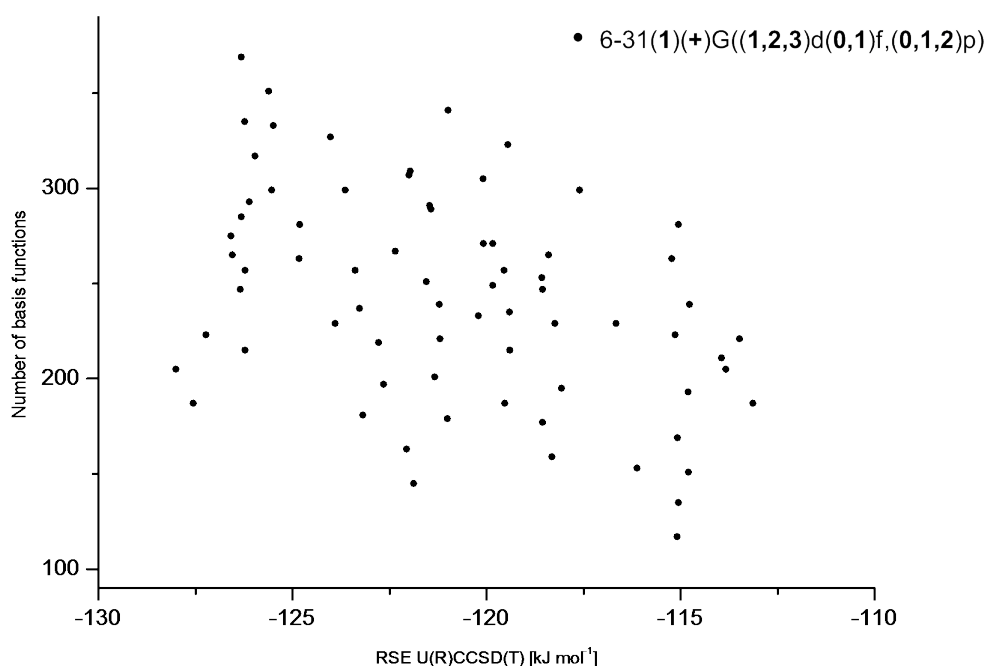
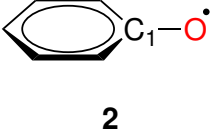
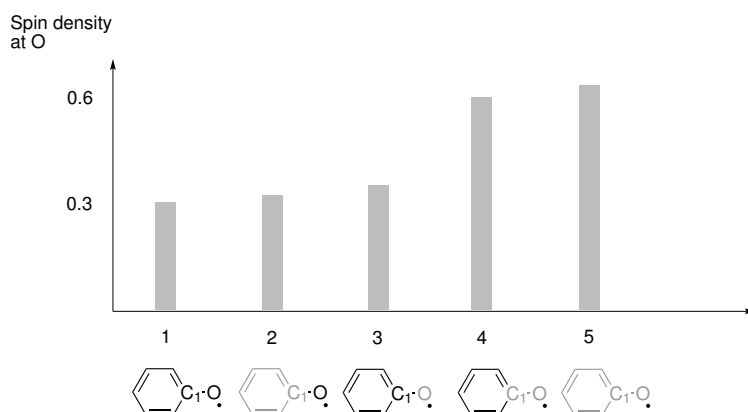
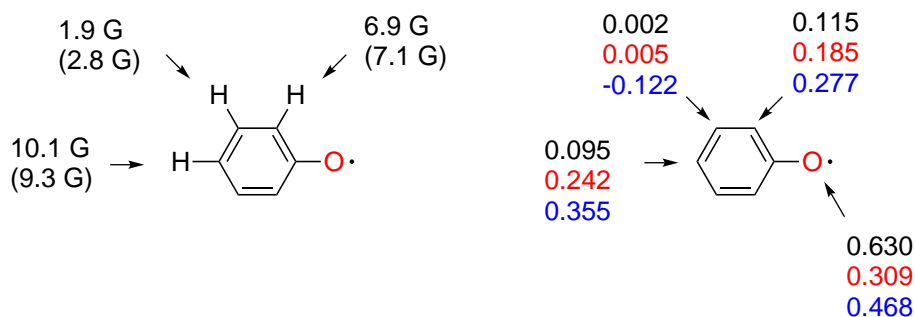


Figure 6.8: Variation of the RSE of phenoxo radical (**2**) with number of basis function at U(R)CCSD(T) level of theories. Black dots •: {6-31(1)(+)G(\mathbf{x} d \mathbf{y} f, \mathbf{z} p) with $\mathbf{x} = 1, 2, 3$; $\mathbf{y} = 0, 1$; $\mathbf{z} = 0, 1, 2$ }.

Natural population analysis on phenoxo radical (**2**) at ROHF-level shows that the spin-density at oxygen drops from 0.63 to 0.31 when the basis set is switched from 6-31G(d) to 6-31+G(2d). Furthermore, a similar spin-population is also found when G3MP2Large basis is applied. Both of these findings indicate a higher delocalization degree of the unpaired spin to the aromatic ring. Surprisingly, increasing the basis function to 6-31+G(2d) to the oxygen only, or to the whole ring is sufficient to achieve lower spin density at oxygen (Table 6.6 and Figure 6.9: Entry number 2 and 3). Blocking the delocalization path by applying the basis 6-31G(d) to the oxygen and the adjacent carbon (C1) raises the localization of unpaired electron at oxygen once more (Table 6.6 and Figure 6.9: Entry number 4).

Table 6.6: Atomic spin density at oxygen atom from natural population analysis at ROHF level.

	Basis set	Entry number in Figure 6.9	Spin-density at oxygen
 2	6-31+G(2d)	1	0.309
	6-31+G(2d) on O 6-31G(d) on others	2	0.323
	6-31G(d) on O 6-31+G(2d) on others	3	0.360
	6-31G(d) on O and C1 6-31+G(2d) on others	4	0.605
	6-31G(d)	5	0.630

**Figure 6.9:** Variation of ROHF spin density at oxygen by applying different basis sets on different local positions. Grey color indicates 6-31G(d), while black indicates 6-31+G(2d).**Figure 6.10:** Left: Experimental isotropic hyperfine coupling constant at *ortho*-, *meta*- and *para*-position protons;^[36] In parentheses: a_{iso} at UB3LYP/EPR-III. Right: Spin density distribution on carbons, and oxygen at ROHF/6-31G(d), ROHF/6-31+G(2d), UB3LYP/EPR-III.

The Fermi-contact coupling of restricted open-shell theory is by formalism always zero when the unpaired electron is located in the p-type orbital, where a nodal plane exists. A comparison between UB3LYP/EPR-III and experiment is performed to verify that the spin density distribution of UB3LYP and ROHF are qualitatively correct (Figure 6.10 (left)).^[36] The isotropic hyperfine coupling constants of hydrogens of the aromatic ring at UB3LYP/EPR-III are relatively in good agreement with the experimental values. This suggests that the order of the amount of unpaired spin at carbon atoms (*ortho*, *meta*, *para*) at UB3LYP level of theory is plausible. Since the spin distribution in the unrestricted picture is resembling more the results of ROHF/6-31+G(2d) rather than ROHF/6-31G(d), it is thus obvious that the reference wavefunction of ROHF/6-31+G(2d) is qualitatively nearer to the experiment (Figure 6.10 (right)). The failure of G3(MP2)-RAD in predicting the stability of phenoxy radical (**2**) seems to lie on the basis set correction term, which is constructed by the extrapolation between the basis set 6-31G(d) and G3MP2Large. The difference of the RSEs at ROMP2/6-31G(d) and ROMP2/G3MP2Large amounts 35.8 kJ mol⁻¹. The apparently too negative RSE for phenoxy radical (**2**) at ROMP2/G3MP2Large has been shown in the previous section to be a consequence of the increase of the correlation energies in the product side, which is originated from open-shell product. Comparison of ROHF orbitals at 6-31G(d), 6-31+G(2d), and G3MP2Large show some orbital rotations when the basis set is altered from 6-31G(d) to 6-31+G(2d) (Figure 6.11). In contrast to ROHF/6-31G(d), ROHF/G3MP2Large seems to be very similar to ROHF/6-31+G(2d).

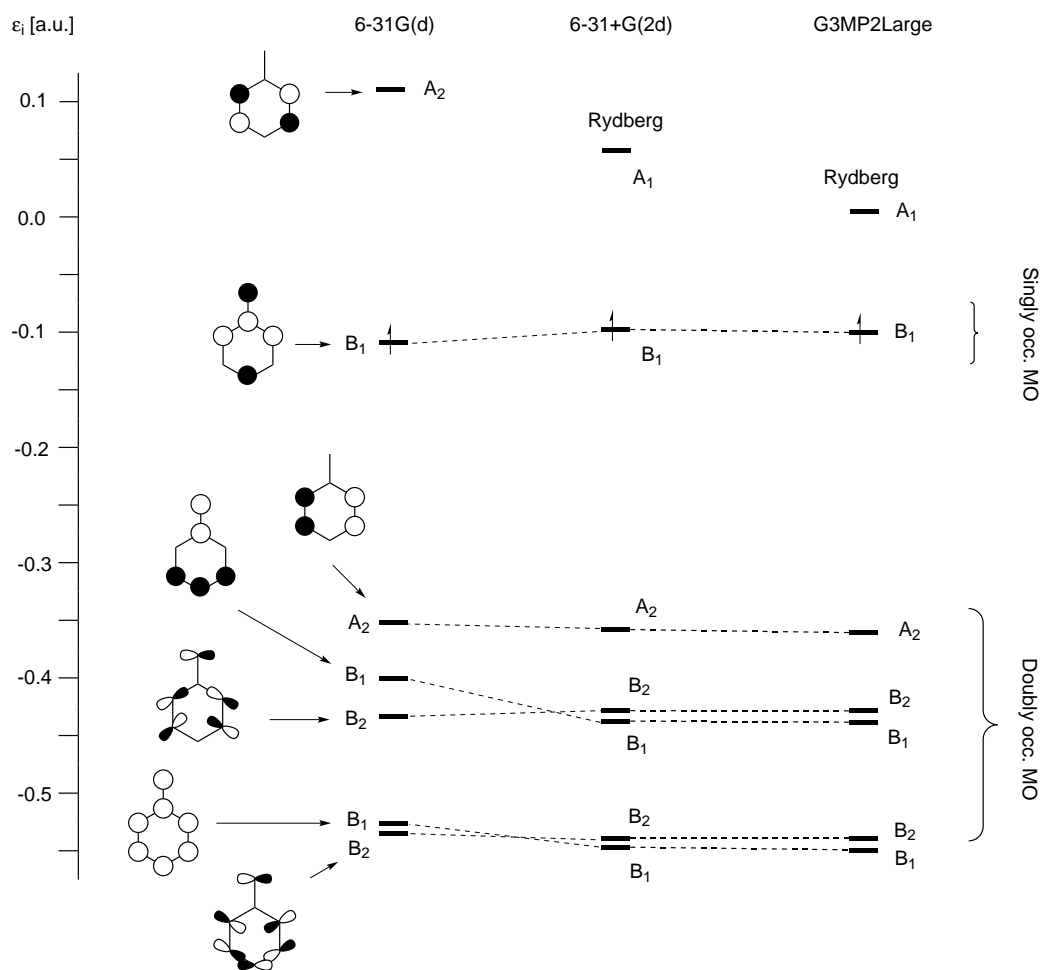


Figure 6.11: Non-canonical ROHF-orbitals at 6-31G(d), 6-31+G(2d) and G3MP2Large.

Furthermore, the T_1 diagnostic at coupled cluster level shows that the wavefunction at ROHF/6-31G(d) is having significant multi-determinant character (T_1 -Diag = 0.031), which indicates that the wavefunction is not applicable to single determinant perturbation theory. Contrary to ROHF/6-31G(d), ROHF/6-31+G(2d) is showing T_1 -diagnostic value of only 0.015. In summary, spin density, orbital analysis and T_1 diagnostic show the rather poor quality of ROHF/6-31G(d) as a reference wavefunction used in the basis set correction term. Finally we find also that RSE calculations of systems (2) and (8) with basis sets 6-31+G(2d) and 6-31G(3d) as starting points, at which the radical stability increases significantly in the basis set correction term, give the expected inductive effects of the methyl substituent. This leads us to test the variant, G3(+2d,MP2)-RAD, in the benchmark calculation against the more expensive G3B3.

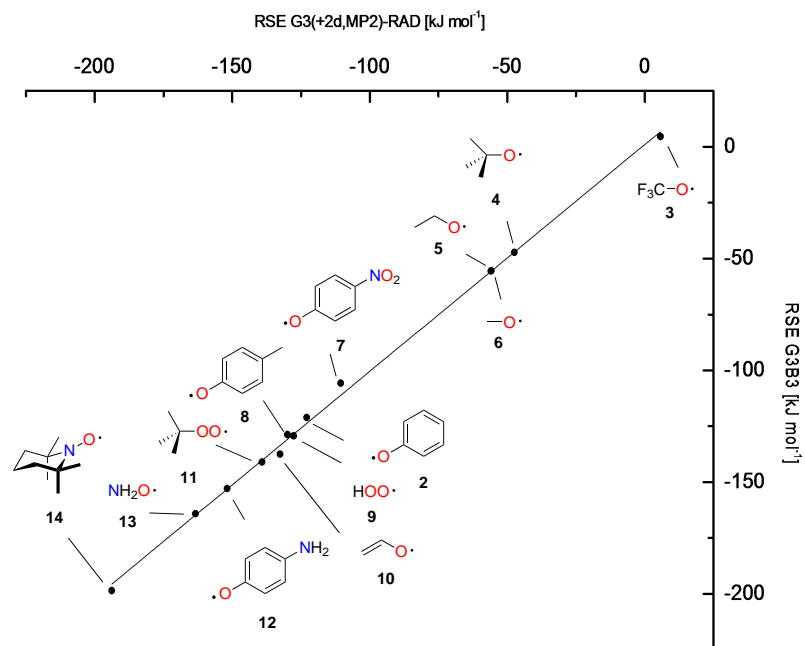


Figure 6.12: RSE (G3B3) vs RSE (G3(+2d,MP2)-RAD). Final fit equation $\Delta H_{298}(\text{G3B3}) = 1.01445\Delta H_{298}(\text{G3(+2d,MP2)-RAD}) + 0.99136$ with correlation coefficient 0.99801. Reference system 1 is excluded.

The correlation coefficient (0.99801) in Figure 6.12 shows the convincing performance of G3(+2d,MP2)RAD. The y-axis intercept is practically zero, which is much better, and the maximum deviation to G3B3 amounts currently only +5.0 kJ/mol (Table 6.7). Despite the good performance of this approach it is important to note that the modified method is in fact expensive, due the significant increase of basis set in U(R)CCSD(T). Two strategies to make G3(+2d,MP2)-RAD more feasible are therefore here presented.

Table 6.7: Radical stabilization enthalpies (RSE, in kJ mol⁻¹) at 298.15 K of 14 O-centered radicals at G3(+2d,MP2)-RAD and G3B3 level.

System	RSE (G3(+2d,MP2)-RAD) ^a	RSE (G3B3) ^b	Deviation
	A	B	A-B
CF ₃ O• (3)	+5.7	+4.5	+1.2
HO• (1)	+0.0	+0.0	+0.0
<i>t</i> -ButO• (4)	-47.4	-47.3	-0.1
CH ₃ CH ₂ O• (5)	-55.8	-55.4	-0.4
CH ₃ O• (6)	-55.9	-55.6	-0.3
<i>p</i> -NO ₂ -PhO• (7)	-110.5	-105.5	-5.0
PhO• (2)	-122.9	-121.1	-1.8
<i>p</i> -me-PhO• (8)	-129.8	-128.8	-1.0
HOO• (9)	-127.7	-129.3	+1.6
CH ₂ CHO• (10)	-132.6	-137.5	+4.9
<i>t</i> -ButOO• (11)	-139.2	-141.0	+1.8
<i>p</i> -NH ₂ -PhO• (12)	-151.8	-152.8	+1.0
NH ₂ O• (13)	-163.4	-164.2	+1.2
TEMPO• (14)	-193.8	-198.5	+4.7

^aScaling factor 0.9806; With full cartesian functions.

^bScaling factor 0.960; With full cartesian functions.

Transfer of +2d correction in coupled cluster to (U)MP4(FC)(SDTQ):

Calculations of CCSD(T) and MP4(SDTQ) scale to the power of 7 with the number of basis functions (n^7) due to the calculation of the connected triples (\hat{T}_3). The main difference between MP4(SDTQ) and CCSD(T) is in the optimization of the single- and all product of double-amplitudes (\hat{T}_2^n , $n = 1, 2, \dots, \infty$). Because the former is a perturbation method, it is obvious that the benefit of transferring the basis functions correction to MP4(SDTQ) is circumventing the iterative optimization of the double amplitudes.

$$E_{\text{tot}}(\text{G3(+2d,MP2,MP4)-RAD}) = E_{\text{tot}}(\text{U(R)CCSD(T)/6-31G(d)}) + \text{B.C.} \quad (6.7)$$

$$\begin{aligned} \text{B.C.} = & E_{\text{tot}}(\text{ROMP2(FC)/G3MP2Large}) - E_{\text{tot}}(\text{ROMP2(FC)/6-31+G(2d)}) \\ & + E_{\text{tot}}(\text{(U)MP4(FC)/6-31+G(2d)}) - E_{\text{tot}}(\text{(U)MP4(FC)/6-31G(d)}) \end{aligned} \quad (6.8)$$

The predictive power of G3(+2d,MP2,MP4)-RAD is comparable with G3(+2d,MP2)-RAD. Both gave the correct stability trend between phenoxy- and *p*-me-phenoxy radicals (**2** and **8**) (Table 6.8 and Figure 6.13). Nevertheless, since the unrestricted reference wavefunction UHF is applied in the UMP4/6-31+G(2d) and UMP4/6-31G(d) calculations, the spin contamination is very possible to appear.

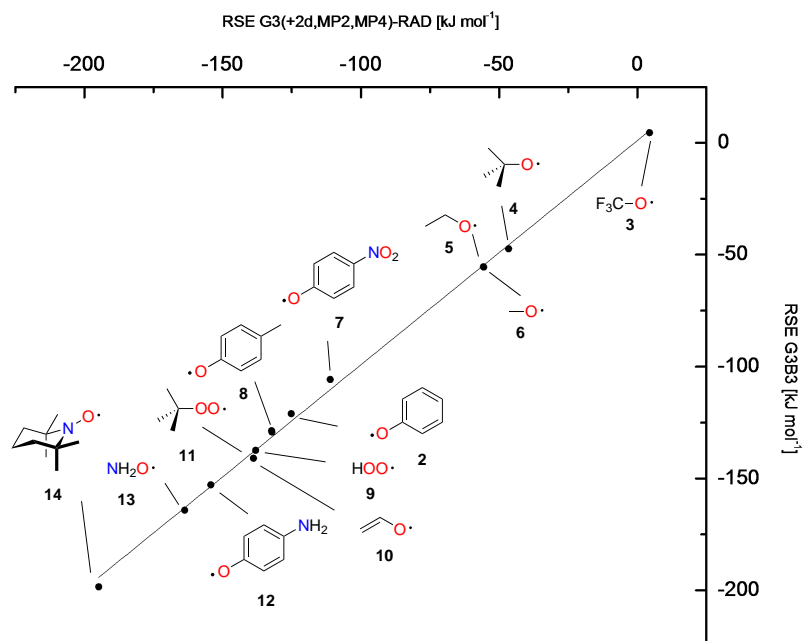


Figure 6.13: RSE (G3B3) vs. RSE (G3(+2d,MP2,MP4)-RAD). Final fit equation $\Delta H_{298}(\text{G3B3}) = 1.00238\Delta H_{298}(\text{G3(+2d,MP2,MP4)-RAD}) + 1.05624$ with correlation coefficient 0.99780. * With full cartesian basis functions for non-hydrogen atoms. Reference system **1** is excluded.

Table 6.8: Radical stabilization enthalpies (RSE, in kJ mol^{-1}) at 298.15 K of 14 O-centered radicals at G3(+2d,MP2,MP4)-RAD and G3B3 level.

System	RSE (G3(+2d,MP2,MP4)-RAD) ^a	RSE (G3B3) ^b	Deviation A-B
	A	B	
CF ₃ O• (3)	+4.5	+4.5	+0.0
HO• (1)	+0.0	+0.0	+0.0
<i>t</i> -ButO• (4)	-46.3	-47.3	+1.0
CH ₃ CH ₂ O• (5)	-55.6	-55.4	-0.2
CH ₃ O• (6)	-55.5	-55.6	+0.1
<i>p</i> -NO ₂ -PhO• (7)	-111.0	-105.5	-5.5
PhO• (2)	-125.2	-121.1	-4.1
<i>p</i> -me-PhO• (8)	-132.3	-128.8	-3.5
HOO• (9)	-132.1	-129.3	-2.8
CH ₂ CHO• (10)	-138.0	-137.5	-0.5
<i>t</i> -ButOO• (11)	-138.8	-141.0	+2.2
<i>p</i> -NH ₂ -PhO• (12)	-154.2	-152.8	-1.4
NH ₂ O• (13)	-163.7	-164.2	+0.8
TEMPO• (14)	-194.8	-198.5	+3.7

^aScaling factor 0.9806; With full cartesian basis functions.

^bScaling factor 0.960; With full cartesian basis functions.

For closed-shell systems, the total spin S is exactly zero for singlet states and thus

expectation value \hat{S}^2 is also zero. For radicals with doublet-state, S is 0.5, and \hat{S}^2 -value in restricted orbital picture amounts to 0.75. Unrestricted orbital picture unfortunately is not the exact eigenfunction of the \hat{S}^2 , and therefore the value of those for open-shells can deviate from $S(S+1)$. This particularly happens in radicals with aromatic substitution where \hat{S}^2 largely deviates from the expectation value. The consequence of the unrestricted orbital picture can be best shown in the calculated RSEs at UMP4 of two systems with different spin delocalization character (Table 6.9). The low stability at UMP4 of phenoxy radical (**2**) corresponds to the unbalanced \hat{S}^2 -value in the reaction scheme at the product side and at the educt side (Figure 6.14). In the other case, \hat{S}^2 -values for hydroxyl-radical (**1**) and the methoxy radical (**6**) are almost equivalent and thus implies a balanced reaction. The corresponding RSEs calculated at ROMP4(FC) and UMP4(FC) for methoxy radical (**6**) are very similar in this case (Table 6.9).

Table 6.9: UHF Spin-contamination and RSE of methoxy radical **6** and phenoxy radical **8** at UMP4(FC)/6-31G(d) and ROMP4(FC)/6-31G(d).

System	\hat{S}^2 (UHF) ^a	RSE (UMP4/6-31G(d))	RSE (ROMP4/6-31G(d))
HO• (1)	0.7555	+0.0	+0.0
CH ₃ O• (6)	0.7581	-42.1	-42.0
PhO• (2)	1.3794	-45.1	-102.6

^aBefore annihilation

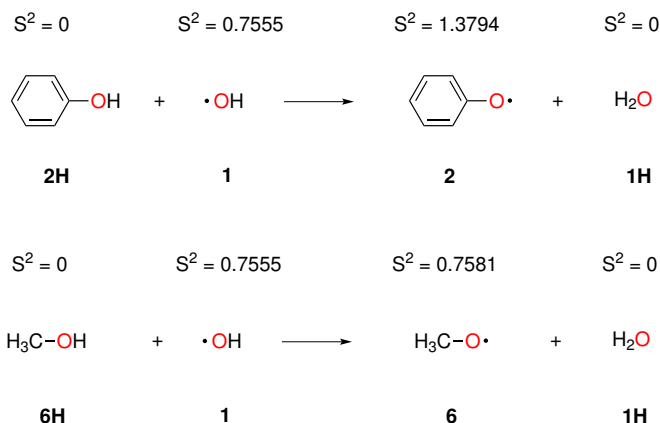


Figure 6.14: Spin contamination arising from using the UHF wavefunction with 6-31G(d).

Despite of the discussed problem with the spin contamination, many composite methods using unrestricted wavefunction such as G3B3 and G4 work fine also for delocalized radicals due to error compensations in the basis correction terms and the highest correlated methods UQCISD(T) or UCCSD(T).

Local density variation on radical center: The basis 6-31+G(2d) will only be added at oxygen atom, which carries the unpaired electron. However, LD-G3(+2d,MP2)-RAD has obviously its own problem in determining the radical center

such as in aromatic systems. The biggest advantage in the local density variant is that the increase of the basis set will be only limited to 10 basis functions per radical center, while the original adds constantly 10 basis functions to every non-hydrogen atom.

$$E_{\text{tot}}(\text{LD-G3(+2d,MP2)-RAD}) = E_{\text{tot}}(\text{LD-U(R)CCSD(T)/6-31+G(2d)}) + \text{B.C.} \quad (6.9)$$

$$\text{B.C.} = E_{\text{tot}}(\text{ROMP2(FC)/G3MP2Large}) - E_{\text{tot}}(\text{LD-ROMP2(FC)/6-31+G(2d)}) \quad (6.10)$$

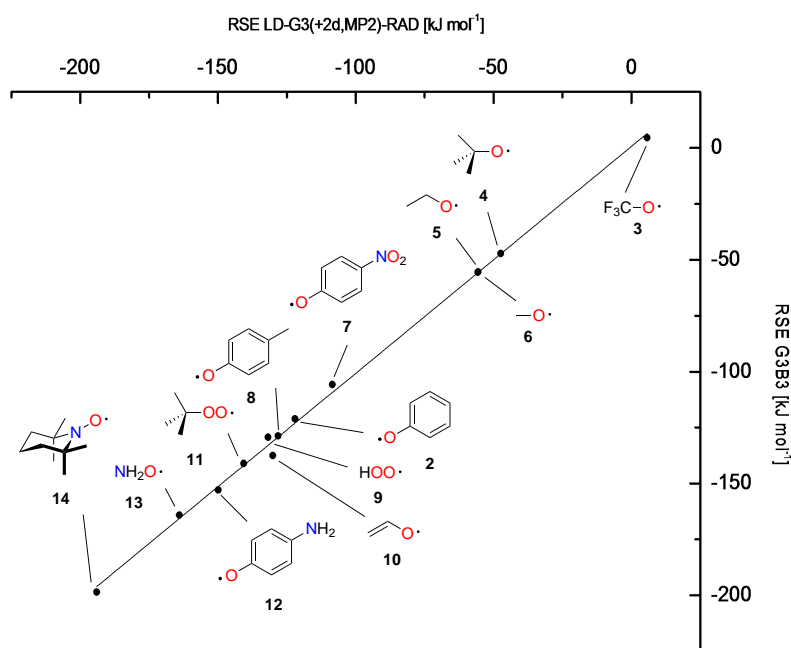


Figure 6.15: RSE (G3B3) vs. RSE (LD-G3(+2d,MP2)-RAD). Final fit equation $\Delta H_{298}(\text{G3B3}) = 1.01362\Delta H_{298}(\text{LD-G3(+2d,MP2)-RAD}) + 0.67439$ with correlation coefficient 0.998584. Reference system 1 is excluded.

Similar to G3(+2d,MP2,MP4)-RAD, LD-G3(+2d,MP2)-RAD shows little deviation to G3B3. The feasibility for moderately large systems is much better than the original G3(+2d,MP2)-RAD. Table 6.11 demonstrates the computational time in the coupled-cluster calculations used in G3(MP2)-RAD, LD-G3(+2d,MP2)-RAD, G3(+2d,MP2)-RAD. As the results show, the average CPU-time for single CCSD iteration in the U(R)CCSD(T)/6-31+G(2d) is approximately three times higher than for LD-U(R)CCSD(T)/6-31+G(2d). The calculation for triples amplitudes in U(R)CCSD(T)/6-31+G(2d) becomes very demanding even for small systems with only 8 non-hydrogen atoms.

Table 6.10: Radical stabilization enthalpies (RSE, in kJ mol⁻¹) at 298.15 K of 14 O-centered radicals at LD-G3(+2d,MP2)-RAD and G3B3 level.

System	RSE (LD-G3(+2d,MP2)-RAD) ^a		RSE (G3B3) ^b	Deviation
	A	B	B	A-B
CF ₃ O• (3)	+5.7	+4.5	+4.5	+1.2
HO• (1)	+0.0	+0.0	+0.0	+0.0
<i>t</i> -ButO• (4)	-47.4	-47.3	-47.3	-0.1
CH ₃ CH ₂ O• (5)	-55.6	-55.4	-55.4	-0.2
CH ₃ O• (6)	-55.7	-55.6	-55.6	-0.1
<i>p</i> -NO ₂ -PhO• (7)	-108.5	-105.5	-105.5	-3.0
PhO• (2)	-122.1	-120.8	-120.8	-1.3
<i>p</i> -me-PhO• (8)	-128.2	-128.4	-128.4	+0.2
HOO• (9)	-131.8	-129.3	-129.3	-2.5
CH ₂ CHO• (10)	-130.1	-137.5	-137.5	+7.4
<i>t</i> -ButOO• (11)	-140.7	-141.0	-141.0	+0.3
<i>p</i> -NH ₂ -PhO• (12)	-149.9	-152.8	-152.8	+2.9
NH ₂ O• (13)	-164.0	-164.2	-164.2	+0.2
TEMPO• (14)	-194.0	-198.5	-198.5	+4.5

^aScaling factor 0.9806; With full cartesian basis functions.

^bScaling factor 0.960; With full cartesian basis functions.

Table 6.11: Computational cost to calculate U(R)CCSD(T) for *p*-me-phenoxy-radical at different levels of theories. Calculated with MOLPRO2012.1 at Intel(R) Xeon(R) CPU E5-2665, 2.40GHz, 8 cores and 1000 MW RAM. MOLPRO2012.1 is compiled with Intel Fortran 12.1.5 using MKL 10.3.

Method	Number	Av. CPU time	CPU time	Disk usage
	of basis function	for CCSD iteration [s]	for triples [s]	[GB]
U(R)CCSD(T)/6-31G(d)	134	7.12	48.20	3.95
LD-U(R)CCSD(T)/6-31+G(2d)	144	9.32	73.65	4.67
U(R)CCSD(T)/6-31+G(2d)	214	29.50	418.73	13.06

Influence of solvents on the stability of oxygen-centered radicals: The current O-H bond dissociation or radical stabilization energies are calculated in gas phase. However, available experimental data of O-H bond strength and kinetic studies for H-abstraction from phenols are usually in solution rather than gas phase. The two are thus, while rather close, not really comparable. In this study, investigation of solvent effects using explicit monosolvation in the gas phase, continuum model (PCM) and cluster continuum model (CCM) is performed. The solvent chosen in this case is water, since the experimental O-H BDEs were mostly measured in aqueous environment. Table 6.12 show the results of monosolvation of chosen oxygen-centered radicals. The RSE of monohydrated *t*-BuO• (**4**) is very similar to that in the gas-phase, which means that the effects of hydrogen bonding in the radical (**4**) and closed-shell (**4H**) are equal. For *p*-nitrophenoxy radical (**5**) and phenoxy radical (**2**), G3(MP2)-RAD is again predicting RSE values, which are very different from G3B3 and G3(+2d,MP2)-RAD.

Table 6.12: Monohydration of oxygen-centered radicals. All RSE is calculated at G3(MP2)-RAD, G3(+2d,MP2)-RAD and G3B3.

Systems	G3(MP2)-RAD	G3(+2d,MP2)-RAD	G3B3
<i>t</i> -BuO• (4) + H ₂ O	-46.9	-47.0	-47.2
<i>p</i> -NO ₂ -PhO• (5) + H ₂ O	-138.9	-99.2	-95.4
PhO• (2) + H ₂ O	-134.4	-121.2	-119.9
<i>p</i> -me-PhO• (8) + H ₂ O	-132.7	-130.5	-129.9
<i>t</i> -BuOO• (11) + H ₂ O	-128.5	-128.4	-129.3
<i>p</i> -NH ₂ -PhO• (12) + H ₂ O	-157.2	-155.9	-157.7
TEMPO• (14) + H ₂ O	-191.9	n.a.	n.a.

This is due to the Boltzmann weighting factor of the conformers of the radicals (**2**) and (**5**), which are artificially stabilized when the water is not located at the oxy-group. Conformational restriction according to the complexation site of the water show clearly that only when the water is near to the oxy-group, G3(MP2)-RAD is able to maintain the accuracy of G3(+2d,MP2)-RAD and G3B3 (Table 6.13).

Table 6.13: RSE of phenoxy radical (**2**) and *para*-substituted phenoxy radicals (**5**, **8**, **12**) with explicit water solvation at different complexation sites.

Systems	G3(MP2)-RAD	G3(+2d,MP2)-RAD	G3B3
Water near to oxy-group			
<i>p</i> -NO ₂ -PhO• (5) + H ₂ O	-100.6	-99.9	-95.8
PhO• (2) + H ₂ O	-122.6	-121.2	-119.9
<i>p</i> -me-PhO• (8) + H ₂ O	-131.6	-130.5	-129.9
<i>p</i> -NH ₂ -PhO• (12) + H ₂ O	-157.2	-155.9	-157.7
Water far from oxy-group			
<i>p</i> -NO ₂ -PhO• (5) + H ₂ O	-153.6	-108.5	-103.8
PhO• (2) + H ₂ O	-144.5	-117.6	-116.3
<i>p</i> -me-PhO• (8) + H ₂ O	-146.0	-128.4	-127.4
<i>p</i> -NH ₂ -PhO• (12) + H ₂ O	-153.4	-152.1	-154.2

The results in Table 6.13 show the strong dependency of G3(MP2)-RAD to the water complexation site. Orbital analysis of water complexed phenoxy radical (**2**) exhibits that similar rotations occur in the reference wavefunction ROHF/6-31G(d) when the water is not interacting with the lone-pair of the oxy-group. The explicit solvent model is clearly not comparable to full aqueous phase, in which the experimental O-H BDE is measured. Probably the best known approach for modelling aqueous phase is the polarizable continuum model (PCM), which creates a cavity for the solute by constructing an overlapping spheres. Combination of explicit solvent model and continuum model is usually termed as the cluster continuum mode (CCM). Previous work by Pliego and coworker has proven the superiority of CCM against other continuum models in predicting the solvation free energy of ions in water.^[37] Nevertheless, it is very obvious that radical interacts quite weakly ions with water. Scheme 6.16 depicts, how the clusterization free energy of phenol in aqueous phase is calculated.

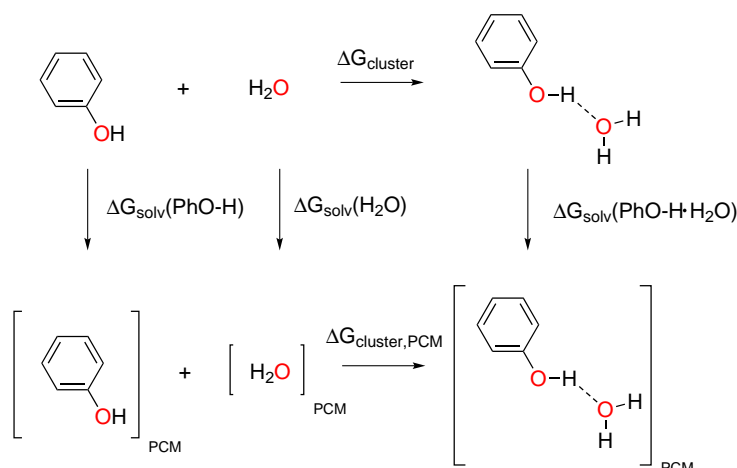


Figure 6.16: Components of clusterization free energy ($\Delta G_{\text{cluster,PCM}}$) of phenol (**2H**) in aqueous phase.

The clusterization free energy of phenol in aqueous phase can be used to determine the amount of explicit water needed to modelize the solution phase. Figure 6.17 shows that the solvation of phenol (**2H**) and phenoxy radical (**2**) in water (ΔG_{solv}), and respectively mono- and dihydrated **2H** and **2**, are thermodynamically not favorable due to the large cavitation energy. The complexation free energy ($\Delta G_{\text{cluster}}$) is also endergonic since the entropy cost is rather dominating than the net stabilization in the enthalpic terms.

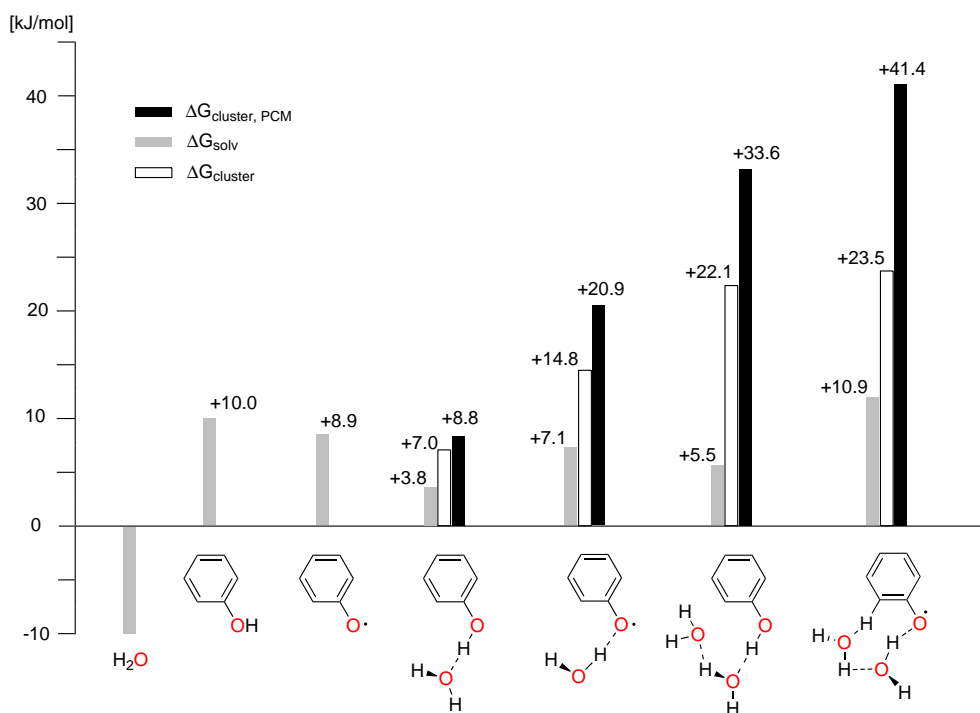


Figure 6.17: Clusterization free energy ($\Delta G_{\text{cluster,PCM}}$) of phenol (**2H**) and phenoxy radical (**2**) in aqueous phase.

In summary, the results in Figure 6.17 indicate that the application of PCM to monohydrated and dihydrated phenol (**2H**) and phenoxy radical (**2**) is not thermodynamically advantageous. Therefore, to modelize the reaction in the aqueous phase standard PCM is sufficient.

6.3 Conclusion

G3(MP2)-RAD fails to predict the stability of phenoxy radical and its derivatives. Any attempts to modify the geometry of phenoxy radical **2** and *p*-me-phenoxy radical (**8**) have yielded relatively large variation in RSEs, but not a correct stability trend. By the upgrade of the starting basis in the basis set correction term and coupled cluster step (G3(+2d,MP2)-RAD), we were able to achieve the accuracy, which is similar to the more expensive method G3B3. The computational cost of G3(+2d,MP2)-RAD can be further reduced by performing the extra basis set correction term at (U)MP4 (G3(+2d,MP2,MP4)-RAD) or applying the basis set +2d only at the radical center (LD-G3(+2d,MP2)-RAD). Both approaches show comparable results to G3(+2d,MP2)-RAD and G3B3, and therefore also a better applicability to larger systems. Nevertheless, further studies using larger training-sets are needed to test the performance and the price of the modified methods. The effect of hydration to the radical stability of O-centered radicals has been studied by explicit solvation and the cluster continuum model. Compared to continuum models the explicit solvation has the benefit of explicit treatment of hydrogen bonding. Our results show that for phenol (**2H**) and phenoxy radical (**2**), CCM is not appropriate to simulate the reaction in aqueous phase. The radical stabilities of alkyloxy radicals are only marginally affected by the monohydration, while those of phenoxy radical and substituted phenoxy radicals are differently shifted depending on the substituent (Figure 6.18).

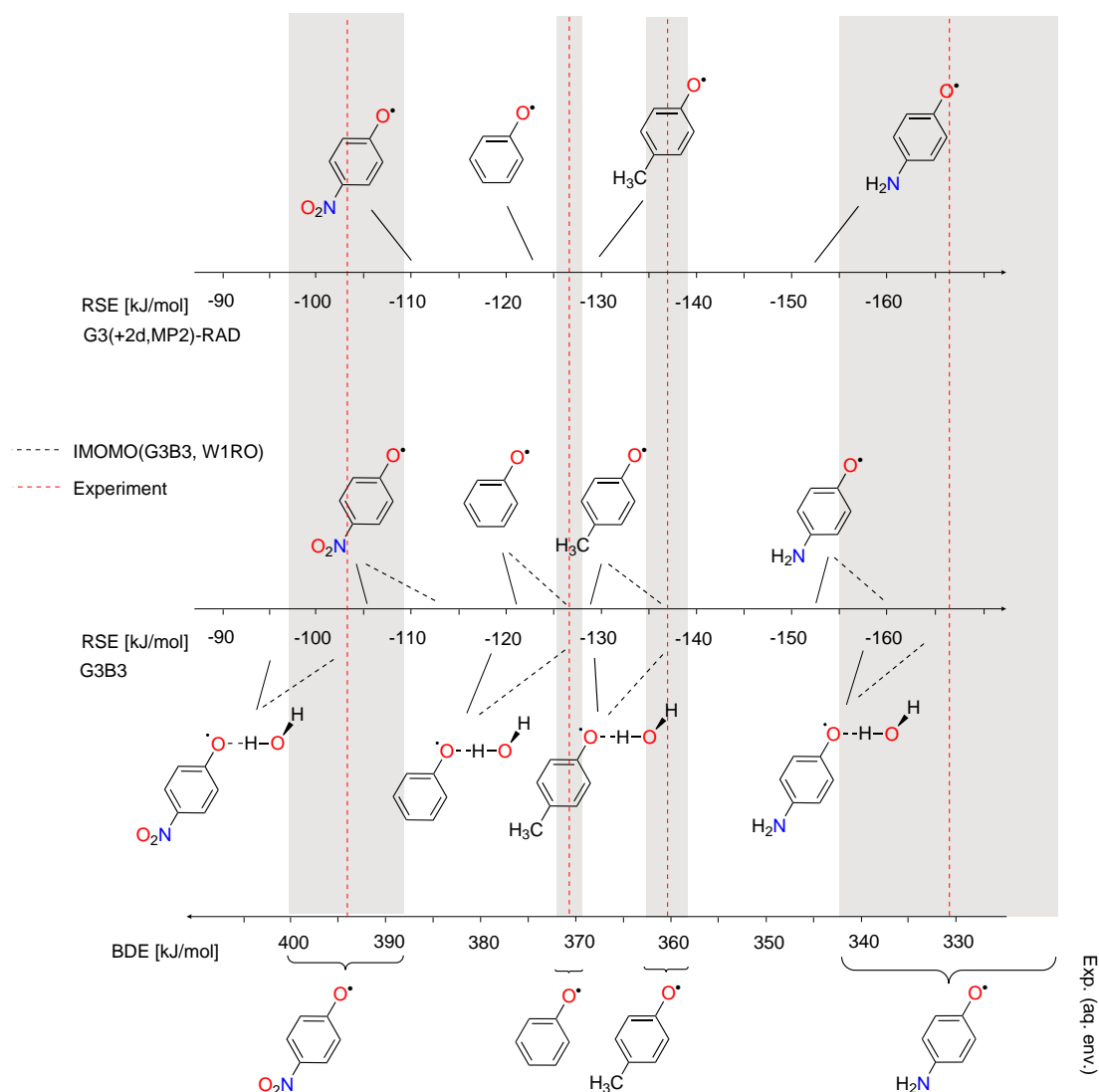


Figure 6.18: Radical stability of phenoxy radical and substituted phenoxy radicals, respectively monohydrated phenoxy radical and substituted phenoxy radicals at G3B3 and IMOMO(G3B3,W1RO) level.

Bibliography

- [1] V. Vaidya, K. U. Ingold, and D. A. Pratt. *Angew. Chem. Intl. Ed.*, 48:157–160, 2009.
- [2] G. Litwinienko and K. U. Ingold. *Acc. Chem. Res.*, 40(3):222–230, 2007.
- [3] D. A. Pratt, G. A. DiLabio, G. Brigati, G. F. Pedulli, and L. Valgimili. *J. Am. Chem. Soc.*, 19:4625–4626, 2001.
- [4] J. M. L. Martin and G. de Oliveira. *J. Chem. Phys.*, 111:1843, 1999.

- [5] L. A. Curtiss, P. C. Redfern, and K. Raghavachari. *J. Chem. Phys.*, 126:084108, 2007.
- [6] D. J. Henry, C. J. Parkinson, and L. Radom. *J. Phys. Chem. A*, 106:7927–7936, 2002.
- [7] D. J. Henry, M. B. Sullivan, and L. Radom. *J. Chem. Phys.*, 118:4849–4860, 2003.
- [8] L. A. Curtiss, P. C. Redfern, K. Raghavachari, V. Rassolov, and J. A. Pople. *J. Chem. Phys.*, 110:4703–4709, 1999.
- [9] H. Zipse J. Hioe. *Faraday Discuss.*, 145:301–313, 2010. and subsequent discussion, p. 381-409.
- [10] J. Hioe and H. Zipse. *Org. Biol. Chem.*, 8:3609–3617, 2010.
- [11] K. Condic-Jurkic, H. Zipse, and D. M. Smith. *J. Comput. Chem.*, 31:1024–1035, 2010.
- [12] K. Condic-Jurkic, V. T. Perchyonok, H. Zipse, and D. M. Smith. *J. Comput. Chem.*, 29:2425–2433, 2008.
- [13] W. Tantawy and H. Zipse. *J. Org. Chem.*, pages 5817–5820, 2007.
- [14] J. Hioe, A. Karton, J. M. L. Martin, and H. Zipse. *Chem. Eur. J.*, 16:6861–6865, 2010. correction: *Chem. Eur. J.*, 16:6722, 2010.
- [15] M. L. Coote, C. Y. Lin, and H. Zipse. *Carbon-Centered Free Radicals and Radicals Cations*, chapter "The Stability of Carbon-Centered Radicals", pages 83–104. M. D. E. Forbes (Ed.), John Wiley & Sons, 2010.
- [16] E. I. Izgorodina, D. R. B. Brittain, J. L. Hodgson, E. H. Krenske, C. Y. Lin, M. Namazian, and M. L. Coote. *J. Phys. Chem. A*, 111:10754–10768, 2007.
- [17] S. D. Wetmore, D. M. Smith, J. T. Bennett, and L. Radom. *J. Am. Chem. Soc.*, 124:14054–14065, 2002.
- [18] S. D. Wetmore, D. M. Smith, B. T. Golding, and L. Radom. *J. Am. Chem. Soc.*, 123:7963–7972, 2001.
- [19] D. M. Smith, W. Buckel, and H. Zipse. *Angew. Chem.*, 115:1867–1870, 2003.
- [20] D. Moran, R. Jacob, G. P. F. Wood, M. L. Coote, M. J. Davies, R. A. J. O’hair, C. J. Easton, and L. Radom. *Helv. Chim. Acta*, 89:2254, 2006.
- [21] Y. Zhao and D. G. Truhlar. *J. Phys. Chem. A*, 112:1095–1099, 2008.
- [22] J. Zheng, Y. Zhao, and D. G. Truhlar. *J. Phys. Chem. A*, 111:4632–4642, 2007.

- [23] H. Zipse. *Top. Curr. Chem.*, 263:163–189, 2006.
- [24] L. A. Curtiss, K. Raghavachari, P. C. Redfern, V. Rassolov, and J. A. Pople. *J. Chem. Phys.*, 109:7764, 1998.
- [25] J. Hioe and H. Zipse. *Encyclopedia of Radicals in Chemistry, Biology and Materials*, chapter "Radical Stability-Thermochemical Aspects", pages 449–476. John Wiley & sons, 2012.
- [26] Y.-R. Luo. *Comprehensive Handbook of Chemical Bond Energies*. CRC Press, 2007.
- [27] J. Lind, X. Shen, T. E. Eriksen, and G. Merényi. *J. Am. Chem. Soc.*, 112(2):479–482, 1990.
- [28] R. M. B. dos Santos and J. A. M. Simoes. *J. Phys. Chem. Ref. Data*, 27(3):707–739, 1998.
- [29] M. G. D. Nix, A. L. Devine, B. Cronin, R. N. Dixon, and M. N. R. Ashfold. *J. Chem. Phys.*, 125:133318, 2006.
- [30] G. A. Kin, M. G. D. Nix, D. E. Kelly, and M. N. R. Ashfold. *Phys. Chem. Chem. Phys.*, 10:6417, 2008.
- [31] C. Schwartz. *Methods in Computational Physics*. Academic, New York, 1963. Edited by B. J. Alder.
- [32] R. N. Hill. *J. Chem. Phys.*, 83:1173–1196, 1985.
- [33] B. Chan, M. L. Coote, and L. Radom. *J. Chem. Theory Comput.*, 6:2647–2653, 2010.
- [34] S. Grimme. *J. Chem. Phys.*, 124:034108, 2006.
- [35] B. J. Lynch, P. L. Fast, M. Harris, and D. G. Truhlar. *J. Phys. Chem. A*, 104:4811–4815, 2000.
- [36] W. T. Dixon and R. O. C. Norman. *J. Chem. Soc.*, pages 4857–4860, 1964.
- [37] J. R. Pliego Jr. and J. M. Riveros. *J. Phys. Chem. A*, 105:7241–7247, 2001.
- [38] H.-J. Werner, P. J. Knowles, R. Lindh, F. R. Manby, M. Schütz, P. Celani, T. Korona, A. Mitrushenkov, G. Rauhut, T. B. Adler, R. D. Amos, A. Bernhardsson, A. Berning, D. L. Cooper, M. J. O. Deegan, A. J. Dobbyn, F. Eckert, E. Goll, C. Hampel, G. Hetzer, T. Hrenar, G. Knizia, C. Köppl, Y. Liu, A. W. Lloyd, R. A. Mata, A. J. May, S. J. McNicholas, W. Meyer, M. E. Mura, A. Nicklaß, P. Palmieri, K. Pflüger, R. Pitzer, M. Reiher, U. Schumann, H. Stoll, A. J. Stone, R. Tarroni, T. Thorsteinsson, M. Wang, and A. Wolf. MOLPRO, version 2012.1, a package of *ab initio* programs.

- [39] M. J. Frisch, G. W. Trucks, H. B. Schlegel, G. E. Scuseria, M. A. Robb, J. R. Cheeseman, J. A. Montgomery, Jr., T. Vreven, K. N. Kudin, J. C. Burant, J. M. Millam, S. S. Iyengar, J. Tomasi, V. Barone, B. Mennucci, M. Cossi, G. Scalmani, N. Rega, G. A. Petersson, H. Nakatsuji, M. Hada, M. Ehara, K. Toyota, R. Fukuda, J. Hasegawa, M. Ishida, T. Nakajima, Y. Honda, O. Kitao, H. Nakai, M. Klene, X. Li, J. E. Knox, H. P. Hratchian, J. B. Cross, V. Bakken, C. Adamo, J. Jaramillo, R. Gomperts, R. E. Stratmann, O. Yazyev, A. J. Austin, R. Cammi, C. Pomelli, J. Ochterski, P. Y. Ayala, K. Morokuma, G. A. Voth, P. Salvador, J. J. Dannenberg, V. G. Zakrzewski, S. Dapprich, A. D. Daniels, M. C. Strain, O. Farkas, D. K. Malick, A. D. Rabuck, K. Raghavachari, J. B. Foresman, J. V. Ortiz, Q. Cui, A. G. Baboul, S. Clifford, J. Cioslowski, B. B. Stefanov, G. Liu, A. Liashenko, P. Piskorz, I. Komaromi, R. L. Martin, D. J. Fox, T. Keith, M. A. Al-Laham, C. Y. Peng, A. Nanayakkara, M. Challacombe, P. M. W. Gill, B. G. Johnson, W. Chen, M. W. Wong, C. Gonzalez, and J. A. Pople, 2009. GAUSSIAN 09 (Revision C.01), Gaussian, Inc., Wallingford, CT.

Chapter 7

Marcus-Analysis of Reaction Barriers for Hydrogen Transfer Reactions

7.1 Introduction

Marcus theory in its formulation given in eq. (7.1) has recently been used to analyze reaction barriers for nucleophilic substitution reactions, where the activation free energy ΔG^\ddagger of a reaction is expressed as a function of the reaction free energy ΔG_0 and the intrinsic barrier ΔG_0^\ddagger for a (hypothetical) process without thermochemical driving force.^[1]

$$\Delta G^\ddagger = \Delta G_0^\ddagger + \frac{1}{2}\Delta G_0 + \frac{\Delta G_0^2}{16\Delta G_0^\ddagger} \quad (7.1)$$

We analyze here whether this model is also appropriate for homolytic hydrogen atom transfer (HAT) reactions whose most general formulation is that given in eq. (7.2).



For symmetric HAT reactions such as (7.3) and (7.4) the activation free energy ΔG^\ddagger is identical to the intrinsic reaction barrier ΔG_0^\ddagger due to the absence of a thermochemical driving force. The intrinsic barrier for an unsymmetrical HAT reaction such as eq. (7.2) can then be derived using the mixing rule expressed in eq. (7.5).

$$\Delta G_0^\ddagger(X/Y) = \frac{1}{2}[\Delta G_0^\ddagger(X/X) + \Delta G_0^\ddagger(Y/Y)] \quad (7.5)$$

A recent survey of rate constants for HAT reactions has indicated that an alternative formulation of Marcus theory based on self-exchange rate constants is capable to predict rate constants over a range of 10^{13} .^[2] While this approach lends it self well to the analysis of experimentally measured rate data, the formulation chosen in eq. (7.1) is very attractive for the purpose of turning known bond dissociation energy (BDE) data^[3-6] into activation barriers.

7.2 Results

The Marcus model (7.1) is first tested in its predictive ability to model gas phase reaction barriers for hydrogen transfer reactions between radicals and hydrogen donors of variable polarity. The intrinsic reaction barriers ΔG_0^\ddagger are those calculated for the respective identity reactions.

Table 7.1: ΔG_0^\ddagger (intrinsic barrier) and ΔG_0^\ddagger calculated relative to separated reactants. In parentheses: Reaction energies ΔG_0 at G3(MP2)-RAD level. Energy unit: [kJ mol⁻¹]

X-H/X•	H ₃ C•	(CH ₃) ₂ H ₂ C•	(CH ₃) ₂ HC•	(CH ₃) ₃ C•	(CH ₃) ₂ N•	(CH ₃)O•	(CH ₃)S•
H ₃ C-H	+103.5; +109.3 ^a (+0.0)	+109.6 (+19.2)	+111.2 (+27.6)	+111.5 (+33.5)	+116.1 (+42.5)	+77.8 (-6.1)	+115.9 (+70.3)
(CH ₃) ₂ H ₂ C-H	+90.4 (-19.2)	+102.7; +104.1 ^a (+0.0)	+102.9 (+8.3)	+99.4 (+14.2)	+104.5 (+23.5)	+64.0 (-25.3)	+99.1 (+51.1)
(CH ₃) ₂ HC-H	+83.7 (-27.6)	+94.6 (-8.3)	+95.5; +97.8 ^a (+0.0)	+92.5 (+5.9)	+95.6 (+15.2)	+51.3 (-33.7)	+87.7 (+42.8)
(CH ₃) ₃ C-H	+78.0 (-33.5)	+85.2 (-14.2)	+86.6 (-5.9)	+87.2; +88.8 ^a (+0.0)	+86.5 (+9.3)	+45.1 (-39.6)	+75.3 (+36.9)
(CH ₃) ₂ N-H	+73.4 (-42.5)	+81.0 (-23.5)	+80.5 (-15.2)	+77.2 (-9.3)	+76.4; +77.4 ^a (+0.0)	+38.5 (-48.8)	+76.4 (+27.6)
(CH ₃)O-H	+83.9; +81.0 ^a (+6.1)	+89.4; +89.0 ^a (+25.3)	+84.9; +90.4 ^a (+33.7)	+84.6; +87.7 ^a (+39.6)	+87.3; +76.7 ^a (+48.8)	+79.1; +78.5 ^a (+0.0)	+131.5 (+76.4)
(CH ₃)S-H	+45.6; +45.2 ^a (-70.3)	+48.1; +47.6 ^a (-51.1)	+44.9; +44.4 ^a (-42.8)	+38.4; +37.3 ^a (-36.9)	+48.8; +47.5 ^a (-27.6)	+52.7; +52.8 ^a (-76.4)	+53.1; +56.1 ^a (+0.0)

^aG3B3.

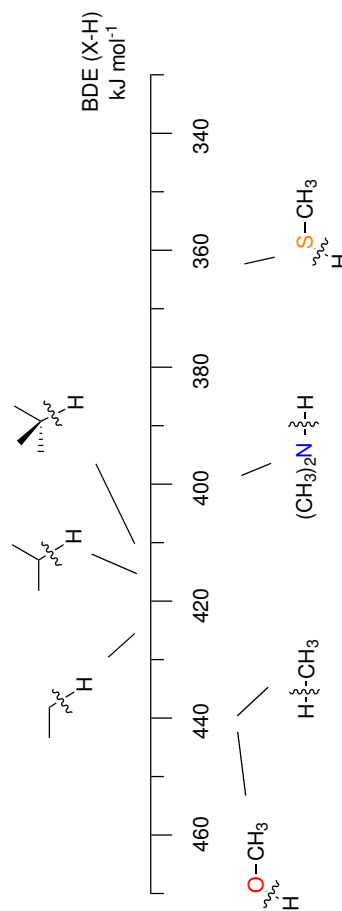


Figure 7.1: X-H bond dissociation energy scale of the listed substances in Table 7.1 at ΔH_{298} (G3(MP2)-RAD).

Correlation of the directly calculated barriers with reaction energies:

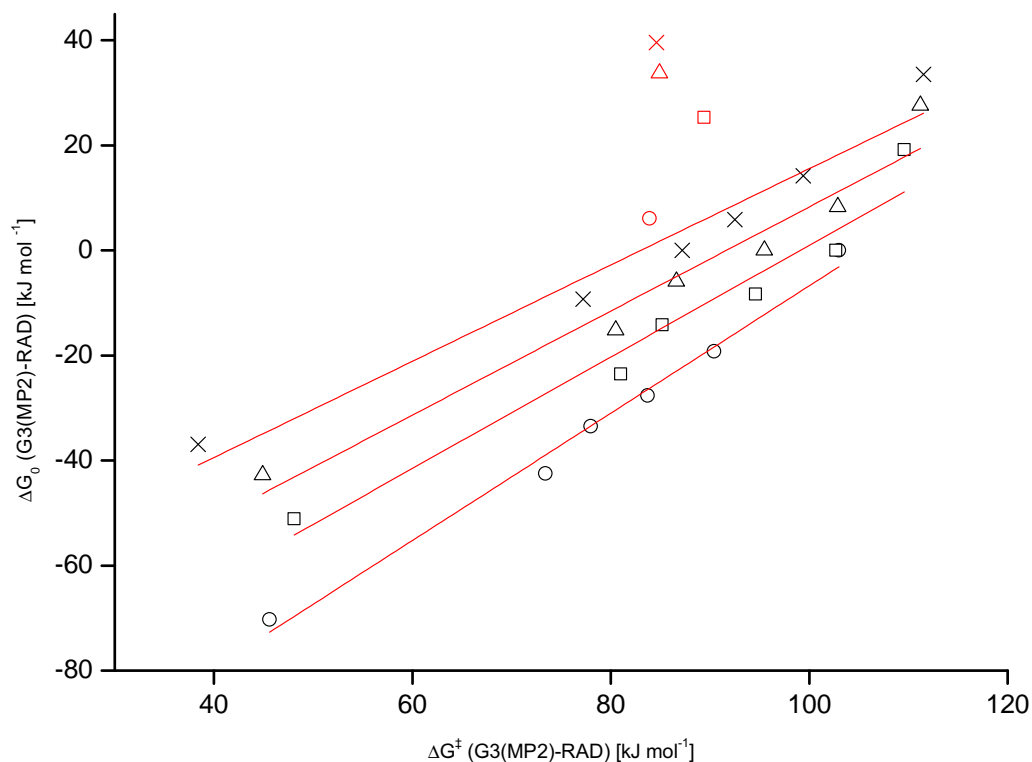


Figure 7.2: Correlation of calculated barriers with the H-abstraction reaction energies from organic compounds listed in Table 7.1 by alkyl radicals. \circ : Methyl radical; \square : 1-Ethyl radical \triangle : 2-Propyl radical; \times : *t*-Butyl radical. Red color: O-H abstraction from methanol.

For accuracy reasons we have calculated several barriers with more elaborate level of theory (G3B3). Table 7.1 shows that the calculated free energy barriers at G3(MP2)-RAD are mostly comparable with those calculated at G3B3. Larger deviations occur within the series of reaction involving methoxy radical with a maximum deviation of 10.6 kJ mol^{-1} . This problem has been pointed out in the previous chapter concerning the accuracy of G3(MP2)-RAD in predicting the stability of O-centered radicals. Figure 7.2 shows that the reaction energies of H-abstraction from selected alkanes by various radicals listed in the first line of Table 7.1 correlate well with the directly calculated barriers in one series, except the abstractions by methoxy radical. The barriers of hydrogen transfer between alkanes to methoxy radical (Table 7.1: Column 5) are usually lower than those between alkanes at similar reaction energies. As an example: The barrier for the transfer from methane to methoxy radical ($+77.8 \text{ kJ mol}^{-1}$) is lower than *t*-butane to 2-propyl radical ($+94.6 \text{ kJ mol}^{-1}$) at similar

exergonic reaction energies (-6.1 kJ mol^{-1} *vs.* -5.9 kJ mol^{-1}). This finding is supported by previous studies, which have revealed the influence of electronegativity on the barrier height. However, it should be noted that the reaction energies correlate better within a series of transfer reactions in one column rather than in one line (Figure 7.3). It seems that the barrier height is somehow more related to the type of the hydrogen abstractor than the hydrogen donor.

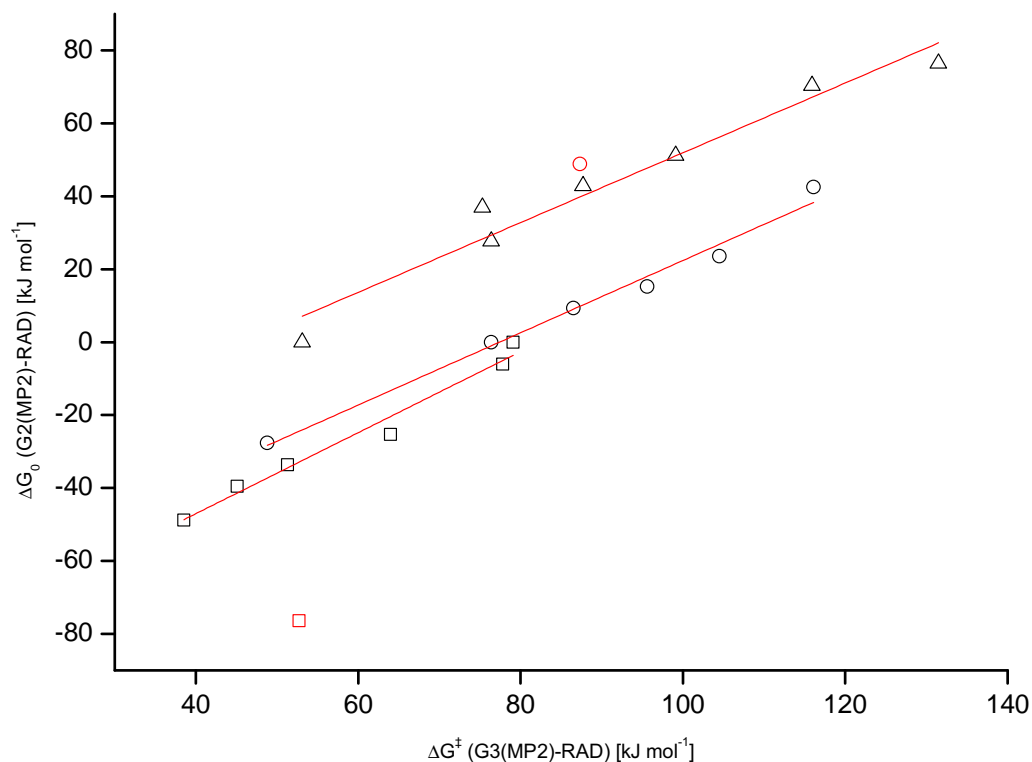


Figure 7.3: Correlation of calculated barriers with the H-abstraction reaction energies from organic compounds listed in Table 7.1 by non-carbon centered radicals. ○: Dimethylaminy radical; □: Methoxy radical △: Methylthiyl radical. Red colored: Abstraction from dimethylamine and methylthiol by methoxy radical.

Application of Marcus model: The results of calculated Marcus barriers are shown in Table 7.2 and are compared with the directly calculated barriers from Table 7.1. Overall deviations in H-transfer processes involving only carbon centered radicals are marginal. In contrast, the deviations for other radical centers are unfortunately not systematic. While the Marcus barriers for the transfer from dimethylamine to alkyl radicals are fairly similar (or slightly lower) to the directly predicted barriers, the deviations of the transfers from methanol to other radicals

are non-negligible. The directly predicted transition states between methoxy radical and alkyl radicals are always located much lower than the transition states obtained by Marcus model. An absence of polar or electronegativity effects in the Marcus formula may be responsible for the deviations in the latter case. Charge analysis (Table 7.2 and Figure 7.4) reveals that the transferred hydrogen carries a significant amount of positive charge in the transition state between methoxy radical and alkyl radicals. Additionally the methoxy radical is in this case negatively charged, while the alkyl radicals can be considered to be charge neutral or marginally positive. Therefore, the transition state is heavily influenced by the partial charge difference between the donor and acceptor. The analysis of the transition states between two alkyl radicals shows that the processes are not contaminated by charges (both donor and acceptor can be considered to be charge neutral). In contrast, the transfer processes from dimethylamine to alkyl radicals (Table 7.2: line 6) are characterized by negatively charged donor and acceptor, whose magnitude are almost equivalent in some of the cases. In addition, the transferred hydrogen carries a significant amount of positive charge as in the case between methoxy radical and alkyl radicals. Taking this together, the partial charge difference between donor and acceptor in this case does exist but the magnitude is smaller than in transfers involving methoxy radical.

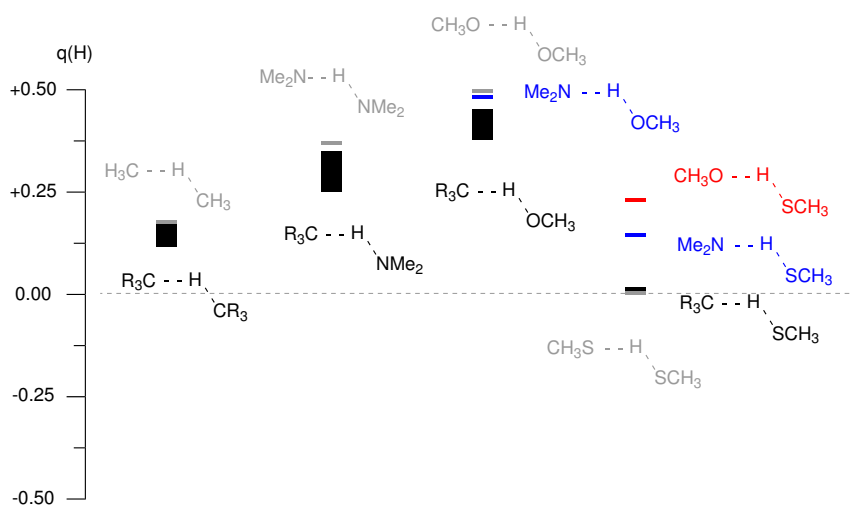


Figure 7.4: Mulliken atomic charge of transferred hydrogen in the transition states at B3LYP/6-31G(d) level of theory.

From the charge analysis a relationship between the partial charge difference Δq and the deviation of the predicted Marcus barrier to the directly calculated barrier can be partially observed. In the series of H-transfers from methylthiol to alkyl radicals (Table 7.2: line 8), the deviation of predicted Marcus barriers is increasing with the increase of partial charge difference. The partial charge difference in the transition state between methylthiyl radical and methyl radical ($\Delta q = -0.121$) are very similar to the transition state between dimethylaminyl radical and *t*-butyl radical ($\Delta q = -0.122$). The deviations of Marcus barriers are in both cases also small and very similar. With the increase of the difference in partial charges, the transfer reaction

is transformed to a more polarity driven process. In this case, the predictive power of Marcus barrier is again deteriorating, resembling to the transfer processes from methanol to other radicals, which shows much higher Marcus barriers compared to direct barriers. However we notice here that the character of the processes is different from those of the transfer processes from methanol (or dimethylamine) to other radicals, since the transferred hydrogen is not carrying a positive charge. The analysis of the transition state between methylthiyl radical and dimethylaminyl radical shows a large partial charge difference ($\Delta q = -0.195$) with a rather small deviation ($+2.9 \text{ kJ mol}^{-1}$) of Marcus barrier and directly predicted barrier. We therefore expect a similar deviation as in the transfer process from methylthiol to *t*-butyl radical.

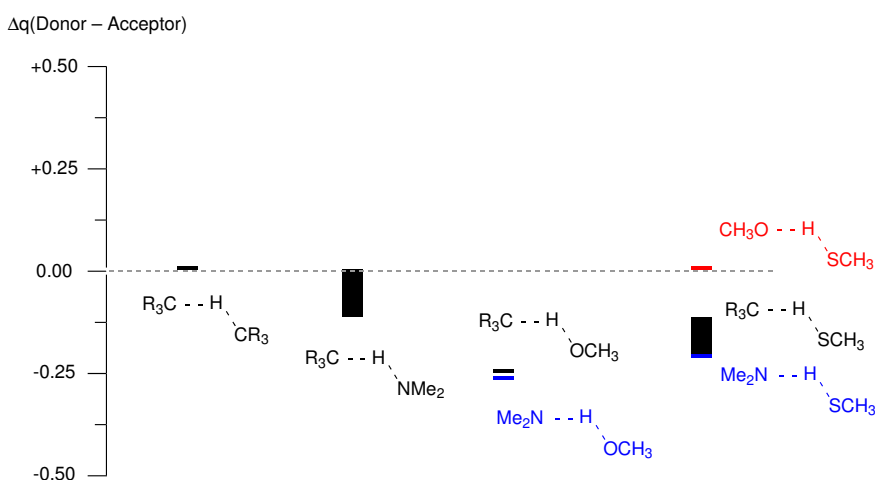


Figure 7.5: Partial charge difference Δq between donor and acceptor at the transition state (B3LYP/6-31G(d)).

However this is not the case as the result shows (Table 7.2: line 8, column 6). Here we observe a significant increase of positive charge on the transferred hydrogen ($q(\text{H}) = +0.139$). The effect of a positively charged hydrogen seems to damp the effect of partial charge difference in this case. While the partial charge difference in this case lowers the direct calculated barriers, the amount of the positive charge counteracts and rises the barrier. In the transition state between methoxy radical and methylthiyl radical the partial charge difference is near to zero, while the transferred hydrogen carries a positive charge. Both, near zero partial charge difference and positively charged hydrogen, imply a higher value of direct calculated barrier. The expected predicted Marcus barrier hence must be too small when compared to the direct calculated barrier according to the previous assumption. The latter is fully in accordance with the result (Table 7.2: line 8, column 7), which showed that the Marcus barrier is by $-20.7 \text{ kJ mol}^{-1}$ too small against the direct calculated barrier. Going back to the series of transfer reactions from dimethylamine to alkyl radicals, we can rationalize why the barrier calculated by Marcus model is lower than the direct calculated barrier. The transition states involving dimethylaminyl

radical and alkyl radicals are marked by a relatively high positive charge on transferred hydrogen, and simultaneously small partial charge difference between donor and acceptor. The most negative deviation, which occurs in the transition state between dimethylaminy radical and alkyl radical, is apparently caused by a high positive charge on hydrogen and near zero partial charge difference. According to our previous analysis, the direct calculated barrier must be therefore high, which in this case $+3.5 \text{ kJ mol}^{-1}$ higher than the Marcus barrier. Moving to the right, the amount of positive charge on transferred hydrogen is decreasing, and at the same time the partial charge difference is increasing. Therefore the magnitude of the deviation becomes more positive since the direct calculated barrier is getting smaller relative to Marcus barrier.

Table 7.2: ΔG_0^\ddagger (intrinsic barrier) and ΔG^\ddagger calculated according to Marcus model relative to separated reactants, Mulliken atomic charge of transferred hydrogen $q(\text{H})$ in the transition states and difference of partial charge between donor and acceptor $\Delta q = q(\text{donor}) - q(\text{acceptor})$. In parentheses: Deviation to directly calculated barriers. Energy unit: kJ mol^{-1} .

X-H/X•	$\text{H}_3\text{C}\cdot$	$(\text{CH}_3)\text{H}_2\text{C}\cdot$	$(\text{CH}_3)_2\text{HC}\cdot$	$(\text{CH}_3)_3\text{C}\cdot$	$(\text{CH}_3)_2\text{N}\cdot$	$(\text{CH}_3)\text{O}\cdot$	$(\text{CH}_3)\text{S}\cdot$
$\text{H}_3\text{C-H}$	+103.5 (+0.0) $q(\text{H}) = 0.178$ $\Delta q = +0.0$	+112.9 (+3.3) $q(\text{H}) = 0.169$ $\Delta q = -0.019$	+113.8 (+2.5) $q(\text{H}) = 0.162$ $\Delta q = -0.028$	+112.9 (+1.4) $q(\text{H}) = 0.154$ $\Delta q = -0.029$	+112.4 (-3.5) $q(\text{H}) = 0.309$ $\Delta q = +0.063$	+88.3 (+10.5) $q(\text{H}) = 0.369$ $\Delta q = +0.227$	+117.4 (+1.5) $q(\text{H}) = 0.048$ $\Delta q = +0.121$
$(\text{CH}_3)\text{H}_2\text{C-H}$	+93.7 (+3.3) $q(\text{H}) = 0.169$ $\Delta q = +0.019$	+102.7 (+0.0) $q(\text{H}) = 0.160$ $\Delta q = +0.0$	+103.3 (+0.4) $q(\text{H}) = 0.151$ $\Delta q = -0.010$	+102.1 (+2.7) $q(\text{H}) = 0.143$ $\Delta q = -0.012$	+101.7 (-2.9) $q(\text{H}) = 0.295$ $\Delta q = +0.098$	+78.7 (+14.6) $q(\text{H}) = 0.352$ $\Delta q = +0.237$	+105.5 (+6.3) $q(\text{H}) = 0.040$ $\Delta q = +0.155$
$(\text{CH}_3)_2\text{HC-H}$	+86.2 (+2.5) $q(\text{H}) = 0.162$ $\Delta q = +0.028$	+95.0 (+0.4) $q(\text{H}) = 0.151$ $\Delta q = +0.010$	+95.5 (+0.0) $q(\text{H}) = 0.142$ $\Delta q = +0.0$	+94.3 (+1.8) $q(\text{H}) = 0.133$ $\Delta q = -0.002$	+93.8 (-1.7) $q(\text{H}) = 0.280$ $\Delta q = +0.114$	+71.3 (+20.1) $q(\text{H}) = 0.338$ $\Delta q = +0.236$	+97.3 (+9.6) $q(\text{H}) = 0.032$ $\Delta q = +0.180$
$(\text{CH}_3)_3\text{C-H}$	+79.4 (+1.4) $q(\text{H}) = 0.154$ $\Delta q = +0.029$	+87.9 (+2.7) $q(\text{H}) = 0.143$ $\Delta q = +0.012$	+88.4 (+1.8) $q(\text{H}) = 0.133$ $\Delta q = +0.002$	+87.2 (+0.0) $q(\text{H}) = 0.124$ $\Delta q = +0.0$	+86.5 (+0.0) $q(\text{H}) = 0.266$ $\Delta q = +0.122$	+64.5 (+19.5) $q(\text{H}) = 0.320$ $\Delta q = +0.232$	+89.8 (+14.5) $q(\text{H}) = 0.024$ $\Delta q = +0.198$
$(\text{CH}_3)_2\text{N-H}$	+69.9 (-3.5) $q(\text{H}) = 0.309$ $\Delta q = -0.063$	+78.2 (-2.9) $q(\text{H}) = 0.295$ $\Delta q = -0.098$	+78.6 (-1.7) $q(\text{H}) = 0.280$ $\Delta q = -0.114$	+77.2 (+0.0) $q(\text{H}) = 0.266$ $\Delta q = -0.122$	+76.4 (+0.0) $q(\text{H}) = 0.399$ $\Delta q = +0.0$	+55.3 (+16.8) $q(\text{H}) = 0.434$ $\Delta q = +0.263$	+79.3 (+2.9) $q(\text{H}) = 0.139$ $\Delta q = +0.195$
$(\text{CH}_3)\text{O-H}$	+94.4 (+10.5) $q(\text{H}) = 0.369$ $\Delta q = -0.227$	+104.0 (+14.6) $q(\text{H}) = 0.352$ $\Delta q = -0.237$	+105.0 (+20.1) $q(\text{H}) = 0.338$ $\Delta q = -0.236$	+104.1 (+19.5) $q(\text{H}) = 0.320$ $\Delta q = -0.232$	+104.1 (+16.8) $q(\text{H}) = 0.434$ $\Delta q = -0.263$	+79.1 (+0.0) $q(\text{H}) = 0.473$ $\Delta q = +0.0$	+108.5 (-20.7) $q(\text{H}) = 0.205$ $\Delta q = -0.056$
$(\text{CH}_3)\text{S-H}$	+47.1 (+1.5) $q(\text{H}) = 0.048$ $\Delta q = -0.121$	+54.4 (+6.3) $q(\text{H}) = 0.040$ $\Delta q = -0.155$	+54.5 (+9.6) $q(\text{H}) = 0.032$ $\Delta q = -0.180$	+52.9 (+14.5) $q(\text{H}) = 0.024$ $\Delta q = -0.198$	+51.7 (+2.9) $q(\text{H}) = 0.139$ $\Delta q = -0.195$	+32.1 (-20.7) $q(\text{H}) = 0.205$ $\Delta q = +0.056$	+53.1 (+0.0) $q(\text{H}) = -0.045$ $\Delta q = +0.0$

7.3 Conclusion

The barrier height of H-transfer reactions are influenced by several factors and substrate dependent. The Marcus model has a limitation in the predictive power since the effects of charge on the transferred hydrogen and partial charge difference between donor and acceptor are non-existent, therefore a lost connection. In this study we provide a qualitative analysis of the deficits in the Marcus model. According to our results, we need to differentiate the reaction set into several cases.

Case 1) Transfer between two alkyl radicals: The Marcus model is fairly able to predict the barriers. The partial charge difference is in this case near to zero and the transferred hydrogen carries a relative small amount of positive charge. Furthermore the donor and the acceptor are almost charge neutral. The effect of charge on the transferred hydrogen is mostly covered in the Marcus model since it is mimicked also in the calculation of the intrinsic barriers of both donor and acceptor.

Case 2) Transfer between methoxy radical and other radicals: The deviations are particularly huge in this series, due to the failure of the Marcus model in reflecting the partial charge difference in the directly calculated barrier, which lowers the barrier. The transferred hydrogen carries a large amount of positive charge, which seems not to have any effects (or very minor) to act against the effect of partial charge difference. In contrary to case 1, the effect of positive charge on the transferred hydrogen is non-existent (in most of the cases) since the atomic charges of the corresponding hydrogens obtained from intrinsic barrier calculations are very different from those in the direct predicted barrier.

Case 3) Transfer between dimethylaminy radical and alkyl radicals: Like in case 1, the Marcus model successfully predicts the barrier height. The transferred hydrogen is carrying here a significant amount of charge. The donor and acceptor are negatively charged in contrast to the case 1. The magnitude of partial charge differences are ranging from near zero to small negative value. The effect of partial charge difference in decreasing the barrier seems to be minor in this value range ($\Delta q = -0.063$ to -0.122) while the amount of positive charge on transferred hydrogen in increasing the barrier is significant. The small deviation of the Marcus model may be hence caused by a relatively large directly predicted barrier. The significant effect of large partial charge difference can be observed in the transfer between dimethylaminy radical and methoxy radical ($\Delta q = -0.263$) which is marked again by a too large Marcus barrier relative to directly predicted barriers. As in the case 2, the effect of positive charge on the transferred hydrogen cannot be obtained by the calculation of the intrinsic barriers.

Case 4) Transfer between methylthiyl radical and other radicals: The transfer processes involving methylthiyl radical are very complex. In reactions with alkyl radicals the effect of positive charge on transferred hydrogen is very similar to

the atomic charge of the corresponding hydrogen calculated in the intrinsic barrier of methylthiol. Therefore the effect should be already incorporated in the Marcus model. The effect of the partial charge difference is steadily increasing in the series, hence the Marcus barrier is becoming too high compared to directly predicted barrier, since the reaction is turning to be polarity driven process. In the transfer between methylthiyl radical and dimethylaminy radical the positive charge on hydrogen counteracts the effect of partial charge difference. The compensation results in a small barrier difference. In the reaction between methylthiyl radical and methoxy radical, the deviation is large and negative due to the effect of positive charge on transferred hydrogen and small partial energy difference, which in synergistic manner increases the directly predicted barrier.

Bibliography

- [1] M. Breugst, H. Zipse, J. P. Guthrie, and H. Mayr. *Angew. Chem. Int. Ed.*, 49:5165–5169, 2010.
- [2] J. M. Mayer. *Acc. Chem. Res.*, 44:36–46, 2011.
- [3] H. Zipse. *Topics Curr. Chem.*, 263:163–189, 2006.
- [4] J. Hioe and H. Zipse. *Faraday Disc.*, 145:301–313, 2010.
- [5] M. L. Coote, C. Y. Lin, and H. Zipse. *Carbon-Centered Free Radicals and Radicals Cations*, chapter "The Stability of Carbon-Centered Radicals", pages 83–104. M. D. E. Forbes (Ed.), John Wiley & Sons, 2010.
- [6] J. Hioe and H. Zipse. *Org. Biol. Chem.*, 8:3609–3617, 2010.
- [7] H.-J. Werner, P. J. Knowles, R. Lindh, F. R. Manby, M. Schütz, P. Celani, T. Korona, A. Mitrushenkov, G. Rauhut, T. B. Adler, R. D. Amos, A. Bernhardsson, A. Berning, D. L. Cooper, M. J. O. Deegan, A. J. Dobbyn, F. Eckert, E. Goll, C. Hampel, G. Hetzer, T. Hrenar, G. Knizia, C. Köppl, Y. Liu, A. W. Lloyd, R. A. Mata, A. J. May, S. J. McNicholas, W. Meyer, M. E. Mura, A. Nicklaß, P. Palmieri, K. Pflüger, R. Pitzer, M. Reiher, U. Schumann, H. Stoll, A. J. Stone, R. Tarroni, T. Thorsteinsson, M. Wang, and A. Wolf. MOLPRO, version 2006.1, *a package of ab initio programs*.
- [8] M. J. Frisch, G. W. Trucks, H. B. Schlegel, G. E. Scuseria, M. A. Robb, J. R. Cheeseman, J. A. Montgomery, Jr., T. Vreven, K. N. Kudin, J. C. Burant, J. M. Millam, S. S. Iyengar, J. Tomasi, V. Barone, B. Mennucci, M. Cossi, G. Scalmani, N. Rega, G. A. Petersson, H. Nakatsuji, M. Hada, M. Ehara, K. Toyota, R. Fukuda, J. Hasegawa, M. Ishida, T. Nakajima, Y. Honda, O. Kitao, H. Nakai, M. Klene, X. Li, J. E. Knox, H. P. Hratchian, J. B. Cross, V. Bakken, C. Adamo, J. Jaramillo, R. Gomperts, R. E. Stratmann, O. Yazyev, A. J. Austin,

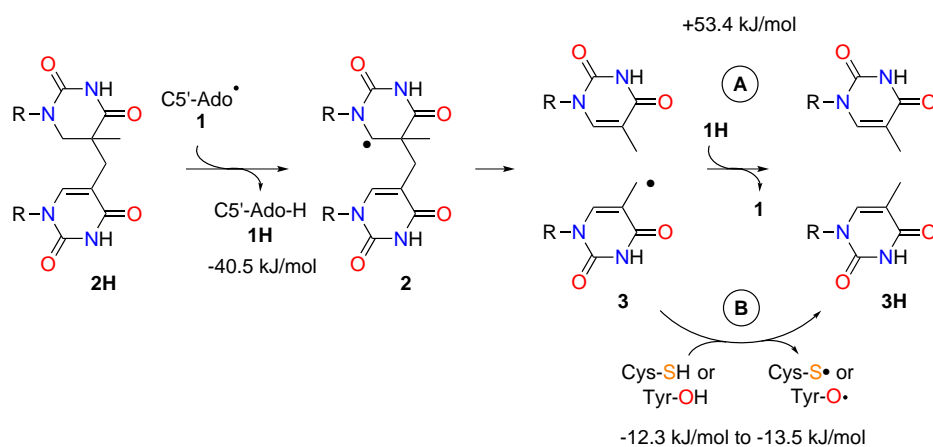
R. Cammi, C. Pomelli, J. Ochterski, P. Y. Ayala, K. Morokuma, G. A. Voth, P. Salvador, J. J. Dannenberg, V. G. Zakrzewski, S. Dapprich, A. D. Daniels, M. C. Strain, O. Farkas, D. K. Malick, A. D. Rabuck, K. Raghavachari, J. B. Foresman, J. V. Ortiz, Q. Cui, A. G. Baboul, S. Clifford, J. Cioslowski, B. B. Stefanov, G. Liu, A. Liashenko, P. Piskorz, I. Komaromi, R. L. Martin, D. J. Fox, T. Keith, M. A. Al-Laham, C. Y. Peng, A. Nanayakkara, M. Challacombe, P. M. W. Gill, B. G. Johnson, W. Chen, M. W. Wong, C. Gonzalez, and J. A. Pople, 2004. GAUSSIAN 03 (Revision D.01), Gaussian, Inc., Wallingford, CT.

Chapter 8

Barrier in Spore Photoproduct Lyase

8.1 Introduction

The proposed repair mechanism of photodimer 5-thyminy-5,6-dihydrothymine using C5'-adenosyl radicals in catalytic fashion remains a mystery due to the thermodynamic profile of the cycle.^[1-18] Previously we have shown according to our stability data that the repair mechanism using SAM as a co-factor and peptide radicals as active catalyst (Scheme 8.1: path **B**) has a flatter thermodynamic profile and hence is more feasible.^[19-25] The X-ray structure of SPL (*G. Thermodenitrificans*) pinpoints cysteine (C140) and tyrosine (Y98) in proximity of the substrate. Mutation experiments of cysteine residue (C140A/S) have shown reduced activity of the enzyme and evidenced the direct involvement of cysteine as hydrogen donor to 3'-thymine instead as a structural seal in the catalytic center to prevent other side reactions.^[26] Recent work concerning the role of tyrosine in the repair cycle has concluded that existence of tyrosine (Y98) is indeed compulsory, probably as a reductant of cysteinyl radical and the real propagator which abstracts the hydrogen of the new substrate.^[27] However the thermodynamic stabilities of tyrosyl and cysteinyl radicals are differing only by about 1-2 kJ mol⁻¹ at higher level theory. Thus no preferences between tyrosine and cysteine as propagators can be made. In this work we therefore present the kinetic profile of the two possible peptides as the second criterion in addition to our thermodynamic data.



Scheme 8.1: Originally proposed and alternative repair mechanisms of photodimer 5-thyminy-5,6-dihydrothymine.

8.2 Results

The free energy barriers of repair mechanisms were evaluated at G3(MP2)-RAD level of theory. In contrast, thermodynamic reaction energies were calculated at the more elaborate methods G3B3 or IMOMO(G3B3,G3(MP2)-RAD) due to the inaccuracy of G3(MP2)-RAD in predicting the stability of phenoxy radicals.

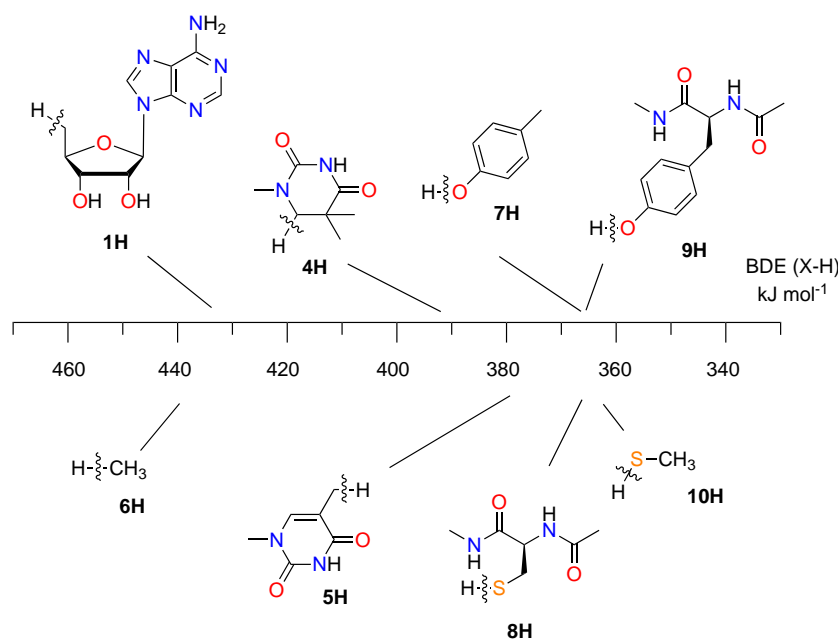


Figure 8.1: BDE scale based on ΔH_{298} G3B3 or ΔH_{298} IMOMO(G3B3,G3(MP2)-RAD) of the models used to estimate reaction enthalpies.

Table 8.1: Bond dissociation energies (BDE) at ΔH_{298} and ΔG_{298} of the systems shown in Figure 8.1.

System	BDE ΔH_{298} [kJ/mol]	BDE ΔG_{298} [kJ mol ⁻¹]	BDE exp. [kJ mol ⁻¹]
6H	n.a.	n.a.	+439.3
1H	+432.4	n.a.	n.a.
4H	+392.0	+391.0 ^a	n.a.
5H	+379.1	n.a.	n.a.
7H	+367.7 (+367.8 ^a)	+370.2 ^a	+360.2
8H	+366.8	n.a.	n.a.
9H	+365.6 ^b	n.a.	n.a.
10H	+363.0 (+363.0 ^a)	+366.8 ^a	+365.7

^aFree energy correction at B3LYP/6-31G(d) with grid ultrafine and scaling factor of 0.960.

^bIMOMO(G3B3/G3(MP2)-RAD).

First step of the repair mechanism: As already proposed in previous studies, C5'-adenosyl radical **1** will abstract the hydrogen at the C6-position from the SPL substrate **2H**. The kinetic barrier will be assessed by using methane **6H** and methyl radical **6** as models to adenosine **1H** and C5'-adenosyl radical **1**. The reaction enthalpy at G3B3 for this step using methyl radical as hydrogen abstractor has been estimated to be exothermic by -47.4 kJ mol⁻¹. The reaction enthalpy with C5'-adenosyl radical has been evaluated at G3(MP2)-RAD to be -40.5 kJ mol⁻¹.^[19;25] The difference in radical stability between methyl radical and C5'-adenosyl radical is known to be -6.9 kJ mol⁻¹ at G3(MP2)-RAD level, implying an identical reaction

enthalpy between the two computational methods. The results show that the entropic contribution to the reaction enthalpy is rather small (-0.9 kJ mol $^{-1}$), giving a free reaction energy of -48.3 kJ mol $^{-1}$. Figure 8.2 shows that the H-abstraction barrier from the substrate model **4H** by methyl radical **6** at G3(MP2)-RAD ($+73.4$ kJ mol $^{-1}$) is the lowest when compared to the abstraction barriers by methylthiyl radical **10** ($+90.3$ kJ mol $^{-1}$) and *p*-me-phenoxy radical **7** ($+84.9$ kJ mol $^{-1}$). However the thermodynamic reaction energy of the abstraction process by methyl radical **6** is 69.1 - 72.5 kJ mol $^{-1}$ lower than the abstraction energy by methylthiyl radical **10** and *p*-me-phenoxy radical **7**.

Table 8.2: Reaction enthalpies (ΔH_{298}) and free energies (ΔG_{298}) at G3B3 level and reaction barriers (ΔH_{298}^\ddagger , ΔG_{298}^\ddagger) at G3(MP2)-RAD level of the reactions shown in Figures 8.2 and 8.3.

	ΔH_{298} [kJ mol $^{-1}$]	ΔG_{298} [kJ mol $^{-1}$]	ΔH_{298}^\ddagger [kJ mol $^{-1}$]	ΔG_{298}^\ddagger [kJ mol $^{-1}$]
4H + 6	-47.4	-48.3	+36.2	+73.4
4H + 7	+24.1	+20.8	+40.9	+84.9
4H + 10	+29.0	+24.2	+47.9	+90.3
6H + 6	+0.0	+0.0	+70.5	+103.5
6H + 7	+71.5	+69.1	+106.7	+139.3
6H + 10	+76.3	+72.5	+89.6	+118.1
10H + 10	+0.0	+0.0	+15.1	+53.1

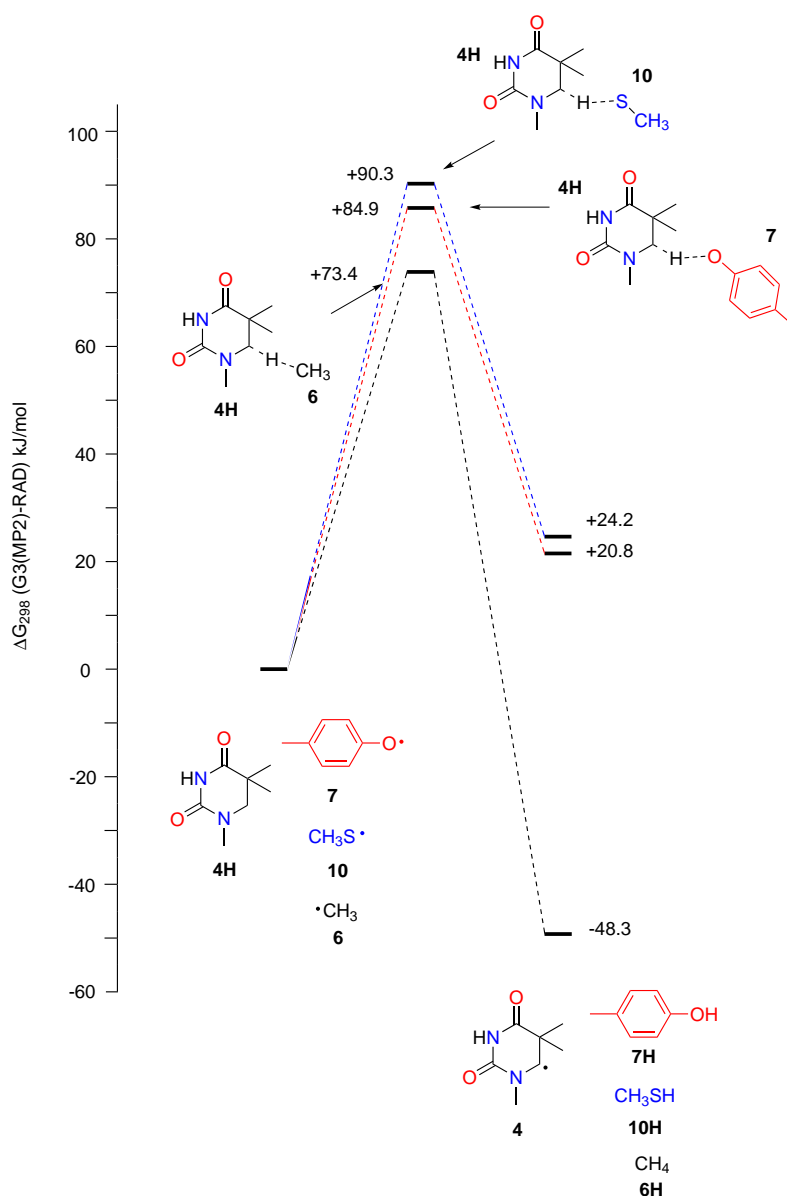


Figure 8.2: Reaction topology of the H-atom transfer of the initiation step in SPL repair mechanism.

The relatively high reaction barrier of the H-abstraction by methyl radical **6** from the SPL substrate model **4H** (+73.4 kJ mol⁻¹) at very exergonic reaction energy (-48.3 kJ mol⁻¹) can be explained by the high intrinsic barrier of C-H bond rupture and the polar effects in the transition state. The intrinsic barrier of symmetric H-abstraction of the pair methane **6H** and **6** is calculated to be +103.5 kJ mol⁻¹ at G3(MP2)-RAD (Figure 8.3). This intrinsic barrier is much higher compared to those of the pair methylthiol **10H** and **10** (+53.1 kJ mol⁻¹). The impact of the height of the intrinsic barrier is demonstrated in Figure 8.3, which shows that the transfer between methylthiol radical **10** and methane **6H** has slightly higher barrier (+118.1 kJ mol⁻¹) at very endergonic reaction energy (+72.5 kJ mol⁻¹) when compared to the

intrinsic barrier of methane **6H** and methyl radical **6** (+103.5 kJ mol⁻¹). According to the Marcus analysis (Chapter 7), the contribution of the intrinsic barrier of the pair **6H/6** and **10H/10** to the barrier height is +78.3 kJ mol⁻¹ for the reaction involving methane **6H** and methylthiyl radical **10**. The other +39.8 kJ mol⁻¹ is a sum of the half of the reaction energy (+36.3 kJ mol⁻¹) and a small cross term.

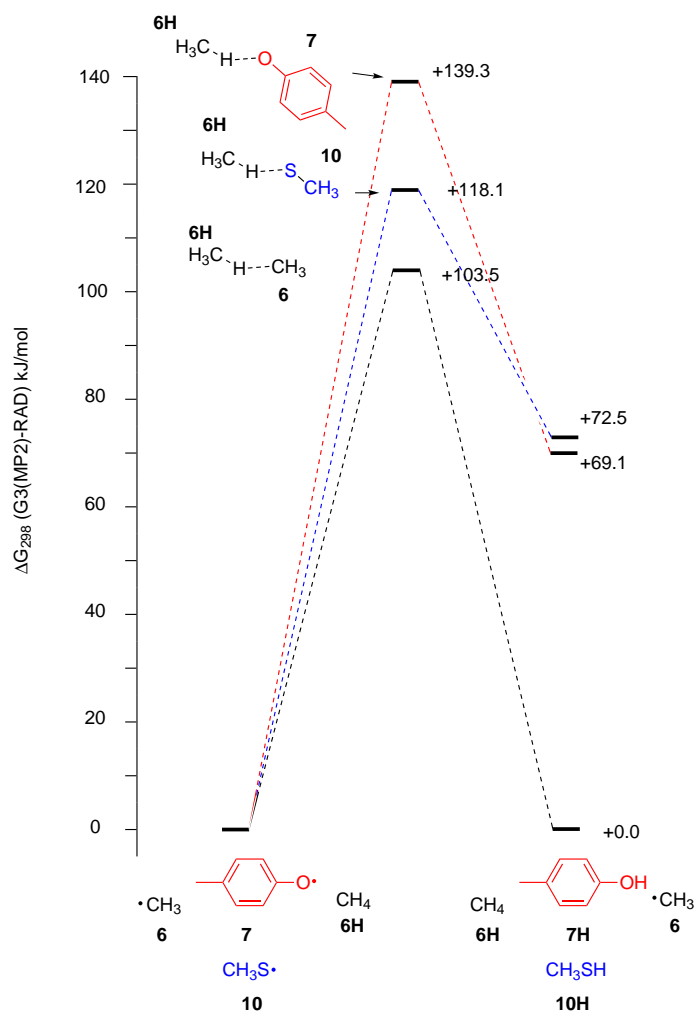
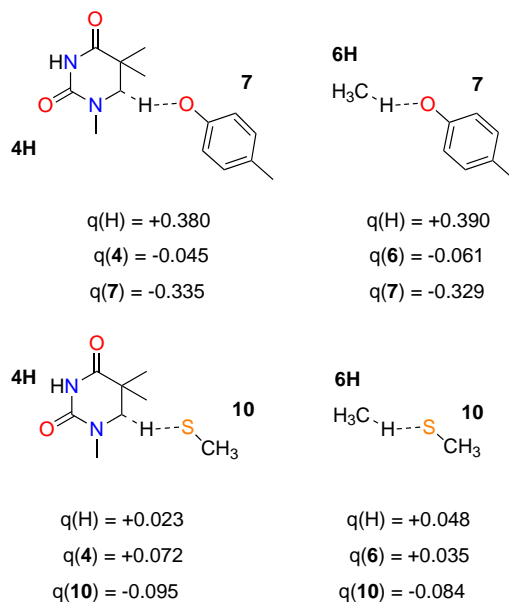


Figure 8.3: Reaction topology of the H-atom abstraction from methane **6H** by *p*-methoxy radical **7**, methylthiyl radical **10** and methyl radical **6**.

For the reaction involving *p*-me-phenoxy radical **7** and methane **6H**, similar reaction energy (+69.1 kJ mol⁻¹) is obtained as for the reaction between methylthiyl radical **10** and methane **6H**. However the barrier height of the transfer process of the former is now much higher than the latter, implying that the intrinsic barrier of the pair *p*-me-phenol **7H** and *p*-me-phenoxy radical **7** is higher than the intrinsic barrier the pair methylthiol **10H** and methylthiyl radical **10**. Previous study of the application of Marcus analysis in predicting barrier height of H-transfer reactions (Chapter 7) shows that polarity may affect the barrier height in the transfer process between oxygen centered radical and various alkanes. In the case where polarity difference is

present in the transition state, the application of Marcus equation is not appropriate since it considers only the contribution of intrinsic barriers, thermodynamic reaction energy and a cross term arising from parabolic treatment of the potential surfaces. Information of other effects, such as the complexity of the transition state geometry and polarity are absent in the Marcus equation.



Scheme 8.2: Mulliken charge on transferred hydrogen atom at B3LYP/6-31G(d) and on the H-acceptor and H-donor.

Scheme 8.2 compiles the Mulliken charge analysis of the all transition states depicted in Figures 8.2 and 8.3. The charge analysis shows that the transferred hydrogen atom carries a significant positive charge in the transfer processes involving *p*-me-phenoxy radical **7** and methane **6H** or substrate model **4H**. Furthermore the partial charge difference between acceptor and donor is also observed in both cases. In contrast, the transfer processes involving methylthiyl radical **10** and methyl radical **6** as H-abstractor can be considered charge neutral. Surprisingly the calculation results show that changing methane **6H** to the SPL model substrate **4H** as hydrogen donor not only reduces the barrier height significantly (Figure 8.2), but now the barrier height for the hydrogen abstraction by *p*-me-phenoxy radical **7** is lower by 5.4 kJ mol⁻¹ than the barrier for the abstraction reaction by methylthiyl radical **10**. The Mulliken charge analysis of the transition states of between SPL model substrate **4H** and *p*-me-phenoxy radical **7**, respectively **10**, does not show any significant difference to abstraction reaction from methane **6H**. This implies that not only polar effects play role here but also geometrical arrangement, which allows other interaction that lowers the barrier between SPL model substrate **4H** and *p*-me-phenoxy radical **7**. Taking this together the first hydrogen abstraction from the SPL-substrate model **4H** occurs very likely by methyl radical **6**, followed by *p*-me-phenoxy radical **7** and methylthiyl radical **10** as the least.

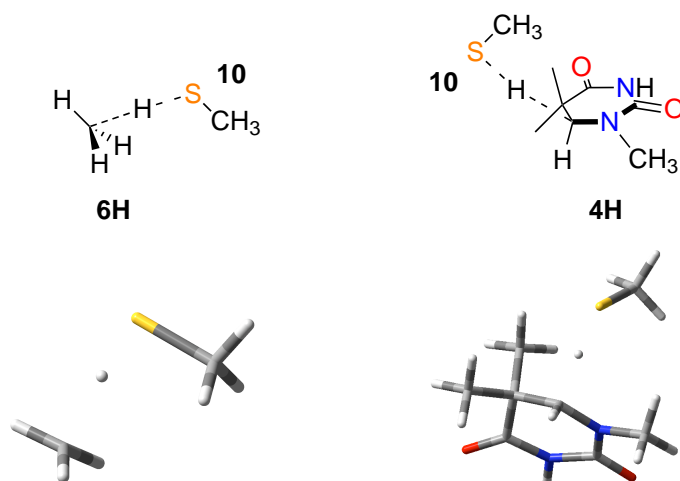


Figure 8.4: Transition states of the hydrogen transfer between methylthiyl radical **10** and methane **6H**, respectively SPL substrate **4H**.

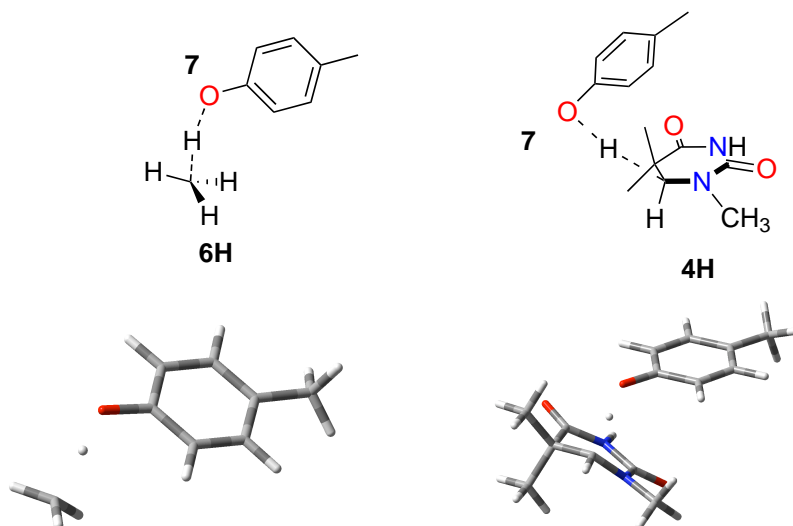


Figure 8.5: Transition states of the hydrogen transfer between *p*-me-phenoxy radical **7** and methane **6H**, respectively SPL substrate **4H**.

Second step of the repair mechanism: The transition states of the second step which closes the cycle will be again modeled by *p*-me-phenol **7H**, methylthiol **10H** and methane **6H** as hydrogen donors to the thymine radical **5** (Figure 8.6). The abstraction process from methane **6H** can be used as an approximation for the regeneration of C5'-adenosyl radical. Figure 8.6 shows that the thermodynamics of the regeneration process of such a primary radical is not favorable.

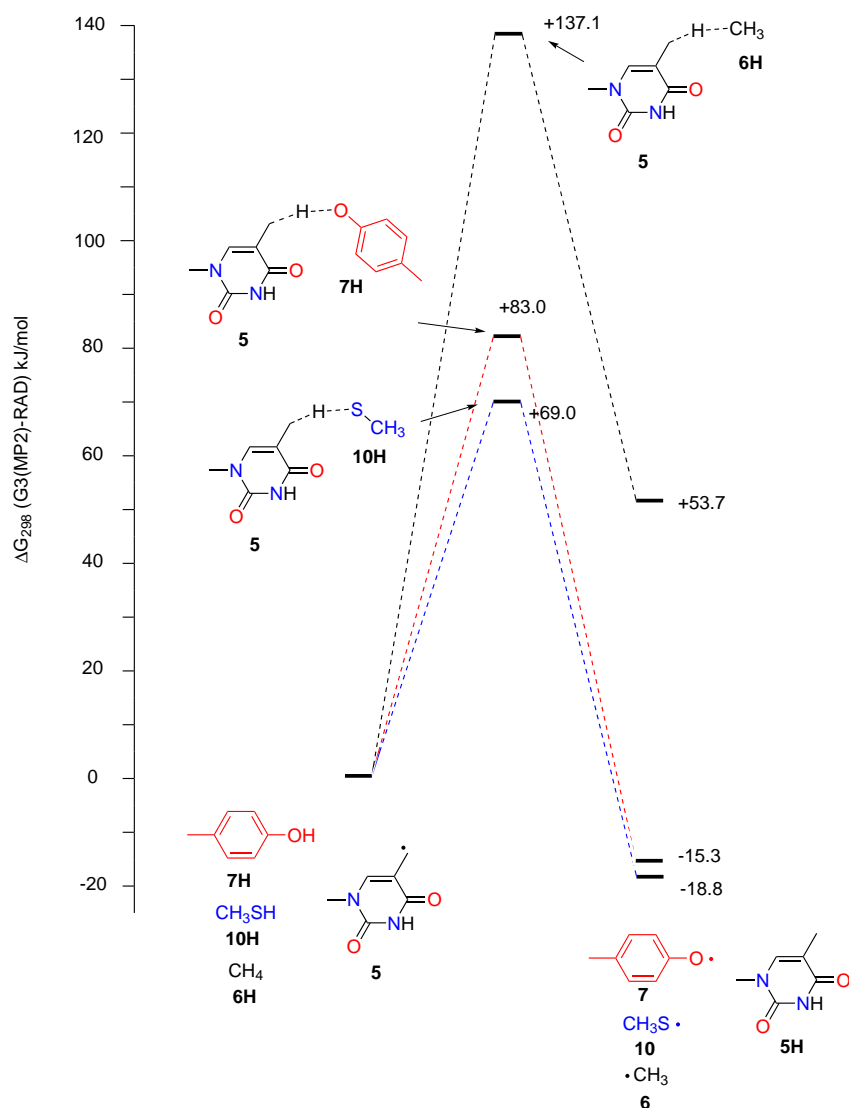


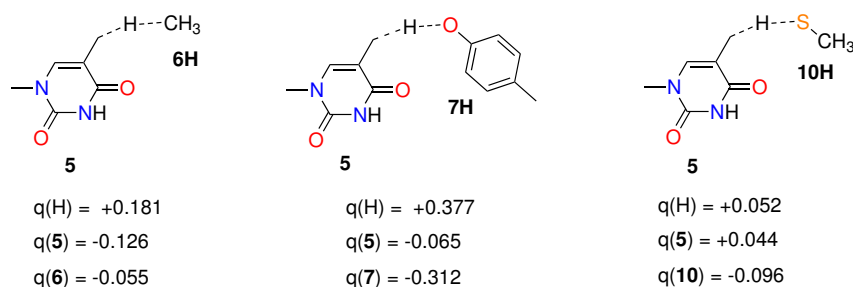
Figure 8.6: Reaction topology of the second H-atom transfer in the SPL repair mechanism.

The alternative use of peptides as hydrogen donors in comparison has a better thermodynamic driving force. Additionally, the kinetic barrier for the H-abstraction from methane **6H** by thymine radical **5** is very high (+137.1 kJ mol⁻¹) and similar to the H-abstraction by *p*-me-phenoxy radical **7** from SPL-substrate model **4H** (+139.3 kJ mol⁻¹). The free reaction energies of the abstraction processes from

p-me-phenol **7H** and methylthiol **10H** at G3B3-level of theory amount to -18.8 kJ mol^{-1} , and -15.3 kJ mol^{-1} , respectively, which are slightly more negative when compared to the previous results due to the entropy contribution.^[19;25] Nevertheless the kinetic barrier of the latter two hydrogen transfer processes differ by 14.0 kJ mol^{-1} with the preference on methylthiol **10H** as the hydrogen donor. Mulliken charge analysis of the transition states between model substrate radical **5** and *p*-me-phenol **7H**, respectively methylthiol **10H**, shows comparable results with the first hydrogen transfer reaction in the repair mechanism (Scheme 8.3). Significant partial charge difference between donor and acceptor is observed only in the transition state between the model substrate radical **5** and *p*-me-phenol **10H**.

Table 8.3: Free reaction energies (ΔG_{298}) at G3B3 level and reaction barriers (ΔG_{298}^\ddagger) at G3(MP2)-RAD level of the reactions shown in Figures 8.6.

	ΔH_{298} [kJ mol^{-1}]	ΔG_{298} [kJ mol^{-1}]	ΔH_{298}^\ddagger [kJ mol^{-1}]	ΔG_{298}^\ddagger [kJ mol^{-1}]
5 + 6H	+63.4	+53.7	+110.5	+137.1
5 + 7H	-8.0	-15.3	+42.5	+83.0
5 + 10H	-12.9	-18.8	+31.2	+69.0



Scheme 8.3: Mulliken charge on transferred hydrogen atom at B3LYP/6-31G(d) and on the H-acceptor and H-donor.

The analysis of the lowest transition states between **5** and **7H**, which amounts to $+83.0$ kJ mol^{-1} at G3(MP2)-RAD level of theory, shows a stacking conformation between the aromatic rings of the two substrates (Figure 8.8). An alternative non-stacked transition state can also be located and displays a barrier of $+102.4$ kJ mol^{-1} , is $+19.4$ kJ mol^{-1} higher than the stacked transition state. However it should be noted here that the non-stacked transition state exhibits hydrogen bonding interactions with a distance of 2.59 Å between the *ortho*-hydrogen of the phenol moiety and a carbonyl oxygen at C4 position of thymine radical **5** (Figure 8.8).

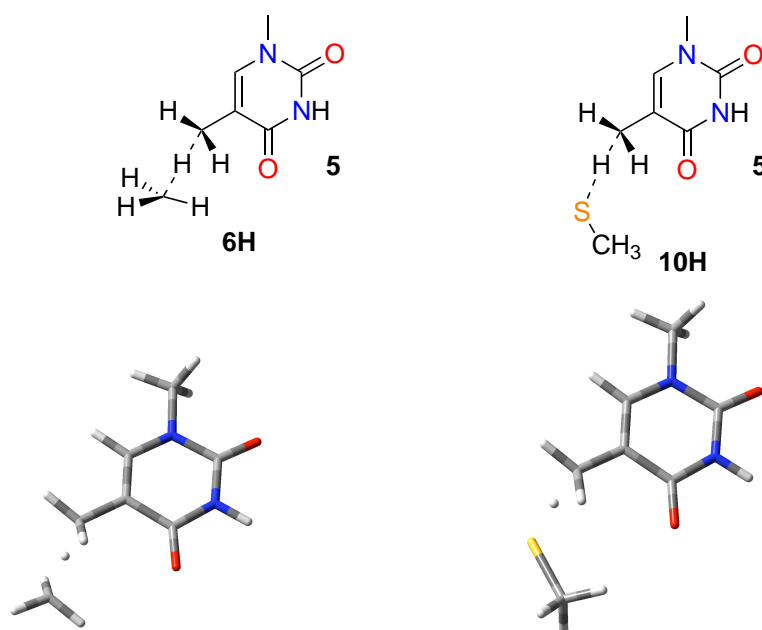


Figure 8.7: Transition states of the transfer between thymine radical **5** and methane **6H**, respectively methylthiol **10H**.

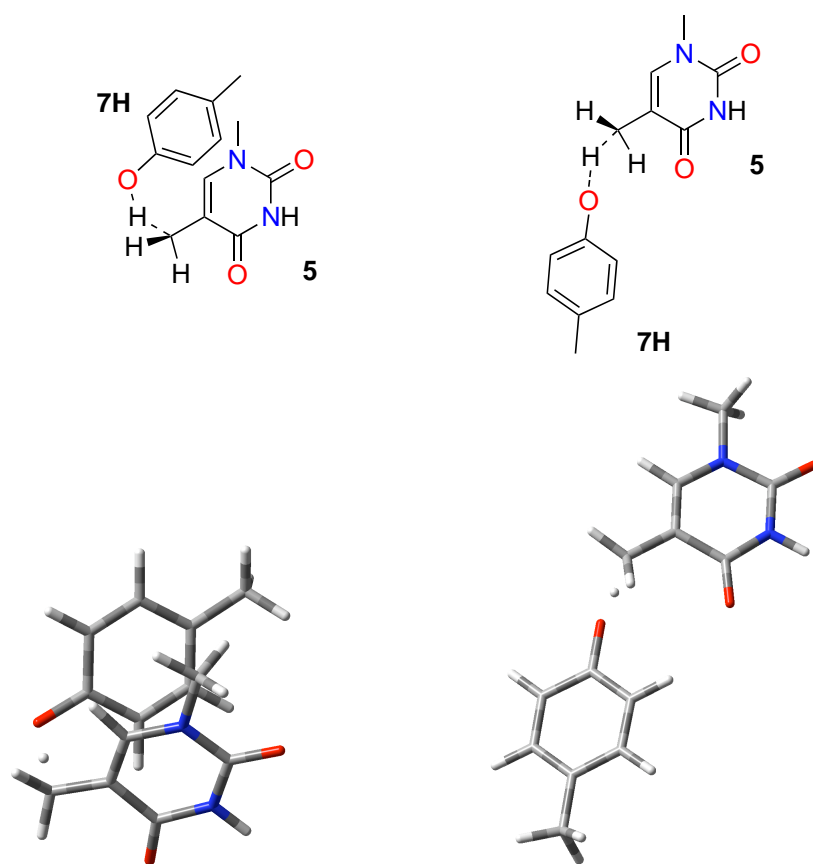


Figure 8.8: Two conformations of the transition states of the hydrogen transfer between thymine radical **5** and *p*-me-phenol **7H**.

8.3 Conclusion

Our results suggest that the SPL repair process is initiated by the adenosyl radical, which is generated from SAM. This process is thermodynamically exergonic by -40.5 kJ/mol with a barrier of $+73.4$ kJ/mol. Subsequent C-C bond cleavage and rearrangement yields thymine and thymine radical. The thymine radical then abstracts a hydrogen atom from peptide side chain in the active site yielding the respective peptide radicals. Both cysteine and tyrosine are possible candidates due to similar S-H and O-H bond strengths. Calculation of barriers for the H-abstraction from peptides using small models *p*-me-phenol **7H** and methylthiol **10H** shows a clear preference for cysteine as hydrogen donor. Regeneration of the C5'-adenosyl radical is not favorable, both due to the high endergonic reaction energy and high kinetic barrier. The catalytic cycle should thus be propagated by a pair of peptides and peptide radicals. The first hydrogen abstraction from the photodimer will occur by either a tyrosyl or a cysteinyl radical. Thermodynamically, the reaction is significantly endergonic when compared to the initiation by the C5'-adenosyl radical. Our results show that the abstraction barrier by *p*-me-phenoxy radical **7** is slightly lower than that by methylthiyl radical **10**. This implies an interplay between cysteine and tyrosine in the repair mechanism. The radical should be transferred back from tyrosyl radical to cysteine in order to close the cycle. The thermodynamics of such a transfer process, of course, is according to our data thermoneutral. Unfortunately the Marcus analysis, cannot provide any information of the composition of the barrier due to the complexity of substrate interaction in the transition states. Further studies with larger systems using QM/MM may broaden the understanding of the repair mechanism.

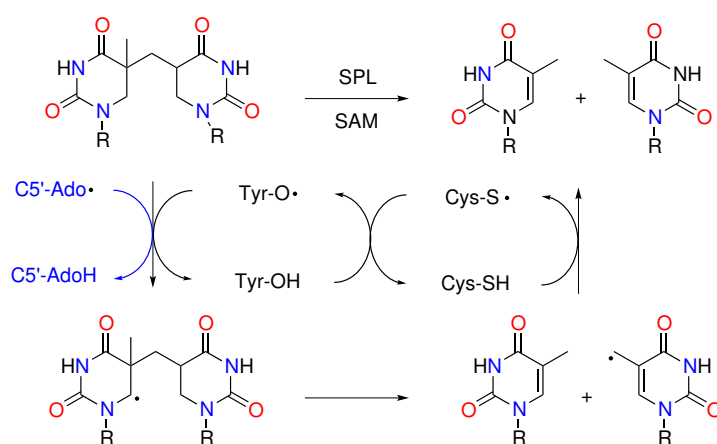


Figure 8.9: Repair mechanism of SPL. The initiation by the C5'-adenosyl radical is shown in blue.

Bibliography

- [1] P. A. Frey, A. D. Hegeman, and F. J. Ruzicka. *Crit. Rev. Biochem. Mol. Biol.*, 43:63–68, 2008.
- [2] E. N. Marsh, D. P. Patterson, and L. Li. *ChemBioChem.*, 11:604–621, 2010.
- [3] L. Li. *BBA - Proteins and Proteomics*, 1824:1264–1277, 2012.
- [4] R. A. Mehl and T. P. Begley. *Org. Lett.*, 1:1065–1066, 1999.
- [5] R. Rebeil and W. L. Nicholson. *Proc. Natl. Acad. Sci. U. S. A.*, 98:9038–9043, 2001.
- [6] M. G. Friedel, O. Berteau, J. C. Pieck, M. Atta, S. Ollagnier de Choudens, M. Fontecave, and T. Carell. *Chem. Commun.*, pages 445–447, 2006.
- [7] J. C. Pieck, D. Kuch, F. Grolle, U. Linne, C. Haas, and T. Carell. *J. Am. Chem. Soc.*, 128:1404–1405, 2006.
- [8] J. C. Pieck, U. Hennecke, A. J. Pierik, M. G. Friedel, and T. Carell. *J. Biol. Chem.*, 281:36317–36326, 2006.
- [9] E. Bürckstümmer and T. Carell. *Chem. Commun*, pages 4037–4039, 2008.
- [10] K. Heil, A. C. Kneuttinger, S. Schneider, U. Lischke, and T. Carell. *Chem. Eur. J.*, 17:9651–9657, 2011.
- [11] J. Cheek and J. B. Broderick. *J. Am. Chem. Soc.*, 124:2860–2861, 2002.
- [12] J. M. Buis, J. Cheek, E. Kalliri, and J. B. Broderick. *J. Biol. Chem.*, 281:25994–26003, 2006.
- [13] T. Chandra, S. C. Silver, E. Zilinskas, E. M. Shepard, W. E. Broderick, and J. B. Broderick. *J. Am. Chem. Soc.*, 131:2420–2421, 2009.
- [14] S. C. Silver, T. Chandra, E. Zilinskas, S. Ghose, W. E. Broderick, and J. B. Broderick. *J. Biol. Inorg. Chem.*, 15:943–955, 2010.
- [15] L. Yang, G. Lin, D. Liu, K. J. Dria, J. Telsler, and L. Li. *J. Am. Chem. Soc.*, 133:10434–10447, 2011.
- [16] G. Lin, C.-H. Chen, M. Pink, J. Pu, and L. Li. *Chem. Eur. J.*, 17:9658–9668, 2011.
- [17] A. Chandor-Proust, O. Berteau, T. Douki, D. Gasparutto, S. Ollagnier-De-Choudens, M. Fontecave, and M. Atta. *J. Biol. Chem.*, 283:36361–36368, 2008.
- [18] A. Chandor, O. Berteau, T. Douki, D. Gasparutto, Y. Sanakis, S. Ollagnier-De-Choudens, M. Atta, and M. Fontecave. *J. Biol. Chem.*, 281:26922–26931, 2006.

- [19] J. Hioe and H. Zipse. *Faraday Discuss.*, 145:301–313, 2010. and subsequent discussion, p. 381-409.
- [20] J. Hioe and H. Zipse. *Org. Biol. Chem.*, 8:3609–3617, 2010.
- [21] H. Zipse. *Top. Curr. Chem.*, 263:163–189, 2006.
- [22] M. L. Coote, C. Y. Lin, and H. Zipse. *Carbon-Centered Free Radicals and Radicals Cations*, chapter "The Stability of Carbon-Centered Radicals", pages 83–104. M. D. E. Forbes (Ed.), John Wiley & Sons, 2010.
- [23] J. Hioe, G. Savasci, H. Brand, and H. Zipse. *Chem. Eur. J.*, 17:3781–3789, 2011.
- [24] J. Hioe and H. Zipse. *Encyclopedia of Radicals in Chemistry, Biology and Materials*, chapter "Radical Stability-Thermochemical Aspects", pages 449–476. John Wiley & sons, 2012.
- [25] J. Hioe and H. Zipse. *Chem. Eur. J.*, 18:16463–16472, 2012.
- [26] A. Benjdia, K. Heil, T. R. M. Barends, T. Carell, and I. Schlichting. *Nucleic Acids Res.*, 40:9308–9318, 2012.
- [27] A.C. Kneuttinger, K. Heil, G. Kashiwazaki, and T. Carell. *Chem. Commun.*, 49:722–724, 2013.
- [28] H.-J. Werner, P. J. Knowles, R. Lindh, F. R. Manby, M. Schütz, P. Celani, T. Korona, A. Mitrushenkov, G. Rauhut, T. B. Adler, R. D. Amos, A. Bernhardsson, A. Berning, D. L. Cooper, M. J. O. Deegan, A. J. Dobbyn, F. Eckert, E. Goll, C. Hampel, G. Hetzer, T. Hrenar, G. Knizia, C. Köppl, Y. Liu, A. W. Lloyd, R. A. Mata, S. J. McNicholas, A. J. May, W. Meyer, M. E. Mura, A. Nicklaß, P. Palmieri, K. Pflüger, R. Pitzer, M. Reiher, U. Schumann, H. Stoll, A. J. Stone, R. Tarroni, T. Thorsteinsson, M. Wang, and A. Wolf. MOLPRO, version 2012.1, *a package of ab initio programs*.
- [29] M. J. Frisch, G. W. Trucks, H. B. Schlegel, G. E. Scuseria, M. A. Robb, J. R. Cheeseman, J. A. Montgomery, Jr., T. Vreven, K. N. Kudin, J. C. Burant, J. M. Millam, S. S. Iyengar, J. Tomasi, V. Barone, B. Mennucci, M. Cossi, G. Scalmani, N. Rega, G. A. Petersson, H. Nakatsuji, M. Hada, M. Ehara, K. Toyota, R. Fukuda, J. Hasegawa, M. Ishida, T. Nakajima, Y. Honda, O. Kitao, H. Nakai, M. Klene, X. Li, J. E. Knox, H. P. Hratchian, J. B. Cross, V. Bakken, C. Adamo, J. Jaramillo, R. Gomperts, R. E. Stratmann, O. Yazyev, A. J. Austin, R. Cammi, C. Pomelli, J. Ochterski, P. Y. Ayala, K. Morokuma, G. A. Voth, P. Salvador, J. J. Dannenberg, V. G. Zakrzewski, S. Dapprich, A. D. Daniels, M. C. Strain, O. Farkas, D. K. Malick, A. D. Rabuck, K. Raghavachari, J. B. Foresman, J. V. Ortiz, Q. Cui, A. G. Baboul, S. Clifford, J. Cioslowski, B. B. Stefanov, G. Liu, A. Liashenko, P. Piskorz, I. Komaromi, R. L. Martin,

D. J. Fox, T. Keith, M. A. Al-Laham, C. Y. Peng, A. Nanayakkara, M. Challacombe, P. M. W. Gill, B. G. Johnson, W. Chen, M. W. Wong, C. Gonzalez, and J. A. Pople, 2009. GAUSSIAN 09 (Revision C.01), Gaussian, Inc., Wallingford, CT.

Chapter 9

General Conclusion

- The enthalpies of hydrogen transfer reactions in the enzymatic radical reactions have been computationally determined. The calculation shows that glycyl **9**, cysteinyl **13** and tyrosyl radicals have comparable radical stabilization enthalpies. The stability of the C5'-adenosyl radical **2**, in contrast, resembles that of a primary alkyl radical (Figure 9.1).

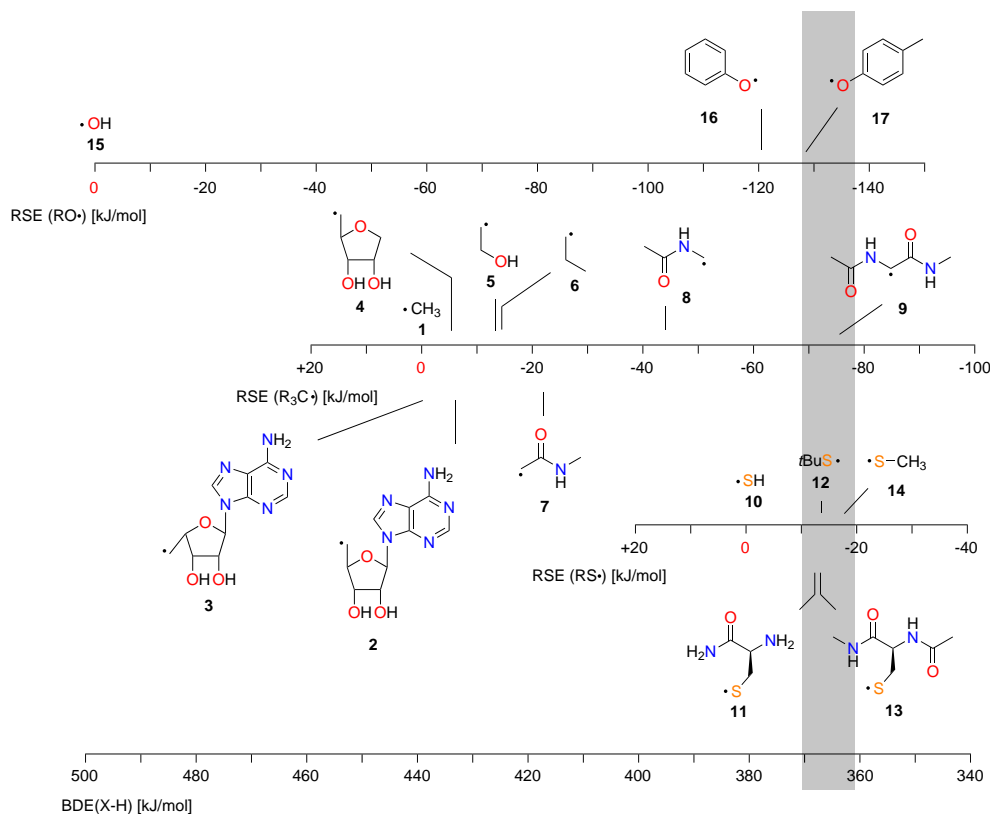


Figure 9.1: Radical stability scale of relevant systems, which are often met in the enzymatic catalysis.

- Thermodynamically glycyl radical **9** is found to be the most stable C_{α} -peptide radical by far. The conformational analysis of the dipeptides and their respective open shells shows that the conformational energies vary strongly with the variation of the peptide backbone. Additionally cis-peptide radicals are predicted to lie near to the global conformational minimum. Compared to other peptide radicals the glycyl radical **9** possesses the broadest variation in the radical stability scale (Figure 9.2).
- The C-H bond dissociation energies (BDE) of glycine and alanine have been reevaluated. Our results show clearly that the choice of the theoretical method and the choice of model system are essential in the determination of the bond strength. Compared to elaborate methods such as G3(MP2)-RAD, G3B3 and W1RO, B3LYP with small basis sets predicts much too low bond dissociation energies and underestimates steric effects. This becomes critical when the

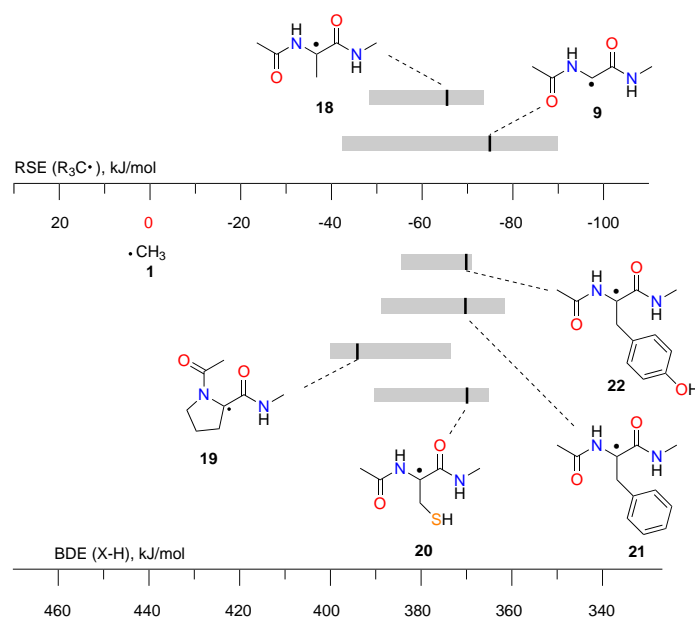


Figure 9.2: Distribution of radical stability of C_{α} -peptide radicals at G3(MP2)-RAD.

dimension of the model systems is switched to larger models (systems **23H** and **24H**) (Figure 9.3). In these cases B3LYP shows that alanine has lower BDE than glycine since it underestimates the steric effects. Finally the choice of reference systems is less critical when higher level theories are applied.

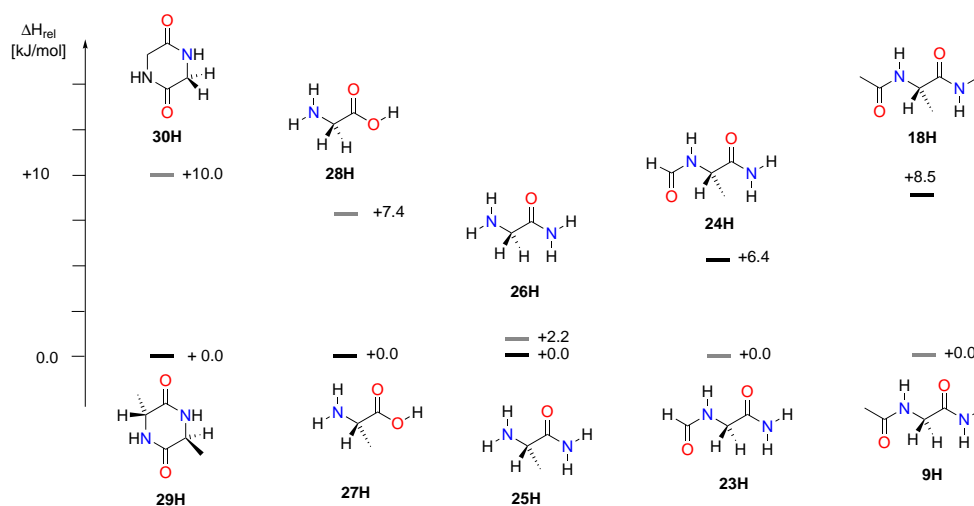


Figure 9.3: Relative C_{α} -H BDE between glycine and alanine at G3B3 level of theory

- The reaction energies of H-transfers in SAM-dependent enzymes have been quantified using our radical stability data (Figure 9.4). SAM can act as co-substrate, which is stoichiometrically used, or used in a catalytic fashion. The reaction energies involving SAM as co-substrate are according to our results

always exothermic due to the reactivity of the SAM-derived C5'-adenosyl radical **2**. In contrast, when SAM is used in a catalytic fashion such as in LAM and SPL, exothermic and endothermic reaction energies are coupled. The originally proposed SPL repair mechanism is very unlikely due to high endothermic reaction energy of the second step (Figure 9.5). Involvement of peptide radicals such as cysteinyl or tyrosyl radical as chain-propagator is more reasonable to avoid endothermicity of second step in the SPL repair mechanism. In RNA methylating enzymes, the application of C5'-adenosyl radical **2** to abstract a hydrogen from adenine, either at C2 or C8, is not favorable, since σ -radicals are generally not stable. In this case alternative mechanism using sulfonium **31H**, respectively dimethylthioether **32H**, and sulfonium radical **31H**, respectively methylthiomethyl radical **32**, are energetically more feasible.

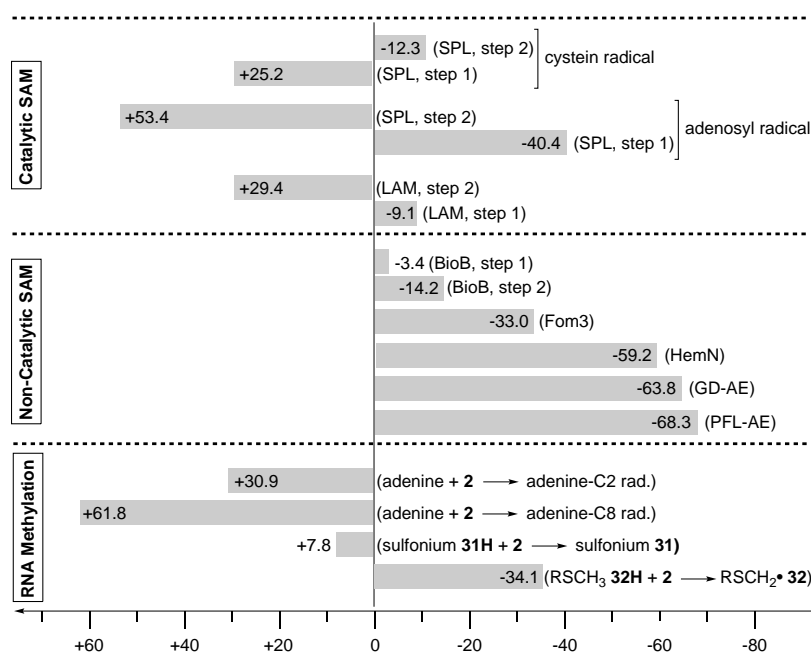


Figure 9.4: Thermodynamics of H-transfer reactions in SAM-dependent enzymes.

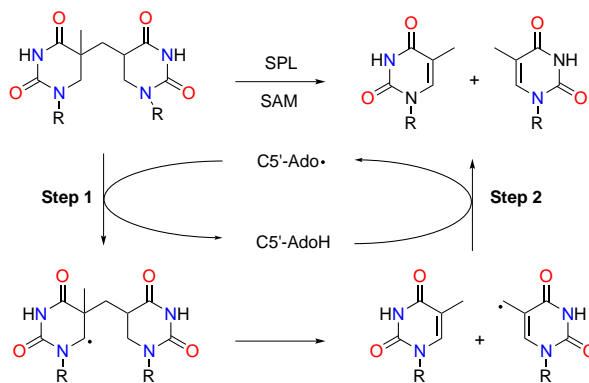


Figure 9.5: Originally proposed SPL repair mechanism.

- The stabilities of oxygen-centered radicals have been calculated with various methods. G3(MP2)-RAD, which is supposed to give thermodynamic reaction energies accurately, has been shown to fail to predict the radical stability of phenoxy radical and *para*-substituted phenoxy radicals (Figure 9.6: **A**). Different geometry optimization methods may vary the stability of phenoxy and *p*-me-phenoxy radicals, but the effect of the geometry variation is shown only to be minor. None of the geometry variations has yielded the correct stability order between phenoxy and *p*-me-phenoxy radicals. The newly modified G3(+2d,MP2)-RAD method has been shown to give similar results as G3B3. Moreover it successfully predicts the effect of substituents at *para*-position of phenoxy radical (Figure 9.6: **B**). Unfortunately G3(+2d,MP2)-RAD method increases the computational effort substantially. Two approaches to reduce the cost, G3(+2d,MP2,MP4)-RAD and LD-G3(+2d,MP2)-RAD have been proposed. Both show good agreement with G3B3 and G3(+2d,MP2)-RAD with much less CPU time (Figure 9.7).

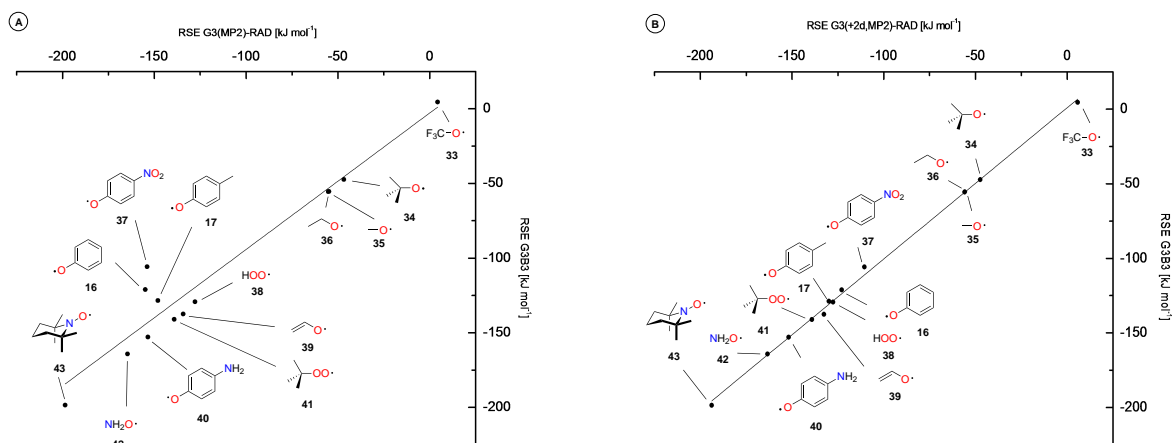


Figure 9.6: Correlation of RSE between G3(MP2)-RAD, respectively G3(+2d,MP2)-RAD, and G3B3.

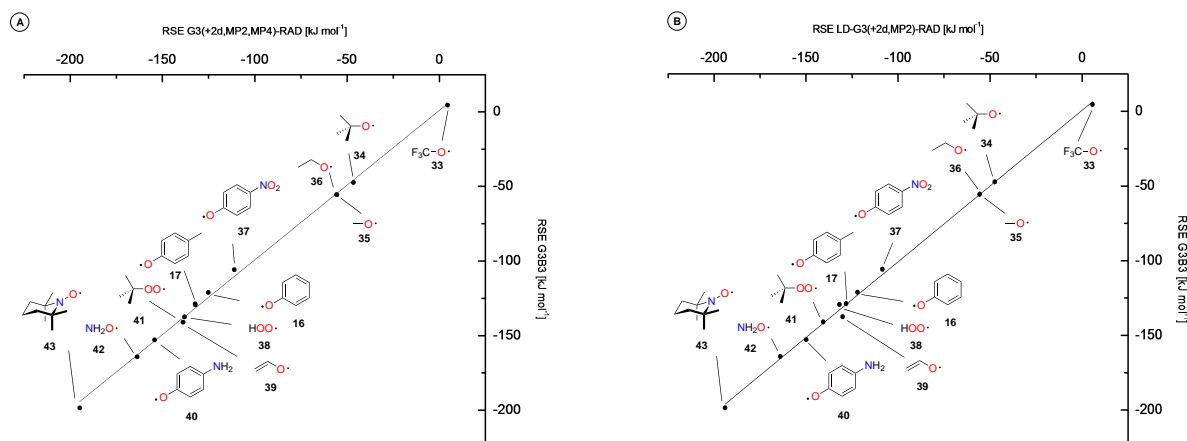


Figure 9.7: Correlation of RSE between G3(+2d,MP2,MP4)-RAD, respectively LD-G3(+2d,MP2)-RAD, and G3B3.

- The Marcus model has been shown to predict barriers of H-transfer reactions between alkyl radicals successfully. However, our results demonstrate that the model exhibits limitations when predicting barrier between O-centered radicals (or S-centered radicals) and alkyl radicals. One possible reason could be strong polarization effects in the transfer process, which is reflected in the charge distributions in the donor and acceptor sides (Figure 9.8).

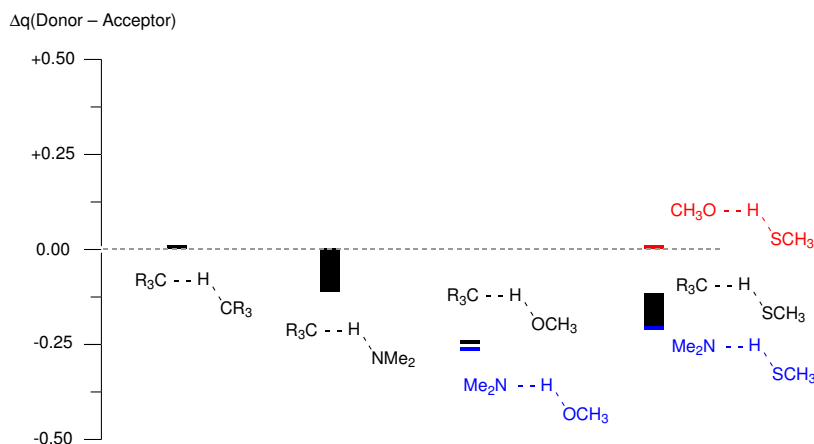


Figure 9.8: Difference in partial charges between the donor and the acceptor side in hydrogen transfer reactions.

- The originally proposed mechanism of spore photoproduct lyase has been shown to suffer from high endothermicity (or endergonicity) of the final step. Crystal structure and analysis via mutagenesis demonstrate that proximal tyrosine and cysteine in the active site are directly involved in the repair mechanism. This is fully supported by our previous calculation and hypothesis,

which have already predict the important role of peptides and peptide radicals as an alternative to the desoxyadenosine and C5'-adenosyl radical. Thermodynamically both tyrosine and cysteine are equivalent due to similar O-H and S-H bond strengths. The calculation of the H-transfer barriers, however, shows a slight preference for tyrosyl radical as hydrogen abstractor in the first step, and a clear preference for cysteine as hydrogen donor in the second step. Taking this together our results are fully in line with the experimental results. The C5'-adenosyl radical seems to be a proper initiator abstracting a hydrogen from the SPL substrate in the first step. Rather than generating C5'-adenosyl radicals at the end of the cycle, the best alternative, which is supported by our calculations, is therefore the use of peptides and peptide radicals, which will also continue the catalytic cycle. This is very surprising, since no SAM enzyme-mediated radical reactions are known up to now to apply SAM as initiator.

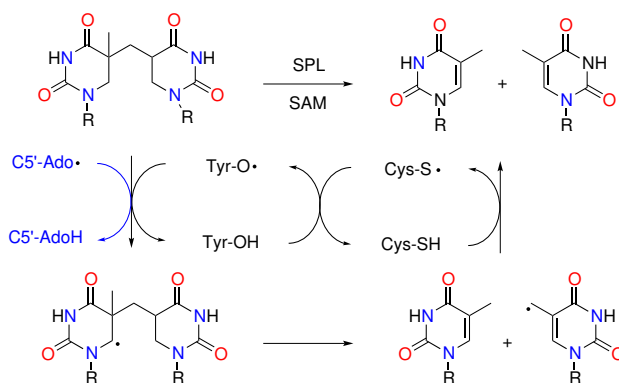


Figure 9.9: Repair mechanism of sporephotoproduct lyase (SPL).

Appendix A

Theoretical Methods

A.1 Composite methods

The Gaussian theories (Gn -theories) are composite extrapolation procedures aiming at accurate thermochemical properties. A general description of this methods can be found in chapter 1 and 6 in this work. Here the exact formulas for the methods, which were used in the projects, are summarized.

G3B3

Geometry optimization for G3B3 is done at B3LYP/6-31G(d), and the thermal correction factor used is 0.960.

$$\begin{aligned}
 E_{\text{tot}}(\text{G3B3}) &= E_{\text{tot}}(\text{QCISD(T)}/6\text{-}31\text{G(d)}) \\
 &\quad + \Delta E(+)\phantom{+ \Delta E(2\text{df,p})} \\
 &\quad + \Delta E(2\text{df,p})\phantom{+ \Delta E(\text{G3Large})} \\
 &\quad + \Delta E(\text{G3Large}) \\
 &\quad + \text{HLC} \\
 &\quad + \text{SO}
 \end{aligned}
 \tag{A.1}$$

With the basis set correction terms,

$$\Delta E(+) = E_{\text{tot}}(\text{MP4}/6\text{-}31\text{+G(d)}) - E_{\text{tot}}(\text{MP4}/6\text{-}31\text{G(d)}) \tag{A.2}$$

$$\Delta E(2\text{df,p}) = E_{\text{tot}}(\text{MP4}/6\text{-}31\text{G(2df,p)}) - E_{\text{tot}}(\text{MP4}/6\text{-}31\text{G(d)}) \tag{A.3}$$

$$\begin{aligned}
 \Delta E(\text{G3Large}) &= E_{\text{tot}}(\text{MP2(Full)}/\text{G3Large}) - E_{\text{tot}}(\text{MP2}/6\text{-}31\text{G(2df,p)}) \\
 &\quad - E_{\text{tot}}(\text{MP2}/6\text{-}31\text{+G(d)}) + E_{\text{tot}}(\text{MP2}/6\text{-}31\text{G(d)})
 \end{aligned}
 \tag{A.4}$$

SO is the spin-orbit correction for atoms. The higher level correction (HLC) for G3B3 is defined as,

$$\text{HLC} = -An_{\beta} - B(n_{\alpha} - n_{\beta}) \tag{A.5}$$

n_{α} and n_{β} are the number of α -valence electrons and β -valence electrons. A and B are parameters fitted to experimental data. For molecules: $A = 6.760$ mHartree and $B = 3.233$ mHartree. For atoms: $A = 6.786$ mHartree and $B = 1.269$ mHartree.

G3(MP2)-RAD

Geometry optimization for G3(MP2)-RAD is done at B3LYP/6-31G(d), and the thermal correction factor used is 0.9806.

$$\begin{aligned}
E_{\text{tot}}(\text{G3}(\text{MP2})\text{-RAD}) &= E_{\text{tot}}(\text{U}(\text{R})\text{CCSD}(\text{T})/6\text{-}31\text{G}(\text{d})) \\
&\quad + \Delta E(\text{G3MP2Large}) \\
&\quad + \text{HLC} \\
&\quad + \text{SO}
\end{aligned} \tag{A.6}$$

With the basis set correction terms,

$$\Delta E(\text{G3MP2Large}) = E_{\text{tot}}(\text{ROMP2}/\text{G3MP2Large}) - E_{\text{tot}}(\text{ROMP2}/6\text{-}31\text{G}(\text{d})) \tag{A.7}$$

SO is the spin-orbit correction for atoms. The higher level correction (HLC) for G3(MP2)-RAD is defined as,

$$\text{HLC} = -An_{\beta} - B(n_{\alpha} - n_{\beta}) \tag{A.8}$$

n_{α} and n_{β} are the number of α -valence electrons and β -valence electrons. A and B are parameters fitted to experimental data. For molecules: $A = 9.413$ mHartree and $B = 3.969$ mHartree. For atoms: $A = 9.438$ mHartree and $B = 1.888$ mHartree.

G3(+2d,MP2)-RAD

Geometry optimization for G3(+2d,MP2)-RAD is done at B3LYP/6-31G(d), and the thermal correction factor used is 0.9086 (not optimized).

$$\begin{aligned}
E_{\text{tot}}(\text{G3}(+2\text{d},\text{MP2})\text{-RAD}) &= E_{\text{tot}}(\text{U}(\text{R})\text{CCSD}(\text{T})/6\text{-}31+\text{G}(2\text{d})) \\
&\quad + \Delta E(+2\text{d})
\end{aligned} \tag{A.9}$$

With the basis set correction terms,

$$\Delta E(+2\text{d}) = E_{\text{tot}}(\text{ROMP2}/\text{G3MP2Large}) - E_{\text{tot}}(\text{ROMP2}/6\text{-}31+\text{G}(2\text{d})) \tag{A.10}$$

No fitted HLC and SO have been optimized yet so far.

LD-G3(MP2)-RAD

Geometry optimization for LD-G3(+2d,MP2)-RAD (local density variant) is done at B3LYP/6-31G(d), and the thermal correction factor used is 0.9086 (not optimized).

$$E_{\text{tot}}(\text{LD-G3}(+2\text{d,MP2})\text{-RAD}) = E_{\text{tot}}(\text{LD-U(R)CCSD(T)/6-31+G}(2\text{d})) + \Delta E(\text{LD},+2\text{d}) \quad (\text{A.11})$$

With the basis set correction terms,

$$\Delta E(\text{LD},+2\text{d}) = E_{\text{tot}}(\text{ROMP2/G3MP2Large}) - E_{\text{tot}}(\text{LD-ROMP2/6-31+G}(2\text{d})) \quad (\text{A.12})$$

No fitted HLC and SO have been optimized yet so far.

G3-RAD

Geometry optimization for G3-RAD is done at B3LYP/6-31G(d), and the thermal correction factor used is 0.9806.

$$E_{\text{tot}}(\text{G3-RAD}) = E_{\text{tot}}(\text{U(R)CCSD(T)/6-31G}(d)) + \Delta E(+)$$

$$+ \Delta E(2\text{df,p})$$

$$+ \Delta E(\text{G3Large})$$

$$+ \text{HLC}$$

$$+ \text{SO} \quad (\text{A.13})$$

With the basis set correction terms,

$$\Delta E(+) = E_{\text{tot}}(\text{ROMP4/6-31+G}(d)) - E_{\text{tot}}(\text{ROMP4/6-31G}(d)) \quad (\text{A.14})$$

$$\Delta E(2\text{df,p}) = E_{\text{tot}}(\text{ROMP4/6-31G}(2\text{df,p})) - E_{\text{tot}}(\text{ROMP4/6-31G}(d)) \quad (\text{A.15})$$

$$\Delta E(\text{G3Large}) = E_{\text{tot}}(\text{ROMP2(Full)/G3Large}) - E_{\text{tot}}(\text{ROMP2/6-31G}(2\text{df,p})) - E_{\text{tot}}(\text{ROMP2/6-31+G}(d)) + E_{\text{tot}}(\text{ROMP2/6-31G}(d)) \quad (\text{A.16})$$

The basis set correction terms apply full cartesian type 6D 10F. SO is the spin-orbit correction for atoms. The higher level correction (HLC) for G3-RAD is defined as,

$$\text{HLC} = -An_{\beta} - B(n_{\alpha} - n_{\beta}) \quad (\text{A.17})$$

n_{α} and n_{β} are the number of α -valence electrons and β -valence electrons. A and B are parameters fitted to experimental data. For molecules: $A = 6.884$ mHartree and $B = 2.741$ mHartree. For atoms: $A = 6.561$ mHartree and $B = 1.341$ mHartree.

G4 and G4-H

Geometry optimization for G4 and G4-5H is done at B3LYP/6-31G(2df,p), and the thermal correction factor is 0.9854.

$$\begin{aligned}
E_{\text{tot}}(\text{G4}) &= E_{\text{tot}}(\text{CCSD(T)}/6\text{-}31\text{G(d)}) \\
&+ \Delta E(+) \\
&+ \Delta E(2\text{df,p}) \\
&+ \Delta E(\text{G3largeXP}) \\
&+ \Delta E(\text{HF}) \\
&+ \text{HLC} \\
&+ \text{SO}
\end{aligned} \tag{A.18}$$

With the basis set correction terms,

$$\Delta E(+) = E_{\text{tot}}(\text{MP4}/6\text{-}31\text{+G(d)}) - E_{\text{tot}}(\text{MP4}/6\text{-}31\text{G(d)}) \tag{A.19}$$

$$\Delta E(2\text{df,p}) = E_{\text{tot}}(\text{MP4}/6\text{-}31\text{G(2df,p)}) - E_{\text{tot}}(\text{MP4}/6\text{-}31\text{G(d)}) \tag{A.20}$$

$$\begin{aligned}
\Delta E(\text{G3LargeXP}) &= E_{\text{tot}}(\text{MP2(Full)}/\text{G3LargeXP}) - E_{\text{tot}}(\text{MP2}/6\text{-}31\text{G(2df,p)}) \\
&- E_{\text{tot}}(\text{ROMP2}/6\text{-}31\text{+G(d)}) + E_{\text{tot}}(\text{ROMP2}/6\text{-}31\text{G(d)})
\end{aligned} \tag{A.21}$$

$$\Delta E(\text{HF}) = E_{\text{tot}}(\text{RHF}/\text{CBS}) - E_{\text{tot}}(\text{RHF}/\text{G3LargeXP}) \tag{A.22}$$

Two points extrapolation style is applied for the calculation of RHF at complete basis set limit (CBS).

$$E_{\text{tot}}(\text{RHF}/\text{CBS}) = \frac{E_{\text{tot}}(\text{RHF}/\text{mod-aug-cc-pV5Z}) - E_{\text{tot}}(\text{RHF}/\text{mod-aug-cc-pVQZ}) \cdot e^{-1.63}}{1 - e^{-1.63}} \tag{A.23}$$

SO is the spin-orbit correction for atoms. The higher level corrections (HLC) for G4 are different for open-shells molecules and closed-shells molecules. For closed-shells:

$$\text{HLC} = -6.967 \text{ mHartree} \cdot n_{\text{val}} \tag{A.24}$$

For open-shells:

$$\text{HLC} = -7.128 \text{ mHartree} \cdot n_{\beta} - 2.441 \text{ mHartree} \cdot (n_{\alpha} - n_{\beta}) \tag{A.25}$$

n_{α} and n_{β} are the number of α -valence electrons and β -valence electrons. n_{val} is the number of valence electron pairs. For atoms the HLC is defined as,

$$\text{HLC} = -7.116 \text{ mHartree} \cdot n_{\beta} - 1.414 \text{ mHartree} \cdot (n_{\alpha} - n_{\beta}) \quad (\text{A.26})$$

G4-5H is a variant of G4, whose closed-shells and open-shells HLCs are identical.

G4(MP2)

Geometry optimization for G4(MP2) is done at B3LYP/6-31G(2df,p), and the thermal correction factor used is 0.9854.

$$\begin{aligned} E_{\text{tot}}(\text{G4(MP2)}) &= E_{\text{tot}}(\text{CCSD(T)/6-31G(d)}) \\ &\quad + \Delta E(\text{G3MP2largeXP}) \\ &\quad + \Delta E(\text{HF}) \\ &\quad + \text{HLC} \\ &\quad + \text{SO} \end{aligned} \quad (\text{A.27})$$

With the basis set correction terms,

$$\Delta E(\text{G3MP2LargeXP}) = E_{\text{tot}}(\text{MP2/G3MP2LargeXP}) - E_{\text{tot}}(\text{MP2/6-31G(2df,p)}) \quad (\text{A.28})$$

$$\Delta E(\text{HF}) = E_{\text{tot}}(\text{RHF/CBS}) - E_{\text{tot}}(\text{RHF/G3MP2LargeXP}) \quad (\text{A.29})$$

Two points extrapolation style is applied for the calculation of RHF at complete basis set limit (CBS).

$$E_{\text{tot}}(\text{RHF/CBS}) = \frac{E_{\text{tot}}(\text{RHF/mod-aug-cc-pVQZ}) - E_{\text{tot}}(\text{RHF/mod-aug-cc-pVTZ}) \cdot e^{-1.63}}{1 - e^{-1.63}} \quad (\text{A.30})$$

SO is the spin-orbit correction for atoms. The higher level corrections (HLC) for G4(MP2) are different for open-shells molecules and closed-shells molecules. For closed-shells:

$$\text{HLC} = -9.472 \text{ mHartree} \cdot n_{\text{val}}. \quad (\text{A.31})$$

For open-shells:

$$\text{HLC} = -9.769 \text{ mHartree} \cdot n_{\beta} - 3.102 \text{ mHartree} \cdot (n_{\alpha} - n_{\beta}) \quad (\text{A.32})$$

n_{α} and n_{β} are the number of α -valence electrons and β -valence electrons. n_{val} is the number of valence electron pairs. For atoms the HLC is defined as,

$$\text{HLC} = -9.741 \text{ mHartree} \cdot n_{\beta} - 2.115 \text{ mHartree} \cdot (n_{\alpha} - n_{\beta}) \quad (\text{A.33})$$

W1RO

The geometry is optimized at B3LYP/cc-pVTZ+1 level. Frequency is scaled by 0.986. The ROCCSD applies restricted open-shells wavefunction for the CCSD(T) calculation. Scalar relativistic calculation is performed at improved models.

$$\begin{aligned} E_{\text{tot}}(\text{W1RO}) &= E_{\text{tot}}(\text{RHF/CBS}) \\ &\quad + E(\text{COR,CCSD,CBS}) \\ &\quad + E(\text{COR,T,CBS}) \\ &\quad + E(\text{CV,DKH}) \end{aligned} \quad (\text{A.34})$$

The calculation of RHF at infinite basis set is using two points extrapolation scheme.

$$E_{\text{tot}}(\text{RHF/CBS}) = E_{\text{tot}}(\text{RHF/AVQZ}) + \frac{E_{\text{tot}}(\text{RHF/AVQZ}) - E_{\text{tot}}(\text{RHF/AVTZ})}{(4/3)^5 - 1} \quad (\text{A.35})$$

CCSD correlation energy and the perturbative triples correlation energy at CBS are estimated by using also two points extrapolation scheme.

$$\begin{aligned} E_{\text{tot}}(\text{COR,CCSD,CBS}) &= E_{\text{tot}}(\text{COR,CCSD,AVTZ}) \\ &\quad + \frac{E_{\text{tot}}(\text{COR,CCSD,AVTZ}) - E_{\text{tot}}(\text{COR,CCSD,AVDZ})}{(4/3)^{3.22} - 1} \end{aligned} \quad (\text{A.36})$$

$$\begin{aligned} E_{\text{tot}}(\text{COR,T,CBS}) &= E_{\text{tot}}(\text{COR,T,AVTZ}) \\ &\quad + \frac{E_{\text{tot}}(\text{COR,T,AVTZ}) - E_{\text{tot}}(\text{COR,T,AVDZ})}{(3/2)^{3.22} - 1} \end{aligned} \quad (\text{A.37})$$

Relativistic effect and core-valence correlation are computed by the Douglas-Kroll-Hess approximation at CCSD(T) level.

$$E_{\text{tot}}(\text{CV,DKF}) = E_{\text{tot}}(\text{CCSD(T,Full)/MTsmall/dkh}) - E_{\text{tot}}(\text{CCSD(T)/MTsmall}) \quad (\text{A.38})$$

Appendix B

Supplementary Information

Supplementary information for chapter 2

Table B.1: H_{298} in a.u. of calculated systems at various level of theory.

System	H_{298}^a		H_{298}^b
	ROMP2/6-311+G(3df,2p)	G3(MP2)-RAD	G3B3
1a	-885.8095616	-886.3897182	n.a.
1c	-885.7983957		
1b	-885.8024874		
1H a	-886.4662887	-887.0522407	n.a.
1H b	-886.4573884	-887.0436679	n.a.
11 (Boltzmann)	-454.8935250	-455.8493335	-455.572847
11 (best conf.)	-454.8938081	-455.8496671	
11H (Boltzmann)	-455.5239405	-455.2124633	-456.209009
11H (best conf.)	-455.5242836	-455.2127203	
2	-39.6983648	-39.7518773	-39.6983648
2H	-40.3573882	-40.4169999	-40.3573882
12	-306.1067562	-306.3440991	-306.1067562
12H	-306.7373021	-306.9722151	-306.7373021
13	-345.3033673	-345.5773961	-345.880743
13H	-345.931822	-346.2081323	-346.518361
3H	-75.6062104	-75.6514326	-75.6062104
3	-76.2935664	-76.3388650	-76.2935664
14a	-700.2659624	-700.5341854	-701.069795
14b	-700.2627431	-700.5313325	
14H a	-700.8975204	-701.1734034	-701.707940
14H b	-700.8955211	-701.1713174	
17	-437.4276964	-437.5379578	-437.863325
17H	-438.0565292	-438.1748149	-438.499110
4	-398.2386425	-398.2970556	-398.593338
4H	-398.8742985	-398.9408183	-399.236045
6a	-420.6211122	-420.9165186	-421.236568
6b	-420.6209188	-420.9163047	
6H a	-421.2791724	-421.5801737	-421.899866
6H b	-421.2788240	-421.5799681	
6H c	-421.2777345	-421.5788272	
16 (Boltzmann)	-891.7999841	-892.2080758	n.a.
16 (Best conf.)	-891.8002669	-892.2082891	n.a.
16H (Boltzmann)	-892.4313403	-892.8467176	n.a.
16H (Best conf.)	-892.4314506	-892.8468226	n.a.
18	-491.74675420	-492.0763724	-492.4751940
18H	-492.38330300	-492.7168535	-493.1159464
19	-532.1113102	-532.4974175	-532.9385613
19H	-532.7539920	-533.1450352	-533.5783865

^a Scaling factor 0.9806

^b Scaling factor 0.960

Supplementary information for chapter 3

Computational details

For the larger closed-shell systems the conformational space has been searched using the MM3 force field and the systematic search routine implemented in the TINKER program suite.^[1] The structures for radicals were then build from those of the respective closed-shell parents. All structures were subsequently reoptimized at the (U)B3LYP/6-31G(d) level of theory. Thermal corrections to enthalpies at 298.15 K have been calculated at this same level of theory using the rigid rotor/harmonic oscillator model and a scale factor of 0.9806. Refined energies have then been obtained using the G3(MP2)-RAD model developed by Radom *et al.*^[2;3] For selected smaller systems evaluation of stability data was also possible at G3B3 level.^[4] Combination of the results for smaller systems at G3B3 level with those obtained for larger systems at G3(MP2)-RAD level allows for improved predictions for the larger systems using a IMOMO(G3B3,G3(MP2)-RAD) scheme.^[5;6] The core regions described in this latter model at G3B3 level are the glycy radical **8** for all C-centered peptide radicals, phenoxy radical **21** for tyrosyl radical **14**, and methylthiyl radical **22** for cysteinyl radical **15**. The URCCSD(T) calculations required in the G3(MP2)-RAD method have been performed with the MOLPRO 2006.1 program package,^[7] and all other calculations have been performed using Gaussian 03, D01.^[8] All calculations have been performed in the gas phase.

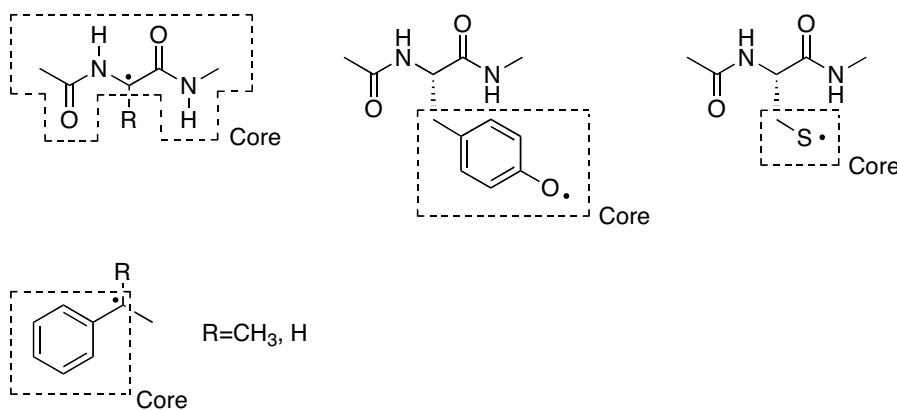
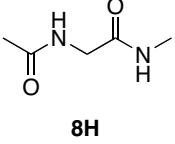
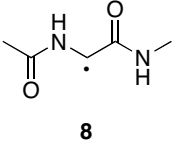
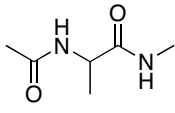
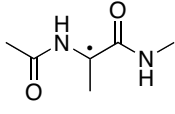
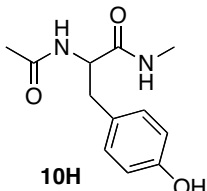
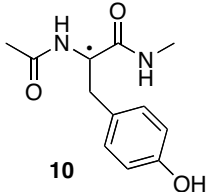
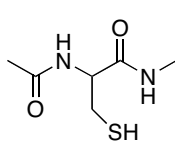
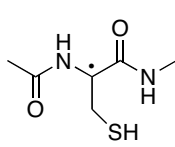


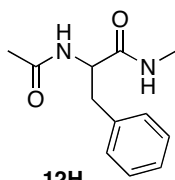
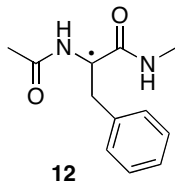
Table B.2: Conformational enthalpies $\Delta H_{298,\text{rel}}$ of dipeptide radicals and their respective closed-shell parent systems at G3(MP2)-RAD level in kJ/mol (complete list).

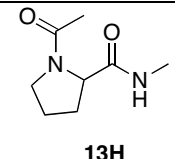
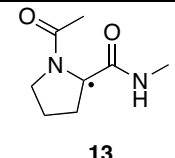
Systems	Backbone geometry	Φ	Ψ	Peptide bond conformations	$\Delta H_{298,\text{rel}}$ [kJ/mol]
 <p>8H</p>	C ₇	-82.2	68.6	Trans-Trans	+0.0
	C ₅	180.0	180.0	Trans-Trans	+4.2
	C ₅	-179.9	-179.8	Trans-Cis	+10.7
	$\beta_2(\alpha')$	-122.7	21.8	Trans-Trans	+11.5
	$\alpha_R(\alpha_L)$	-94.5	-1.7	Cis-Trans	+16.5
	C ₇	-93.9	117.4	Trans-Cis	+19.6
	C ₅	180.0	180.0	Cis-Trans	+23.7
	$\beta(\alpha_D)$	-74.9	-151.7	Cis-Trans	+27.0
	C ₅	179.7	179.5	Cis-Cis	+30.3
	$\alpha_R(\alpha_L)$	-70.0	-43.4	Trans-Cis	+38.8
	$\alpha_R(\alpha_L)$	-77.0	-70.8	Cis-Cis	+38.9
	$\beta_2(\alpha')$	-152.3	64.9	Cis-Cis	+41.6
 <p>8</p>	C ₅	180.0	180.0	Trans-Trans	+0.0
	C ₅	179.9	179.5	Trans-Cis	+6.0
	C ₅	180.0	180.0	Cis-Trans	+10.3
	C ₅	180.0	180.0	Cis-Cis	+13.6
	$\beta_2(\alpha')$	-176.4	14.9	Trans-Trans	+26.7
	$\beta_2(\alpha')$	-173.9	13.6	Cis-Trans	+27.4
	C ₇	-5.4	-0.6	Trans-Trans	+31.4
	$\beta(\alpha_D)$	-38.1	174.2	Cis-Trans	+38.8
	$\beta_2(\alpha')$	179.5	17.5	Trans-Cis	+41.4
	$\beta_2(\alpha')$	-179.5	18	Cis-Cis	+43.4
	$\alpha_R(\alpha_L)$	-55.9	-12.1	Cis-Trans	+44.3
	$\beta(\alpha_D)$	-42.5	163.2	Trans-Cis	+57.1

 <p>9H</p>	C _{7eq.}	-82.9	72.9	Trans-Trans	+0.0
	C ₅	-158.1	164.1	Trans-Trans	+6.1
	C _{7ax.}	72.8	-56.3	Trans-Trans	+9.8
	β ₂	126.7	20.9	Trans-Trans	+14.3
	C ₅	-157.1	158.7	Trans-Cis	+15.8
	α _R	-94.1	-4.0	Cis-Trans	+18.8
	α _L	68.2	26.8	Trans-Trans	+19.5
	C _{7eq.}	-96.5	111.6	Trans-Cis	+20.4
	α'	-169.1	-39.3	Trans-Trans	+26.8
	C ₅	-151.1	150.6	Cis-Trans	+27.8
	α _L	74.5	26.1	Cis-Trans	+29.0
	α'	-80.0	-92.6	Cis-Trans	+34.4
	C ₅	-150.0	153.7	Cis-Cis	+37.8
	α _L	52.4	53.3	Trans-Cis	+40.2
	α _R	-65.7	-37.1	Trans-Cis	+40.5
	β ₂	-151.8	88.2	Cis-Cis	+40.7
	α _R	-66.7	-42.0	Cis-Cis	+41.6
α'	-161.0	-45.8	Trans-Cis	+44.8	
α _L	59.6	59.8	Cis-Cis	+45.3	
C _{7ax.}	111.3	-56.1	Trans-Cis	+48.2	
 <p>9</p>	C ₅	180.0	180.0	Trans-Trans	+0.0
	C ₇	-31.9	6.5	Trans-Trans	+17.4
	β ₂ (α')	-167.7	15.2	Trans-Trans	+17.7
	C ₅	-170.6	177.1	Cis-Trans	+18.6
	C ₅	-175.1	172.8	Trans-Cis	+19.3
	α _R (α _L)	-62.5	-10.9	Cis-Trans	+26.2
	β(α _D)	-37.2	168.4	Cis-Trans	+28.7
	β ₂ (α')	-173.8	15.5	Trans-Cis	+31.8
	C ₅	-169.6	173.4	Cis-Cis	+37.7
	α _R (α _L)	-46.6	-23.9	Cis-Cis	+41.3
	β ₂ (α')	-168.6	16.7	Cis-Cis	+41.8
	β(α _D)	-43.0	150.1	Trans-Cis	+45.2
α _R (α _L)	-31.5	-40.6	Trans-Cis	+45.5	

 <p>10H</p>	C ₅	-158.7	170.8	Trans-Trans	+0.0
	C _{7eq.}	-82.8	78.2	Trans-Trans	+2.8
	β ₂	-122.4	19.5	Trans-Trans	+5.7
	C _{7ax.}	72.3	-54.9	Trans-Trans	+6.3
	C _{7eq.}	-108.0	7.4	Cis-Trans	+14.7
	C ₅	-155.5	162.0	Trans-Cis	+16.3
	α'	-174.6	-32.1	Trans-Trans	+18.0
	β ₂	-133.2	15.1	Cis-Trans	+17.5
	C ₅	-133.5	142.7	Cis-Trans	+22.1
	β ₂	-125.2	58.5	Trans-Cis	+22.8
	C _{7eq.}	-99.2	109.9	Trans-Cis	+24.2
	α _L	49.4	43.4	Trans-Trans	+25.6
	α _L	69.9	35.6	Cis-Trans	+28.3
	α _R	-81.8	-27.0	Cis-Trans	+30.2
	α _L	51.5	50.2	Trans-Cis	+35.8
	C ₅	-145.0	159.6	Cis-Cis	+41.0
	α _L	61.2	60.1	Cis-Cis	+43.5
	β ₂	-143.5	46.8	Cis-Cis	+43.6
	α _R	-72.9	-38.4	Cis-Cis	+44.7
	α _R	-55.2	-49.1	Trans-Cis	+48.9
α'	-157.6	-59.3	Trans-Cis	+49.1	
C _{7ax.}	101.3	-77.4	Trans-Cis	+54.7	
 <p>10</p>	C ₅	-170.3	177.2	Trans-Trans	+0.0
	C ₇	40.6	-19.3	Trans-Trans	+14.6
	β ₂ (α')	-165.0	17.7	Trans-Trans	+18.1
	C ₅	171.1	-178.4	Cis-Trans	+21.0
	C ₅	-171.6	172.4	Trans-Cis	+25.6
	α _R (α _L)	-61.8	-14.6	Cis-Trans	+26.9
	β ₂ (α')	-168.5	18.6	Trans-Cis	+33.0
	α _R (α _L)	-47.5	-25.5	Cis-Cis	+42.2
	C ₅	-170.2	-167.2	Cis-Cis	+43.0
	α _R (α _L)	-28.5	-47.0	Trans-Cis	+44.5
β ₂ (α')	-166.5	21.3	Cis-Cis	+48.2	

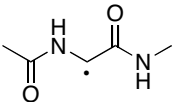
 <p style="text-align: center;">11H</p>	C _{7eq.}	-82.5	66.0	Trans-Trans	+0.0
	C ₅	-160.4	173.0	Trans-Trans	+8.7
	C _{7ax.}	75.6	-54.9	Trans-Trans	+18.6
	β ₂	-131.9	25.8	Trans-Trans	+19.2
	β ₂	-125.5	62.4	Trans-Cis	+23.4
	α _L	68.0	26.3	Trans-Trans	+23.7
	β ₂	-126.3	19.4	Cis-Trans	+24.0
	C ₅	-155.5	133.4	Trans-Cis	+27.0
	α'	-161.6	-40.2	Trans-Trans	+30.1
	β	-111.7	150.6	Trans-Cis	+30.7
	C _{7eq.}	-94.9	117.4	Trans-Cis	+31.8
	C ₅	-149.0	162.5	Cis-Trans	+35.0
	C _{7eq.}	-106.2	7.3	Cis-Trans	+35.4
	β	-118.8	141.6	Cis-Trans	+36.1
	α _L	71.3	28.0	Cis-Trans	+36.3
	α _R	-79.1	-36.6	Cis-Trans	+44.1
	C ₅	-120.2	150.4	Cis-Cis	+46.0
	β ₂	-145.0	52.6	Cis-Cis	+47.9
	α _L	54.9	51.6	Trans-Cis	+49.2
	α'	-146.0	-49.8	Cis-Trans	+53.8
	β	-116.9	147.5	Cis-Cis	+55.7
	α'	-154.7	-54.2	Trans-Cis	+55.9
	α _L	56.6	60.1	Cis-Cis	+56.2
α _R	-63.7	-36.5	Trans-Cis	+57.5	
α _R	-68.7	-37.0	Cis-Cis	+59.9	
C _{7ax.}	110.7	-49.6	Trans-Cis	+61.2	
 <p style="text-align: center;">11</p>	C ₅	-168.3	172.2	Trans-Trans	+0.0
	C ₇	-38.7	16.6	Trans-Trans	+16.4
	C ₅	-178.0	173.2	Trans-Cis	+21.0
	β ₂ (α')	-172.1	16.6	Trans-Trans	+23.4
	C ₅	-177.0	171.6	Cis-Trans	+26.8
	α _R (α _L)	-63.3	-8.9	Cis-Trans	+31.8
	β ₂ (α')	-154.7	18.5	Cis-Trans	+32.2
	β ₂ (α')	-172.8	21.6	Trans-Cis	+37.0
	α _R (α _L)	-24.9	-51.0	Trans-Cis	+46.9
	α _R (α _L)	-47.9	-22.1	Cis-Cis	+47.3
	β ₂ (α')	-162.9	26.7	Cis-Cis	+50.1
C ₅	170.3	174.9	Cis-Cis	+53.6	

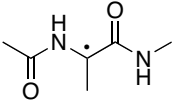
 <p>12H</p>	C ₅	-159.0	170.8	Trans-Trans	+0.0
	C _{7eq.}	-82.8	78.8	Trans-Trans	+3.0
	β ₂	-120.6	17.6	Trans-Trans	+5.7
	C _{7ax.}	76.2	-54.9	Trans-Trans	+5.8
	C ₅	-158.7	140.4	Trans-Cis	+11.0
	C _{7eq.}	-102.4	6.9	Cis-Trans	+14.5
	α'	-132.3	15.2	Cis-Trans	+17.8
	β ₂	-125.2	57.2	Trans-Cis	+23.3
	C _{7eq.}	-99.7	110.1	Trans-Cis	+24.7
	β ₂	-172.6	-33.5	Trans-Trans	+17.7
	α _L	49.0	44.1	Trans-Trans	+24.5
	α _L	69.5	35.4	Cis-Trans	+28.2
	α _R	-81.4	-27.6	Cis-Trans	+29.9
	C ₅	-145.8	161.8	Cis-Trans	+30.1
	C ₅	-131.6	149.2	Cis-Cis	+33.7
	α _L	50.8	53.9	Trans-Cis	+34.9
	α _L	60.6	60.3	Cis-Cis	+40.5
	β ₂	-142.6	42.2	Cis-Cis	+41.1
α _R	-72.8	-37.7	Cis-Cis	+41.3	
α'	-156.8	-50.2	Trans-Cis	+48.0	
α _R	-58.2	-47.9	Trans-Cis	+49.1	
C _{7ax.}	101.0	-77.5	Trans-Cis	+54.4	
 <p>12</p>	C ₅	-171.7	177.3	Trans-Trans	+0.0
	C ₇	40.0	-18.2	Trans-Trans	+15.0
	β ₂ (α')	-164.5	17.6	Trans-Trans	+18.3
	C ₅	170.8	-178.2	Cis-Trans	+21.0
	α _R (α _L)	-62.0	-14.3	Cis-Trans	+26.9
	C ₅	175.0	177.4	Trans-Cis	+28.4
	β ₂ (α')	-167.9	18.7	Trans-Cis	+33.5
	α _R (α _L)	-47.4	-25.5	Cis-Cis	+41.7
	C ₅	-169.2	167.2	Cis-Cis	+43.5
	α _R (α _L)	-30.3	-41.1	Trans-Cis	+46.0
	β ₂ (α')	-166.2	21.3	Cis-Cis	+48.2

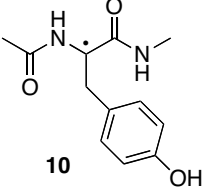
 <p>13H</p>	C _{7eq.}	-84.0	71.0	Trans-Trans	+0.0
	α _R	-93.0	-1.8	Cis-Trans	+11.9
	β	-74.0	144.5	Cis-Trans	+23.9
	β	-76.9	123.9	Cis-Cis	+24.6
	β	-71.2	163.2	Trans-Cis	+33.9
 <p>13</p>	C ₇	-26.4	2.2	Trans-Trans	+0.0
	β(α _D)	-40.9	171.9	Cis-Trans	+4.3
	α _R (α _L)	-54.8	-9.8	Cis-Trans	+8.4
	β(α _D)	-41.5	167.3	Cis-Cis	+16.3
	β(α _D)	-44.8	159.0	Trans-Cis	+31.8

System	H ₂₉₈ G3(MP2)RAD
CH ₄	-40.4169999
•CH ₃	-39.7518773

Table B.3: RSE values of conformationally restricted dipeptide radicals at G3(MP2)-RAD level in kJ/mol (complete list).

System	Backbone geometry	Peptide bond conformations	RSE [kJ/mol]
 <p>8</p>	C ₇	Trans-Trans	-42.6
	α _R	Cis-Trans	-46.0
	β ₂	Trans-Trans	-58.8
	β	Cis-Trans	-62.1
	β ₂	Cis-Cis	-72.2
	C ₅	Trans-Trans	-78.2
	C ₅	Trans-Cis	-79.6
	C ₅	Cis-Trans	-87.4
	C ₅	Cis-Cis	-90.7

 <p>9</p>	C ₇	Trans-Trans	-47.4
	α _R	Cis-Trans	-57.4
	α _L	Trans-Cis	-59.4
	α _R	Trans-Cis	-59.7
	C ₅	Trans-Cis	-61.3
	β ₂	Trans-Trans	-61.4
	β ₂	Cis-Cis	-63.7
	C ₅	Cis-Cis	-64.9
	α _R	Cis-Cis	-65.1
	α _L	Cis-Trans	-67.5
	α _L	Cis-Cis	-68.7
	C ₅	Trans-Trans	-70.9
	α'	Trans-Trans	-73.9
	C ₅	Cis-Trans	-73.9
	α'	Trans-Cis	-77.8

 <p>10</p>	β ₂	Trans-Trans	-55.7
	C ₇	Trans-Trans	-56.3
	β ₂	Trans-Cis	-57.9
	C ₅	Trans-Cis	-59.3
	α _L	Trans-Cis	-59.4
	β ₂	Cis-Cis	-63.5
	C ₅	Cis-Cis	-66.1
	α'	Trans-Trans	-68.0
	C ₅	Trans-Trans	-68.1
	α _L	Cis-Cis	-69.4
	α _L	Cis-Trans	-69.5
	C ₅	Cis-Trans	-70.4
	α _R	Cis-Cis	-70.6
	α _R	Cis-Trans	-71.4
	α _R	Trans-Cis	-72.5
α'	Trans-Cis	-84.2	

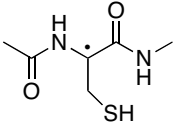
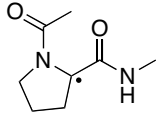
 <p style="text-align: center;">11</p>	C ₇	Trans-Trans	-48.3
	β ₂	Cis-Trans	-56.4
	C ₅	Cis-Cis	-57.0
	β ₂	Trans-Trans	-60.5
	β ₂	Cis-Cis	-62.5
	α _L	Trans-Cis	-66.0
	α _L	Cis-Trans	-69.2
	C ₅	Trans-Cis	-70.7
	α'	Trans-Trans	-71.4
	C ₅	Cis-Trans	-72.9
	C ₅	Trans-Trans	-73.4
	α _L	Cis-Cis	-73.6
	α _R	Trans-Cis	-75.2
	α _R	Cis-Trans	-77.0
	α _R	Cis-Cis	-77.2
β ₂	Trans-Cis	-81.4	
α'	Trans-Cis	-83.5	
α'	Cis-Trans	-86.2	
 <p style="text-align: center;">13</p>	β	Trans-Cis	-39.1
	C ₇	Trans-Trans	-46.3
	α _R	Cis-Trans	-49.8
	β	Cis-Cis	-63.8
	β	Cis-Trans	-65.9

Table B.4: Conformational enthalpies H₂₉₈ of glycine dipeptide radicals and their respective closed-shell parent systems at G3(MP2)-RAD level in kJ/mol (complete list).

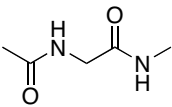
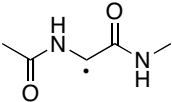
Systems	Backbone geometry	Peptide bond conformations	H ₂₉₈ G3(MP2)RAD
 <p style="text-align: center;">8H</p>	C ₇	Trans-Trans	-455.8496671
	C ₅	Trans-Trans	-455.8480607
	C ₅	Trans-Cis	-455.8456046
	β ₂ (α')	Trans-Trans	-455.8452950
	α _R (α _L)	Cis-Trans	-455.8433928
	C ₇	Trans-Cis	-455.8421975
	C ₅	Cis-Trans	-455.8406313
	β(α _D)	Cis-Trans	-455.8394035
	C ₅	Cis-Cis	-455.8381207
	α _R (α _L)	Trans-Cis	-455.8348896
	α _R (α _L)	Cis-Cis	-455.8348340
	β ₂ (α')	Cis-Cis	-455.8338319
 <p style="text-align: center;">8</p>	C ₅	Trans-Trans	-455.2127203
	C ₅	Trans-Cis	-455.2104202
	C ₅	Cis-Trans	-455.2088008
	C ₅	Cis-Cis	-455.2075282
	β ₂ (α')	Trans-Trans	-455.2025543
	β ₂ (α')	Cis-Trans	-455.2022851
	C ₇	Trans-Trans	-455.2007780
	β(α _D)	Cis-Trans	-455.1979359
	β ₂ (α')	Trans-Cis	-455.1969383
	β ₂ (α')	Cis-Cis	-455.1962031
	α _R (α _L)	Cis-Trans	-455.1957964
	β(α _D)	Trans-Cis	-455.1909809

Table B.5: Conformational enthalpies H_{298} of alanine dipeptide radicals and their respective closed-shell parent systems at G3(MP2)-RAD level in kJ/mol (complete list).

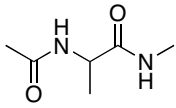
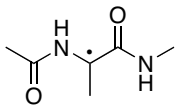
Systems	Backbone geometry	Peptide bond conformations	H_{298} G3(MP2)RAD
 <p style="text-align: center;">9H</p>	$C_{7eq.}$	Trans-Trans	-495.0879664
	C_5	Trans-Trans	-495.0856290
	$C_{7ax.}$	Trans-Trans	-495.0842540
	β_2	Trans-Trans	-495.0825223
	C_5	Trans-Cis	-495.0819643
	α_R	Cis-Trans	-495.0808073
	α_L	Trans-Trans	-495.0805354
	$C_{7eq.}$	Trans-Cis	-495.0802090
	α'	Trans-Trans	-495.0777641
	C_5	Cis-Trans	-495.0773833
	α_L	Cis-Trans	-495.0769348
	α'	Cis-Trans	-495.0748829
	C_5	Cis-Cis	-495.0735716
	α_L	Trans-Cis	-495.0726734
	α_R	Trans-Cis	-495.0725548
	β_2	Cis-Cis	-495.0724790
	α_R	Cis-Cis	-495.0721085
α'	Trans-Cis	-495.0709082	
α_L	Cis-Cis	-495.0707196	
$C_{7ax.}$	Trans-Cis	-495.0696237	
 <p style="text-align: center;">9</p>	C_5	Trans-Trans	-494.4475184
	C_7	Trans-Trans	-494.4409077
	$\beta_2(\alpha')$	Trans-Trans	-494.4407734
	C_5	Cis-Trans	-494.4404175
	C_5	Trans-Cis	-494.4401775
	$\alpha_R(\alpha_L)$	Cis-Trans	-494.4375304
	$\beta(\alpha_D)$	Cis-Trans	-494.4366020
	$\beta_2(\alpha')$	Trans-Cis	-494.4354063
	C_5	Cis-Cis	-494.4331778
	$\alpha_R(\alpha_L)$	Cis-Cis	-494.4317735
	$\beta_2(\alpha')$	Cis-Cis	-494.4316033
	$\beta(\alpha_D)$	Trans-Cis	-494.4302934
	$\alpha_R(\alpha_L)$	Trans-Cis	-494.4301827

Table B.6: Conformational enthalpies H_{298} of tyrosine dipeptide radicals and their respective closed-shell parent systems at G3(MP2)-RAD level in kJ/mol (complete list).

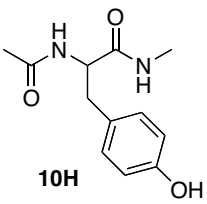
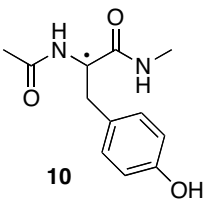
Systems	Backbone geometry	Peptide bond conformations	H_{298} G3(MP2)RAD
 <p>10H</p>	C_5	Trans-Trans	-800.8873015
	$C_{7eq.}$	Trans-Trans	-800.8862296
	β_2	Trans-Trans	-800.8851417
	$C_{7ax.}$	Trans-Trans	-800.8849001
	$C_{7eq.}$	Cis-Trans	-800.8817176
	C_5	Trans-Cis	-800.8809273
	α'	Trans-Trans	-800.8804491
	β_2	Cis-Trans	-800.8806294
	C_5	Cis-Trans	-800.8784240
	β_2	Trans-Cis	-800.8786087
	$C_{7eq.}$	Trans-Cis	-800.8780847
	α_L	Trans-Trans	-800.8775671
	α_L	Cis-Trans	-800.8765260
	α_R	Cis-Trans	-800.8758168
	α_L	Trans-Cis	-800.8736588
	C_5	Cis-Cis	-800.8717021
	α_L	Cis-Cis	-800.8707446
	β_2	Cis-Cis	-800.8706835
	α_R	Cis-Cis	-800.8702839
	α_R	Trans-Cis	-800.8686683
α'	Trans-Cis	-800.8686013	
$C_{7ax.}$	Trans-Cis	-800.8664636	
 <p>10</p>	C_5	Trans-Trans	-800.2481158
	C_7	Trans-Trans	-800.2425384
	$\beta_2(\alpha')$	Trans-Trans	-800.2412316
	C_5	Cis-Trans	-800.2401053
	C_5	Trans-Cis	-800.2383832
	$\alpha_R(\alpha_L)$	Cis-Trans	-800.2378675
	$\beta_2(\alpha')$	Trans-Cis	-800.2355364
	$\alpha_R(\alpha_L)$	Cis-Cis	-800.2320405
	C_5	Cis-Cis	-800.2317547
	$\alpha_R(\alpha_L)$	Trans-Cis	-800.2311608
$\beta_2(\alpha')$	Cis-Cis	-800.2297530	

Table B.7: Conformational enthalpies H_{298} of cysteine dipeptide radicals and their respective closed-shell parent systems at G3(MP2)-RAD level in kJ/mol (complete list).

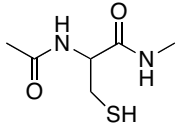
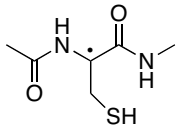
Systems	Backbone geometry	Peptide bond conformations	H_{298} G3(MP2)RAD
 <p>11H</p>	$C_{7eq.}$	Trans-Trans	-892.8468226
	C_5	Trans-Trans	-892.8435077
	$C_{7ax.}$	Trans-Trans	-892.8397246
	β_2	Trans-Trans	-892.8394998
	β_2	Trans-Cis	-892.8379065
	α_L	Trans-Trans	-892.8377853
	β_2	Cis-Trans	-892.8376956
	C_5	Trans-Cis	-892.8365372
	α'	Trans-Trans	-892.8353759
	β	Trans-Cis	-892.8351431
	$C_{7eq.}$	Trans-Cis	-892.8347088
	C_5	Cis-Trans	-892.8334901
	$C_{7eq.}$	Cis-Trans	-892.8333525
	β	Cis-Trans	-892.8330763
	α_L	Cis-Trans	-892.8330043
	α_R	Cis-Trans	-892.8300247
	C_5	Cis-Cis	-892.8293024
	β_2	Cis-Cis	-892.8285914
	α_L	Trans-Cis	-892.8280694
	α'	Cis-Trans	-892.8263501
	β	Cis-Cis	-892.8256232
	α'	Trans-Cis	-892.8255471
	α_L	Cis-Cis	-892.8254037
α_R	Trans-Cis	-892.8249319	
α_R	Cis-Cis	-892.8240277	
$C_{7ax.}$	Trans-Cis	-892.8235052	
 <p>11</p>	C_5	Trans-Trans	-892.2063314
	C_7	Trans-Trans	-892.2001000
	C_5	Trans-Cis	-892.1983382
	$\beta_2(\alpha')$	Trans-Trans	-892.1974346
	C_5	Cis-Trans	-892.1961289
	$\alpha_R(\alpha_L)$	Cis-Trans	-892.1942372
	$\beta_2(\alpha')$	Cis-Trans	-892.1940527
	$\beta_2(\alpha')$	Trans-Cis	-892.1922316
	$\alpha_R(\alpha_L)$	Trans-Cis	-892.1884520
	$\alpha_R(\alpha_L)$	Cis-Cis	-892.1883199
	$\beta_2(\alpha')$	Cis-Cis	-892.1872542
	C_5	Cis-Cis	-892.1859060

Table B.8: Conformational enthalpies H_{298} of phenylalanine dipeptide radicals and their respective closed-shell parent systems at G3(MP2)-RAD level in kJ/mol (complete list).

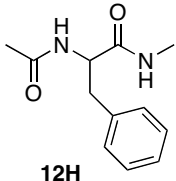
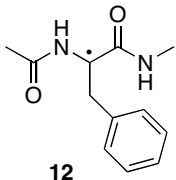
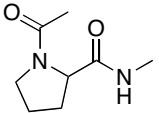
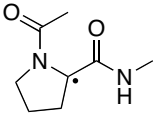
Systems	Backbone geometry	Peptide bond conformations	H_{298} G3(MP2)RAD
 <p>12H</p>	C ₅	Trans-Trans	-725.7383683
	C _{7eq.}	Trans-Trans	-725.7372180
	β ₂	Trans-Trans	-725.7361877
	C _{7ax.}	Trans-Trans	-725.7361493
	C ₅	Trans-Cis	-725.7341815
	C _{7eq.}	Cis-Trans	-725.7328575
	α'	Trans-Trans	-725.7316465
	β ₂	Cis-Trans	-725.7315880
	C _{7eq.}	Trans-Cis	-725.7294898
	β ₂	Trans-Cis	-725.7293348
	α _L	Trans-Trans	-725.7290321
	α _L	Cis-Trans	-725.7276283
	α _R	Cis-Trans	-725.7269664
	C ₅	Cis-Trans	-725.7268907
	C ₅	Cis-Cis	-725.7255501
	α _L	Trans-Cis	-725.7250590
	α _L	Cis-Cis	-725.7217933
	β ₂	Cis-Cis	-725.7215574
	α _R	Cis-Cis	-725.7214784
	α'	Trans-Cis	-725.7200690
α _R	Trans-Cis	-725.7196756	
C _{7ax.}	Trans-Cis	-725.7176561	
 <p>12</p>	C ₅	Trans-Trans	-725.0992692
	C ₇	Trans-Trans	-725.0935482
	β ₂ (α')	Trans-Trans	-725.0923122
	C ₅	Cis-Trans	-725.0912683
	α _R (α _L)	Cis-Trans	-725.0890104
	C ₅	Trans-Cis	-725.0884427
	β ₂ (α')	Trans-Cis	-725.0865069
	α _R (α _L)	Cis-Cis	-725.0834016
	C ₅	Cis-Cis	-725.0826994
	α _R (α _L)	Trans-Cis	-725.0817630
	β ₂ (α')	Cis-Cis	-725.0809066

Table B.9: Conformational enthalpies H_{298} of proline dipeptide radicals and their respective closed-shell parent systems at G3(MP2)-RAD level in kJ/mol (complete list).

Systems	Backbone geometry	Peptide bond conformations	H_{298} G3(MP2)RAD
 <p>13H</p>	C _{7eq.}	Trans-Trans	-572.3627496
	α _R	Cis-Trans	-572.3582267
	β	Cis-Trans	-572.3536381
	β	Cis-Cis	-572.3533720
	β	Trans-Cis	-572.3498476
 <p>13</p>	C ₇	Trans-Trans	-571.7152625
	β(α _D)	Cis-Trans	-571.7136126
	α _R (α _L)	Cis-Trans	-571.7120599
	β(α _D)	Cis-Cis	-571.7090401
	β(α _D)	Trans-Cis	-571.7031512

Bibliography

- [1] J. W. Ponder. Tinker 4.2, 2004. Washington University, St. Louis.
- [2] D. J. Henry, C. J. Parkinson, and L. Radom. *J. Phys. Chem. A*, 106:7927, 2007.
- [3] D. J. Henry, M. B. Sullivan, and L. Radom. *J. Chem. Phys.*, 118:4849–4860, 2003.
- [4] A. G. Baboul, L. A. Curtiss, P. C. Redfern, and K. Ragahavachari. *J. Chem. Phys.*, 110:7650–7657, 1999.
- [5] T. Vreven and K. Morokuma. *J. Chem. Phys.*, 111:8799–8803, 1999.
- [6] T. Vreven and K. Morokuma. *J. Comp. Chem.*, 21:1419–1432, 2000.
- [7] H.-J. Werner, P. J. Knowles, R. Lindh, F. R. Manby, M. Schütz, P. Celani, T. Korona, A. Mitrushenkov, G. Rauhut, T. B. Adler, R. D. Amos, A. Bernhardsson, A. Berning, M. J. O. Deegan D. L. Cooper, A. J. Dobbyn, F. Eckert, E. Goll, G. Hetzer C. Hampel, G. Knizia T. Hrenar, C. Köppl, A. W. Lloyd Y. Liu, R. A. Mata, S. J. McNicholas A. J. May, W. Meyer, M. E. Mura, A. Nicklaß, P. Palmieri, K. Pflüger, R. Pitzer, M. Reiher, U. Schumann, H. Stoll, A. J. Stone, R. Tarroni, T. Thorsteinsson, M. Wang, and A. Wolf. MOLPRO, version 2006.1, *a package of ab initio programs*.
- [8] M. J. Frisch, G. W. Trucks, H. B. Schlegel, G. E. Scuseria, M. A. Robb, J. R. Cheeseman, J. A. Montgomery, Jr., T. Vreven, K. N. Kudin, J. C. Burant, J. M. Millam, S. S. Iyengar, J. Tomasi, V. Barone, B. Mennucci, M. Cossi, G. Scalmani, N. Rega, G. A. Petersson, H. Nakatsuji, M. Hada, M. Ehara, K. Toyota, R. Fukuda, J. Hasegawa, M. Ishida, T. Nakajima, Y. Honda, O. Kitao, H. Nakai, M. Klene, X. Li, J. E. Knox, H. P. Hratchian, J. B. Cross, V. Bakken, C. Adamo, J. Jaramillo, R. Gomperts, R. E. Stratmann, O. Yazyev, A. J. Austin, R. Cammi, C. Pomelli, J. Ochterski, P. Y. Ayala, K. Morokuma, G. A. Voth, P. Salvador, J. J. Dannenberg, V. G. Zakrzewski, S. Dapprich, A. D. Daniels, M. C. Strain, O. Farkas, D. K. Malick, A. D. Rabuck, K. Raghavachari, J. B. Foresman, J. V. Ortiz, Q. Cui, A. G. Baboul, S. Clifford, J. Cioslowski, B. B. Stefanov, G. Liu, A. Liashenko, P. Piskorz, I. Komaromi, R. L. Martin, D. J. Fox, T. Keith, M. A. Al-Laham, C. Y. Peng, A. Nanayakkara, M. Challacombe, P. M. W. Gill, B. G. Johnson, W. Chen, M. W. Wong, C. Gonzalez, and J. A. Pople, 2004. GAUSSIAN 03 (Revision D.01), Gaussian, Inc., Wallingford, CT.

Supplementary information for chapter 4

Table B.10: Rate constants for hydrogen abstraction by thiyl radicals **12** and BDE(C_{α} -H) values for selected peptide models.

System	Rate constant [$M^{-1} s^{-1}$]	C-H BDE (G3B3) [kJ/mol]	C-H BDE (B3LYP/6-31G(d)) [kJ/mol]
6H_a	8.0×10^4	+359.2 ^a	+341.0
N-Ac-Gly-NH ₂	3.2×10^4	+363.8 ^c (2H_a)	+337.7 (2H_a)
N-Ac-Ala-NH ₂	1.0×10^4	+372.3 ^b (2H_b)	+340.4 (2H_b)
N-Ac-Pro-NH ₂	0.18×10^4	+391.5 ^b (Proline) ^c	+364.6 (Proline) ^c

^a G3B3; ^b IMOMO(G3B3/G3(MP2)-RAD); ^c Taken from ref. 3.

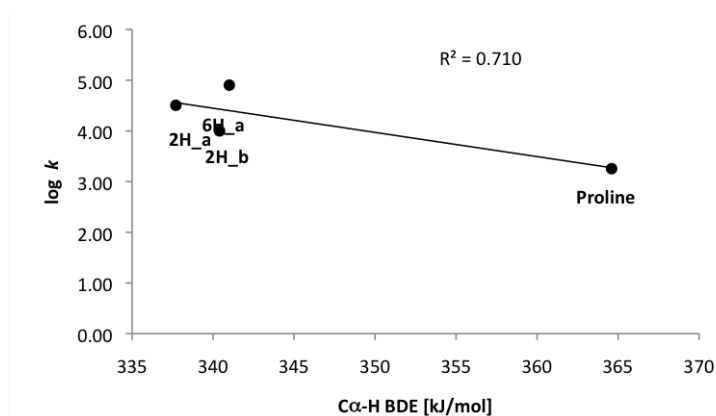
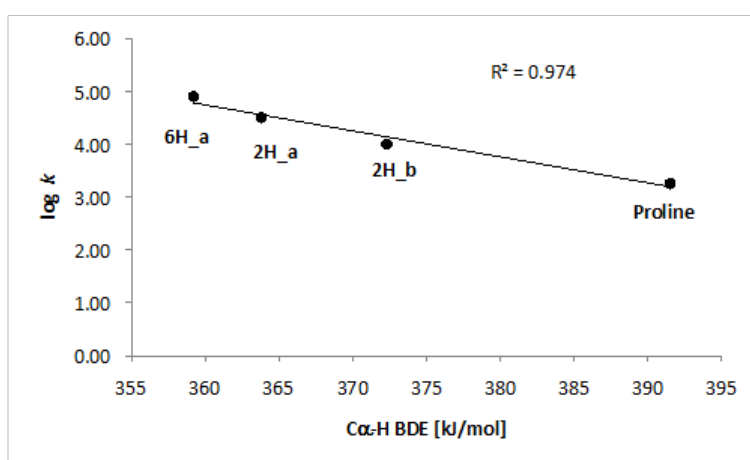


Table B.11: Complete list of C $_{\alpha}$ -H BDE of peptides, amino acids and anhydrides with different reference systems and theoretical methods.

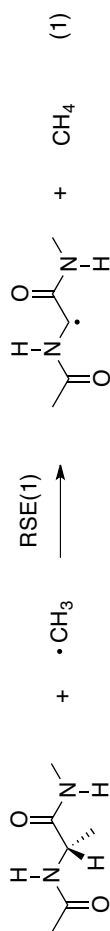
Reference	C-H BDE of reference	System	BDE C $_{\alpha}$ -H B3LYP ^a	BDE C $_{\alpha}$ -H G3(MP2)-RAD	BDE C $_{\alpha}$ -H G3B3 or IMOMO		
CH ₄ /•CH ₃	+439.3 ± 0.4 (exp.)	2H_a	+337.7	+365.2	+363.8		
		2H_b	+340.4	+373.8	+372.3 ^b		
		3H_a	+338.9	+363.4	+361.7		
		3H_b	+338.3	+369.7	+368.1		
		4H_a	+331.2	+353.7	+351.6		
		4H_b	+325.6	+352.2	+349.4		
		5H_a	+320.5	+343.5	+340.3		
		5H_b	+308.5	+336.8	+332.9		
		6H_a	+341.0	+361.4	+359.2		
		6H_b	+324.7	+351.6	+349.2		
		CH ₃ NH ₂ /•CH ₂ NH ₂	+392.9 ± 8.4 (exp.) +383.4 (B3LYP) ^c +394.4 (G3(MP2)-RAD) ^c +392.4 (G3B3) ^c	2H_a	+347.2	+363.7	+364.3
				2H_b	+350.0	+372.3	+372.8 ^b
3H_a	+348.1			+361.9	+362.0		
3H_b	+348.1			+368.2	+368.6		
4H_a	+341.3			+352.3	+352.1		
4H_b	+335.5			+350.7	+349.9		
5H_a	+330.2			+342.0	+340.8		
5H_b	+318.2			+335.3	+333.4		
6H_a	+350.5			+359.9	+359.7		
6H_b	+334.2			+350.1	+349.7		
CH ₃ CHCH ₂ /•CH ₂ CHCH ₂	+368.6 ± 2.9 (exp.) +335.9 (B3LYP) ^c +367.3 (G3(MP2)-RAD) ^c +368.8 (G3B3) ^c			2H_a	+350.3	+366.3	+363.6
				2H_b	+353.1	+374.9	+372.1 ^b
		3H_a	+351.3	+364.5	+361.3		
		3H_b	+351.3	+370.8	+367.9		
		4H_a	+344.4	+354.8	+351.4		
		4H_b	+338.6	+353.2	+349.2		
		5H_a	+333.3	+344.6	+340.1		
		5H_b	+321.3	+337.9	+332.7		
		6H_a	+353.6	+362.5	+359.0		
		6H_b	+337.3	+352.7	+349.2		
		5H_a/5_a	+331.0 ^d	2H_a	+348.3	+352.7	+354.5
				2H_b	+351.0	+361.3	+362.7 ^b
3H_a	+349.4			+350.8	+352.2		
3H_a (C₅)	+348.9			+353.4	+350.4		
3H_b	+348.8			+357.2	+358.8		
3H_b (C₅)	+344.8			+357.1	+354.5		
4H_a	+341.8			+341.2	+342.3		
4H_b	+336.2			+339.7	+340.1		
6H_a	+351.5			+348.9	+349.9		
6H_b	+335.3			+339.1	+339.9		

Table B.12: H_{298} of reference systems, peptides, amino acids, anhydrides and their respective open shells at various level of theories.

System	H_{298} B3LYP/6-31G(d)	H_{298} G3(MP2)-RAD	H_{298} G3B3	H_{298} G+5H	H_{298} WIRO	H_{298} G2(MP2)	H_{298} G3X(MP2)-RAD	G_{obs}	B3LYP/6-31G(d)
	[a.u.]	[a.u.]	[a.u.]	[a.u.]	[a.u.]	[a.u.]	[a.u.]	[kcal/mol]	
CH ₄	-40.4693510	-40.4169999	-40.4544536	-40.460604		-40.405849	-40.4188481		3.29
•CH ₃	-39.8044070	-39.7518765	-39.7895467	-39.795364		-39.739661	-39.7533909		2.98
CH ₃ NH ₂	-95.784448	-95.6808713	-95.7579170						
•CH ₂ NH ₂	-95.140791	-95.0328567	-95.1108822						
CH ₃ CHCH ₃	-117.822453	-117.6662905	-117.7797155						
•CH ₂ CHCH ₂	-117.189239	-117.0285033	-117.1416547						
3H_a	-377.7910035	-377.3822685	-377.6646443	-377.7217460					
3_a	-377.1643090	-376.7460668	-377.0293563	-377.0863812					
3H_b	-417.0791835	-416.6203750	-416.9409716						
3_b	-416.4527109	-415.9817492	-416.3031673						
4H_a	-264.4572682	-264.1774801	-264.3771516	-264.4170515					
4_a	-263.8334805	-263.5449422	-263.7456465	-263.7856841					
4H_b	-303.7452297	-303.4147559	-303.6526214						
4_b	-303.1235712	-302.7828142	-303.0219614						
5H_a	-284.3365448	-284.0472385	-284.2493855	-284.2931825	-284.4997116	-284.0029182	-284.0511497		
5_a	-283.7168552	-283.4185933	-283.6221765	-283.6656951	-283.8734810	-283.3739639	-283.4222416		
5H_b	-323.6253926	-323.2856566	-323.5239870						
5_b	-323.0102522	-322.6595893	-322.8996172						

6H_a	-415.888512	-415.4210565	-415.7429686	-2.34
6_a	-415.260998	-414.7856127	-415.1085792	-2.68
6H_b	-494.465387	-493.8979223	-494.2963331	1.66
6_b	-493.844074	-493.2661897	-493.6657485	1.09

IMOMO(G3B3,G3(MP2)-RAD) for alanyl radical can be described as the difference of calculated reaction enthalpies of a small system (eq. 2) at G3B3 and G3(MP2)-RAD plus the reaction enthalpies calculated G3(MP2)-RAD for the big system (eq. 1).



$$\begin{aligned}
 \text{RSE(1) IMOMO(G3B3/G3(MP2)-RAD)} &= \text{RSE(1) G3(MP2)-RAD} \\
 &+ \text{RSE(2) G3B3} - \text{RSE(2) G3(MP2)-RAD}
 \end{aligned}$$

Supplementary information for chapter 5

Computational details

The Gaussian theories (G2, G3 and G4) are developed to determine correct reaction energies within an error threshold of 1 kcal/mol to the experimental data or to higher theoretical methods. One of the most popular G3-method is G3B3. It contains a calculation at the highly correlated QCISD(T) level of theory and three separated basis set correction terms. G3(MP2)-RAD belongs to the G3-theories, which is specially designed to predict accurate thermochemistry for open shell structures. Different from G3B3, the QCISD(T) calculation in G3(MP2)-RAD is replaced by a more consistent coupled cluster calculation and it has only a single basis set correction term. G3(+2d,MP2)-RAD is a minor variation to G3(MP2)-RAD by scaling down the basis set correction term, and a simultaneous scaling up of the coupled cluster part. The double- ζ basis set is extended through addition of a d-polarization function and a diffusefunction. In summary, in G3(+2d,MP2)-RAD ten additional basis functions are added to each non hydrogen center. For the details of the composite methods please refer to appendix A.1.

$$E_{U(R)CCSD(T),INF} = \frac{\left(\frac{9}{2}\right)^4 E_{U(R)CCSD(T),cc-pVQZ} - \left(\frac{7}{2}\right)^4 E_{U(R)CCSD(T),cc-pVTZ}}{\left(\frac{9}{2}\right)^4 - \left(\frac{7}{2}\right)^4} \quad \text{Eq. (1)}$$

$$E_{SCF,INF} = E_{SCF,cc-pVQZ} + \frac{E_{SCF,cc-pVQZ} - E_{SCF,cc-pVTZ}}{(4/3)^5 - 1} \quad \text{Eq. (2a)}$$

$$E_{COR,CCSD,INF} = E_{COR,CCSD,cc-pVQZ} + \frac{E_{COR,CCSD,cc-pVQZ} - E_{COR,CCSD,cc-pVTZ}}{(4/3)^{3.22} - 1} \quad \text{Eq. (2b)}$$

$$E_{COR,T,INF} = E_{COR,T,cc-pVTZ} + \frac{E_{COR,T,cc-pVTZ} - E_{COR,T,cc-pVDZ}}{(3/2)^{3.22} - 1} \quad \text{Eq. (2c)}$$

Several extrapolation approaches are proposed to match the distinct purposes depending on the calculated systems. The first approach extrapolates the whole coupled cluster energies using the extrapolation formula as it is described in eq. 1. The second approach used different extrapolation formulas for different levels of theories, that is, the ground state energies are extrapolated differently from the correlation energies. An example for this approach can be seen in Weizmann-theories (W1). In this study, the extrapolation schemes from W1-method are used, but the basis sets cc-pVTZ and cc-pVQZ are applied to the extrapolations of SCF-energy and CCSD correlation energy (eq. 2a and eq. 2b), and the basis set cc-pVDZ and cc-pVTZ are applied to the extrapolation of the triples excitations energies (eq. 2c). Furthermore the relativistic effect is also neglected here. Finally these two extrapolation approaches are applied to determine the RSE of pyrimidinyl radical **9**.

Table B.13: Total energies in a.u. at coupled cluster level of theory used for CBS extrapolation.

System		cc-pVDZ	cc-pVTZ	cc-pVQZ	CBS ^a	CBS ^b
3H						
A	SCF	-40.1987615	-40.2132302	-40.2160390	-40.2169130	n.a.
B	CCSD-Correlation Energies	-0.1860289	-0.2194120	-0.2285092	-0.2344737	n.a.
C	Triples-Contribution	-0.0038581	-0.0063702	-0.0070146	-0.0073042	n.a.
	U(R)CCSD(T)	-40.3886485	-40.4390124	-40.4515628	-40.4586908	-40.4588065
System		cc-pVDZ	cc-pVTZ	cc-pVQZ	CBS ^a	CBS ^b
32H						
A	SCF	-262.7137736	-262.7795108	-262.7960030	-262.7086423	n.a.
B	CCSD-Correlation Energies	-0.8688926	-1.0321140	-1.0857442	-0.8337308	n.a.
C	Triples-Contribution	-0.0397793	-0.0567093	-0.0612912	-0.0334853	n.a.
	U(R)CCSD(T)	-263.6224455	-263.8683341	-263.9430384	-263.9850436	-263.9861551
System		cc-pVDZ	cc-pVTZ	cc-pVQZ	CBS ^a	CBS ^b
3						
A	SCF	-39.5596813	-39.5728899	-39.5756061	-39.5764512	n.a.
B	CCSD-Correlation Energies	-0.1549363	-0.1840038	-0.1920209	-0.1972772	n.a.
C	Triples-Contribution	-0.0027536	-0.0048620	-0.0054439	-0.0056459	n.a.
	U(R)CCSD(T)	-39.71737121	-39.76175578	-39.77307088	-39.7793743	-39.7796015
System		cc-pVDZ	cc-pVTZ	cc-pVQZ	CBS ^a	CBS ^b
32						
A	SCF	-262.0650969	-262.1293634	-262.1456677	-262.1507405	n.a.
B	CCSD-Correlation Energies	-0.8408223	-0.9994405	-1.0520804	-1.0865930	n.a.
C	Triples-Contribution	-0.0400267	-0.0567092	-0.0612433	-0.0629111	n.a.
	U(R)CCSD(T)	-262.9459459	-263.1855131	-263.2589914	-263.3002447	-263.3014004
RSE	U(R)CCSD(T)	+13.7(+18.7) kJ/mol ^c	+14.6(+19.6) kJ/mol ^c	+14.6(+19.6) kJ/mol ^c	+14.4 (+19.4) kJ/mol ^c	+14.6 (+19.6) kJ/mol ^c

^a CBS extrapolation using Weizmann-1 extrapolation schemes. ^b CBS extrapolation using Schwartz two points extrapolation schemes ^c In brackets: ΔH_{298} with thermal correction at B3LYP/6-31G(d).

Table B.14: H_{298} in a.u. of model systems (closed shells) in enzymatic catalysis using SAM at various level of theories.

Systems	H_{298} B3LYP/6-31G(d) ^a	H_{298} G3MP2Large	H_{298} G3(MP2)-RAD	H_{298} G3(+2d,MP2)-RAD ^b	H_{298} G3B3
2H	n.a.	n.a.	-887.0522407 ^[8,9]	n.a.	n.a.
3H	-40.470224	-40.3559600	-40.4169999	-40.3802496	-40.4544536
4H	-56.510280	-56.4103792	-56.4659305	-56.4287357	-56.5044867
31H	-467.199678	-466.3089263	-466.6348363	-466.3998972	-467.0309016
32H	-264.242763	-263.6981312	-263.9032200	-263.7620108	-264.1373323
33H	-232.144443	-231.6088872	-231.8230504	-231.6798795	-232.0516995
34H	-248.192386	-247.6523321	-247.8615089	-247.7192947	-248.0929017
36H	-226.139912	-225.6887464	-225.8631018	-225.7407937	-226.0584345
37H	-467.561515	-466.6573746	-466.9877425	-466.7532798	-467.3843621
38H	-467.563896	-466.6604694	-466.9903567	-466.7558847	-467.3868715
40H	-467.528384	-466.6288478	-466.9568454	-466.7223032	-467.3527950
41H	-596.126288	-595.1480480	-595.4338118	-595.2589012	-595.9198740
42H	-517.548823	-516.7630413	-516.9603438	-516.8412567	-517.3701485
43H	-477.933089	-477.2449172	-477.3951597	-477.3037611	-477.7672474
5H	n.a.	n.a.	-455.8496670 ^[8,9]	n.a.	-456.2090090 ^[8,9]
7H ^c	-362.909117	-362.2343852	-362.5161528	n.a.	n.a.
7H-1	-362.909720	-362.2348360	-362.5166434	n.a.	n.a.
7H-2	-362.908697	-362.2346932	-362.5164230	n.a.	n.a.
7H-3	-362.907471	-362.2333832	-362.5151328	n.a.	n.a.
7H-4	-362.907443	-362.2324695	-362.5142149	n.a.	n.a.
7H-5	-362.906784	-362.2337295	-362.5153761	n.a.	n.a.
7H-6	-362.905210	-362.2316592	-362.5135076	n.a.	n.a.
7H-7	-362.904666	-362.2307234	-362.5126760	n.a.	n.a.
11H	-420.428161	-419.5749953	-419.9332743	-419.6926500	-420.2871413
14H ^c	-516.49238867	-515.48125118	-515.8843673	n.a.	n.a.
14H-1	-516.492908	-515.4819100	-515.8850203	n.a.	n.a.
14H-2	-516.492335	-515.4799406	-515.8833278	n.a.	n.a.
14H-3	-516.491859	-515.4804905	-515.8835723	n.a.	n.a.
14H-4	-516.490844	-515.4802522	-515.8832438	n.a.	n.a.
14H-5	-516.490432	-515.4797826	-515.8826127	n.a.	n.a.
17H	-722.618960	-721.7147525	-721.8753296	-721.6754353	-722.4134521
20H ^c	-400.98648431	-400.53338241	-400.5333824	n.a.	n.a.
20H-1	-400.987330	-400.2219118	-400.5342118	n.a.	n.a.
20H-2	-400.986458	-400.2208132	-400.5329940	n.a.	n.a.
20H-3	-400.986298	-400.2211251	-400.5332446	n.a.	n.a.
20H-4	-400.986082	-400.2211510	-400.5333507	n.a.	n.a.
20H-5	-400.985605	-400.2202348	-400.5324921	n.a.	n.a.
20H-6	-400.985780	-400.2209300	-400.5329546	n.a.	n.a.
20H-7	-400.985003	-400.2189607	-400.5312784	n.a.	n.a.
20H-8	-400.984846	-400.2191801	-400.5314499	n.a.	n.a.
20H-9	-400.984097	-400.2193535	-400.5317716	n.a.	n.a.
20H-10	-400.983846	-400.2186130	-400.5310878	n.a.	n.a.
21H ^c	-400.99269530	-400.22849248	-400.5406369	n.a.	n.a.
21H-1	-400.993306	-400.2291154	-400.5412493	n.a.	n.a.
21H-2	-400.992569	-400.2275045	-400.5397281	n.a.	n.a.
21H-3	-400.991335	-400.2273788	-400.5393704	n.a.	n.a.
21H-4	-400.990906	-400.2264854	-400.5384518	n.a.	n.a.
21H-5	-400.990144	-400.2252980	-400.5371844	n.a.	n.a.
21H-6	-400.989776	-400.2244855	-400.5369773	n.a.	n.a.
21H-7	-400.989109	-400.2243907	-400.5363172	n.a.	n.a.

21H-8	-400.987942	-400.2231894	-400.5354308	n.a.	n.a.
21H-9	-400.987855	-400.2233621	-400.5358434	n.a.	n.a.
21H-10	-400.987480	-400.2229153	-400.5351658	n.a.	n.a.
24H	n.a.	n.a.	-533.1450347 ^[8,9]	n.a.	-533.5819120 ^[8,9]
25H	n.a.	n.a.	-492.7168417 ^[8,9]	n.a.	-493.1159350 ^[8,9]
27H	n.a.	n.a.	-892.8468224 ^[8,9]	n.a.	-893.5411760 ^[8,9]

^a Scaling factor 0.9806

^b Without HLC

^c Boltzmann averaged value

Table B.15: H_{298} in a.u. of model systems (open shells) in enzymatic catalysis using SAM at various level of theories.

Systems	H_{298} B3LYP/6-31G(d) ^a	H_{298} G3MP2Large	H_{298} G3(MP2)-RAD	H_{298} G3(+2d,MP2)-RAD ^b	H_{298} G3B3
2	n.a.	n.a.	-886.3897182 ^[8,9]	n.a.	n.a.
3	-39.804978	-39.6971464	-39.7518775	-39.7205433	-39.7895467
4	-55.850231	-55.7439369	-55.7969166	-55.7656772	-55.8357987
31	-466.531239	-465.6395443	-465.9605771	-465.7315146	-466.3581085
32	-263.574058	-263.0290258	-263.2292208	-263.0938671	-263.4627283
33	-231.469971	-230.9341895	-231.1438720	-231.0065158	-231.3707971
34	-247.526255	-246.9850216	-247.1899100	-247.0536684	-247.4201585
35	-466.519505	-465.6265995	-465.9488117	-465.7198339	-466.3463812
36	-225.458360	-225.0053212	-225.1761501	-225.0597763	-225.3731052
37	-466.886553	-465.9804999	-466.3063390	-466.0777484	-466.7040403
38	-466.886382	-465.9807982	-466.3066796	-466.0780833	-466.7043838
39	-466.547736	-465.6414643	-465.9717128	-465.7421494	-466.3655226
40	-466.914228	-465.9987753	-466.3289808	-466.1007535	-466.7261745
41	-595.464586	-594.4879907	-594.7683317	-594.5991560	-595.2550644
42	-516.885677	-516.1022096	-516.2939505	-516.1806212	-516.7044425
43	-477.284737	-476.6679735	-476.7456566	-476.6603164	-477.1186876
5	n.a.	n.a.	-455.2127519 ^[8,9]	n.a.	-455.5728470 ^[8,9]
7^b	-362.25114538	-361.57962267	-361.8554887	n.a.	n.a.
7-1	-362.251682	-361.5800287	-361.8559220	n.a.	n.a.
7-2	-362.251162	-361.5799191	-361.8557838	n.a.	n.a.
7-3	-362.250330	-361.5786050	-361.8544514	n.a.	n.a.
7-4	-362.249473	-361.5774836	-361.8533726	n.a.	n.a.
7-5	-362.249165	-361.5792498	-361.8549605	n.a.	n.a.
7-6	-362.247035	-361.5768201	-361.8526758	n.a.	n.a.
7-7	-362.246694	-361.5757925	-361.8517859	n.a.	n.a.
11a	-419.770746	-418.9196209	-419.2720811	-419.0369221	n.a.
11b	-419.777499	-418.9233331	-419.2761808	-419.0411350	n.a.
14^c	-515.8586873	-514.8444356	-515.2426263	n.a.	n.a.
14-1	-515.859204	-514.8447194	-515.2431016	n.a.	n.a.
14-2	-515.858012	-514.8446363	-515.2424804	n.a.	n.a.
14-3	-515.857144	-514.8431354	-515.2412375	n.a.	n.a.
14-4	-515.855489	-514.8419840	-515.2400792	n.a.	n.a.
14-5	-515.855977	-514.8413864	-515.2400714	n.a.	n.a.
17	-721.975379	-720.9572109	-721.2254190	-721.0311347	-721.7643155
20^c	-400.33355775	-399.56758524	-399.8744389	n.a.	n.a.
20-1	-400.334209	-399.5679840	-399.8748025	n.a.	n.a.
20-2	-400.333845	-399.5681484	-399.8750748	n.a.	n.a.
20-3	-400.333372	-399.5673881	-399.8742087	n.a.	n.a.
20-4	-400.333108	-399.5671785	-399.8738973	n.a.	n.a.
20-5	-400.332624	-399.5661075	-399.8730783	n.a.	n.a.
20-6	-400.332360	-399.5662167	-399.8732143	n.a.	n.a.
20-7	-400.332066	-399.5664372	-399.8733765	n.a.	n.a.
20-8	-400.330920	-399.5648131	-399.8719379	n.a.	n.a.
20-9	-400.330291	-399.5641252	-399.8713470	n.a.	n.a.
21^c	-400.34886540	-399.58153268	-399.8880592	n.a.	n.a.
21-1	-400.349247	-399.5818853	-399.8884478	n.a.	n.a.

21-2	-400.347899	-399.5805255	-399.8871395	n.a.	n.a.
21-3	-400.345660	-399.5774931	-399.8844975	n.a.	n.a.
21-4	-400.345032	-399.5776971	-399.8846308	n.a.	n.a.
21-5	-400.344133	-399.5762922	-399.8833173	n.a.	n.a.
21-6	-400.343389	-399.5760728	-399.8830835	n.a.	n.a.
21-7	-400.341364	-399.5749997	-399.8819647	n.a.	n.a.
21-TS	-400.333370	-399.5675115	-399.8743956	n.a.	n.a.
24	n.a.	n.a.	-532.4973859 ^[8,9]	n.a.	-532.9350080 ^[8,9]
25	n.a.	n.a.	-492.0751977 ^[8,9]	n.a.	-492.4739650 ^[8,9]
27	n.a.	n.a.	-892.208289 ^[8,9]	n.a.	-892.9039690 ^[8,9]

^a Scaling factor 0.9806

^b Without HLC

^c Boltzmann averaged value

Supplementary information for chapter 6

Table B.16: H_{298} in a.u. of monohydrated O-centered radicals and their closed shells at various level of theories.

	H_{298} G3(MP2)-RAD ^{a,b}	H_{298} G3(+2d,MP2)-RAD ^{a,b}	H_{298} G3B3 ^{b,c}
<i>Closed shells</i>			
4H + H ₂ O	-309.4347264	-309.4390968	-309.7377656
7H + H ₂ O	-587.6437874	-587.6472861	-587.5759759
2H + H ₂ O	-383.3365641	-383.3371710	-383.2862779
8H + H ₂ O	-422.5733625	-422.5743794	-422.5173999
11H + H ₂ O	-384.4666156	-384.4729192	-384.8244526
12H + H ₂ O	-438.6179476	-438.6190051	-438.5609231
14H + H ₂ O	-559.4936110		
<i>Open shells</i>			
4 + H ₂ O	-308.7708171	-308.7761566	-309.0722154
7 + H ₂ O	-587.0094551	-586.9987786	-586.9258549
2 + H ₂ O	-382.7005457	-382.6970260	-382.6455079
8 + H ₂ O	-421.9366875	-421.9377858	-421.8804320
11 + H ₂ O	-383.8337834	-383.8409680	-384.1901625
12 + H ₂ O	-437.9909348	-437.9924706	-437.9349201
14 + H ₂ O	-558.8848281		

^a Scaling factor 0.9806.

^b With 6D 10F polarization functions.

^c Scaling factor 0.960.

Table B.17: H_{298} and G_{298} in a.u. of dihydrated phenoxy radical and phenol at various level of theories.

	H_{298} G3(MP2)-RAD ^{a,b}	H_{298} G3(+2d,MP2)-RAD ^{a,b}	H_{298} G3B3 ^{b,c}
<i>Closed shells</i>			
2H + 2 * H ₂ O	-459.6908947	-459.6930380	-459.6328862
<i>Open shells</i>			
2 + 2 * H ₂ O	-459.0493783	-459.0518479	-458.9912010
	G_{298} G3(MP2)-RAD ^{a,b}	G_{298} G3(+2d,MP2)-RAD ^{a,b}	G_{298} G3B3 ^{b,c}
<i>Closed shells</i>			
1H	-76.3649435	-76.3658248	-76.3561001
2H + 2 * H ₂ O	-459.7404108	-459.7425472	-459.6827563
<i>Open shells</i>			
1	-75.6765249	-75.6783358	-75.6684541
2 + 2 * H ₂ O	-459.1052819	-459.1024450	-459.0422024

^a Scaling factor 0.9806.

^b With 6D 10F polarization functions.

^c Scaling factor 0.960.

Table B.18: H₂₉₈ in a.u. of O-centered radicals and their closed shells at various level of theories.

	H ₂₉₈ G3(MP2)-RAD ^b	H ₂₉₈ G3(+2d,MP2)-RAD ^b	H ₂₉₈ G3(+2d,MP2,MP4)-RAD ^b	H ₂₉₈ LD-G3(+2d,MP2)-RAD ^b	H ₂₉₈ G3B3 ^{b,c}
<i>Closed shells</i>					
3H	-412.9518636	-412.9588340	-412.99536655	-412.9533408	-413.2263723
1H	-76.3058471	-76.3067279	-76.3075155	-76.3067279	-76.3607481
4H	-233.1226966	-233.1257563	-233.1264314	-233.1239730	-233.3703191
5H	-154.6974653	-154.6998152	-154.71068867	-154.6987095	-154.8489301
6H	-115.4873974	-115.4892692	-115.49849115	-115.4885881	-115.5908293
7H	-511.0454086	-511.0475460	-511.0517682	-511.0465586	-511.5376331
2H	-306.8159784	-306.8153075	-306.8174865	-306.8170211	-307.1489996
8H	-346.0249932	-346.0247208	-346.0270712	-346.0260240	-346.4063812
9H	-151.3234185	-151.3261401	-151.3257575	-151.3249651	-151.4326467
10H	-153.5014670	-153.5029545	-153.51341126	-153.5027355	-153.6499648
11H	-308.1527603	-308.1575733	-308.1594317	-308.1542934	-308.4547788
12H	-362.0700160	-362.0698389	-362.0724265	-362.0710409	-362.4538389
13H	-131.4892697	-131.4912122	-131.4923392	-131.4906851	-131.5947854
14H	-483.1770484	-483.1818810	-483.1844724	-483.1785095	-483.7138970
<i>Open shells</i>					
3	-412.2684635	-412.2758241	-412.31201275	-412.2703173	-412.5411165
1	-75.6240702	-75.6258814	-75.6258561	-75.6258814	-75.6772042
4	-232.4586980	-232.4629508	-232.46241416	-232.4611691	-232.7048067
5	-154.0366032	-154.0402091	-154.05020941	-154.0390530	-154.1864664
6	-114.8266304	-114.8297029	-114.83797847	-114.8289544	-114.9284730
7	-510.4223166	-510.4073987	-510.4111360	-510.4070465	-510.8942618
2	-306.1932044	-306.1812685	-306.1835211	-306.1826631	-306.5114717
8	-345.3995962	-345.3933073	-345.3957910	-345.3940145	-345.7717325
9	-150.6903227	-150.6939276	-150.6944146	-150.6943116	-150.7983513
10	-152.8708356	-152.8726011	-152.88426990	-152.8714280	-153.0187969
11	-307.5239486	-307.5297520	-307.5306199	-307.5270250	-307.8249540
12	-361.4467069	-361.4468150	-361.4495070	-361.4472985	-361.8284823
13	-130.8701691	-130.8725940	-130.8730467	-130.8722967	-130.9737821
14	-482.5709608	-482.5748386	-482.5770107	-482.5715632	-483.1059620

^a Scaling factor 0.9806.

^b With 6D 10F polarization functions.

^c Scaling factor 0.960.

Table B.19: H_{298} in a.u. of systems **1H**, **2H** and **8H**, and their respective radicals at various level of theories.

	E_{h} B3LYP 6-31G(d)	H_{298} B3LYP 6-31G(d) ^b	H_{298} ROMP2 6-31G(d) ^b	H_{298} ROMP2 G3MP2Large ^{a,b}	H_{298} U(R)CCSD(T) 6-31G(d) ^b	H_{298} G3(MP2)-RAD ^a	
<i>Closed shells</i>							
1H	-76.4089533	-76.384421	-76.1723126	-76.1814455	-76.135207	-76.3058471	
2H	-307.4648705	-307.355553	-306.3816178	-306.4586750	-306.3977468	-306.8159784	
8H	-346.7822486	-346.644017	-345.5229143	-345.6280796	-345.5598355	-346.0249932	
<i>Open shells</i>							
1	-75.7234548	-75.712007	-75.5096031	-75.5148078	-75.4866975	-75.6240702	
2	-306.8276418	-306.731339	-305.7594325	-305.8330834	-305.7836597	-306.1932044	
8	-346.1477848	-346.022525	-344.9079003	-345.0050134	-344.9484446	-345.3995962	
	H_{298} ROMP2 6-311+G(3df,2p) ^{a,b}	H_{298} SCS-ROMP2 6-31G(d) ^b	H_{298} SCS-ROMP2 G3MP2Large ^{a,b}	H_{298} G3(MP2)-RAD ^{a,b} With SCS-ROMP2	H_{298} G3(MP2)-RAD ^c	H_{298} G3-RAD ^b	H_{298} G3B3 ^{b,d}
<i>Closed shells</i>							
1H	-76.4052559	-76.1682859	-76.2916617	-76.3066817	-76.3083070	-76.3603000	-76.3607481
2H	-307.1225852	-306.3505403	-306.7128167	-306.8208071	-306.8523034	-307.1460634	-307.1489996
8H	-346.3899396	-345.4900988	-345.9066290	-346.0313652	-346.0471316	-346.4027957	-346.4063812
<i>Open shells</i>							
1	-75.6253232	-75.5096084	-75.6106692	-75.6267305	-75.6252643	-75.6771500	-75.6772042
2	-306.4622454	-305.7327560	-306.0888636	-306.2008366	-306.2072534	-306.5204902	-306.5114717
8	-345.7316743	-344.8793713	-345.2844211	-345.4084219	-345.4199791	-345.7744912	-345.7717325
	H_{298} G4 ^{b,e}	H_{298} G4-5H ^{b,e}	H_{298} G4(MP2) ^{b,e} Without HLC	H_{298} G4(MP2) ^{b,e} With HLC	H_{298} U(R)CCSD(T) ^{a,b,f} CBS	H_{298} WIRO ^g	
<i>Closed shells</i>							
1H	-76.4037967	-76.3760087	-76.3580953	-76.3202073	-76.3526857	-76.458282	
2H	-307.3243498	-307.1993038	-307.0320686	-306.8615726	-306.9747143	-307.467281	
8H	-346.6088704	-346.4629834	-346.2748380	-346.0762790	-346.2068276	-346.763973	
<i>Open shells</i>							
1	-75.7162246	-75.6923996	-75.6702200	-75.6377340	-75.6652499	-75.770649	
2	-306.6851028	-306.5614858	-306.3917873	-306.2225353	-306.3359185	-306.828448	
8	-345.9729344	-345.8279334	-345.6390749	-345.4401629	-345.5709088	-346.127997	

Table B.20: H_{298} in a.u. of systems **1H**, **2H** and **8H**, and their respective radicals with different geometry.

	H_{298} G3(MP2)-RAD //B3LYP/6-31G(2df,p) ^e	H_{298} G3(MP2)-RAD //B3LYP/6-31+G(2df,p) ^h	H_{298} G3(MP2)-RAD //B3LYP/cc-pVDZ ^h	H_{298} G3(MP2)-RAD //MPW1K/6-31+G(d) ^h	H_{298} G3(MP2)-RAD //B2PLYP/6-31G(d) ^h
<i>Closed shells</i>					
1H	-76.3056690	-76.3053744	-76.35522069	-76.3045755	-76.3052673
2H	-306.8158944	-306.8146960	-307.03606197	-306.8101800	-306.813690
8H	-346.0251593	-346.0237159	-346.30280868	-346.0180685	-346.0218802
<i>Open shells</i>					
1	-75.6240002	-75.6238572	-75.64698514	-75.6235539	-75.6238402
2	-306.1856874	-306.1879667	-306.38474918	-306.1851218	-306.1885034
8	-345.3934264	-345.3920920	-345.64470336	-345.3876695	-345.3900490

^a Scaling factor 0.9806.

^b With 6D 10F polarization functions.

^c See ref 16 in chapter 6.

^d Scaling factor 0.960.

^e Scaling factor 0.9854.

^f CBS extrapolation using Schwartz scheme with cc-pVIZ ($l = 3, 4$).

^g W.IRO as implemented in Gaussian 09 C.01.

^h No scaling factor.

Table B.21: Total energies in a.u. of systems **1H**, **2H** and **8H**, and their respective radicals at MP2 and CCSD(T) level of theories.

Basis set	System 2H		System 1H		System 2		System 1	
	E_{tot} ROMP2 ^a	E_{tot} U(R)CCSD(T) ^a						
6-31g(d)	-306.4909353	-306.5678481	-76.1968449	-76.2078382	-305.8557353	-305.9410317	-75.5210509	-75.5371174
6-31g(d,p)	-306.5419633	-306.6210263	-76.2196843	-76.2314988	-305.8946906	-305.9817903	-75.5320192	-75.5483718
6-31+g(d)	-306.5119486	-306.5885969	-76.2096736	-76.2203112	-305.8791216	-305.9609979	-75.5340499	-75.5504710
6-311g(d)	-306.6185757	-306.6967774	-76.2389868	-76.2506556	-305.9824381	-306.0685767	-75.5458640	-75.5632575
6-31g(d,2p)	-306.5517843	-306.6311929	-76.2245694	-76.2364150	-305.9020531	-305.9895464	-75.5567039	-75.5742877
6-31g(2d)	-306.5699197	-306.6468094	-76.2261475	-76.2385391	-305.9332495	-306.0166575	-75.5575241	-75.5750798
6-31+g(d,p)	-306.5625929	-306.6411813	-76.2329928	-76.2442847	-305.9176488	-306.0012351	-75.5516721	-75.5690316
6-311g(d,p)	-306.6680630	-306.7484021	-76.2676363	-76.2797035	-306.0172717	-306.1056124	-75.5622310	-75.5797821
6-31g(2d,p)	-306.6184260	-306.6971949	-76.2480471	-76.2610929	-305.9708383	-306.0556107	-75.5630349	-75.5805236
6-311+g(d)	-306.6287957	-306.7067768	-76.2484457	-76.2597034	-305.9950699	-306.0784687	-75.5296087	-75.5462231
6-31+g(d,2p)	-306.5723928	-306.6512943	-76.2380091	-76.2493652	-305.9248256	-306.0088841	-75.5409558	-75.5577800
6-31+g(2d)	-306.5900604	-306.6663023	-76.2394004	-76.2512745	-305.9627970	-306.0361575	-75.5430794	-75.5599706
6-311g(d,2p)	-306.6807195	-306.7603058	-76.2773769	-76.2895716	-306.0258944	-306.1133942	-75.5545986	-75.5724763

6-31g(df)	-306.6511428	-306.7356976	-76.2333751	-76.2468671	-306.0093810	-306.1023574	-75.5657203	-75.5837401
6-31g(2d)	-306.6855321	-306.7638898	-76.2652448	-76.2772437	-306.0455541	-306.1298035	-75.5665954	-75.5845681
6-31g(2d,2p)	-306.6248178	-306.7034935	-76.2501076	-76.2630047	-305.9758251	-306.0606043	-75.5603774	-75.5780906
6-31+g(d,p)	-306.6785894	-306.7586104	-76.2783994	-76.2898694	-306.0297761	-306.1154665	-75.5709951	-75.5888715
6-31g(3d)	-306.5998165	-306.6782818	-76.2346388	-76.2467549	-305.9710763	-306.0468388	-75.5715663	-75.5893846
6-31+g(2d,p)	-306.6380268	-306.7160058	-76.2615570	-76.2739891	-305.9995947	-306.0745784	-75.5628042	-75.5786628
6-31g(df,p)	-306.6854158	-306.7700058	-76.2496837	-76.2632138	-306.0352089	-306.1282874	-75.5769946	-75.5930149
6-31g(2d,p)	-306.7254066	-306.8053687	-76.2819247	-76.2944022	-306.0768196	-306.1622897	-75.5808608	-75.5970645
6-31+g(d,2p)	-306.6905370	-306.7698359	-76.2872848	-76.2989520	-306.0379053	-306.1228312	-75.5823642	-75.5993652
6-31+g(df)	-306.6682387	-306.7520577	-76.2449935	-76.2577915	-306.0282149	-306.1180027	-75.5907013	-75.6078569
6-31g(3d,p)	-306.6443536	-306.7243259	-76.2561807	-76.2689300	-306.0048361	-306.0820117	-75.5936183	-75.6108188
6-31+g(2d)	-306.6951445	-306.7731300	-76.2746331	-76.2860333	-306.0640510	-306.1390725	-75.5894219	-75.6064641
6-31g(df)	-306.7429604	-306.8271102	-76.2637294	-76.2769943	-306.1021826	-306.1945107	-75.5971697	-75.6143702
6-31+g(2d,2p)	-306.6443766	-306.7222285	-76.2635104	-76.2758048	-306.0046022	-306.0795196	-75.5989676	-75.6160975
6-31g(df,2p)	-306.6959543	-306.7805801	-76.2552156	-76.2688212	-306.0431737	-306.1362337	-75.5690572	-75.5852375
6-31+g(3d)	-306.6156163	-306.6934182	-76.2462423	-76.2579469	-305.9858011	-306.0608236	-75.5836436	-75.5999423
6-31g(2d,2p)	-306.7371675	-306.8164327	-76.2889475	-76.3014578	-306.0854360	-306.1702952	-75.5873375	-75.6038041
6-31g(2df)	-306.7174035	-306.8009511	-76.2630706	-76.2777944	-306.0760573	-306.1656071	-75.5886156	-75.6057422
6-31+g(df,p)	-306.7023690	-306.7861061	-76.2617636	-76.2744868	-306.0537479	-306.1436208	-75.5973490	-75.6145949
6-31g(3d)	-306.7100486	-306.7879845	-76.2750505	-76.2871386	-306.0780253	-306.1528584	-75.5999855	-75.6172808
6-31g(3d,2p)	-306.6488508	-306.7284802	-76.2580650	-76.2706346	-306.0084692	-306.0853910	-75.5958842	-75.6131124
6-31+g(2d,p)	-306.7351815	-306.8146881	-76.2923108	-76.3040684	-306.0949271	-306.1714516	-75.6040328	-75.6213855
6-31g(df,p)	-306.7769019	-306.8616476	-76.2892590	-76.3028785	-306.1234512	-306.2164595	-75.6056213	-75.6229061
6-31+g(3d,p)	-306.6596580	-306.7388847	-76.2678544	-76.2801187	-306.0194554	-306.0958254	-75.5524704	-75.5703700
6-31g(2df,p)	-306.7511063	-306.8345793	-76.2794859	-76.2940368	-306.1016459	-306.1910084	-75.5602024	-75.5780709
6-31+g(df)	-306.7527398	-306.8365145	-76.2730320	-76.2857632	-306.1143571	-306.2038768	-75.5626098	-75.5805510
6-31+g(df,2p)	-306.7128642	-306.7966131	-76.2674825	-76.2802942	-306.0615686	-306.1514261	-75.5782340	-75.5972328
6-31g(3d,p)	-306.7494623	-306.8292238	-76.2900404	-76.3025929	-306.1096365	-306.1862296	-75.5863332	-75.6052450
6-31+g(2d,2p)	-306.7463267	-306.8251353	-76.2985217	-76.3103871	-306.1032738	-306.1790918	-75.5873595	-75.6062303
6-31+g(2df)	-306.7339845	-306.8165691	-76.2751090	-76.2888754	-306.1016453	-306.1809558	-75.5842177	-75.6031289
6-31g(df,2p)	-306.7895334	-306.8736022	-76.2982460	-76.3118887	-306.1326709	-306.2249223	-75.5914586	-75.6102745
6-31+g(3d)	-306.7181031	-306.7956925	-76.2847600	-76.2962825	-306.0854724	-306.1601367	-75.5925908	-75.6113566
6-31g(2df)	-306.8020000	-306.8848947	-76.2908417	-76.3046592	-306.1578737	-306.2468457	-75.5601489	-75.5781893
6-31+g(3d,2p)	-306.6640008	-306.7428601	-76.2692438	-76.2813420	-306.0230663	-306.0991701	-75.5681823	-75.5861452

6-31g(2df,2p)	-306.7567688	-306.8398728	-76.2819148	-76.2963360	-306.1058426	-306.1949326	-75.5707080	-75.5887422
6-311+g(df,p)	-306.7868512	-306.8711276	-76.2998057	-76.3127077	-306.1353451	-306.2256387	-75.5860477	-75.6051200
6-311g(3d,2p)	-306.7571595	-306.8359444	-76.2944581	-76.3068370	-306.1153095	-306.1910109	-75.5942821	-75.6132410
6-31g(3df)	-306.7445887	-306.8285529	-76.2717352	-76.2860244	-306.1106619	-306.1913729	-75.5954017	-75.6143083
6-31+g(2df,p)	-306.7671469	-306.8495785	-76.2916074	-76.3052512	-306.1265421	-306.2058495	-75.5919149	-75.6108296
6-311+g(3d,p)	-306.7573514	-306.8366788	-76.3006567	-76.3125364	-306.1167284	-306.1931327	-75.5992577	-75.6180550
6-311g(2df,p)	-306.8287298	-306.9119512	-76.3036098	-76.3175891	-306.1859184	-306.2672914	-75.6001905	-75.6189449
6-311+g(df,2p)	-306.7988590	-306.8825026	-76.3080151	-76.3210175	-306.1441692	-306.2337684	-75.5839050	-75.6011048
6-31g(3df,p)	-306.7732587	-306.8569186	-76.2866866	-76.3008830	-306.1320147	-306.2126306	-75.5965446	-75.6139068
6-311+g(2df)	-306.8105822	-306.8929645	-76.3000821	-76.3131800	-306.1757882	-306.2549008	-75.6001179	-75.6176084
6-31+g(2df,2p)	-306.7727240	-306.8547571	-76.2939977	-76.3075159	-306.1306710	-306.2096508	-75.6041520	-75.6226566
6-311+g(3d,2p)	-306.7649061	-306.8432620	-76.3042976	-76.3160632	-306.1224646	-306.1979840	-75.6105140	-75.6290388
6-31+g(3df)	-306.7577749	-306.8409566	-76.2822370	-76.2958606	-306.1231259	-306.2030871	-75.6131720	-75.6317086
6-311g(2df,2p)	-306.8400949	-306.9225917	-76.3099474	-76.3238806	-306.1867973	-306.2752817	-75.6115167	-75.6299477
6-311g(3df)	-306.8254263	-306.9078619	-76.3008821	-76.3146419	-306.1898517	-306.2689754	-75.6172023	-75.6356552
6-31g(3df,2p)	-306.7776129	-306.8607916	-76.2891576	-76.3032258	-306.1352493	-306.2154604	-75.6188367	-75.6372087
6-311+g(2df,p)	-306.8374116	-306.9200411	-76.3136553	-76.3267972	-306.1957444	-306.2752033	-75.5900400	-75.6074108
6-31+g(3df,p)	-306.7860574	-306.8688984	-76.2973672	-76.3108390	-306.1443562	-306.2241576	-75.6030577	-75.6205500
6-311g(3df,p)	-306.8493020	-306.9320908	-76.3118422	-76.3257533	-306.2080434	-306.2875593	-75.6064914	-75.6241029
6-311+g(2df,2p)	-306.8482693	-306.9301984	-76.3193084	-76.3324866	-306.2041175	-306.2829074	-75.6102987	-75.6287848
6-311+g(3df)	-306.8325065	-306.9145125	-76.3104161	-76.3234933	-306.1964020	-306.2752068	-75.6169697	-75.6354400
6-31+g(3df,2p)	-306.7902304	-306.8725763	-76.2994048	-76.3127653	-306.1475169	-306.2269050	-75.6193948	-75.6378886
6-311g(3df,2p)	-306.8575241	-306.9394753	-76.3157535	-76.3294566	-306.2145961	-306.2933789	-75.6178478	-75.6363209
6-311+g(3df,p)	-306.8563039	-306.9385885	-76.3221376	-76.3352678	-306.2143848	-306.2935724	-75.6238763	-75.6423397
6-311+g(3df,2p)	-306.8643763	-306.9458306	-76.3253479	-76.3383335	-306.2209249	-306.2993913	-75.6253232	-75.6437123

^a With 6D 10F polarization functions.

Supplementary information for chapter 7

Table B.22: Total energies of closed shell and open shell systems at G3(MP2)-RAD and G3B3 [a.u.].

System	G ₂₉₈ G3(MP2)-RAD ^a [a.u.]	G ₂₉₈ G3B3 ^a [a.u.]
H ₃ C-H	-40.4004958	-40.4485656
(CH ₃)H ₂ C-H	-79.6049048	-79.6989801
(CH ₃) ₂ HC-H	-118.8135787	-118.9536409
(CH ₃) ₃ C-H	-158.0236947	-158.2097513
(CH ₃) ₂ N-H	-134.8400292	-134.9820719
(CH ₃)O-H	-115.5086684	-115.6071780
(CH ₃)S-H	-438.1283326	-438.4806554
H ₃ C•	-39.7418718	-39.7882540
(CH ₃)H ₂ C•	-78.9536075	-79.0460971
(CH ₃) ₂ HC•	-118.1654502	-118.3040523
(CH ₃) ₃ C•	-157.3778115	-157.5626515
(CH ₃) ₂ N•	-134.1976746	-134.3383127
(CH ₃)O•	-114.8477213	-114.9449612
(CH ₃)S•	-437.4964859	-437.8479539

^a Total energies without HLC

Table B.23: Total energies of transition states at G3(MP2)-RAD and in parentheses at G3B3 [a.u.].

X-H/X•	H ₃ C•	(CH ₃)H ₂ C•	(CH ₃) ₂ HC•	(CH ₃) ₃ C•	(CH ₃) ₂ N•	(CH ₃)O•	(CH ₃)S•
H ₃ C-H	-80.1029322 (-80.1951942)						
(CH ₃)H ₂ C-H	-119.3123632	-158.5194162 (-158.7053082)					
(CH ₃) ₂ HC-H	-158.5235858	-197.7311649	-236.9426421 (-237.2204293)				
(CH ₃) ₃ C-H	-197.7358570	-236.9448427	-276.1561550	-315.3683018 (-315.7385852)			
(CH ₃) ₂ N-H	-174.5539445	-213.7627725	-252.9748345	-292.1884304	-269.0086037 (-269.2909221)		
(CH ₃)O-H	-155.2185780 (-155.3645802)	-194.4282392 (-194.6193823)	-233.6417771 (-233.8767942)	-272.8542433 (-273.1364136)	-249.6731124 (-249.9162977)	-230.3262659 (-230.5222348)	
(CH ₃)S-H	-477.8528256 (-478.2516879)	-517.0636364 (-517.5086269)	-556.2766694 (-556.7677896)	-595.4915185 (-596.0289323)	-552.9526995 (-553.4055037)	-572.3074169 (-572.8008789)	-875.6046131 (-876.3072464)

^aTotal energies without HLC

Supplementary information for chapter 8

Table B.24: G_{298} of the respective closed shells and open shells used in the calculation of barrier and thermodynamic reaction energies.

System	G_{298} G3(MP2)-RAD ^a [a.u.]	G_{298} G3B3 ^a [a.u.]
CH ₄ (6)	-40.4004958	-40.4274136
•CH ₃ (6H)	-39.7418718	-39.7660337
4H	-532.9020922	-533.4215845
4	-532.2613485	-532.7796713
5H	-492.5086805	-492.9797024
5	-491.8710504	-492.3398610
7H	-346.0519524	-346.4181360
7	-345.4267956	-345.7841322
10H	-438.1283326	-438.4806554
10	-437.4964859	-437.8479539
Transition state		
<i>Intrinsic</i>		
4H/4	-1065.1332653	n.a.
5H/5 stacked	-984.3456644	n.a.
5H/5	-984.3391857	n.a.
<i>First step of SPL mechanism</i>		
4H/6	-572.6156265	n.a.
4H/7	-878.2888605	n.a.
4H/10	-970.3644823	n.a.
6H/7	-385.7670644	n.a.
6H/10	-477.8528256	n.a.
<i>Second step of SPL mechanism</i>		
6H/5	-532.2193282	n.a.
7H/5 stacked	-837.8913738	n.a.
7H/5	-837.8839714	n.a.
10H/5	-929.9731027	n.a.

^aTotal energies without HLC

The barrier height for the first step is calculated in a reversed step due to the inaccuracy in the calculation of *p*-me-phenoxy radical **7** at G3(MP2)-RAD (Figure B.1). This can cause too high barrier due to artificial stabilization of *p*-me-phenoxy

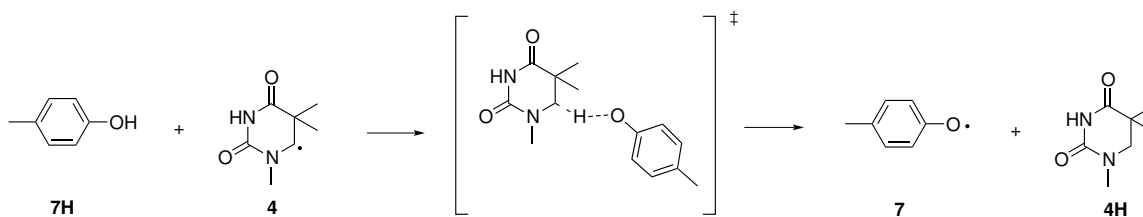


Figure B.1: Reversed barrier used to determine barrier height of the first step.

radical **7** (See chapter 6). The hydrogen abstraction from SPL substrate **4H** by *p*-me-phenoxy radical **7** is thus obtained by adding the thermodynamic reaction energy, which is calculated at G3B3, to the reversed barrier. In contrary, the second hydrogen transfer step does not have the problem of the inaccuracy occurring due to *p*-me-phenoxy radical **7**, since the starting point is the respective closed shells **7H** and thymine radical **5**. Nevertheless the free reaction energy should be still evaluated at G3B3.